

EXPLORING SOURCES AND METABOLIC CONSEQUENCES OF 2-AMINOACRYLATE
STRESS IN BACTERIA AND YEAST

by

DUSTIN CASEY ERNST

(Under the Direction of Diana Downs)

ABSTRACT

Reactive metabolites are produced by many biochemical pathways within a given metabolic network. The inherent reactivity of these metabolites presents a challenge to cells, where integrated biochemical pathways often coexist in densely packed spaces, paving the way for aberrant metabolic interactions to arise. Many networks produce reactive metabolite degradation systems to prevent these labile metabolites from damaging the cell. The broadly conserved Rid protein superfamily represents a key line of defense against reactive enamine stress. Reactive enamines, specifically 2-aminoacrylate generated by pyridoxal 5'-phosphate-dependent serine/threonine dehydratases, accumulate in *Salmonella enterica* lacking its native enamine deaminase, RidA. Persistence of 2-aminoacrylate in the absence of RidA triggers the inactivation of several distinct pyridoxal 5'-phosphate-dependent enzymes, diminishing cell fitness. The research described herein was performed to characterize diversity in the mechanisms of 2-aminoacrylate production, to improve our understanding of the key growth-limiting metabolic consequence of 2-aminoacrylate stress in *S. enterica*, and to assess conservation of the RidA-2-aminoacrylate paradigm in eukaryotic organisms. The data show that multiple mechanisms of 2-aminoacrylate production are found in *S. enterica*, the primary growth-limiting defect caused by

2-aminoacrylate stress in *S. enterica ridA* mutant strains is diminished glycine/one-carbon unit biosynthesis, and the RidA paradigm for reactive enamine control is conserved in yeast, where disruption of the mitochondrial RidA homolog (Mmf1p) leads to 2-aminoacrylate-induced loss of the mitochondrial genome.

INDEX WORDS: Enamine, 2-aminoacrylate, Metabolic stress, Pyridoxal 5'-phosphate, RidA

EXPLORING SOURCES AND METABOLIC CONSEQUENCES OF 2-AMINOACRYLATE
STRESS IN BACTERIA AND YEAST

by

DUSTIN CASEY ERNST
B.A., The University of San Diego, 2007

A Dissertation Submitted to the Graduate Faculty of The University of Georgia in Partial
Fulfillment of the Requirements for the Degree

DOCTOR OF PHILOSOPHY

ATHENS, GEORGIA

2017

© 2017

Dustin Casey Ernst

All Rights Reserved

EXPLORING SOURCES AND METABOLIC CONSEQUENCES OF 2-AMINOACRYLATE
STRESS IN BACTERIA AND YEAST

by

DUSTIN CASEY ERNST

Major Professor: Diana Downs

Committee: Jorge Escalante
Robert Maier
Robert Phillips

Electronic Version Approved:

Suzanne Barbour
Dean of The Graduate School
The University of Georgia
December 2017

ACKNOWLEDGEMENTS

I am thankful to all those who supported me in this endeavor. Special thanks to Dr. Diana Downs for her wonderful mentorship throughout my doctoral training. I appreciate the support and feedback provided by committee members Dr. Jorge Escalante, Dr. Rob Maier and Dr. Rob Phillips. Dr. David Garfinkel was instrumental in getting the yeast work off the ground. My labmates have kept me entertained and focused over the years, and I am especially indebted to Lauren Palmer, Jannell Bazurto and Jeff Flynn for their advice and guidance in navigating graduate school and preparing for life beyond.

I appreciate the many fantastic scientific mentors I have worked with to date. Dr. Jeffery Long and Dr. Michael Hannon provided me with a stimulating undergraduate research experience that sparked my interest in scientific exploration. Dr. Thomas Ishoey and Dr. Stuart Underwood provided exceptional mentorship during my time in industry and encouraged me to pursue graduate training. Dr. James G. Ferry recommended I consider the University of Wisconsin for graduate school, and Diana's lab in particular, which turned out to be great advice.

Lastly, the love and support of my family and friends has motivated me in unquantifiable ways. To my partner, Erin, your care and patience has meant the world to me. To my parents, Mary and David, I have tried to live by the examples you have set and am lucky to have you in my corner. And to my siblings and close friends who have encouraged me, I hope to pay it forward someday.

TABLE OF CONTENTS

	Page
ACKNOWLEDGEMENTS	iv
CHAPTERS	
1 INTRODUCTION AND LITERATURE REVIEW	1
2 ENDOGENOUS SYNTHESIS OF 2-AMINOACRYLATE CONTRIBUTES TO CYSTEINE SENSITIVITY IN <i>SALMONELLA ENTERICA</i>	31
3 L-2,3-DIAMINOPROPIONATE GENERATES DIVERSE METABOLIC STRESSES IN <i>SALMONELLA ENTERICA</i>	62
4 2-AMINOACRYLATE STRESS INDUCES A CONTEXT-DEPENDENT GLYCINE REQUIREMENT IN <i>RIDA</i> STRAINS OF <i>SALMONELLA ENTERICA</i>	100
5 MMF1P COUPLES AMINO ACID METABOLISM TO MITOCHONDRIAL DNA MAINTENANCE IN <i>SACCHAROMYCES CEREVISIAE</i>	129
6 ENHANCED CYSTATHIONINE β -LYASE PRODUCTION SUPPRESSES 2- AMINOACRYLATE STRESS IN <i>SALMONELLA ENTERICA</i>	160
7 CONCLUSIONS	186
APPENDICES	
A <i>SACCHAROMYCES CEREVISIAE</i> LACKING MMF1P HAVE LOW HEME LEVELS AND ARE SENSITIVE TO IRON	192

B	THE <i>STM4195</i> GENE PRODUCT (PANS) TRANSPORTS COENZYME A PRECURSORS IN <i>SALMONELLA ENTERICA</i>	206
C	PERTURBATION OF THE METABOLIC NETWORK IN <i>SALMONELLA ENTERICA</i> REVEALS CROSS-TALK BETWEEN COENZYME A AND THIAMINE PATHWAYS	240

CHAPTER 1

INTRODUCTION AND LITERATURE REVIEW

Metabolic networks are webs of integrated enzymatic and non-enzymatic reactions organized according to the chemical constraints of the cell. These networks must be arranged to maximize the output of chemical compounds necessary for cell growth and survival, while minimizing the detrimental impact reactive metabolite accumulation can have on cell fitness. One strategy to prevent aberrant reactive metabolite accumulation is targeted enzymatic degradation. A variety of enzymatic reactive metabolite defense systems, including those that degrade reactive oxygen species, have been described to date. The content that follows describes ongoing work to characterize reactive enamine stress and associated enamine degradation systems throughout life. This introduction provides historical context for the discovery of reactive enamine stress in *Salmonella enterica*, and describes our current understanding of the role RidA/YER057c/UK114 family proteins play in degrading reactive enamine/imine intermediates.

1.1 Organization of metabolic networks

Origins of metabolism and metabolic stress. The origin of metabolism was an early evolutionary adaptation that allowed primitive life forms to generate chemical compounds necessary for life (1). Unsettled hypotheses abound regarding the mechanisms of transition from heterogeneous mixtures of diverse chemicals in the prebiotic world, into more complex entities capable of self organization and self replication (2). Regardless, as self-replicating proto-

organisms grew more complex, metabolic pathways became increasingly important to provide precursors for macromolecule synthesis. In the absence of metabolism, life would be constrained by environmental parameters and dependent on geochemistry to supply diverse chemical building blocks (3). The emergence of catalytic macromolecules (e.g. ribozymes) conferred a higher degree of order to metabolism and provided an alternative to non-enzymatic chemistry (4), allowing organisms to expand into nutrient-limited growth environments by employing a variety of metabolic strategies (5). The precise origin of proteinaceous catalysts remains unclear, but ultimately, their genetic underpinnings gave rise to heritability (6). Metabolic capabilities likely expanded as gene duplications arose and diverged through mutation, giving rise to altered enzyme activities and patchwork expansion of biochemical pathways (7, 8). Extant metabolic networks are organized into intertwined biochemical pathways comprised of both enzymatic and non-enzymatic reactions (4). The diversity of metabolites and catalysts contained within cells and organelles generates robust networks with wide-ranging metabolic potential. However, the varied reactivity of metabolites and catalysts within the cell requires quality control measures to optimize cell fitness by preventing or repairing deleterious chemistries (9). The focus here will be on mechanisms of preventing metabolic stress, while damage repair systems have been described elsewhere (10).

Metabolic stress prevention strategies. The regulation of metabolism at a variety of levels, from gene expression to enzyme activity, provides temporal control over which pathways are active in the cell at any given time (11–13). However, temporal control of metabolism fails to completely prevent metabolic stress as many reactive metabolites are introduced from the environment or produced by core metabolic pathways (14, 15). Thus, a variety of additional evolutionary solutions have emerged to manage chemical reactivity within metabolic networks.

Damage-prone metabolites can be protected from the cellular milieu through substrate channeling or scaffolding, in which metabolites in a given pathway are handed off from one enzyme to the next (16, 17). Reactive chemical moieties attached to intermediates can be transiently modified to prevent undesirable side reactions from occurring (18, 19). Physical constraints can be placed on the location a given reaction is allowed to occur, exemplified by bacterial microcompartments or eukaryotic organelles, to limit interactions between reactive metabolites and the cellular milieu (20, 21). Elimination systems enable compartmentalized degradation (e.g. lysosomes) or excretion of useless or potentially harmful metabolites (22, 23). Lastly, a variety of enzymatic degradation systems act by converting highly-reactive metabolites into less-reactive products (10). Taken together, these quality control systems serve to minimize the threat of metabolic stress in a variety of cell types. The work herein focuses on enzymes that degrade reactive species produced during normal metabolic processes.

Reactive metabolite degradation systems. Several reactive metabolite degradation systems have been described, but perhaps none is better characterized than reactive oxygen species (ROS) defense (Figure 1.1A) (24). Many organisms maintain high concentrations of enzymes that degrade superoxide (O_2^-) and hydrogen peroxide (H_2O_2) (25). These reactive metabolites are produced as a repercussion of metabolism in aerobic environments and lead to damage of a variety of macromolecules, particularly enzymes containing iron as a cofactor (26, 27). Additionally, O_2^- and H_2O_2 are indirectly mutagenic, as the generation of hydroxyl radicals ($\bullet OH$) can damage DNA (28). The main source of intracellular ROS is promiscuous interactions between molecular oxygen and electron-transfer enzymes, predominantly flavoenzymes, that result in one (e.g. O_2^-) or two (e.g. H_2O_2) electron transfer reactions (29). The universality of ROS stress indicates it is an unavoidable by-product of life in oxygenated environments.

In many aerobic and facultative anaerobic bacteria, including *Escherichia coli*, basal defense against ROS accumulation is sufficient to prevent drastic changes in fitness (25). However, when presented with growth conditions that elicit high ROS burdens (e.g. redox-cycling antibiotics), defense systems are induced to scavenge excess ROS. Superoxide dismutase (SOD) and peroxidase/catalase serve as the primary ROS defense systems in *E. coli* and most other bacteria. SOD is required to enhance the rate of spontaneous O_2^- dismutation, while low levels of H_2O_2 are reduced by NADH-dependent peroxidase, and high levels of H_2O_2 induce the peroxide dismutase, catalase. Operating in concert, these enzymes prevent ROS from accumulating to toxic levels inside the cell. In total, the ROS-defense paradigm represents the best understood reactive metabolite stress pre-emption system studied to date.

Other examples of reactive metabolite control are found throughout nature. Many reactive carbonyl species, including the dicarbonyl methylglyoxal (a.k.a. pyruvaldehyde), are potent cytotoxic agents in a variety of organisms (Figure 1.1B) (30). In *E. coli*, methylglyoxal is produced by multiple pathways and acts as a potent electrophile capable of modifying DNA and proteins (31). Despite the toxicity of methylglyoxal in *E. coli*, it is paradoxically generated from dihydroxyacetone-phosphate (DHAP) by a dedicated methylglyoxal synthase (MGS) (32). MGS serves as a bypass pathway for glycolysis to prevent sugar phosphate accumulation, especially under limiting inorganic phosphate conditions (33). The fitness benefit of this bypass system only makes sense in light of co-occurring mechanisms of methylglyoxal degradation. *E. coli* is dependent on a well-conserved glyoxalase system and glutathione (GSH) for efficient detoxification of methylglyoxal (34). The degradation process is initiated by spontaneous reaction between methylglyoxal and GSH to form GSH-hemithioacetal, followed by glyoxalase I catalyzed formation of *S*-lactoylglutathione. The *S*-lactoylglutathione formed by glyoxalase I is hydrolyzed

by glyoxylase II to relatively non-toxic metabolites D-lactate and GSH. Thus, methylglyoxal degradation can be viewed as a two-tiered process reliant on non-enzymatic chemistry to initiate the reaction, followed by enzymatic catalysis to complete the degradation pathway. Similar to ROS defense systems, the broad conservation of glyoxylase systems across all domains of life indicates methylglyoxal (or related carbonyl species) stress is encountered by virtually all organisms as a consequence of normal metabolic processes.

Influence of reactive metabolites on metabolic robustness. Although the reactive metabolites outlined above clearly elicit toxic effects in the cell, they also impact fitness in potentially beneficial ways. In many eukaryotes, particularly plants, ROS is viewed as a versatile signaling molecule integrated into different signaling networks (35, 36). ROS signaling in higher plants was found to regulate redox levels, development, cellular differentiation, cell death and interactions with other organisms (37). In *Saccharomyces cerevisiae*, methylglyoxal production increases in response to osmotic stress, leading to activation of Ca^{2+} uptake systems and a cascade of regulatory events linked to improved osmotolerance (38).

Beyond ROS and methylglyoxal, the aberrant production of reactive metabolites has been shown to promote metabolic plasticity by enabling new pathways to emerge. Work by Kim *et al.* demonstrated that enhancing the production of a putative NUDIX hydrolase (YeaB) in *E. coli* uncovered a promiscuous enzyme activity that generated 3-hydroxypyruvate (3HP) from the serine precursor, 3-phosphohydroxypyruvate (39). 3HP is not normally produced by *E. coli*; the 3HP formed by YeaB served as the first intermediate in a non-canonical pyridoxal 5'-phosphate (PLP) biosynthetic pathway that bypassed a block ($\Delta pdxH$) in the canonical PLP pathway. Increasing levels of 3HP through exogenous supplementation diminished growth of *E. coli* under standard growth conditions, indicating 3HP was partially toxic. Thus, the impact of 3HP on *E. coli* fitness

ranged from deleterious to beneficial and proved to be context dependent. In instances where PLP was limiting, the synthesis of 3HP facilitated an additional mechanism of PLP production, but when 3HP concentrations exceeded a certain threshold, growth was limited as a consequence of 3HP toxicity.

Taken together, these examples demonstrate that reactive metabolites influence the fitness and metabolic flexibility of organisms in both harmful and beneficial ways. Therefore, the control of reactive metabolite accumulation must be coordinated to promote fitness-enhancing chemistries, while limiting undesirable perturbations. The sections that follow describe an emerging paradigm of intracellular reactive enamine stress and its mechanism of control.

1.2 Reactive enamines produced enzymatically can act as mechanism-based inhibitors.

Reactive enamine/imine production by pyridoxal phosphate-dependent enzymes.

Enamines are unsaturated nitrogen-containing compounds that are useful as labile intermediates in a variety of biochemical and chemical reactions (40). Biochemical studies have demonstrated that many pyridoxal 5'-phosphate (PLP)-dependent enzymes generate enamine intermediates from α -amino acid substrates (41). In some cases, the cofactor-bound enamine is processed further prior to release from the enzyme (42, 43). In other cases, the enamine is released into the reaction milieu and undergoes spontaneous tautomerization to the corresponding imine, followed by spontaneous hydrolysis in solvent water that results in production of a keto acid (44, 45).

PLP-dependent enzymes are generally grouped according to structural similarities or catalytic mechanisms, but there is not a universal correlation between structure and function (41). The majority of PLP-dependent enzymes belong to one of five fold types, with fold type II comprising the largest number of α,β -eliminases (46). A number of PLP-dependent enzymes

assigned to the other fold types also catalyze β -elimination reactions as side-reactions to their primary activity (47). Many amino acids with electronegative side chains, including non-canonical β -substituted amino acids (e.g. 3-chloro-L-alanine), serve as substrates for dedicated (or promiscuous) α,β -eliminases. Amino acid substrates with only hydrogens and a leaving group attached to C-3 are precursors to the highly reactive enamine, 2-aminoacrylate (2AA). As mentioned above, the fate of 2AA formed in a given active site depends on the active site configuration and mechanism employed by the enzyme of origin.

Tryptophanase (TnaA; EC 4.1.99.1), a fold type I PLP-dependent lyase, is the main enzyme in *E. coli* responsible for the catabolism (α,β -elimination) of tryptophan into indole, pyruvate and ammonia (48). This enzyme can additionally generate tryptophan (β -substitution) in the presence of serine and indole following the β -elimination of water from serine (49). The versatility of this enzyme is further exemplified by its role in cysteine detoxification (via α,β -elimination) (50). In these reactions, PLP-bound 2AA is formed as an intermediate. Instead of being released via transaldimination, 2AA is first protonated (or condensed with indole) on C-3 in a stereospecific manner, and is subsequently released and hydrolyzed to pyruvate (or released as tryptophan) (43). This represents a mechanism where PLP-bound 2AA is produced, but not released until 2AA is modified further.

PLP-dependent serine/threonine dehydratase (EC 4.3.1.19) is a representative fold type II β -lyase that generates unbound enamine intermediates that undergo spontaneous tautomerization and hydrolysis to stable keto acid products (Figure 1.1C). In *S. enterica*, anabolic serine/threonine dehydratase (IlvA) catalyzes the first step in isoleucine biosynthesis by generating and releasing an unstable enamine, 2-aminoacronate (2AC), from threonine (45). Some reaction schemes incorrectly depict IlvA-catalyzed dehydration of threonine as leading directly to 2-ketobutyrate

formation (2KB) (51, 52). In reality, 2AC released by IlvA serves as the relevant precursor to 2KB. IlvA also catalyzes the promiscuous dehydration of serine to form unbound 2AA (53). Like 2AC, the breakdown of 2AA to pyruvate occurs spontaneously in solvent water. The relevance of unbound 2AA and 2AC to the overall reaction scheme of serine/threonine dehydratases is sometimes overlooked due to the short half-life of these reactive enamines in aqueous solution. The stability of enamine intermediates is dependent on the pH and temperature of the reaction buffer. 2AC has an estimated half-life of ~3 minutes at 30 °C and pH 7-8 (54), while the imine derived from serine (2-iminopropionate) has a half-life of ~1.5 seconds (42). Thus, the occurrence of these unbound enamine metabolites is often ignored.

Mechanism based inactivation of PLP-dependent enzymes by 2AA. While TnaA and IlvA are dedicated lyases, a variety of non-lyase PLP-dependent enzymes catalyze α,β -elimination reactions when provided substrates with strong leaving groups attached to the β -carbon (41). Strong leaving groups tend to be atoms or molecules that are more electronegative (e.g. -Cl, -SO₃⁻) than the functional groups attached to amino acids normally encountered (e.g. -OH, -SH). Thus, amino acid substrates with favorable leaving groups can be acted on by otherwise poor catalysts of β -elimination reactions. PLP-dependent transaminases are particularly susceptible to such promiscuous α,β -eliminations, while some decarboxylases, racemases and retro-aldolases have also been reported to have moonlighting β -eliminase activity (55–58).

The broad range of PLP-dependent enzymes that catalyze (promiscuous) β -elimination reactions led to the identification of reactive enamine mechanism-based inhibitors. Numerous *in vitro* biochemical studies highlighted the potential for 2AA or related α,β -unsaturated amino acids to damage PLP-dependent enzymes (55, 56). These studies demonstrated that the elimination of functional groups from β -substituted α -amino acids (e.g. 3-chloro-L-alanine, L-serine-*O*-sulfate,

etc.) led to 2AA inactivation of the enzyme. Independent reports showed that a variety of transaminases, including those that typically act on aspartate, valine, isoleucine, alanine and ornithine, were all inactivated to varying degrees by 2AA produced within each enzyme's respective active site (59). The mechanisms of inactivation ranged from attack of the 2AA-PLP adduct by active-site nucleophilic residues (56), to release of 2AA and subsequent nucleophilic attack of the electrophilic enzyme-bound PLP Schiff base (Figure 1.2) (58). Furthermore, the consequences of mechanism-based 2AA inactivation can be detected *in vivo*; feeding 3-chloro-L-alanine to *E. coli* inhibits growth and inactivates alanine-valine transaminase (AvtA) and isoleucine transaminase (IlvE) in turnover-dependent manners (60). In all of the above cases, 2AA explicitly inactivated the enzyme that generated it and was not reported to diffuse from one enzyme to another.

Some PLP-dependent enzymes can be sensitized to mechanism-based inactivation by 2AA through site-directed mutagenesis (61). The tryptophan synthase $\alpha_2\beta_2$ complex catalyzes the last two reactions in the biosynthesis of tryptophan (62). The PLP-dependent β subunit catalyzes β -elimination and β -substitution reactions, but when in the $\alpha_2\beta_2$ complex, has very low activity in β -elimination reactions (63). Variant β subunits (in an $\alpha_2\beta_2$ complex) with altered active site residues displayed unique catalytic properties; some variants biased reactions towards β -elimination relative to the wild-type $\alpha_2\beta_2$ complex (63). Several of the variants became susceptible to inactivation by 2AA produced from L-serine or 3-chloro-L-alanine, whereas the wild-type enzyme was unmodified by serine and infrequently modified by 3-chloro-L-alanine. These data demonstrated that a fine line exists between substrate-based inactivation and successful elimination reactions; changing a single active-site residue profoundly influenced susceptibility to 2AA inactivation. Insights from this study are useful when examining how enzymes that routinely

generate 2AA are less-prone to 2AA inactivation, while enzymes that haphazardly generate 2AA are more susceptible to inactivation. The fact that enzymes proficient at α,β -elimination are still susceptible to mechanism based inactivation (64), albeit less so than promiscuous eliminases, highlights the reactivity and potential toxicity of 2AA.

1.3 Reactive enamines cause stress unless degraded by RidA family proteins.

Diffusible 2-aminoacrylate damages *S. enterica* lacking RidA. Pioneering work in the Downs laboratory demonstrated that 2AA generated by one enzyme could diffuse into the active site of another enzyme and inactivate it. This discovery was made based on biochemical genetic studies of *S. enterica* harboring mutations in a well-conserved gene of then-unknown function, *ridA* (previously *yjgF*). Early work showed that *ridA* mutants were sensitive to serine when grown on minimal glucose medium unless isoleucine was provided in the growth medium (Figure 1.3) (65). The ability of isoleucine to reverse the serine sensitivity of a *ridA* strain was influenced by the status of IlvA. Because IlvA catalyzes the first step in isoleucine biosynthesis, it is feedback inhibited by isoleucine ($K_i = 0.003$ mM) (53). Replacing the wild-type *ilvA* allele with an allele (*ilvA219*) encoding the feedback-insensitive IlvA^{L447F} variant prevented isoleucine from restoring growth to a *ridA* strain (66, 67). This observation confirmed that isoleucine inhibition of IlvA was required to prevent serine sensitivity in a *ridA* strain background. By extension, these data indicated that RidA was required to prevent IlvA-dependent serine sensitivity in wild type cells.

Earlier biochemical work established that IlvA generates and releases 2AA from serine (see above). In aqueous solution, the dehydration of serine by IlvA ultimately produces pyruvate, indicating that 2AA is unstable and susceptible to spontaneous tautomerization and hydrolysis by water. The Downs laboratory demonstrated that despite the short half-life of 2AA in solution, RidA

added to reactions containing IlvA and serine enhanced the rate of pyruvate formation (68). Changing a conserved arginine to alanine (R105A) in the purported RidA active site abolished the rate-enhancing properties of RidA. Taken together, these data indicated that RidA binds 2AA (and/or the corresponding imine) and enhances its rate of conversion to pyruvate. This finding was groundbreaking given that RidA enhanced the rate of a reaction previously assumed to be strictly non-enzymatic. RidA had a similar rate-enhancing effect on reactions containing IlvA and threonine, indicating RidA uses 2AC as a substrate (68). RidA homologs derived from organisms spanning the tree of life displayed conserved enamine/imine hydrolase activity *in vitro* (68). This finding ultimately led to the renaming of the broadly conserved YjgF/YER057c/UK114 protein family as the Rid (reactive enamine deaminase) protein superfamily (69).

The combined biochemical and genetic data indicated that *ridA* mutant strains were likely sensitive to intracellular 2AA accumulation. Growth phenotypes suggested multiple metabolic pathways were inactivated in a *ridA* strain exposed to IlvA-dependent 2AA stress. In minimal glucose medium, *ridA* strains display a minor growth defect relative to wild type (Figure 1.3). The minor growth defect is reversed by isoleucine supplementation, indicating that basal 2AA stress is generated by IlvA from endogenous pools of serine (not shown). Assaying PLP-dependent enzymes in crude extracts following growth in minimal glucose medium showed that serine hydroxymethyltransferase (GlyA; EC 2.1.2.1), isoleucine transaminase (IlvE; EC 2.6.1.42) and alanine racemases (Alr/DadX; EC 5.1.1.1) all had lower activity in a *ridA* strain (Table 1.1) (70–72). These enzyme defects correlated with the pleiotropic phenotypes summarized in Table 1.1. Protein recovery and analytical evaluation (e.g. UV/Vis, mass spectrometry and/or HPLC) confirmed that the inhibited PLP-dependent enzymes were covalently inactivated by 2AA. Although detailed mechanisms of inactivation remain unsettled, these findings proved that 2AA

generated by IlvA i) could persist *in vivo* and ii) diffuse into the active site of a distinct PLP-dependent enzyme and inactivate it. These *in vivo* findings were corroborated by *in vitro* work that showed reactions containing IlvA, serine and IlvE led to inactivation of IlvE, but including RidA in the reaction mixture prevented IlvE from becoming inactivated by 2AA (72). The work described above established the RidA paradigm: 2AA produced by PLP-dependent serine/threonine dehydratases can be degraded by RidA to prevent 2AA from accumulating and inactivating distinct PLP-dependent enzymes in the cell.

2AC derived from threonine contributes to metabolic plasticity. Work that preceded our understanding of RidA activity demonstrated that some reactive enamine/imine metabolites positively influence network plasticity. This discovery was made following a mutant hunt to look for suppressors of a thiamine-deficient *purF gnd* mutant strain of *S. enterica* (65). The most common suppressors isolated contained mutations in *ridA*. Disruption of *ridA* uncovered a PurF-independent mechanism of phosphoribosyl amine (PRA) formation in support of thiamine biosynthesis. Isoleucine supplementation inhibited PRA/thiamine biosynthesis in the *purF gnd ridA* mutant strain. The ability of isoleucine to reverse the thiamine proficiency of a *purF gnd ridA* mutant was influenced by IlvA feedback sensitivity, analogous to the role of isoleucine in limiting 2AA production. Subsequent work showed that 2AC, produced by IlvA from threonine, accumulated in the absence of RidA and supported PurF-independent PRA formation (73–75). The promiscuous formation of PRA via condensation of 2AC with phosphoribosyl pyrophosphate occurred in an anthranilate phosphoribosyl transferase (TrpD)-dependent manner (74). These data showed that *S. enterica* lacking RidA enamine deaminase activity possessed an alternative mechanism of PRA formation that was contingent upon 2AC accumulation. Recent work demonstrated that this mechanism of 2AC-dependent PRA formation is active in wild type *E. coli*

despite the presence of active RidA homologs in this organism (76). These findings indicate *E. coli* has a metabolic configuration distinct from *S. enterica* that enables IlvA- and TrpD-dependent PRA formation despite the presence of RidA. This work emphasizes that reactive enamines can influence metabolic networks in various ways, and the mere presence of RidA does not indicate reactive enamines are absent from the intracellular milieu.

RidA proteins are found across all domains of life. The broad conservation of RidA proteins likely reflects the production of unbound reactive enamines throughout life. Genomes that encode at least one RidA homolog often encode one or more (putative) PLP-dependent α,β -eliminases (69), though this correlation has not been rigorously tested. Most free-living organisms possess at least one RidA homolog; while eukaryotes typically encode one or two true RidA proteins, many prokaryotes encode additional Rid proteins (Rid1-7) that are often embedded in operons. The Rid1-7 proteins display primary sequence divergence from the archetypal RidA, especially at several well-conserved residues, suggesting these enzymes have altered or specialized activity relative to RidA. Our current model dictates that true RidA proteins serve as housekeeping enamine/imine deaminases, while Rid1-7 proteins found in prokaryotes are induced in response to specific signals. Ongoing work in the Downs laboratory suggests that some Rid proteins may be less important for enamine/imine detoxification *per se*, but are instead required to enhance pathway efficiency (77).

The molecular mechanism used by RidA to convert enamines/imines to keto acids is still undetermined. A universal feature of all Rid proteins demonstrated to have enamine/imine deaminase activity is conservation of the Arg-105-equivalent from *S. enterica* RidA (69, 77). This residue is predicted to coordinate the enamine/imine intermediate adjacent to a nucleophilic water molecule, oriented by hydrogen bonding with active site residues (Figure 1.4) (78, 79). *In vitro*,

RidA clearly has an affinity for imines generated by flavin adenine dinucleotide (FAD)-dependent L-amino acid oxidase (LOX); this enzyme generates and releases an imine directly without proceeding through an enamine intermediate (69). However, evidence is lacking to support the relevance of exclusive imine hydrolysis in preventing reactive enamine stress. Therefore, we predict RidA binds the enamine (e.g. 2AA), or a transition state between the enamine and imine, and facilitates a near simultaneous tautomerization and hydrolysis event to generate a keto acid (Figure 1.4). This model is based in part on the anticipated greater intracellular stability of the enamine relative to the imine, necessitating an enzyme capable of scavenging enamines directly (45).

Beyond *S. enterica*, the role of RidA homologs in most other organisms has yet to be experimentally defined. Several alternative biochemical functions have been ascribed to RidA homologs from a variety of organisms (80–84). Importantly, conclusions regarding the function of RidA in these other cases were based largely on *in vitro* observations and lacked the power of our robust biochemical genetics approach in *Salmonella enterica*. The fact that all true RidA enzymes assayed possess enamine/imine deaminase activity supports our model of conserved RidA deaminase activity across domains of life. Thus, the RidA paradigm outlined above serves as a template for investigating the function of RidA in other organisms, including mammals. A variety of reports have described correlations in the production of the mammalian RidA homolog (UK114), immune cell behavior and tumor cell differentiation (85–87). In fact, some reports have determined that UK114 can be targeted to cancer cell surfaces, facilitating anti-UK114 antibody mediated cytotoxicity (88–91). Our understanding of RidA dynamics in mammals stands to benefit from preliminary investigation of Rid protein function in eukaryotic model organisms. Reports have described phenotypic characteristics of *Saccharomyces cerevisiae* lacking the mitochondrial

RidA homolog (Mmf1p), but a clear connection to 2AA stress was not made since these findings predated our understanding of RidA deaminase activity (92, 93). Work described in Chapter 5 addresses the function of Mmf1p in preventing 2AA stress in yeast, providing the first example of 2AA stress occurring in a eukaryotic organism.

1.4 Summary

The findings summarized here show that reactive enamines generated by PLP-dependent enzymes are significant *in vivo*; in some cases (i.e. 2AA) they are deleterious, but in other cases (i.e. 2AC) they enhance the robustness of metabolic systems. Work in the Downs laboratory has defined a clear role for RidA in controlling reactive enamine accumulation in *S. enterica*. The primary consequence in strains lacking RidA is the accumulation of 2AA that inactivates a variety of metabolic PLP-dependent enzymes. These findings showed that a reaction (e.g. 2AA/imine hydrolysis) achieved spontaneously in solvent water is not readily attained *in vivo*, possibly reflecting the lack of free water in the cell. These insights raise questions about other purportedly spontaneous intracellular reactions; perhaps enzymes are actually required to facilitate or enhance these reactions. There is growing speculation that many of the extant genes of unknown function in model organisms may encode enzymes like RidA, that improve seemingly spontaneous reactions involving labile intermediates (94). Disruption of these enzymes would be expected to harm the cell, but may not lead to strong, detectable phenotypes under standard laboratory growth conditions. Here it is important to emphasize that the function of RidA was determined using a genetic approach; an epistatic interaction between thiamine biosynthesis and enamine accumulation set the stage for defining RidA activity. Thus, in an era where systems level

approaches are growing more powerful, there is still a need for rigorous biochemical genetics approaches to help define unknown aspects of cellular metabolism.

1.5 Dissertation Outline

In the dissertation that follows, I describe my efforts to expand our understanding of the sources and metabolic consequences of 2AA stress in bacteria and yeast. Our early interest was in assessing the diversity of enzymes capable of potentiating 2AA stress in *ridA* strains of *S. enterica*. In Chapters 2 and 3, I describe IlvA-independent mechanisms of 2AA production.

Chapter 2 highlights the role of PLP-dependent cysteine desulfhydrase (CdsH) in generating 2AA from cysteine. Whereas IlvA acts promiscuously on serine, CdsH is induced specifically in response to cysteine and serves as a cysteine detoxification pathway dependent on RidA to avoid concomitant 2AA stress.

A similar paradigm is explored in Chapter 3 through the characterization of PLP-dependent diaminopropionate ammonia lyase (DpaL). We show that DpaL contributes to 2AA stress when diaminopropionate is provided to RidA-defective strains. We also explore the direct inhibition by diaminopropionate of proline, pantothenate and isoleucine biosynthetic pathways.

In Chapter 4, attention is turned to explaining the underlying metabolic perturbations caused by 2AA that limit growth of *ridA* strains. Building on previous work, we show that 2AA inactivation of serine hydroxymethyltransferase (GlyA) creates a context-dependent glycine requirement. Under circumstances where serine is abundant in the growth medium, glycine is necessary to regulate activity of the GcvB small RNA, presumably to limit serine uptake. In contrast, when 2AA stress is exacerbated by enhancing turnover of endogenous serine, glycine is

required to supply one-carbon units through the glycine cleavage complex (GCV), bypassing damage to GlyA.

Chapter 5 details the first comprehensive study of 2AA stress in a eukaryote. We confirm that *Saccharomyces cerevisiae* lacking the nuclear-encoded, mitochondrial-active RidA homolog, Mmf1p, lose their mtDNA and capacity to respire. We demonstrate that the loss of mtDNA in an *mmf1*Δ strain is caused by 2AA stress generated by PLP-dependent serine/threonine dehydratases.

In Chapter 6 I describe our current model of cystathionine β-lyase (MetC)-mediated suppression of 2AA sensitivity in *S. enterica* lacking RidA. The current data indicate MetC overproduction in a *ridA* background indirectly reduces 2AA levels, and is consistent with a model where MetC generates a reactive metabolite that sequesters 2AA.

Chapter 7 summarizes the main conclusions from the work herein and offers suggestions for future research.

Appendix A describes preliminary data from our efforts to identify the mechanism of mtDNA loss in *mmf1*Δ mutants of *S. cerevisiae* exposed to 2AA stress.

Appendix B represents a divergence from the RidA storyline; it reflects work done to explore metabolic robustness surrounding the coenzyme A metabolic node. These published findings highlight a previously unknown transporter (PanS) of pantoate, ketopantoate and other unknown coenzyme A precursors.

Appendix C presents unpublished data indicating that cross-talk between thiamine and coenzyme A biosynthesis is influenced by mutations in the LysR-type transcriptional regulator gene, *ilvY*.

1.6 References

1. Ralser M. 2014. The RNA world and the origin of metabolic enzymes. *Biochem Soc Trans* 42:985–988.
2. Krishnamurthy R. 2017. Giving rise to life: transition from prebiotic chemistry to protobiology. *Acc Chem Res* 50:455–459.
3. Braakman R, Smith E. 2012. The emergence and early evolution of biological carbon-fixation. *PLoS Comput Biol* 8:e1002455.
4. Keller MA, Piedrafita G, Ralser M. 2015. The widespread role of non-enzymatic reactions in cellular metabolism. *Curr Opin Biotechnol* 34:153–161.
5. Fondi M, Emiliani G, Fani R. 2009. Origin and evolution of operons and metabolic pathways. *Res Microbiol* 160:502–512.
6. Woese CR. 1987. Bacterial evolution. *Microbiol Rev* 51:221–271.
7. Jensen RA. 1976. Enzyme recruitment in evolution of new function. *Annu Rev Microbiol* 30:409–425.
8. Lazcano A, Diaz-Villagomez E, Mills T, Oro J. 1995. On the levels of enzymatic substrate specificity: implications for the early evolution of metabolic pathways. *Adv Space Res Off J Comm Space Res COSPAR* 15:345–356.
9. de Lorenzo V, Sekowska A, Danchin A. 2015. Chemical reactivity drives spatiotemporal organisation of bacterial metabolism. *FEMS Microbiol Rev* 39:96–119.
10. Linster CL, Van Schaftingen E, Hanson AD. 2013. Metabolite damage and its repair or pre-emption. *Nat Chem Biol* 9:72–80.
11. Thieffry D, Huerta AM, Perez-Rueda E, Collado-Vides J. 1998. From specific gene regulation to genomic networks: a global analysis of transcriptional regulation in *Escherichia coli*. *BioEssays News Rev Mol Cell Dev Biol* 20:433–440.
12. Goodey NM, Benkovic SJ. 2008. Allosteric regulation and catalysis emerge via a common route. *Nat Chem Biol* 4:474–482.
13. Tu BP, Kudlicki A, Rowicka M, McKnight SL. 2005. Logic of the yeast metabolic cycle: temporal compartmentalization of cellular processes. *Science* 310:1152–1158.

14. Attia SM. 2010. Deleterious effects of reactive metabolites. *Oxid Med Cell Longev* 3:238–253.
15. Metallo CM, Vander Heiden MG. 2013. Understanding metabolic regulation and its influence on cell physiology. *Mol Cell* 49:388–398.
16. Arentson BW, Sanyal N, Becker DF. 2012. Substrate channeling in proline metabolism. *Front Biosci J Virtual Libr* 17:375.
17. Hardwick SW, Gubbey T, Hug I, Jenal U, Luisi BF. 2012. Crystal structure of *Caulobacter crescentus* polynucleotide phosphorylase reveals a mechanism of RNA substrate channelling and RNA degradosome assembly. *Open Biol* 2:120028–120028.
18. Dairi T, Kuzuyama T, Nishiyama M, Fujii I. 2011. Convergent strategies in biosynthesis. *Nat Prod Rep* 28:1054.
19. Snell K. 1986. The duality of pathways for serine biosynthesis is a fallacy. *Trends Biochem Sci* 11:241–243.
20. Bobik TA, Lehman BP, Yeates TO. 2015. Bacterial microcompartments: widespread prokaryotic organelles for isolation and optimization of metabolic pathways. *Mol Microbiol* 98:193–207.
21. Mühlenhoff U, Hoffmann B, Richter N, Rietzschel N, Spantgar F, Stehling O, Uzarska MA, Lill R. 2015. Compartmentalization of iron between mitochondria and the cytosol and its regulation. *Eur J Cell Biol* 94:292–308.
22. Lloyd-Price J, Hakkinen A, Kandhavelu M, Marques IJ, Chowdhury S, Lihavainen E, Yli-Harja O, Ribeiro AS. 2012. Asymmetric disposal of individual protein aggregates in *Escherichia coli*, one aggregate at a time. *J Bacteriol* 194:1747–1752.
23. Danchin A. 2017. Coping with inevitable accidents in metabolism. *Microb Biotechnol* 10:57–72.
24. Imlay JA. 2013. The molecular mechanisms and physiological consequences of oxidative stress: lessons from a model bacterium. *Nat Rev Microbiol* 11:443–454.
25. Imlay JA. 2008. Cellular defenses against superoxide and hydrogen peroxide. *Annu Rev Biochem* 77:755–776.
26. Kuo CF, Mashino T, Fridovich I. 1987. alpha,beta-Dihydroxyisovalerate dehydratase. A superoxide-sensitive enzyme. *J Biol Chem* 262:4724–4727.

27. Flint DH, Tuminello JF, Emptage MH. 1993. The inactivation of Fe-S cluster containing hydro-lyases by superoxide. *J Biol Chem* 268:22369–22376.
28. Keyer K, Gort AS, Imlay JA. 1995. Superoxide and the production of oxidative DNA damage. *J Bacteriol* 177:6782–6790.
29. Messner KR, Imlay JA. 1999. The identification of primary sites of superoxide and hydrogen peroxide formation in the aerobic respiratory chain and sulfite reductase complex of *Escherichia coli*. *J Biol Chem* 274:10119–10128.
30. Semchyshyn HM. 2014. Reactive carbonyl species *in vivo*: generation and dual biological effects. *Sci World J* 2014:1–10.
31. Töttemeyer S, Booth NA, Nichols WW, Dunbar B, Booth IR. 1998. From famine to feast: the role of methylglyoxal production in *Escherichia coli*. *Mol Microbiol* 27:553–562.
32. Lee C, Park C. 2017. Bacterial responses to glyoxal and methylglyoxal: reactive electrophilic species. *Int J Mol Sci* 18:169.
33. Booth IR, Ferguson GP, Miller S, Li C, Gunasekera B, Kinghorn S. 2003. Bacterial production of methylglyoxal: a survival strategy or death by misadventure? *Biochem Soc Trans* 31:1406–1408.
34. Ferguson GP. 1999. Protective mechanisms against toxic electrophiles in *Escherichia coli*. *Trends Microbiol* 7:242–247.
35. D'Autréaux B, Toledano MB. 2007. ROS as signalling molecules: mechanisms that generate specificity in ROS homeostasis. *Nat Rev Mol Cell Biol* 8:813–824.
36. Mittler R, Vanderauwera S, Suzuki N, Miller G, Tognetti VB, Vandepoele K, Gollery M, Shulaev V, Van Breusegem F. 2011. ROS signaling: the new wave? *Trends Plant Sci* 16:300–309.
37. Mittler R. 2017. ROS Are Good. *Trends Plant Sci* 22:11–19.
38. Aguilera J, Rodríguez-Vargas S, Prieto JA. 2005. The HOG MAP kinase pathway is required for the induction of methylglyoxal-responsive genes and determines methylglyoxal resistance in *Saccharomyces cerevisiae*: Role of the HOG MAP kinase pathway in the response to methylglyoxal. *Mol Microbiol* 56:228–239.
39. Kim J, Copley SD. 2012. Inhibitory cross-talk upon introduction of a new metabolic pathway into an existing metabolic network. *Proc Natl Acad Sci* 109:E2856–E2864.

40. West JA. 1963. The chemistry of enamines. *J Chem Educ* 40:194.
41. Eliot AC, Kirsch JF. 2004. Pyridoxal phosphate enzymes: mechanistic, structural, and evolutionary considerations. *Annu Rev Biochem* 73:383–415.
42. Hillebrand GG, Dye JL, Suelter CH. 1979. Formation of an intermediate and its rate of conversion to pyruvate during the tryptophanase-catalyzed degradation of S-o-nitrophenyl-L-cysteine. *Biochemistry (Mosc)* 18:1751–1755.
43. Vederas JC, Schleicher E, Tsai M-D, Floss HG. 1978. Stereochemistry and mechanism of reactions catalyzed by tryptophanase *Escherichia coli*. *J Biol Chem* 253:5350–5354.
44. Flavin M, Slaughter C. 1969. Enzymic reactions of enamines with N-ethylmaleimide. *J Biol Chem* 244:1434–1444.
45. Datta P, Bhadra R. 1978. Biodegradative threonine dehydratase. Reduction of ferricyanide by an intermediate of the enzyme-catalyzed reaction. *Eur J Biochem* 91:527–532.
46. Schneider G, Käck H, Lindqvist Y. 2000. The manifold of vitamin B6 dependent enzymes. *Structure* 8:R1–R6.
47. John RA. 1995. Pyridoxal phosphate-dependent enzymes. *Biochim Biophys Acta BBA-Protein Struct Mol Enzymol* 1248:81–96.
48. Newton WA, Snell EE. 1964. Catalytic properties of tryptophanase, a multifunctional pyridoxal phosphate enzyme. *Proc Natl Acad Sci U S A* 51:382.
49. Watanabe T, Snell EE. 1972. Reversibility of the tryptophanase reaction: synthesis of tryptophan from indole, pyruvate, and ammonia. *Proc Natl Acad Sci* 69:1086–1090.
50. Awano N, Wada M, Mori H, Nakamori S, Takagi H. 2005. Identification and functional analysis of *Escherichia coli* cysteine desulfhydrases. *Appl Environ Microbiol* 71:4149–4152.
51. LaRossa RA, Van Dyk TK, Smulski DR. 1987. Toxic accumulation of alpha-ketobutyrate caused by inhibition of the branched-chain amino acid biosynthetic enzyme acetolactate synthase in *Salmonella typhimurium*. *J Bacteriol* 169:1372–1378.
52. Zhang C, Qi J, Li Y, Fan X, Xu Q, Chen N, Xie X. 2016. Production of α -ketobutyrate using engineered *Escherichia coli* via temperature shift. *Biotechnol Bioeng* 113:2054–2059.

53. Burns RO, Hofler JG, Luginbuhl GH. 1979. Threonine deaminase from *Salmonella typhimurium*. Substrate-specific patterns of inhibition in an activator site-deficient form of the enzyme. *J Biol Chem* 254:1074–1079.
54. Flavin M, Slaughter C. 1964. An intermediate trapped by maleimides in a pyridoxal-phosphate potentiated enzymatic elimination reaction. *Biochemistry (Mosc)* 3:885–893.
55. Likos JJ, Ueno H, Feldhaus RW, Metzler DE. 1982. A novel reaction of the coenzyme of glutamate decarboxylase with L-serine O-sulfate. *Biochemistry (Mosc)* 21:4377–4386.
56. Ueno H, Likos JJ, Metzler DE. 1982. Chemistry of the inactivation of cytosolic aspartate aminotransferase by serine O-sulfate. *Biochemistry (Mosc)* 21:4387–4393.
57. Wang EA, Kallen R, Walsh C. 1981. Mechanism-based inactivation of serine transhydroxymethylases by D-fluoroalanine and related amino acids. *J Biol Chem* 256:6917–6926.
58. Esaki N, Walsh CT. 1986. Biosynthetic alanine racemase of *Salmonella typhimurium*: purification and characterization of the enzyme encoded by the *alr* gene. *Biochemistry (Mosc)* 25:3261–3267.
59. Walsh C. 1982. Suicide substrates: mechanism-based enzyme inactivators. *Tetrahedron* 38:871–909.
60. Whalen WA, Wang MD, Berg CM. 1985. beta-Chloro-L-alanine inhibition of the *Escherichia coli* alanine-valine transaminase. *J Bacteriol* 164:1350–1352.
61. Ahmed SA, Ruvinov SB, Kayastha AM, Miles EW. 1991. Mechanism of mutual activation of the tryptophan synthase alpha and beta subunits. Analysis of the reaction specificity and substrate-induced inactivation of active site and tunnel mutants of the beta subunit. *J Biol Chem* 266:21548–21557.
62. Schleicher E, Mascaro K, Potts R, Mann DR, Floss HG. 1976. Stereochemistry and mechanism of reactions catalyzed by tryptophanase and tryptophan synthetase. *J Am Chem Soc* 98:1043–1044.
63. Rhee S, Parris KD, Hyde CC, Ahmed SA, Miles EW, Davies DR. 1997. Crystal structures of a mutant (betaK87T) tryptophan synthase alpha2beta2 complex with ligands bound to the active sites of the alpha- and beta-subunits reveal ligand-induced conformational changes. *Biochemistry (Mosc)* 36:7664–7680.
64. Phillips AT, Wood WA. 1965. The mechanism of action of 5'-adenylic acid-activated threonine dehydrase. *J Biol Chem* 240:4703–4709.

65. Enos-Berlage JL, Langendorf MJ, Downs DM. 1998. Complex metabolic phenotypes caused by a mutation in *yjgF*, encoding a member of the highly conserved YER057c/YjgF family of proteins. *J Bacteriol* 180:6519–6528.
66. Schmitz G, Downs DM. 2004. Reduced transaminase B (IlvE) activity caused by the lack of *yjgF* is dependent on the status of threonine deaminase (IlvA) in *Salmonella enterica* serovar Typhimurium. *J Bacteriol* 186:803–810.
67. Christopherson MR, Schmit GE, Downs DM. 2008. YjgF is required for isoleucine biosynthesis when *Salmonella enterica* is grown on pyruvate medium. *J Bacteriol* 190:3057–3062.
68. Lambrecht JA, Flynn JM, Downs DM. 2012. Conserved YjgF protein family deaminates reactive enamine/imine intermediates of pyridoxal 5'-phosphate (PLP)-dependent enzyme reactions. *J Biol Chem* 287:3454–3461.
69. Niehaus TD, Gerdes S, Hodge-Hanson K, Zhukov A, Cooper AJ, ElBadawi-Sidhu M, Fiehn O, Downs DM, Hanson AD. 2015. Genomic and experimental evidence for multiple metabolic functions in the RidA/YjgF/YER057c/UK114 (Rid) protein family. *BMC Genomics* 16:382.
70. Flynn JM, Downs DM. 2013. In the absence of RidA, endogenous 2-aminoacrylate inactivates alanine racemases by modifying the pyridoxal 5'-phosphate cofactor. *J Bacteriol* 195:3603–3609.
71. Flynn JM, Christopherson MR, Downs DM. 2013. Decreased coenzyme A levels in *ridA* mutant strains of *Salmonella enterica* result from inactivated serine hydroxymethyltransferase: *ridA* mutants are deficient in one carbon metabolism. *Mol Microbiol* 89:751–759.
72. Lambrecht JA, Schmitz GE, Downs DM. 2013. RidA proteins prevent metabolic damage inflicted by PLP-dependent dehydratases in all domains of life. *MBio* 4:e00033-13.
73. Browne BA, Ramos AI, Downs DM. 2006. PurF-independent phosphoribosyl amine formation in *yjgF* mutants of *Salmonella enterica* utilizes the tryptophan biosynthetic enzyme complex anthranilate synthase-phosphoribosyltransferase. *J Bacteriol* 188:6786–6792.
74. Lambrecht JA, Downs DM. 2012. Anthranilate phosphoribosyl transferase (TrpD) generates phosphoribosylamine for thiamine synthesis from enamines and phosphoribosyl pyrophosphate. *ACS Chem Biol* 8:242–248.

75. Lambrecht JA, Browne BA, Downs DM. 2010. Members of the YjgF/YER057c/UK114 family of proteins inhibit phosphoribosylamine synthesis *in vitro*. *J Biol Chem* 285:34401–34407.
76. Bazurto JV, Farley KR, Downs DM. 2016. An unexpected route to an essential cofactor: *Escherichia coli* relies on threonine for thiamine biosynthesis. *mBio* 7:e01840–15.
77. Hodge-Hanson KM, Downs DM. 2017. Members of the Rid protein family have broad imine deaminase activity and can accelerate the *Pseudomonas aeruginosa* D-arginine dehydrogenase (DauA) reaction *in vitro*. *PloS One* 12:e0185544.
78. Flynn JM. 2013. Toward a metabolic understanding of 2-aminoacrylate stress in *ridA* mutants of *Salmonella enterica*. Ph.D., University of Wisconsin.
79. Liu X, Zeng J, Chen X, Xie W. 2016. Crystal structures of RidA, an important enzyme for the prevention of toxic side products. *Sci Rep* 6.
80. Müller A, Langklotz S, Lupilova N, Kuhlmann K, Bandow JE, Leichert LIO. 2014. Activation of RidA chaperone function by N-chlorination. *Nat Commun* 5:5804.
81. Lindemann C, Lupilova N, Muller A, Warscheid B, Meyer HE, Kuhlmann K, Eisenacher M, Leichert LI. 2013. Redox proteomics uncovers peroxynitrite-sensitive proteins that help *Escherichia coli* to overcome nitrosative stress. *J Biol Chem* 288:19698–19714.
82. Farkas A, Nardai G, Csermely P, Tompa P, Friedrich P. 2004. DUK114, the *Drosophila* orthologue of bovine brain calpain activator protein, is a molecular chaperone. *Biochem J* 383:165–170.
83. Schmiedeknecht G, Kerkhoff C, Orsó E, Stöhr J, Aslanidis C, Nagy GM, Knuechel R, Schmitz G. 1996. Isolation and characterization of a 14.5-kDa trichloroacetic-acid-soluble translational inhibitor protein from human monocytes that is upregulated upon cellular differentiation. *Eur J Biochem* 242:339–351.
84. Oka T, Tsuji H, Noda C, Sakai K, Hong Y, Suzuki I, Muñoz S, Natori Y. 1995. Isolation and characterization of a novel perchloric acid-soluble protein inhibiting cell-free protein synthesis. *J Biol Chem* 270:30060–30067.
85. Chong CL, Huang SF, Hu C p., Chen YL, Chou HY, Chau GY, Shew JY, Tsai YL, Chen CT, Chang C, Chen ML. 2008. Decreased expression of UK114 is related to the differentiation status of human hepatocellular carcinoma. *Cancer Epidemiol Biomarkers Prev* 17:535–542.

86. Kanouchi H, Matsuo A, Oka T, Tachibana H, Yamada K. 2003. Recombinant perchloric acid-soluble protein suppresses the immunoglobulin production of human-human hybridoma HB4C5 cells. *Vitro Cell Dev Biol-Anim* 39:263–265.
87. Kanouchi H, Tachibana H, Oka T, Yamada K. 2001. Recombinant expression of perchloric acid-soluble protein reduces cell proliferation. *Cell Mol Life Sci CMLS* 58:1340–1343.
88. Bartorelli A, Bussolati B, Millesimo M, Gugliotta P, Bussolati G. 1996. Antibody-dependent cytotoxic activity of human cancer cells expressing UK114 membrane antigen. *Int J Oncol* 8:543–548.
89. Bussolati G, Geuna M, Bussolati B, Millesimo M, Botta M, Bartorelli A. 1997. Cytolytic and tumor inhibitory antibodies against UK114 protein in the sera of cancer patients. *Int J Oncol* 10:779–785.
90. Funaro A, Horenstein AL, Ghisolfi G, Bussolati B, Bartorelli A, Bussolati G. 1999. Identification of a 220-kDa membrane tumor-associated antigen by human anti-UK114 monoclonal antibodies selected from the immunoglobulin repertoire of a cancer patient. *Exp Cell Res* 247:441–450.
91. Racca S, Di Carlo F, Bartorelli A, Bussolati B, Bussolati G. 1997. Growth inhibition of DMBA-induced rat mammary carcinomas by UK114. *Virchows Arch* 431:323–328.
92. Oxelmark E, Marchini A, Malanchi I, Magherini F, Jaquet L, Hajibagheri MAN, Blight KJ, Jauniaux J-C, Tommasino M. 2000. Mmf1p, a novel yeast mitochondrial protein conserved throughout evolution and involved in maintenance of the mitochondrial genome. *Mol Cell Biol* 20:7784–7797.
93. Kim J-M, Yoshikawa H, Shirahige K. 2001. A member of the YER057c/yjgf/Uk114 family links isoleucine biosynthesis and intact mitochondria maintenance in *Saccharomyces cerevisiae*. *Genes Cells* 6:507–517.
94. Hanson AD, Pribat A, Waller JC, Crécy-Lagard V de. 2010. “Unknown” proteins and “orphan” enzymes: the missing half of the engineering parts list – and how to find it. *Biochem J* 425:1–11.

TABLE 1.1 *RidA* paradigm in *S. enterica*: generators and targets of 2AA stress

PLP enzymes	Protein	Activity in <i>ridA</i> bkg. (% of Wt)	Phenotype	Ref.
Endogenous 2AA generators				
Ser/Thr dehydratase (anabolic)	IlvA			
Ser/Thr dehydratase (catabolic)	TdcB*			
Endogenous 2AA targets				
Ser hydroxymethyltransferase	GlyA	20	Keto acid excretion	(71)
Transaminase B	IlvE	30	Ile limitation on Pyr	(66, 67)
Alanine racemase	Alr	60	Ala poor N source	(70)
Alanine racemase	DadX	70	Ala poor N source	(70)

* TdcB is only produced anaerobically in response to threonine and does not contribute to 2AA stress under standard aerobic growth conditions.

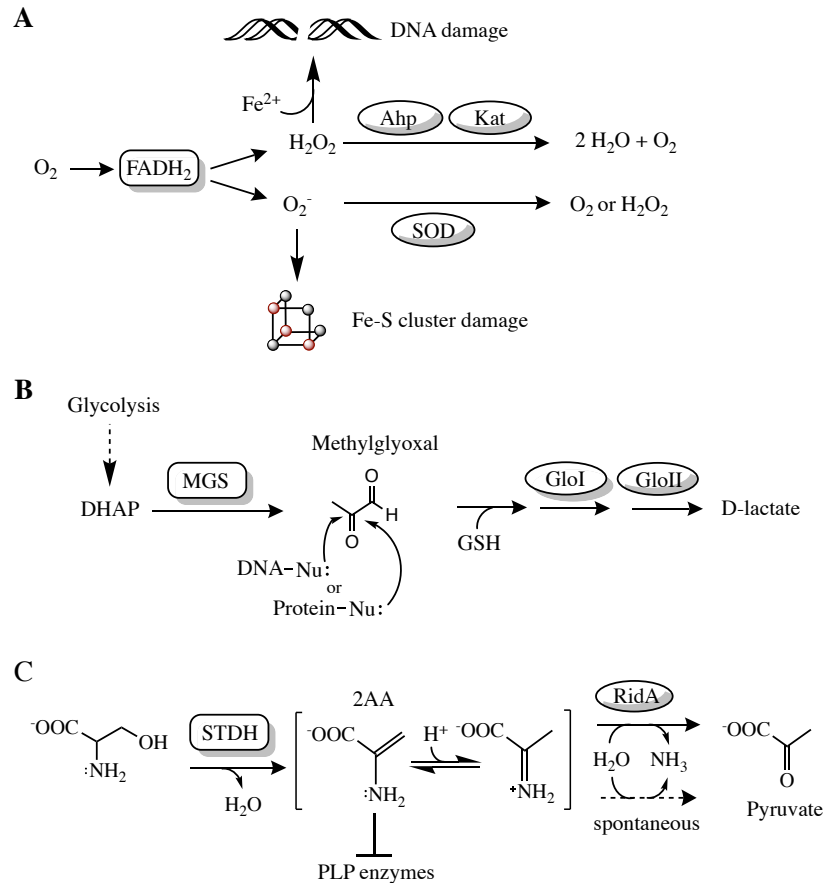


FIGURE 1.1. Reactive metabolite production and mechanisms of control. A) Molecular oxygen gives rise to reactive oxygen species, O_2^- and H_2O_2 , through promiscuous interaction with electron-donating flavoenzymes ($FADH_2$). H_2O_2 levels are reduced by enzymes alkyl hydroperoxide reductase (Ahp) and catalase (Kat); O_2^- is degraded by superoxide dismutase (SOD). B) Methylglyoxal synthase (MGS) generates methylglyoxal, which behaves as a potent electrophile capable of modifying macromolecules in the cell. A dedicated glyoxylase system degrades methylglyoxal to lactate. C) The RidA enamine defense system degrades reactive enamines, including 2-aminoacrylate (2AA). In the absence of RidA, 2AA can accumulate and damage a variety of PLP-dependent enzymes.

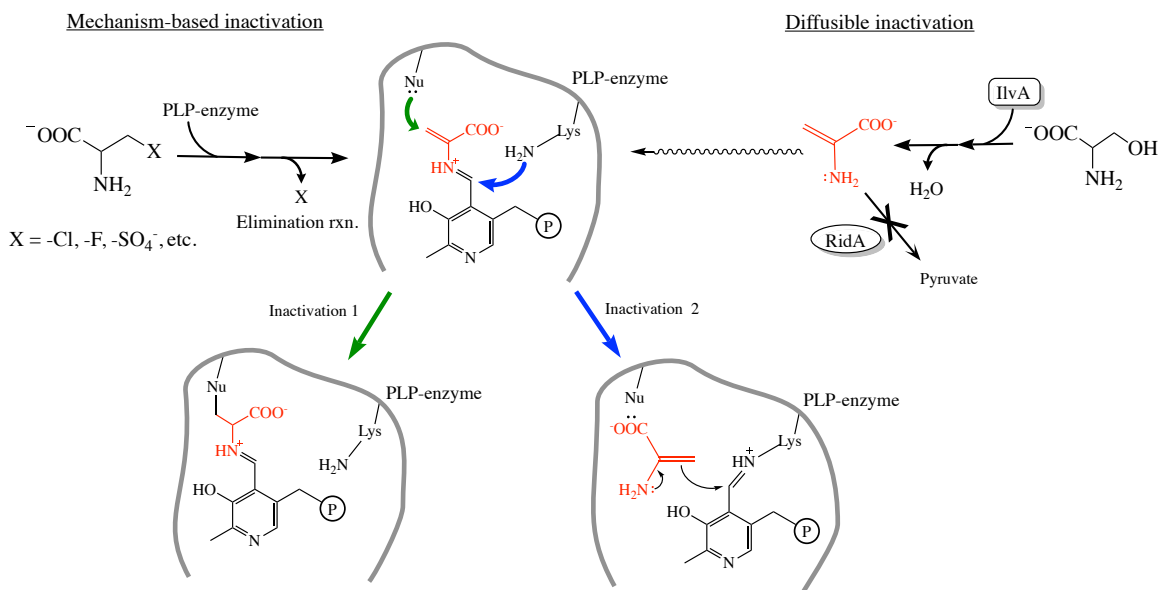


FIGURE 1.2. 2-aminoacrylate as a mechanism-based inhibitor and diffusible stressor. (Left)

A variety of PLP-dependent enzymes, even those possessing poor β -eliminase activity, can catalyze elimination reactions when acting on substrates with strong leaving groups. In some cases, production of 2AA in the active site leads to mechanism-based inactivation of the enzyme. Inactivation mechanisms differ between enzymes, with two representative mechanisms displayed. (Right) Investigation of the RidA paradigm revealed that 2AA produced by PLP-dependent serine/threonine dehydratases can diffuse through the cell and inactivate a variety of distinct PLP-dependent enzyme targets. Undulating line represents diffusion.

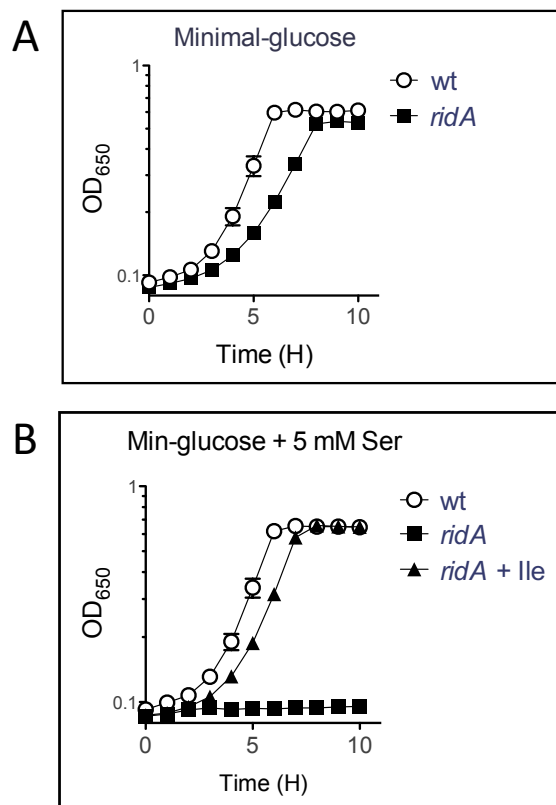


FIGURE 1.3. *S. enterica* *ridA* mutant strains are sensitive to serine. A) A lesion in *S. enterica* *ridA* creates a small growth defect when strains are grown in minimal glucose medium. Importantly, this minor growth defect correlates with inactivation of several PLP-dependent enzymes detailed in Table 1.1. Isoleucine abolishes the minor growth defect and preserves 2AA target-enzyme activity (not shown). B) Feeding exogenous serine to a *ridA* strain leads to complete growth inhibition. However, isoleucine supplementation inhibits IlvA activity, thus alleviating serine sensitivity in a *ridA* strain.

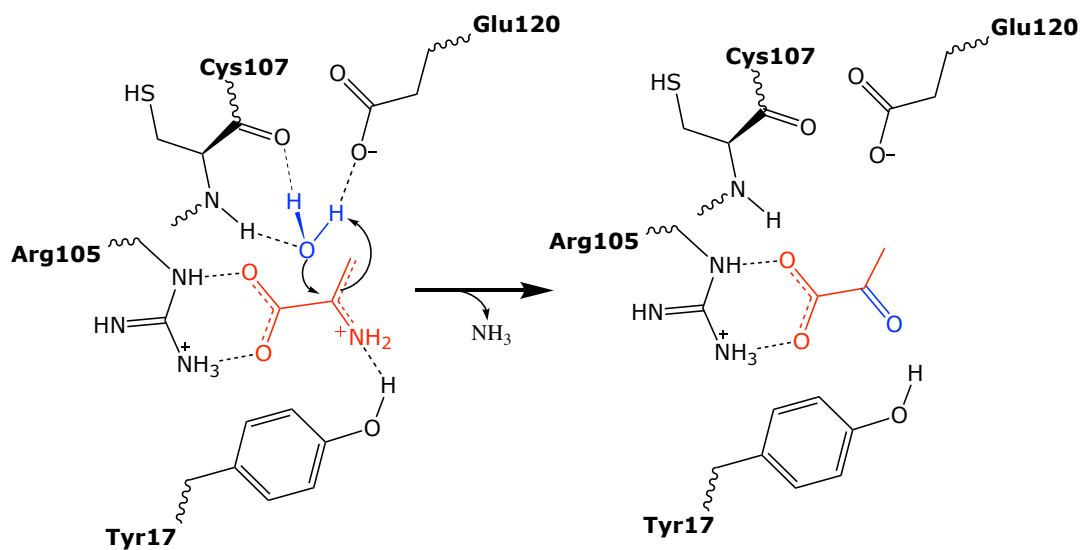


FIGURE 1.4. Proposed mechanism of RidA 2-aminoacrylate deaminase activity. Arginine-105 is universally conserved in Rid enzymes possessing enamine/imine hydrolase activity. The proposed model is speculative and demonstrates a near-simultaneous tautomerization/protonation event coupled to imine hydrolysis. The resulting product is pyruvate.

CHAPTER 2

ENDOGENOUS SYNTHESIS OF 2-AMINOACRYLATE CONTRIBUTES TO CYSTEINE SENSITIVITY IN *SALMONELLA ENTERICA*¹

¹Ernst DC, Lambrecht JA, Schomer RA, Downs DM. 2014. *Journal of Bacteriology* 196:3335–3342.
Reprinted here with permission of the publisher.

2.1 ABSTRACT

RidA, the archetype member of the widely-conserved RidA/YER057c/UK114 family of proteins, prevents reactive enamine/imine intermediates from accumulating in *Salmonella enterica* by catalyzing their hydrolysis to stable keto acid products. In the absence of RidA, endogenous 2-aminoacrylate persists in the cellular environment long enough to damage a growing list of essential metabolic enzymes. Prior studies have focused on the dehydration of serine by the PLP-dependent serine/threonine dehydratases, IlvA and TdcB, as sources of endogenous 2-aminoacrylate. The current study describes an additional source of endogenous 2-aminoacrylate derived from cysteine. The results of *in vivo* analysis show that the cysteine sensitivity of a *ridA* strain is contingent upon CdsH, the predominant cysteine desulfhydrase in *S. enterica*. The impact of cysteine on 2-aminoacrylate accumulation is shown to be unaffected by the presence of serine/threonine dehydratases, revealing another mechanism of endogenous 2-aminoacrylate production. Experiments *in vitro* suggest that 2-aminoacrylate is released from CdsH following cysteine desulfhydration, resulting in an unbound aminoacrylate substrate for RidA. This work expands our understanding of the role served by RidA in preventing enamine stress resulting from multiple normal metabolic processes.

2.2 BACKGROUND

The RidA/YER057c/UK114 family of proteins is highly conserved across all domains of life. In *Salmonella enterica*, RidA catalyzes the hydrolysis of reactive enamine/imine intermediates produced as a consequence of serine/threonine dehydratase activity (1). The pyridoxal 5'-phosphate (PLP)-dependent serine/threonine dehydratases (EC 4.3.1.19), IlvA and TdcB, dehydrate serine and threonine to generate enamine intermediates, 2-aminoacrylate (2AA)

and 2-aminocrotonate, respectively (2, 3). The unstable enamine intermediates tautomerize to their respective imine forms prior to a hydration event that releases ammonia and generates a stable keto acid product (Figure 2.1) (2, 4). Despite the relatively short half-life of 2AA in aqueous solution, RidA increased the rate of IlvA-dependent pyruvate formation from serine *in vitro* (1). This result suggested that RidA had an affinity for 2AA and may impact accumulation of this toxic metabolite *in vivo*, where molecular crowding and the lack of abundant free-water could increase the half-life of 2AA (5). In fact, removal of RidA from the metabolic network in *S. enterica* led to pleiotropic phenotypes that were attributed to 2AA accumulation (6–10)

A number of PLP-enzymes can be inactivated by 2AA *in vitro* by a mechanism that modifies the PLP cofactor in the active site (11–15). Previous studies suggested that inactivation by 2AA and related species was restricted to the active site of origin (5, 16). *In vivo* analysis showed that in the absence of RidA, endogenously generated free 2AA persists in the cell long enough to damage distinct PLP-enzymes in *S. enterica*, including those that are involved in isoleucine biosynthesis, one-carbon metabolism and cell-wall synthesis (9, 10, 17). Prior to this study, the characterized sources of endogenous 2AA were the PLP-dependent serine/threonine dehydratases (17). It remains to be determined if the enamine stress caused by serine/threonine dehydratases is unique, or if this stress is a general feature of metabolic enzymes with similar PLP-dependent catalytic mechanisms.

Many prokaryotic and eukaryotic organisms are sensitive to high concentrations of cysteine (18–24). Various mechanisms have been proposed to explain cysteine toxicity, including inhibition of electron transport, inactivation of anabolic enzymes and stimulation of Fenton chemistry resulting in hydroxyl radical production (18, 19, 23, 25). In *E. coli*, cysteine has been shown to cause transient amino acid starvation as a result of threonine deaminase (IlvA) inhibition,

which can be overcome by the addition of branched-chain amino acids (BCAAs) (19). The specific mechanism of cysteine toxicity in *S. enterica* is less clear, but seems to be due in part to the generation of reactive oxygen species leading to DNA damage (18, 23). The enzymatic desulfhydration of cysteine has been described previously as a method of cysteine detoxification in many bacterial species and higher organisms, including mammals (26). *S. enterica* and *E. coli* have several metabolic enzymes with cysteine desulfhydrase activity, including cystathionine β -lyase (MetC), cysteine synthase A (CysK), cysteine synthase B (CysM), β -cystathionase (MalY) and tryptophanase (TnaA; *E. coli* only) (25, 27). In contrast to *E. coli*, *S. enterica* encodes a dedicated cysteine desulfhydrase activity that is strongly induced in response to cysteine (26, 28, 29). It was recently demonstrated that this dedicated cysteine desulfhydrase (CDS; EC 2.5.1.47) is encoded by *stm0458*, which was renamed *cdsH* (25). CDS is thought to participate in the detoxification of excess cysteine (26), and recent reports suggest an additional role for this enzyme in maintaining sulfide concentrations at a high enough level to support antibiotic resistance and pathogenesis (25, 30, 31). In general, a PLP-dependent CDS performs chemistry similar to that of IlvA, catalyzing β -elimination of the sulfhydryl group from cysteine yielding sulfide, ammonia and pyruvate (26, 29). 2-aminoacrylate has been implicated as an intermediate in CDS-mediated cysteine degradation *in vitro* (29), making the enzyme mechanism reminiscent of the dehydratase enzymes that contribute to metabolic phenotypes observed for *ridA* mutants of *S. enterica* (1, 3, 32). This study was initiated to address the impact of cysteine on strains that lack RidA and are unable to respond to 2AA stress.

2.3 MATERIALS AND METHODS

Bacterial strains, media and chemicals. Bacterial strains used in this study were derived from *Salmonella enterica* serovar Typhimurim LT2 and are listed with their genotype in Table 1. *Tn10(d)* refers to the transposition defective mini-*Tn10* (*Tn10*Δ16 Δ17) described by Way et al. (33). *MudJ* refers to the *Mud1734* transposon described previously (34).

Minimal medium was no-carbon E medium (NCE) supplemented with 1 mM MgSO₄ (35), trace minerals (36) and 11 mM D-glucose as the sole carbon source. Bacto vitamin-free casamino acids (CAAs) were added at 0.1% w/v when necessary. Difco nutrient broth (NB) (8 g/liter) with NaCl (5 g/liter) was used as rich media. Superbroth consisting of tryptone (32 g/liter), yeast extract (20 g/liter), sodium chloride (5 g/liter) and sodium hydroxide (0.2 g/liter) was used when high cell densities were required. Difco BiTek agar (15 g/liter) was added for solid medium. Antibiotics were added as necessary to reach the following concentrations in rich and minimal medium, respectively: tetracycline 20 and 10 μg/ml; ampicillin 150 and 30 μg/ml; and chloramphenicol 20 and 5 μg/ml. L-cysteine was prepared fresh for each experiment and added at the indicated concentrations. L-isoleucine was added to a final concentration of 1 mM when needed. Unless otherwise stated, all chemicals were purchased from Sigma-Aldrich Chemical Company, St. Louis, MO.

Genetic techniques and growth analysis. Transductional crosses were carried out using the high-frequency general transducing mutant of bacteriophage P22 (HT105/1, *int-201*) (37). Methods for performing transductional crosses, purifying transductants from phage and identifying phage-free recombinants were described previously (38, 39). All mutant strains listed in Table 1 were constructed using standard genetic techniques. Gene replacements were made using the λ-Red recombinase system described by Datsenko and Wanner (40).

Growth phenotypes were determined in solid medium by using agar overlays and in liquid medium using growth curves as described previously (6). Briefly, strains to be analyzed in liquid culture were grown to full density in NB at 37°C. Cells were pelleted and resuspended in an equal volume of saline solution (85 mM), and 5 µl of the resuspension were used to inoculate 195 µl of the relevant defined growth medium contained in 96-well microtitre plates. Microtitre plates were incubated at 37°C while shaking using the Biotek EL808 ultra microplate reader. Growth was monitored as the change in absorbance at 650 nm over time. Data were plotted using GraphPad Prism 5.0f.

Mutant isolation. A culture of DM3480 (*ridA3::MudJ*) was grown overnight in NB medium. Cells were pelleted and suspended in an equal volume of saline solution (85 mM). Approximately 10⁸ cells were spread onto solid glucose medium containing 5 mM L-cysteine. Diethyl sulfate (DES) was spotted in the center of each plate (5 µl), which was incubated at 37°C for 24-48 hrs. Colonies that arose were streaked out on non-selective medium prior to confirming their cysteine-resistant phenotype in liquid minimal medium.

Genome sequencing. Whole-genome sequencing was used to identify the causative suppressor mutation in DM13827 (*ridA3::MudJ cdsH3*). High molecular-weight genomic DNA was isolated using a phenol-chloroform extraction method. A 1 ml culture was grown to full density in superbrot, pelleted in a microcentrifuge tube, and resuspended in buffer (0.1 M Tris pH 8, 0.15 M NaCl and 0.1 M EDTA). Lysozyme (0.5 mg) was added, followed by incubation at 37°C for 10 minutes. Proteinase K (1 mg) and SDS (1%) were added and incubation was allowed to continue at 37°C for 30 minutes. 1 ml of Tris saturated phenol-chloroform was added and mixed gently, followed by centrifugation at 17,000 x g for 1 minute. The aqueous layer was removed, washed twice with 1 ml of chloroform, and transferred to a clean microcentrifuge tube. The sample

was overlaid with 1 ml of ice-cold 100% ethanol and the DNA was spooled out using a hooked Pasteur pipet. The spooled DNA was washed by submerging in ethanol, air dried for 5 minutes, and suspended overnight in 1 ml of Tris-EDTA buffer (10 mM Tris pH 8.0 and 1mM EDTA). The concentration of recovered DNA was determined using a NanoDrop 2000 (Thermo Scientific). DNA gel electrophoresis was performed to ensure high-molecular weight DNA (>10,000 kbp) was abundant prior to sequencing.

Genomic DNA was submitted to the Georgia Genomics Facility (GGF) at the University of Georgia for paired-end (2 x 250 bp) sequencing using the Illumina MiSeq platform. DNA samples were fragmented and tagged with sequencing adapters using the Nextera XT DNA sample preparation kit (Illumina). Processing and assembly of the sequencing data was done by the Georgia Advanced Computing Resource Center (GACRC) at the University of Georgia. Briefly, the raw sequencing data was cleaned up using Trimmomatic (Usadel) with a read length cut-off of 100 bp, resulting in >300-fold coverage of the 4.95 Mb *S. enterica* LT2 genome (41). Trimmed reads were mapped to the published genome using Bowtie 2 (Source Forge). Variant calling was performed using the Genome Analysis Toolkit (Broad Institute), and single nucleotide polymorphisms (SNPs) were identified using the Integrative Genomics Viewer (Broad Institute).

Molecular methods. The *cdsH* gene was amplified by PCR with Herculase II Fusion DNA polymerase (Agilent) using primers STM0458_NdeI_F (5'-gagacatatgatgagtagcaattggggttaa -3') and STM0458_XhoI_R (5'- gagactcgagctagtcgccgtaagtaatt -3'). The resulting PCR product was either used for sequence analysis or for cloning. In the latter case, the PCR product was gel purified, digested with *NdeI* (New England Biolabs) and *XhoI* (New England Biolabs) and ligated into *NdeI/XhoI*-cut pET14b (Novagen), forming pDM1375. Constructs were transformed into

Escherichia coli strain DH5 α and screened for vectors containing inserts. Plasmid inserts were confirmed by sequence analysis, performed by Genewiz.

Isoleucine transaminase (IlvE) assays. Permeabilized cells were used to assay IlvE activity as previously described (42). Strains were grown to stationary phase in 5 mL minimal glucose medium containing 0.1% CAAs, 1 mM isoleucine and cysteine added as indicated. Cells were pelleted, washed once with NCE medium, and frozen at -20°C. Frozen cell pellets were thawed, resuspended in 50 mM potassium phosphate buffer pH 8.0 and permeabilized by PopCulture (Novagen). 50 μ M PLP and 10 mM 2-ketoglutarate were mixed with an aliquot (30 μ l) of the permeabilized cell suspension, and isoleucine was added (20 mM) to initiate reactions. Reaction mixes were incubated for 20 minutes at 37°C, and activity was determined based on the amount of 2-keto-3-methylvalerate (2KMV) formed. 2KMV was derivatized with 2,4-dinitrophenylhydrazine (DNPH) to enable hydrazone formation, followed by organic extraction. The organic layer was washed once with 0.5 N HCl, separated and then mixed with 1.5 N NaOH to allow chromophore formation. The absorbance of the aqueous layer (containing the chromophore) was measured at 540 nm using a Spectramax M2. The protein content of each cell extract was determined using the BCA assay (Pierce). Activity is reported as nmol 2KMV/min/mg protein in permeabilized cells. GraphPad Prism 5.0f was used to perform one-way ANOVA and Tukey's test was used to assess significant changes in IlvE activity ($p < 0.01$).

Purification of CdsH. Wild-type *cdsH* cloned into the pET14b vector (Novagen) was transformed into *E. coli* BL21AI (DM14430) for overexpression and His₆ tag purification. Cells were inoculated into 10 ml of superbroth containing ampicillin and grown overnight at 37°C. Overnight cultures were inoculated into 3 liters of superbroth containing ampicillin and grown at 37°C until an A₆₅₀ of 0.4-0.7 was reached. Arabinose (0.02%) was added to induce expression and

cultures were shifted to 22°C for 18 h. Cells were harvested at 4°C by centrifugation (15 minutes at 8,000 x g) and resuspended in 50 mM Tris-HCl pH 7.5 containing 200 mM sodium chloride, 5 mM imidazole, 10 µM PLP and 10% glycerol. Lysozyme (1 mg/ml), phenylmethylsulfonyl fluoride (100 µg/ml) and DNase (25 µg/ml) were added to the cell suspension, which then sat on ice for 1 h. Cells were mechanically lysed using a French pressure cell (5 passes at 10,342 kPa). The resulting lysate was clarified by centrifugation (45 minutes at 48,000 x g) and filtered through a 0.45-µm membrane. The filtered lysate was loaded onto a Ni-NTA superflow resin (5 ml) and CdsH was purified according to the manufacturer's protocol (Qiagen). Purified protein was concentrated by centrifugation with a 10,000 molecular weight cut-off filter unit (Millipore) and the buffer was replaced with 50 mM Tris-HCl pH 7.5 containing 10 M PLP and 10% Glycerol using a PD-10 desalting column (GE Healthcare). Protein recovery as determined by the BCA assay (Pierce) was approximately 5.5 mg/ml. Protein aliquots were frozen in liquid nitrogen and stored at -80°C.

Purification of RidA. RidA protein was purified from a BL21AI strain harboring the pET20b-*ridA* overexpression construct previously described (DM12740) (8). Briefly, an overnight culture of DM12740 grown in superbrotth containing ampicillin was inoculated into 3 L of superbrotth with ampicillin. Cultures were grown ~3 hours at 37°C with aeration until an A_{650} of 0.6 was reached. Fresh arabinose was added to a final concentration of 0.2% and cultures were allowed to incubate while shaking at 37°C for an additional 10 hours. Cells were harvested by centrifugation and resuspended in 50 mM Tris-HCl pH 8 containing 100 mM sodium chloride, 5 mM imidazole and 12.5% glycerol. Following lysis, the extract was clarified, filtered and injected onto a Ni-NTA superflow resin (5 ml) and RidA was purified according to the manufacturer's protocol (Qiagen). Purified protein was concentrated by centrifugation with a 4,000 molecular weight cut-off filter

unit (Millipore) and the concentrated protein sample (~ 5 ml) was sequentially dialyzed in 1 L of 10 mM HEPES pH 8 containing 10 mM EGTA for 1 hour, 1 L of HEPES buffer for 1 hour and 1 L of HEPES buffer containing 20% glycerol overnight. Protein recovery as determined by the BCA assay (Pierce) was approximately 15.2 mg/ml. Protein aliquots were frozen in liquid nitrogen and stored at -80°C.

Cysteine desulfhydrase assay. Cysteine desulfhydrase activity was measured by coupling pyruvate formation to NADH oxidation using lactate dehydrogenase (Sigma) and monitoring the decrease in absorbance at 340 nm as described previously (29). Assays consisted of 100 mM Tris-HCl pH 8.5 containing 0.25 mM NADH, 30 μ M PLP and 15 U/ml lactate dehydrogenase. CdsH and RidA were added to the reaction at final monomeric concentrations of 0.19 μ M and 0.27 μ M, respectively. Because RidA is a trimer (43) and CdsH is a hexamer (44), the oligomeric ratio of RidA:CdsH was ~ 3:1. Concentrations of fresh L-cysteine ranging from 0 to 20 mM were added to initiate the reaction. Reactions (300 μ l) were monitored continuously at 22°C in a 96-well quartz plate using a Spectramax M2. Initial rates were calculated from the change in A_{340} due to the consumption of NADH over the initial 20 seconds. The extinction coefficient of NADH at 340 nm ($6,220 \text{ M}^{-1} \text{ cm}^{-1}$) was used to calculate enzyme activity. Initial activity is reported as the initial rate of pyruvate formation in μ mol/min. Experiments were performed in triplicate and the resulting data were plotted using GraphPad Prism 5.0f.

2.4 RESULTS AND DISCUSSION

Growth of a *ridA* strain is affected by exogenous cysteine. Growth of wild-type *S. enterica* in glucose minimal medium is unaffected by cysteine concentrations up to 0.1 mM. Concentrations above that affect growth by increasing the lag phase before the culture enters

logarithmic growth (Figure 2.2A). The concentration of cysteine that prevented recovery after an extended lag was not determined. In contrast to wild-type, a *ridA* strain is sensitive to a concentration of cysteine as low as 0.1 mM and displayed a concentration-dependent extension of the lag phase prior to entering exponential growth. A *ridA* strain had no significant growth within 20 hours when cysteine concentrations were 0.25 mM or higher (Figure 2.2B). The growth inhibition caused by 0.25 mM cysteine was transient and after 24 hours the *ridA* strain grew exponentially, ultimately reaching the same final cell density as the wild-type strain. Together these data showed that a strain lacking RidA was substantially more sensitive to exogenous cysteine than a wild-type strain.

Serine/threonine dehydratase is not required for the cysteine sensitivity of a *ridA* strain. Strains lacking RidA are sensitive to the accumulation of 2-aminoacrylate generated from serine by the serine/threonine dehydratase IlvA (9, 10, 17). Given that cysteine is a β -substituted amino acid akin to serine, it was formally possible that the cysteine sensitivity of a *ridA* strain would directly or indirectly depend on IlvA activity. Cysteine was shown to have a mixed inhibitory effect on the threonine dehydratase activity of IlvA isolated from *E. coli*, suggesting it may serve as a competitive substrate of the enzyme (45). IlvA is the only serine/threonine dehydratase expressed in *S. enterica* under aerobic conditions (46). Two experiments ruled out a role for IlvA in the cysteine sensitivity of a *ridA* strain. The growth data in Figure 2.3 showed that in the presence of 1 mM cysteine, neither isoleucine nor threonine (data not shown) restored growth to a strain lacking RidA. In contrast, both isoleucine and threonine suppressed the growth defects of a *ridA* mutant caused by the activity of IlvA (6, 42, 47). Further, the deletion of *ilvA* did not affect the growth of *ridA* mutant strains in the presence of cysteine. These data ruled out a

role for IlvA in mediating cysteine sensitivity in a *ridA* strain, and indicated a distinct cellular component was involved in the cysteine sensitivity of *ridA* strains.

Exogenous cysteine increases the level of free 2AA in the cell. Based on the *in vitro* activity associated with RidA (1), a simple scenario was that a non-IlvA enzyme generated 2AA or a related enamine from cysteine that resulted in the cysteine sensitivity observed. In the absence of RidA, endogenous 2AA can react with the PLP cofactor of isoleucine transaminase B (IlvE), forming a covalent active-site modification that renders the enzyme inactive (17, 41, 45). Therefore, the activity of IlvE has been used as a proxy for the levels of 2AA in the cells of strains lacking RidA (17, 42, 47). Wild-type and *ridA* mutant strains were grown in minimal medium containing casamino acids and isoleucine, with and without the addition 0.25 mM cysteine, and IlvE activity was assayed. The addition of 0.1% casamino acids to the growth medium resulted in similar growth patterns for each strain. The data in Figure 2.4 showed that cysteine did not affect the level of IlvE activity in strains with a functional RidA. In contrast, the transaminase B activity was decreased by ~ 35% in a *ridA* mutant strain when 0.25 mM cysteine was present in the growth media. Consistent with the growth data, the impact of cysteine on the activity of IlvE was not affected by the presence or absence of IlvA. Additionally, in an *in vitro* system, neither cysteine alone nor IlvA and cysteine decreased the activity of IlvE (data not shown). In total, these data suggested that an indirect consequence of cysteine, or a metabolite of cysteine was responsible for the decreased IlvE activity and growth defect of a *ridA* mutant.

Multiple enzymes in *S. enterica* use cysteine as a substrate and have the potential to generate 2AA as a reaction intermediate. Based on *E. coli*, three enzymes were identified that may have cysteine desulfhydrase activity in *S. enterica*: CysK, CysM, STM1557 (34% identical to *E. coli* MalY) (27). These PLP-dependent enzymes generate pyruvate, hydrogen sulfide, and

ammonia from cysteine, and it was plausible that these reactions would proceed through a 2AA intermediate (29, 48, 49). Deletions of *cysK*, *cysM*, and *stm1557* were generated by gene replacement (40), and strains that contained each mutation alone or in combination with a *ridA* mutation were constructed. None of the double mutants *ridA cysK*, *ridA cysM*, or *ridA stm1557* grew in the presence of 0.25 mM cysteine, while the growth of *ridA*⁺ derivatives of each strain was unaffected by the presence of cysteine (data not shown). CysK and CysM are isozymes involved in cysteine biosynthesis and a *cysK cysM* double mutant strain is a cysteine auxotroph. A concentration of cysteine exceeding 0.5 mM was needed to satisfy the cysteine requirement of this strain. If either CysK or CysM contributed to 2AA stress arising from cysteine, a *cysK cysM ridA* triple mutant would be expected to grow in the presence of cysteine despite the *ridA* mutation. The triple mutant strain failed to grow in the presence of 0.5 mM or 1 mM cysteine. These data suggested that CysK, CysM and STM1557 did not contribute significantly to the production of 2AA in *S. enterica*.

Mutations in *cdsH* partially relieve cysteine sensitivity. Mutations that restored growth of a *ridA* mutant in the presence of cysteine were isolated. Approximately 10⁸ cells of *ridA* mutant strain DM3480 were spread on minimal cysteine (5 mM) plates. Despite numerous attempts, no spontaneous mutants that allowed growth were recovered after 3-5 days of incubation. When the same process was repeated, and diethyl sulfate (DES) was spotted in the middle of the cysteine plate, multiple colonies arose. The cysteine-resistant phenotypes were verified and two of these mutants were selected for further analysis. Whole-genome sequencing of a representative mutant, DM13827, revealed a G-to-A substitution in the gene encoding STM0458, changing residue 295 from a tryptophan to a stop codon (W295STOP). The same mutation was observed in both of the suppressor strains. In the course of our studies it was reported that *stm0458* encoded the major

CDS in *Salmonella* and the gene was renamed *cdsH* to reflect this finding (25). The *cdsH* mutation (*cdsH3*) was reconstructed to confirm it was the causative lesion. Subsequently, an insertion linked to *cdsH3* was used to generate an isogenic pair of strains in both the *ridA* (DM3480) and wild-type strain (DM9404) background.

Anticipating that a nonsense mutation would be recessive and display the phenotype of a null allele, a deletion of *cdsH* was generated ($\Delta cdsH1::Cm$). Growth analysis showed that while both alleles of *cdsH* increased growth of a *ridA* mutant in the presence of cysteine, they displayed different levels of suppression (Figure 2.5). Both *cdsH* alleles significantly reduced the growth lag of the *ridA* mutant in the presence of 0.1 mM cysteine (data not shown). In the presence of 0.25 mM cysteine, when a *ridA* mutant had no growth after 20 hours, the *cdsH3* allele restored growth while the *cdsH1::Cm* deletion had a lesser effect (Figure 2.5). The difference between the two alleles was presumed to be due to the periodic read-through of the UGA (opal) nonsense codon (50) or reduced activity of the partial protein. The positive growth response allowed by decreasing or eliminating CdsH activity was consistent with the general hypothesis that CDS was generating 2AA, which was toxic in the absence of RidA. However, a few observations about growth of the mutant strains indicated additional complexities were present in the cell. First, if the generation of 2AA were the only deleterious consequence of cysteine, deletion of *cdsH* would have the best suppressing effect. In addition, if the generation of 2AA from cysteine was by CdsH alone, a *ridA cdsH1::Cm* double-mutant (DM14254) should grow similarly to the *cdsH1::Cm* single-mutant (DM14240). The growth discrepancy between the *ridA* + and *ridA* - strains suggested that an additional enzyme generates a RidA substrate from cysteine.

Loss of CdsH exacerbates cysteine toxicity in wild-type *Salmonella*. The inability of the *cdsH* deletion to restore wild-type growth to a *ridA* mutant in the presence of cysteine indicated

that 2AA was not the only metabolic problem generated by the presence of cysteine. During this study another group reported that the deletion of *cdsH* resulted in a 10-fold decrease in CDS activity, and caused increased sensitivity to cysteine (25). Consistently, both the *cdsH* deletion mutant and the nonsense mutant had an extended lag phase when grown in medium containing 0.25 mM cysteine (Figure 2.5). When 0.5 mM cysteine was present the defect was more severe (data not shown).

Collectively, these results revealed the opposing consequences of eliminating *cdsH*, and the complexity of dissecting the physiological status of strains lacking both RidA and CdsH. On the one hand, deletion of *cdsH* affected the ability of the cell to remove, or detoxify, cysteine. This led to the accumulation of cysteine, which inhibited growth by poorly characterized mechanisms. On the other hand, cells without CdsH produce less 2AA because the desulfhydrase reaction is not proceeding. Therefore, the toxic effects of 2AA derived from cysteine in a *ridA* mutant are negated. Taken together these data suggest that the detoxification of cysteine by CDS enzymes proceeds through a reactive intermediate, which itself is toxic and must be quenched by RidA. The results herein indicated that the decreased growth of *S. enterica* in the presence of cysteine was a consequence of both features.

RidA increases the rate of cysteine desulfhydrase-dependent pyruvate formation *in vitro*.

The scenario above predicted RidA would have a detectable influence on the products of the CdsH protein *in vitro*. CdsH activity was assessed by a coupled assay with lactate dehydrogenase to measure the formation of pyruvate. The rate of the reaction was calculated over time in the presence or absence of RidA protein (Figure 2.6). From these data a number of points were noted. In the absence of RidA, the rate of pyruvate formation decreased at concentrations of cysteine above 1 mM. This behavior of CdsH was observed previously, and was attributed to the

spontaneous reaction of L-cysteine with a 2AA intermediate, leading to the formation of the cyclized compound 2-methyl-2,4-thiazolidine-dicarboxylate (MTD) (29). The relevant reaction is schematically shown in Figure 2.7. An alternative assay monitoring sulfide release from cysteine determined the K_m of CdsH for L-cysteine was 0.17 - 0.21 mM, and found sulfide inhibited the reaction with a K_i of 0.010 mM (26, 29). The data presented in Figure 2.6 displayed sigmoidal kinetics of CdsH, consistent with the positive cooperatively ($n = 1.9$) reported for this enzyme (29).

The addition of RidA to the CdsH reaction increased the rate of pyruvate formation at all cysteine concentrations (Figure 2.6). The CdsH-dependent rate of pyruvate formation was greatest at 1 mM cysteine, where including RidA in the reaction increased the rate 3.8-fold. Increasing the concentration of cysteine to 2 mM decreased the rate of CdsH-catalyzed pyruvate formation and is attributed to the diversion of 2AA by cysteine as depicted in Figure 2.7. However, the addition of RidA had the greatest relative effect at 2 mM cysteine, increasing the rate 5.8-fold. At concentrations of cysteine above 4 mM the rate of pyruvate formation decreased in a cysteine dependent manner despite the presence of RidA (Figure 2.6). Additional controls substituting bovine serum albumin (10 $\mu\text{g}/\mu\text{l}$) for RidA had no affect on CDS activity. These data, when viewed in light of the reaction mechanism previously described, suggest that at high concentrations of cysteine, there is a competition between cysteine and RidA for the 2AA intermediate (Figure 2.7).

Conclusions. The purpose of this study was to describe the mechanism of cysteine sensitivity provoked by removing RidA from the metabolic network in *S. enterica*. Previous reports had focused on the dehydration of serine by PLP-dependent serine/threonine dehydratases (IlvA and TdcB) as sources of endogenous 2AA (7, 9, 10, 17, 42). The work here describes an additional mechanism of endogenous 2AA formation that is dependent on the cysteine desulphydrase activity

of CdsH. *In vitro* analysis showed that RidA enhanced the rate of CdsH-dependent pyruvate formation from cysteine, consistent with the hypothesis that an unbound 2AA intermediate is formed by CdsH and subsequently acted upon by RidA to increase the rate of enamine/imine hydrolysis. Eliminating CdsH partially decreased the cysteine sensitivity of *ridA* mutants while increasing the sensitivity of the wild-type strain.

The findings presented here introduce an interesting dichotomy in which the detoxification of cysteine, which is itself toxic to wild-type *Salmonella* when present at high concentrations, relies on an enzyme-catalyzed reaction that proceeds through a dangerous reactive intermediate, 2-aminoacrylate. *S. enterica* has a built-in defense against 2AA stress in the form of RidA. Therefore, it seems that the benefit of detoxifying cysteine via a toxic intermediate outweighs the potential consequence given the robust protection afforded to the cell by RidA. *Salmonella* relies on the dedicated cysteine desulfhydrase encoded by *cdsH* to prevent cysteine from accumulating to toxic levels. The PLP-dependent mechanism used by CdsH dictates that 2AA be generated as a deliberate intermediate in the cysteine detoxification pathway, and demands the presence of RidA to prevent 2AA stress.

This is the first example of a role for RidA in a dedicated detoxification pathway and potentially represents a conserved role for RidA proteins in cysteine detoxification in other organisms. In contrast, the dehydration of serine by IlvA is a side reaction of an enzyme that acts primarily to convert threonine to 2-ketobutyrate in isoleucine biosynthesis. The generation of 2AA in this context is therefore a consequence of substrate promiscuity, as serine degradation by IlvA does not serve a crucial role in metabolism. In fact, the *S. enterica* genome encodes three Fe-S-dependent serine deaminases (EC 4.3.1.17), SdaA, SdaB and TdcG, which specifically prevent the accumulation of toxic levels of serine (51). The serine deaminase reactions catalyzed by these

enzymes are thought to proceed through a 2AA intermediate (52), yet current data suggests that these enzymes do not contribute to free 2AA accumulation in *Salmonella* (unpublished data).

The unusual kinetics we observed for CdsH *in vitro* are in agreement with Kredich *et al.* They reported that under similar assay conditions, the amount of free pyruvate generated by CdsH in the presence of 2 mM cysteine was less than 10% of that expected based on the relative amount of sulfide produced (29). The remaining ~ 90% of unrecovered pyruvate had been diverted to MTD (Figure 2.7). The relevance of this side reaction forming MTD *in vivo* is questionable given the differences between the assay conditions and cell environment. The neutral pH and relatively low concentrations of cysteine found in the cell may prevent MTD from being formed (29), especially when RidA is present. Furthermore, the physiological relevance of MTD in any organism remains unclear (21, 53). However, there is interest in the use of thiazolidine derivatives in therapeutic applications (21). MTD and other thiazolidine derivatives can be converted to cysteine non-enzymatically or enzymatically, and are viewed as a means of delivering adequate doses of cysteine to mammalian systems without causing cysteine toxicity (21). Given that cysteine behaves as a nucleophile when attacking 2AA, future studies will address the possibility that additional nucleophilic species react with 2AA *in vitro*. The results herein describe a new role for RidA in metabolism and raise the possibility that other detoxification pathways could proceed through reactive intermediates that are quenched by RidA.

ACKNOWLEDGMENTS

The authors would like to thank Lauren Palmer for constructing the pET14b-*cdsH* plasmid for protein overproduction. This work was supported by competitive grant GM095837 from the NIH.

2.5 REFERENCES

1. Lambrecht JA, Flynn JM, Downs DM. 2012. Conserved YjgF protein family deaminates reactive enamine/imine intermediates of pyridoxal 5'-phosphate (PLP)-dependent enzyme reactions. *J Biol Chem* 287:3454–3461.
2. Chargaff E, Sprinson DB. 1943. Studies on the mechanism of deamination of serine and threonine in biological systems. *J Biol Chem* 151:273–280.
3. Phillips AT, Wood WA. 1965. The mechanism of action of 5'-adenylic acid-activated threonine dehydrase. *J Biol Chem* 240:4703–4709.
4. Layer RW. 1963. The chemistry of imines. *Chem Rev* 63:489–510.
5. Hillebrand GG, Dye JL, Suelter CH. 1979. Formation of an intermediate and its rate of conversion to pyruvate during the tryptophanase-catalyzed degradation of So-nitrophenyl-L-cysteine. *Biochemistry (Mosc)* 18:1751–1755.
6. Enos-Berlage JL, Langendorf MJ, Downs DM. 1998. Complex metabolic phenotypes caused by a mutation in *yjgF*, encoding a member of the highly conserved YER057c/YjgF family of proteins. *J Bacteriol* 180:6519–6528.
7. Christopherson MR, Schmitz GE, Downs DM. 2008. YjgF is required for isoleucine biosynthesis when *Salmonella enterica* is grown on pyruvate medium. *J Bacteriol* 190:3057–3062.
8. Lambrecht JA, Browne BA, Downs DM. 2010. Members of the YjgF/YER057c/UK114 family of proteins inhibit phosphoribosylamine synthesis *in vitro*. *J Biol Chem* 285:34401–34407.
9. Flynn JM, Christopherson MR, Downs DM. 2013. Decreased coenzyme A levels in *ridA* mutant strains of *Salmonella enterica* result from inactivated serine hydroxymethyltransferase: *ridA* mutants are deficient in one carbon metabolism. *Mol Microbiol* 89:751–759.
10. Flynn JM, Downs DM. 2013. In the absence of RidA, endogenous 2-aminoacrylate inactivates alanine racemases by modifying the pyridoxal 5'-phosphate cofactor. *J Bacteriol* 195:3603–3609.
11. Arfin SM, Koziell DA. 1971. Inhibition of growth of *Salmonella typhimurium* and of threonine deaminase and transaminase B by β -chloroalanine. *J Bacteriol* 105:519–522.

12. Silverman RB, Abeles RH. 1976. Inactivation of pyridoxal phosphate dependent enzymes by mono-and polyhaloalanines. *Biochemistry (Mosc)* 15:4718–4723.
13. Likos JJ, Ueno H, Feldhaus RW, Metzler DE. 1982. A novel reaction of the coenzyme of glutamate decarboxylase with L-serine O-sulfate. *Biochemistry (Mosc)* 21:4377–4386.
14. Ueno H, Likos JJ, Metzler DE. 1982. Chemistry of the inactivation of cytosolic aspartate aminotransferase by serine O-sulfate. *Biochemistry (Mosc)* 21:4387–4393.
15. Walsh C. 1982. Suicide substrates: mechanism-based enzyme inactivators. *Tetrahedron* 38:871–909.
16. Walsh CT. 1984. Suicide substrates, mechanism-based enzyme inactivators: recent developments. *Annu Rev Biochem* 53:493–535.
17. Lambrecht JA, Schmitz GE, Downs DM. 2013. RidA proteins prevent metabolic damage inflicted by PLP-dependent dehydratases in all domains of life. *mBio* 4:e00033-13-e00033-13.
18. Gomez RF, Montville T, Blais K. 1980. Toxic effect of cysteine against *Salmonella typhimurium*. *Appl Environ Microbiol* 39:1081–1083.
19. Harris CL. 1981. Cysteine and growth inhibition of *Escherichia coli*: threonine deaminase as the target enzyme. *J Bacteriol* 145:1031–1035.
20. Cowman RA, Baron SS, Fitzgerald RJ. 1983. Cysteine toxicity for oral streptococci and effect of branched-chain amino acids. *Infect Immun* 39:1107–1113.
21. Wlodek L, Rommelspacher H, Susilo R, Radomski J, Höfle G. 1993. Thiazolidine derivatives as source of free L-cysteine in rat tissue. *Biochem Pharmacol* 46:1917–1928.
22. Sørensen MA, Pedersen S. 1991. Cysteine, even in low concentrations, induces transient amino acid starvation in *Escherichia coli*. *J Bacteriol* 173:5244–5246.
23. Park S, Imlay JA. 2003. High levels of intracellular cysteine promote oxidative DNA damage by driving the Fenton reaction. *J Bacteriol* 185:1942–1950.
24. Kumar A, John L, Alam MM, Gupta A, Sharma G, Pillai B, Sengupta S. 2006. Homocysteine- and cysteine-mediated growth defect is not associated with induction of oxidative stress response genes in yeast. *Biochem J* 396:61.
25. Oguri T, Schneider B, Reitzer L. 2012. Cysteine catabolism and cysteine desulfhydrase (CdsH/STM0458) in *Salmonella enterica* serovar Typhimurium. *J Bacteriol* 194:4366–4376.

26. Collins JM, Monty KJ. 1973. The cysteine desulfhydrase of *Salmonella typhimurium* kinetic and catalytic properties. *J Biol Chem* 248:5943–5949.
27. Awano N, Wada M, Mori H, Nakamori S, Takagi H. 2005. Identification and functional analysis of *Escherichia coli* cysteine desulfhydrases. *Appl Environ Microbiol* 71:4149–4152.
28. Guarneros G, Ortega M V. 1970. Cysteine desulfhydrase activities of *Salmonella typhimurium* and *Escherichia coli*. *Biochim Biophys Acta BBA-Enzymol* 198:132–142.
29. Kredich NM, Foote LJ, Keenan BS. 1973. The stoichiometry and kinetics of the inducible cysteine desulfhydrase from *Salmonella typhimurium*. *J Biol Chem* 248:6187–6196.
30. Turnbull AL, Surette MG. 2008. L-cysteine is required for induced antibiotic resistance in actively swarming *Salmonella enterica* serovar Typhimurium. *Microbiology* 154:3410–3419.
31. Shatalin K, Shatalina E, Mironov A, Nudler E. 2011. H₂S: a universal defense against antibiotics in bacteria. *Science* 334:986–990.
32. Chargaff E, Sprinson DB. 1943. Studies on the mechanism of deamination of serine and threonine in biological systems. *J Biol Chem* 151:273–280.
33. Way JC, Davis MA, Morisato D, Roberts DE, Kleckner N. 1984. New Tn10 derivatives for transposon mutagenesis and for construction of *lacZ* operon fusions by transposition. *Gene* 32:369–379.
34. Castilho B, Olfson P, Casadaban MJ. 1984. Plasmid insertion mutagenesis and *lac* gene fusion with mini-*mu* bacteriophage transposons. *J Bacteriol* 158:488–95.
35. Vogel HJ, Bonner DM. 1956. Acetylornithinase of *Escherichia coli*: partial purification and some properties. *J Biol Chem* 218:97–106.
36. Balch WE, Wolfe RS. 1976. New approach to the cultivation of methanogenic bacteria: 2-mercaptoethanesulfonic acid (HS-CoM)-dependent growth of *Methanobacterium ruminantium* in a pressurized atmosphere. *Appl Environ Microbiol* 32:781–791.
37. Schmieger H. 1972. Phage P22-mutants with increased or decreased transduction abilities. *Mol Gen Genet* 119:75.
38. Chan RK, Botstein D, Watanabe T, Ogata Y. 1972. Specialized transduction of tetracycline resistance by phage P22 in *Salmonella typhimurium*. II. Properties of a high-frequency-transducing lysate. *Virology* 50:883–898.

39. Downs DM, Petersen L. 1994. *apbA*, a new genetic locus involved in thiamine biosynthesis in *Salmonella typhimurium*. *J Bacteriol* 176:4858–64.
40. Datsenko KA, Wanner BL. 2000. One-step inactivation of chromosomal genes in *Escherichia coli* K-12 using PCR products. *Gene* 1:H2.
41. McClelland M, Sanderson KE, Spieth J, Clifton SW, Latreille P, Courtney L, Porwollik S, Ali J, Dante M, Du F, Hou S, Layman D, Leonard S, Nguyen C, Scott K, Holmes A, Grewal N, Mulvaney E, Ryan E, Sun H, Florea L, Miller W, Stoneking T, Nhan M, Waterston R, Wilson RK. 2001. Complete genome sequence of *Salmonella enterica* serovar Typhimurium LT2. *Nature* 413:852–856.
42. Schmitz G, Downs DM. 2004. Reduced transaminase B (IlvE) activity caused by the lack of *yjgF* is dependent on the status of threonine deaminase (IlvA) in *Salmonella enterica* serovar Typhimurium. *J Bacteriol* 186:803.
43. Burman JD, Stevenson CE, Sawers RG, Lawson DM. 2007. The crystal structure of *Escherichia coli* TdcF, a member of the highly conserved YjgF/YER057c/UK114 family. *BMC Struct Biol* 7:30.
44. Kredich NM, Keenan BS, Foote LJ. 1972. The purification and subunit structure of cysteine desulhydrase from *Salmonella typhimurium*. *J Biol Chem* 247:7157–7162.
45. Harris CL. 1981. Cysteine and growth inhibition of *Escherichia coli*: threonine deaminase as the target enzyme. *J Bacteriol* 145:1031–1035.
46. Umbarger HE, Brown B. 1957. Threonine deamination in *E. coli* II: evidence for two l-threonine deaminases. *J Bacteriol* 73:105.
47. Christopherson MR, Lambrecht JA, Downs D, Downs DM. 2012. Suppressor analyses identify threonine as a modulator of *ridA* mutant phenotypes in *Salmonella enterica*. *PLoS ONE* 7:e43082.
48. Miles EW, Hatanaka M, Crawford IP. 1968. A new thiol-dependent transamination reaction catalyzed by the B protein of *Escherichia coli* tryptophan synthetase. *Biochemistry (Mosc)* 7:2742–2753.
49. Ågren D, Schnell R, Schneider G. 2009. The C-terminal of CysM from *Mycobacterium tuberculosis* protects the aminoacrylate intermediate and is involved in sulfur donor selectivity. *FEBS Lett* 583:330–336.
50. Bertram G, Innes S, Minella O, Richardson JP, Stansfield I. 2001. Endless possibilities: translation termination and stop codon recognition. *Microbiology* 147:255–269.

51. Zhang X, El-Hajj ZW, Newman E. 2010. Deficiency in L-serine deaminase interferes with one-carbon metabolism and cell wall synthesis in *Escherichia coli* K-12. *J Bacteriol* 192:5515–5525.
52. Grabowski R, Hofmeister A, Buckel W. 1993. Bacterial L-serine dehydratases: a new family of enzymes containing iron-sulfur clusters. *Trends Biochem Sci* 18:297–300.
53. Wlodek L. 1964. Formation of MTD from L-cysteine in rat tissues. *Acta Biochim Pol* 31:279–288.

TABLE 2.1 Bacterial strains^a

Strain	Genotype ^b
DM9404	<i>ridA</i> ⁺ in DM3480 background (wild-type)
DM3480	<i>ridA3</i> ::MudJ
DM4748	<i>ilvA595</i> ::Tn10d(Tc)
DM5062	<i>ridA3</i> ::MudJ <i>ilvA595</i> ::Tn10d(Tc)
DM12740	BL21AI pET20b- <i>ridA</i>
DM13827	<i>ridA3</i> ::MudJ <i>cdsH3</i>
DM14240	<i>cdsH1</i> ::Cm
DM14254	<i>ridA3</i> ::MudJ <i>cdsH1</i> ::Cm
DM14317	<i>cdsH1</i> ::Cm <i>ilvA595</i> ::Tn10d(Tc)
DM14319	<i>ridA3</i> ::MudJ <i>cdsH</i> ::Cm <i>ilvA595</i> ::Tn10d(Tc)
DM14430	BL21AI pET14b- <i>cdsH</i>
DM14497	<i>ampG</i> ::Tn10d(Tc)
DM14498	<i>ampG</i> ::Tn10d(Tc) <i>cdsH3</i> (CdsH ^{W295Stop})
DM14499	<i>ampG</i> ::Tn10d(Tc) <i>ridA</i> ::MudJ <i>cdsH3</i> (CdsH ^{W295Stop})
DM14500	<i>ampG</i> ::Tn10d(Tc) <i>ridA</i> ::MudJ

^a All strains were derived from *Salmonella enterica* serovar Typhimurium LT2 and were obtained from the lab archive or made for this study.

^b MudJ refers to the MudJ1734 insertion element (34). Tn10d(Tc) refers to the transposition-defective mini-Tn10 (Tn10Δ16Δ17) (33).

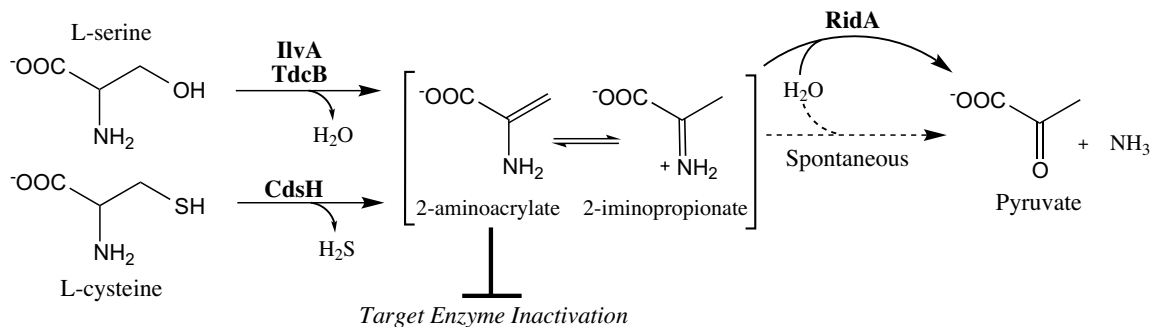


FIGURE 2.1. RidA catalyzes the hydrolysis of reactive intermediates. The PLP-dependent α,β -elimination of serine and cysteine proceeds through an unbound aminoacrylate intermediate. RidA protein enhances the rate of intermediate hydrolysis.

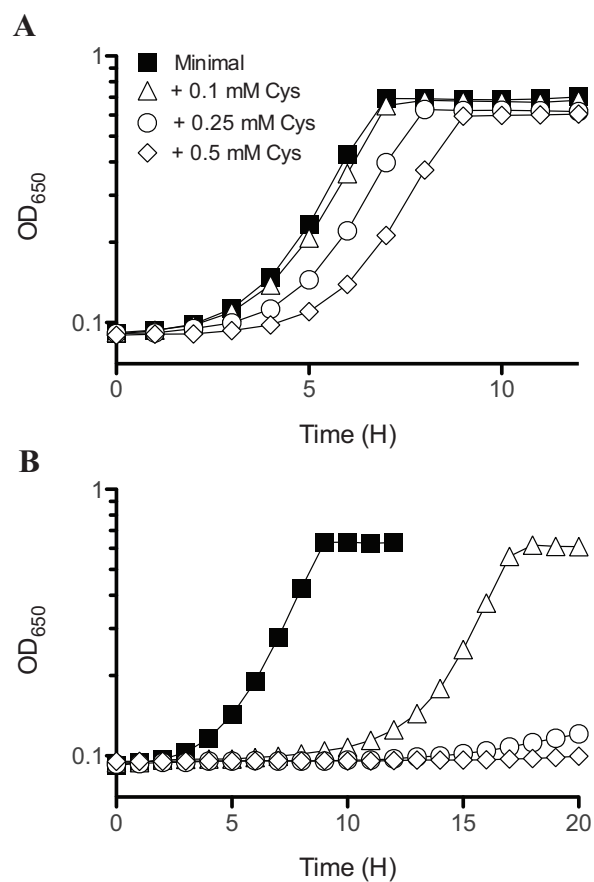


FIGURE 2.2. Growth inhibition increases with cysteine concentration. A) Wild-type (DM9404) and B) *ridA* (DM3480) strains were grown at 37°C in minimal glucose medium with cysteine excluded (closed squares) or added to a final concentration of 0.1 mM (open triangles), 0.25 mM (open circles) or 0.5 mM (open diamonds). Error bars representing the standard error (SEM) of three replicates are excluded as the replicates deviated less than 5% from the average value.

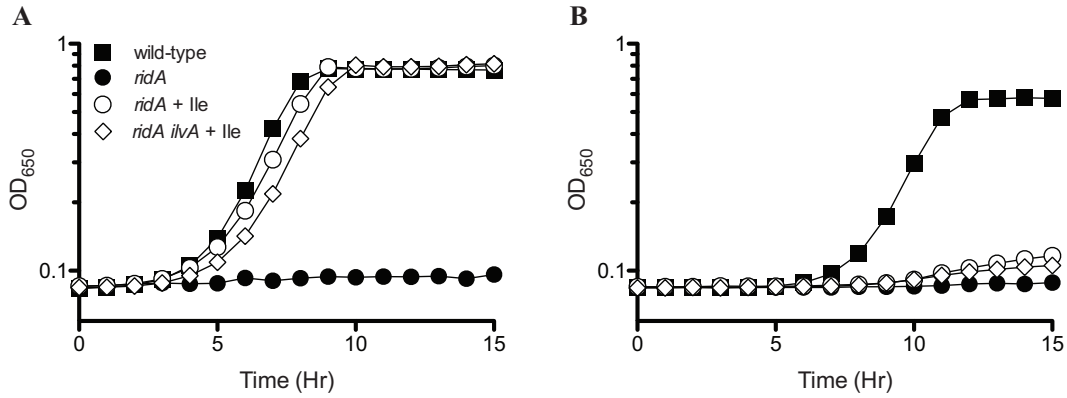


FIGURE 2.3. The cysteine sensitivity of a *ridA* strain does not require *IlvA*. Strains were grown at 37°C in glucose minimal medium containing A) 5 mM serine or B) 1 mM cysteine. Open symbols indicate the addition of 1 mM isoleucine. Growth is displayed for wild-type (DM9404; squares), *ridA* (DM3480; circles) and *ridA ilvA* (DM5062; diamonds). Error bars representing the standard error (SEM) of three replicates are excluded as the replicates deviated less than 5% from the average value.

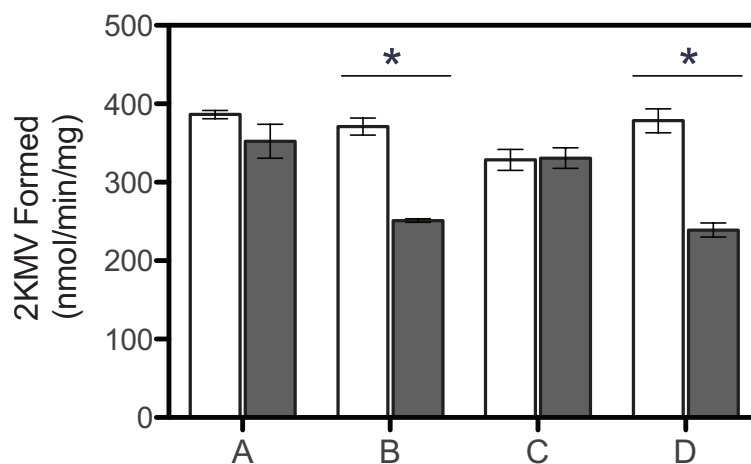


FIGURE 2.4. IlvE activity is reduced in *ridA* strains grown in the presence of exogenous cysteine. Cultures were grown to stationary phase in glucose minimal medium containing 0.1% casamino acids and 1 mM isoleucine, without exogenous cysteine (white bars) or with 0.25 mM cysteine (gray bars). The specific activity of IlvE from three independent cultures was determined based on 2-ketomethylvalerate (2KMV) formation in crude extracts. Error bars represent the standard error (SEM). A) Wild-type (DM9404), B) *ridA* (DM3480), C) *ilvA* (DM4748) and D) *ridA ilvA* (DM5062). * indicates a significant difference based on one-way ANOVA and Tukey's test ($p < 0.01$).

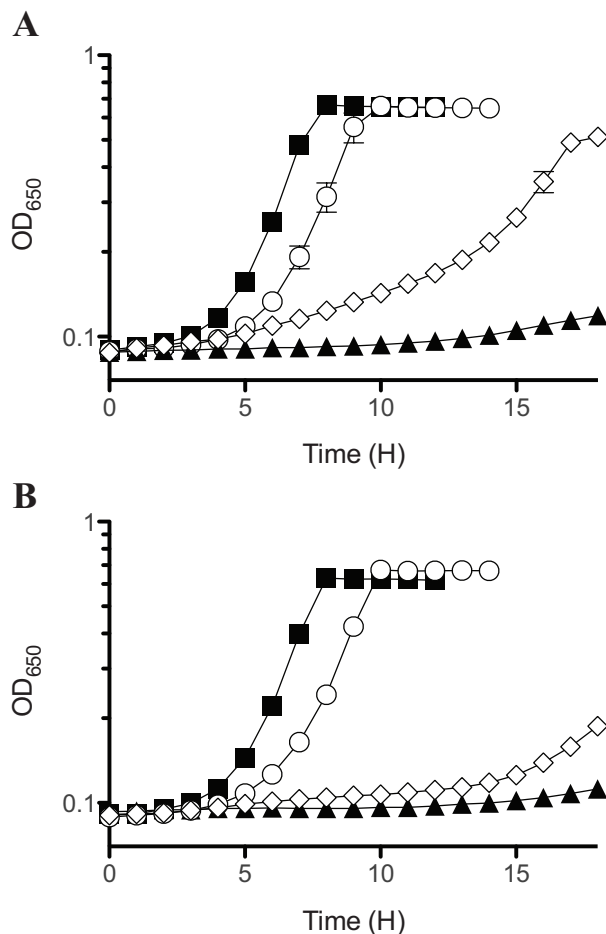


FIGURE 2.5. Lesions in *cdsH* improve growth of a *ridA* strain in the presence of cysteine.

Strains were grown in glucose minimal medium containing 0.25 mM cysteine. A) Growth of wild-type (DM14497; closed squares), *ridA* (DM14500; closed triangles), *cdsH3* (DM14498; open circles) and *ridA cdsH3* (open diamonds). B) Growth of wild-type (DM9404; closed squares), *ridA* (DM3480; closed triangles), *cdsH1::Cm* (DM14240; open circles) and *ridA cdsH1::Cm* (DM14254; open diamonds). Experiments were done in triplicate. Error bars represent the standard error (SEM).

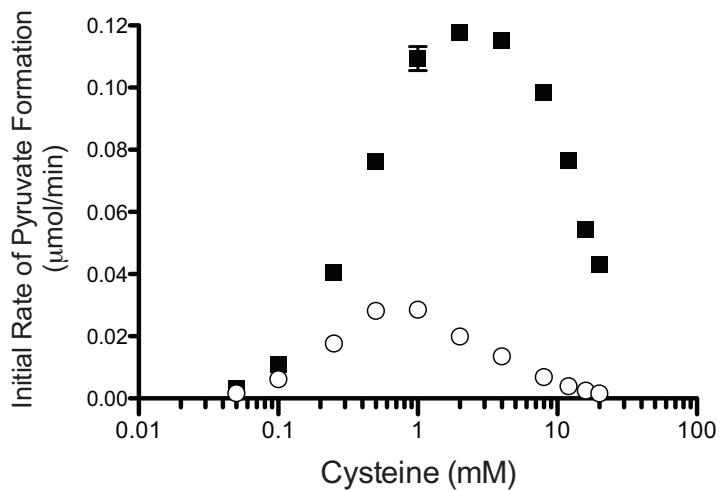


FIGURE 2.6. The initial rate of CdsH-catalyzed pyruvate formation is improved by RidA.

The initial rate of pyruvate formation versus cysteine concentration is plotted for CdsH alone (open circles) and CdsH + RidA (squares). Experiments were performed in triplicate and the resulting data are displayed with error bars representing the standard error (SEM).

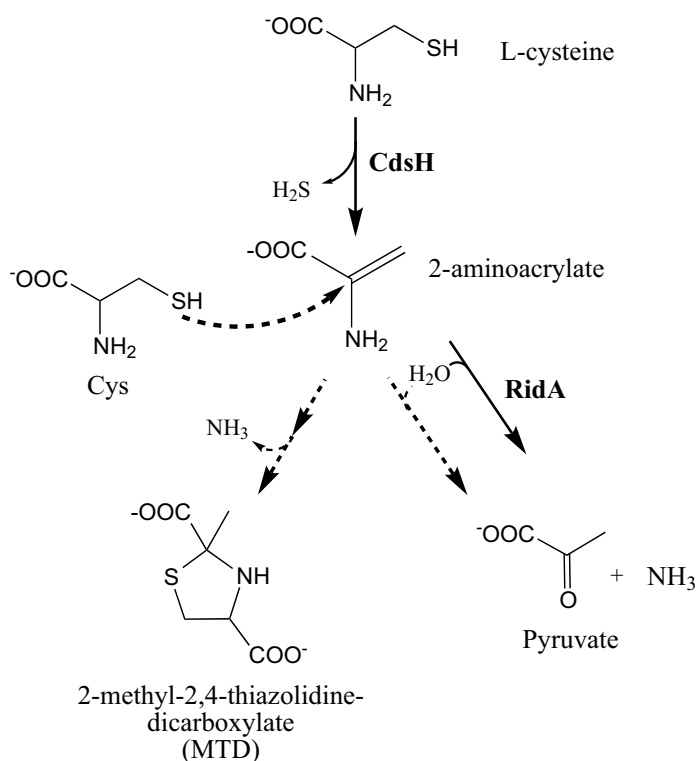


FIGURE 2.7. Nucleophilic attack by cysteine reduces the amount of 2-aminoacrylate converted to pyruvate. The PLP-dependent α,β -elimination reaction catalyzed by CdsH converts cysteine to 2-aminoacrylate and hydrogen sulfide. In solvent water, 2-aminoacrylate can be hydrolyzed to pyruvate spontaneously or enzymatically through the activity of RidA. The nucleophilic sulfhydryl group of cysteine can also attack the $\text{C}=\text{C}$ double bond of 2-aminoacrylate, ultimately leading to the formation of the cyclized thiazolidine derivative, 2-methyl-2,4-thiazolidine-dicarboxylate (MTD) (29). Solid arrows indicate enzyme-catalyzed steps and dashed arrows indicate spontaneous reactions.

CHAPTER 3

L-2,3-DIAMINOPROPIONATE GENERATES DIVERSE METABOLIC STRESSES IN

*SALMONELLA ENTERICA*¹

¹Ernst DC, Anderson ME, Downs DM. 2016. *Molecular microbiology* 101:210–223.

Reprinted here with permission of the publisher.

3.1 ABSTRACT

Unchecked amino acid accumulation in living cells has the potential to cause stress by disrupting normal metabolic processes. Thus, many organisms have evolved degradation strategies that prevent endogenous accumulation of amino acids. L-2,3-diaminopropionate (Dap) is a non-protein amino acid produced in nature where it serves as a precursor to siderophores, neurotoxins, and antibiotics. Dap accumulation in *S. enterica* was previously shown to inhibit growth by unknown mechanisms. The production of diaminopropionate ammonia-lyase (DpaL) alleviated Dap toxicity in *S. enterica* by catalyzing the degradation of Dap to pyruvate and ammonia. Here, we demonstrate that Dap accumulation in *S. enterica* elicits a proline requirement for growth and specifically inhibits coenzyme A and isoleucine biosynthesis. Additionally, we establish that the DpaL-dependent degradation of Dap to pyruvate proceeds through an unbound 2-aminoacrylate (2AA) intermediate, thus contributing to 2AA stress inside the cell. The reactive intermediate deaminase, RidA, is shown to prevent 2AA damage caused by DpaL-dependent Dap degradation by enhancing the rate of 2AA hydrolysis. The results presented herein inform our understanding of the effects Dap has on metabolism in *S. enterica*, and likely other organisms, and highlight the critical role played by RidA in preventing 2AA stress stemming from Dap detoxification.

3.2 BACKGROUND

The robustness of a given metabolic network is influenced by the availability and reactivity of metabolites. Reactive metabolites, along with enzyme catalysts, facilitate the chemistry necessary to sustain life. However, reactive metabolites can cause damage to cellular components if they accumulate aberrantly. Systems for pre-empting damage caused by reactive metabolites often include degradation, chemical modification, compartmentalization, or excretion of the relevant

stressor (1, 2). The significance of this problem has been recognized by a recent suggestion that many genes of unknown function are involved in protecting the cell from metabolic errors (1). Aberrant amino acid accumulation represents a broadly encountered form of metabolic stress. For example, human diseases such as phenylketonuria, branched-chain ketoaciduria, homocysteinuria, cystinosis, and others are associated with amino acid build-up (3). In bacteria, several amino acids, including serine and cysteine, cause metabolic stress and disrupt normal metabolic processes if they accumulate (4–6). Organisms such as *Escherichia coli* and *Salmonella enterica* possess independent degradative enzymes for serine and cysteine that keep the levels of these amino acids low enough to minimize stress (4, 6).

L-2,3-diaminopropionate (Dap) is an amino acid produced by some plants and bacteria where it serves as a precursor to secondary metabolites, including neurotoxins, antibiotics, siderophores and polyamino acids (7–10). Chemically synthesized Dap derivatives are reported to act as potent scavengers of reactive aldehyde species, including those implicated in neurodegenerative diseases (11). Recent reports describing Dap synthesis in *Staphylococcus aureus* and *Streptomyces albulus* revealed two distinct mechanisms of Dap production in bacteria, and demonstrated the importance of this metabolite in iron acquisition and poly(L-diaminopropionic acid) production, respectively (10, 12). Dap is not produced by *E. coli* or *S. enterica*, but it directly impairs growth of these organisms by unknown mechanisms (13). The pyridoxal 5'-phosphate (PLP)-dependent degradation of Dap to pyruvate catalyzed by diaminopropionate ammonia-lyase (DpaL; EC 4.3.1.15) helped alleviate Dap stress in *E. coli* and *S. enterica* (13). Expression of *dpaL* and protein production were specifically induced in *S. enterica* when exposed to Dap (13). Furthermore, the narrow substrate range observed for DpaL *in vitro* and its favorable affinity for Dap ($K_m = 0.1\text{--}0.3$ mM) support a specific role for DpaL in degrading Dap to avoid metabolic stress (14–16).

The mechanism proposed for DpaL was reminiscent of other PLP-dependent eliminases, including serine/threonine dehydratases (IlvA/TdcB; EC 4.3.1.19) and cysteine desulfhydrase (CdsH; EC 4.4.1.1), and suggested 2-aminoacrylate (2AA) was generated as an intermediate in the degradation of Dap to pyruvate (17, 18). Strains of *S. enterica* lacking the enamine/imine deaminase, RidA (EC 3.5.99.10), were more sensitive than wild type strains to the accumulation of 2AA produced by IlvA and CdsH from serine and cysteine, respectively (19–23). Extrapolating these results suggested that RidA could be an important component of DpaL-mediated Dap detoxification in *S. enterica*.

This study was initiated to further characterize the mechanism of Dap sensitivity in *S. enterica* and to expand our current understanding of the role RidA plays in preventing 2AA stress arising from amino acid degradation. Here we show that Dap provokes a requirement for proline and directly inhibits the biosynthesis of coenzyme A and isoleucine. Furthermore, we show that the degradation of Dap by DpaL yields 2AA and exacerbates metabolic stress in the absence of RidA. The work presented here adds to mounting evidence that RidA participates broadly in amino acid detoxification pathways by preventing associated 2AA stress.

3.3 MATERIALS AND METHODS

Bacterial strains, media and chemicals. The bacterial strains used in this study were generated from *Salmonella enterica* serovar Typhimurium LT2. Tn10d indicates the transposition-defective mini-Tn10 (Tn10Δ16Δ17) described previously (24). Minimal medium consisted of no-carbon E medium (NCE) supplemented with 1 mM MgSO₄ (25), trace minerals (26) and 11 mM D-glucose as the sole carbon source. Standard rich medium was Difco nutrient broth (8 g/liter) with sodium chloride (5 g/liter). Superbroth containing tryptone (32 g/liter), yeast extract (20

g/liter), sodium chloride (5 g/liter) and sodium hydroxide (0.2 g/liter) was used when high cell densities were required. Solid medium was made by adding Difco BiTek agar (15 g/liter). Antibiotics were added as needed to minimal and rich growth medium at the following concentrations, respectively: tetracycline, 10 and 20 $\mu\text{g/ml}$; kanamycin, 12.5 and 50 $\mu\text{g/ml}$; chloramphenicol, 5 and 20 $\mu\text{g/ml}$; ampicillin, 15 and 150 $\mu\text{g/ml}$. L-2,3-diaminopropionate was purchased from Chem-Impex International, Inc., Wood Dale, IL. Amino acids and vitamins used in growth and enzyme activity assays were purchased from Sigma-Aldrich Chemical Company, St. Louis, MO.

Genetic techniques and growth analysis. Genetic crosses were performed by transduction using the high-frequency general transducing mutant of bacteriophage P22 (HT105/1, *int-201*) (27). Standard methods used for performing transductions, purifying transductants from phage and identifying phage-free recombinants were described previously (28, 29). The gene replacement made in *STM1002* (*dpaL*) was constructed using the λ -Red recombinase system described by Datsenko and Wanner (30). To be consistent with the described activity of diaminopropionate ammonia-lyase, the *STM1002* gene locus was renamed *dpaL*.

Growth phenotypes were established in solid medium by using agar overlays. Concentrated amino acid or vitamin stocks were spotted (5 μl) on the overlay surface and plates were incubated overnight at 37°C. Growth phenotypes were determined in liquid medium by growing cultures to full density in NB at 37°C. Cells were then pelleted and resuspended in an equal volume of saline solution (85 mM), and 2 μl of the resuspension was inoculated into 198 μl of the relevant defined growth medium contained in a 96-well microtiter plate. Microtiter plates were incubated at 37°C while shaking in a Biotek EL808 ultra microplate reader. Growth was measured as the change in

absorbance at 650 nm (OD_{650}) over time. Data were plotted as the average and standard deviation of three biological replicates using GraphPad Prism 5.0f with the Y-axis displayed in \log_{10} format.

Proline cross-feeding experiments were performed in agar overlays. Reporter strains (proline auxotrophs) were grown overnight in NB liquid at 37°C, washed once with NaCl and overlaid in soft-agar on solid minimal glucose medium containing 1.3 mM L-arabinose (Sigma). L-diaminopropionate was included in the growth medium at a final concentration of 0.25 mM, where appropriate. Producer strains were freshly streaked for isolation and grown overnight at 37°C on NB medium containing ampicillin. Single colonies were picked and stabbed into the solid overlay of the reporter strain and incubated at 37°C for 48 hours. Growth of the reporter strain was assessed based on the change in turbidity in the embedded agar overlay surrounding the stab site. Growth of the producer strain was determined based on outgrowth from the surface of the inoculation site and was clearly distinguishable from growth of the embedded reporter strain.

Molecular methods. The *dpaL* gene was amplified by PCR using Q5 High-fidelity DNA polymerase (New England BioLabs) with primers, DpaL-for-NdeI (5'-AGAGAGCATATGCATGAGCTTAT-3') and DpaL-rev-BamHI (5'-AGAGAGGGA TCCTTAAGCACT-3'). The resulting PCR product was gel purified, digested with NdeI (New England BioLabs) and BamHI (New England BioLabs), and ligated into pET-15b (Novagen) vector digested with the same restriction enzymes, forming pDM1451. Constructs were transformed into *Escherichia coli* strain DH5 α and the resulting transformants were screened for vectors containing the appropriate insert. Plasmid inserts were confirmed by sequence analysis, performed by Genewiz.

The *proB* and *proA* genes from *S. enterica* were amplified by PCR as a single amplicon using GoTaq Green Master Mix (Promega) with primers, proAB_NcoI_F (5'-

GAGACCATGGCCATGAGTGACAGCCAGACG -3') and proAB_PstI_R (5'-GAGACTGCAGTTACGCACGAATCGTACC -3'). The PCR reaction was cleaned-up, digested with NcoI (New England BioLabs) and PstI (New England BioLabs), gel purified and ligated into pBAD24 (Guzman *et al.*, 1995) previously digested with the same restriction enzymes, forming pDM1457. Constructs were transformed into DH5 α and the resulting transformants were screened by PCR for the appropriate insert and confirmed by sequence analysis through Eton Bioscience Inc. The *proB* gene encoded by pDM1457 was altered by site-directed mutagenic PCR using the primer proAB_D107N (5'-CGGGCAGATGCTGTTGACGCGTGCGAATATGGAAGACAGAGAGCGCTTTCTG -3') and *PfuUltra* High-Fidelity DNA polymerase (Agilent), forming pDM1462. As a result, basepair 319 of *proB* was changed from G-to-A, altering the encoded protein to ProB^{D107N}, consistent with a previously reported feedback-resistant variant of ProB from *E. coli* (31). The *proB*^{G319A} allele generated in pDM1462 was confirmed by sequence analysis, performed by Eton Bioscience Inc.

Purification of diaminopropionate ammonia-lyase (DpaL). Wild type *dpaL* cloned into pET-15b (pDM1451), containing an N-terminal polyhistidine-tag, was transformed into *E. coli* BL21-AI for overexpression and Ni-affinity purification. Cells were inoculated into 10 ml of superbroth containing ampicillin and grown overnight at 37°C. Overnight cultures were subcultured into 3 liters of superbroth containing ampicillin and grown at 37°C while shaking at 250 rpm until an OD₆₅₀ of 0.5 was reached. Expression was induced by adding arabinose (0.2 %) and IPTG (0.1 mM) and cultures were shifted to 30°C for 16 hours. Cells were pelleted at 4°C by centrifugation (15 min at 8,000 x g) and resuspended in buffer A (50 mM potassium phosphate pH 7.5 containing 100 mM sodium chloride, 5 mM imidazole and 10 % glycerol). Lysozyme (30 mg) and DNase (1 mg) were added to the cell suspension and incubated on ice for 30 minutes. Cells

were mechanically lysed using a French pressure cell (3 passes at 10,342 kPa). The resulting crude cell lysate was clarified by centrifugation (1 hr at 48,000 x g) and filtered through a 0.22- μ m polyethersulfone membrane (Whatman). The filtered lysate was added to a column containing 5 ml of Ni-nitriloacetic acid (NTA) Superflow resin (Qiagen). The column was washed with 50 ml of buffer A, then eluted with buffer B (buffer A + 500 mM imidazole) added to the column in a linear gradient over 10 column volumes. The resulting fractions were analyzed for purity, then pooled and dialyzed against 2 x 1 L of 20 mM Tris-HCl pH 8 containing 100 mM NaCl for 3 hrs, followed by 1 x 1 L of 20 mM Tris-HCl pH 8 containing 5 % glycerol overnight. Protein recovery as determined by the BCA assay (Pierce) was 4.2 mg/ml. Protein aliquots were frozen in liquid nitrogen and stored at -80°C.

Diaminopropionate ammonia-lyase (DpaL) assays. Diaminopropionate ammonia-lyase (DpaL) activity was measured by coupling pyruvate formation to NADH oxidation using lactate dehydrogenase (Sigma) and monitoring the decrease in absorbance at 340 nm as previously described (16). RidA was purified and its activity was confirmed previously (23). Assays consisted of 100 mM Tris-HCl pH 8, 0.25 mM NADH, and 5 U lactate dehydrogenase. DpaL and RidA were added at final monomeric concentrations of 0.2 μ M and 0.9 μ M, respectively, achieving a 1:3 ratio of oligomeric DpaL (dimer) to RidA (trimer). L-2,3-diaminopropionate was added at final concentrations ranging from 0 - 80 mM to initiate reactions. Each reaction consisted of 300 μ l and was monitored continuously at 22°C in a 96-well quartz plate using a SpectraMax M2 (Molecular Devices) microplate reader. Initial rates of NADH consumption were calculated from the linear change in absorbance at 340 nm over the course of 2 minutes following an initial non-linear phase (~60 seconds). A standard curve of NADH concentration based on A_{340} was used to calculate enzyme activity, reported as the initial rate of pyruvate formation in μ mol/min. Experiments were

performed in triplicate, and the resulting data were plotted using GraphPad Prism 5.0f and fit to the Michaelis-Menten model where appropriate.

Purification of γ -glutamate kinase (ProB) and glutamyl 5-semialdehyde dehydrogenase (ProA). ProB and ProA, encoded by the respective genes from *E. coli*, were purified from ASKA strains possessing the appropriate pCA24N constructs (32). The resulting proteins contained N-terminal hexahistidine tags. Strains were grown overnight at 37°C in 10 ml of superbrotch containing chloramphenicol. Overnight cultures were inoculated into 1 L each of superbrotch containing chloramphenicol and cultures were grown at 37°C with aeration until an OD₆₅₀ of 0.5 was reached. Expression was induced by adding IPTG (0.02 %) and cultures were shifted to the appropriate growth conditions. Expression of *proB* was performed at 37°C for 8 hours. Expression of *proA* was carried out at 20°C overnight (~16 hours). Cells were then harvested by centrifugation (15 min at 8,000 x *g*) and frozen at -80°C overnight. Cell pellets were thawed and resuspended in 50 mM Tris-HCl pH 7.2 containing 200 mM NaCl, 1 mM TCEP and 10 mM imidazole. Lysozyme (10 mg), DNase (0.25 mg) and phenylmethanesulfonyl fluoride (1 mg) were added and the cell suspensions were incubated on ice for 45 minutes. Cells were mechanically lysed using a French pressure cell (3 passes at 10,342 kPa). The resulting lysates were clarified by centrifugation and passed through 0.45- μ m polyethersulfone filters (Whatman). A 50 % slurry of Ni-NTA Superflow (Qiagen) resin was added (2 ml) to each lysate and incubated at 4°C with gentle shaking for 1 hour. The resin-lysate mixes were added to 10 ml Poly-Prep (Bio-Rad) chromatography columns and allowed to settle. Each column was washed with 30 ml of 50 mM Tris-HCl pH 7.2 containing 200 mM NaCl, 1 mM TCEP, 40 mM imidazole and 10 % glycerol. ProB and ProA were then eluted from each column by adding 5 ml of elution buffer (50 mM Tris-HCl pH 7.2 containing 200 mM NaCl, 1 mM TCEP, 300 mM imidazole and 10 % glycerol).

Fractions (0.5 ml) were collected and pooled together following SDS-PAGE analysis to determine protein purity. The buffer was exchanged with 50 mM Tris-HCl pH 7.2 containing 10 % glycerol using a PD-10 Sephadex G25 column (GE Healthcare). The concentration of ProB and ProA protein recovered as determined by the BCA assay (Pierce) was 1.2 mg/ml and 8.1 mg/ml, respectively. Protein aliquots were frozen in liquid nitrogen and stored at -80°C until use.

γ -glutamate kinase (ProB) and glutamyl 5-semialdehyde dehydrogenase (ProA) assays. *Continuous assays.* ProB and ProA were assayed together by measuring the rate of NADPH oxidation catalyzed by ProA, with the labile substrate (γ -glutamyl phosphate) generated from glutamate by ProB, as previously described (33). Assays consisted of 100 mM Tris-HCl pH 7.2 containing 16 mM MgCl₂, 4 mM ATP, 0.3 mM NADPH, 0.2 μ M ProB and 0.6 μ M ProA. L-2,3-diaminopropionate was added at various concentrations (0 – 10 mM) to determine the impact on ProAB activity. Reactions (300 μ l) were initiated by adding L-glutamate (12 mM) and the change in A₃₄₀ corresponding to NADPH oxidation was monitored for 5 minutes. Experiments were performed in a 96-well quartz plate using a SpectraMax M2 (Molecular Devices) microplate reader. Initial rates were calculated based on the extinction coefficient of NADPH ($\epsilon = 6,220 \text{ M}^{-1} \text{ cm}^{-1}$), and were reported in $\mu\text{mol}/\text{min}$. Representative data are presented in the text as the average and standard deviation of three independent experiments.

End-point assays. ProAB endpoint assays were completed in 0.5 ml reaction volumes consisting of 50 mM MES/HEPES/TAPS pH 7.5 containing 16 mM MgCl₂, 4 mM ATP, 1 mM NADPH, 0.4 μ M ProB and 2 μ M ProA. NADPH was excluded in a subset of reactions intended to accumulate γ -glutamyl phosphate. L-2,3-diaminopropionate (10 mM) was included when appropriate and L-glutamate (12 mM) was added to initiate reactions, followed by incubation at 30°C for 16 hours. Protein was removed using a 10,000 Da molecular weight cutoff

microcentrifuge filter (Millipore). Aliquots (20 μ l) of the resulting protein-free solution were derivatized with *o*-phthalaldehyde (OPA; 80 μ l) for 90 seconds and directly injected onto a Gemini C18 column (Phenomenex) pre-equilibrated with methanol-tetrahydrofuran-50 mM sodium acetate buffer pH 6.6 (24:1:75). The concentration of methanol was increased in a linear gradient to 80% over the course of 20 minutes while absorbance ($\lambda = 190 - 600$ nm) and fluorescence (Ex: 340 nm; Em: 455 nm) were monitored in tandem using the SPD-M20A (Shimadzu) and RF-20Axs (Shimadzu) detectors, respectively. Peaks corresponding to all known reaction components were accounted for. In an alternative approach to derivatization and HPLC analysis, protein-free reaction aliquots were submitted directly for LC/MSD-TOF analysis at the University of Wisconsin Biotechnology Center (Madison, WI) and were analyzed in the positive mode following reverse phase separation.

Pantothenate synthetase (PanC) assays. PanC was provided by J. V. Bazarro and was purified as previously described (34).

Continuous assays. PanC assays were performed using a coupled enzyme system according to previous reports (34, 35). Briefly, the ATP-dependent ligation of pantoate to β -alanine produced AMP. AMP and ATP were converted to 2 moles of ADP by myokinase. The resulting ADP was used to accept a phosphate from phosphoenolpyruvate in a reaction catalyzed by pyruvate kinase, generating pyruvate. Finally, lactate dehydrogenase catalyzed the oxidation of NADH to reduce pyruvate to lactate.

Reactions (200 μ l) consisted of 100 mM Tris-HCl pH 7.5 containing 10 mM MgCl₂, 0.3 mM NADH, 1.5 mM phosphoenolpyruvate, 2.5 mM ATP, 5 U myokinase, 5 U pyruvate kinase, 5 U lactate dehydrogenase, 4 mM pantoate and 0.05 μ M PanC. L-2,3-diaminopropionate and/or β -alanine were added at increasing concentrations to initiate reactions. Assays were performed in a

96-well quartz plate and monitored for 5 minutes using a SpectraMax M2 (Molecular Devices) microplate reader. Initial rates were calculated from the change in A_{340} corresponding to NADH oxidation. Based on the coupling assay design, 1 mol of pantothenate (or pantothenate analog) was produced per 2 moles of NADH oxidized. A standard curve of A_{340} plotted as a function of NADH concentration was used to calculate rates, reported as nmol NADH consumed per min. The resulting data were fit with a curve using the Michaelis-Menten equation in GraphPad Prism 5.0f.

Endpoint assays. PanC endpoint assays were performed in 0.5 mls and consisted of 50 mM potassium phosphate buffer pH 8 containing 10 mM $MgCl_2$, 2.5 mM ATP, 4 mM pantoate and 1 μ M PanC. L-2,3-diaminopropionate (5 mM) was added when appropriate. Reactions were initiated by adding β -alanine and assays were incubated at 28°C for 16 hours. PanC was removed from the reactions using a 30,000 Da molecular weight cutoff centrifuge filter (Millipore). Aliquots (40 μ l) of the resulting protein-free solution were mixed with OPA (80 μ l) and allowed to react for 90 seconds at room temperature, while the remainder of the sample was frozen at -20°C. Derivatized samples were then analyzed by reverse-phase high-performance liquid chromatography using the Shimadzu Prominence HPLC system. Absorbance and fluorescence were monitored in tandem by using the SPD-M20A photo diode array detector ($\lambda = 190 - 600$ nm) and the RF-20Axs fluorescence detector (Ex: 340 nm; Em: 455 nm), respectively. A Gemini C18 column (Phenomenex) equipped with a C18 SecurityGuard (Phenomenex) cartridge was pre-equilibrated with 60 % mobile phase A (water containing 0.1 % trifluoroacetic acid pH 2.5) and 40 % mobile phase B (methanol containing 0.1 % trifluoroacetic acid pH 2.5). Samples (20 μ l) were introduced onto the column at a flowrate of 1 ml/min and eluted by increasing the concentration of mobile phase B to 100 % over 20 minutes. Samples displaying unique product peaks indicative of Dap-derivatization were identified for follow-up analysis by mass spectrometry (MS). The

corresponding non-derivatized samples and appropriate controls were submitted for MS analysis at the University of Wisconsin Biotechnology Center (Madison, WI). Crude samples (5 μ l) were pre-separated by liquid chromatography using a Zorbax SB-C18 column (Agilent) and mass data were obtained by MSD-TOF analyzed in the positive mode.

Threonine dehydratase (IlvA) assays. IlvA was provided by K. Hodge-Hanson and was purified following a previously described protocol (36). Reactions (300 μ l) consisted of 50 mM potassium phosphate pH 8 and 65 nM IlvA. L-2,3-diaminopropionate was added at increasing concentrations. Experiments were performed in triplicate and measured in a 96-well quartz plate using a SpectraMax M2 (Molecular Devices) microplate reader. Reactions were initiated by adding L-threonine and monitored continuously at 230 nm for 60 seconds. Initial rates were determined based on the increase in A_{230} corresponding to α -ketobutyrate (AKB) production. A standard curve of AKB concentrations relative to A_{230} was generated and used to calculate reaction rates, reported as μ mol of AKB produced per minute. The data, reported as the average and standard deviation of three independent experiments, were fit with curves corresponding to a mixed model of inhibition using GraphPad Prism 5.0f. Lineweaver-Burke plots were generated and used to confirm the mode of inhibition.

3.4 RESULTS AND DISCUSSION

L-2,3-diaminopropionate elicits a proline requirement in wild type *S. enterica*. Wild type *S. enterica* (DM14828) failed to grow in glucose minimal medium containing 0.25 mM Dap within 12 hours (Figure 3.1A). Growth of the wild type strain resumed after 12 hours, whereas a *dpaL* mutant (DM14881) failed to grow within 24 hours, suggesting DpaL was required to overcome Dap inhibition (data not shown). To understand the growth defect, the wild type strain

was embedded in soft-agar overlays on solid minimal glucose medium containing 1 mM Dap. Each of the 20 common amino acids and various vitamins were individually spotted on the agar surface. Growth stimulation was assessed after overnight incubation at 37°C. Of the supplements spotted, only L-proline stimulated growth. Liquid growth studies confirmed that 1 mM L-proline eliminated the growth inhibition caused by Dap (Figure 3.1A). In addition to serving as a building block of proteins, proline behaves as an osmoprotectant in many prokaryotes and eukaryotes (37). The alternative osmolyte, glycine betaine (1 mM), was added to cultures of wild type *S. enterica* grown in the presence of 0.25 mM Dap. Glycine betaine failed to restore growth in the presence of Dap (data not shown), suggesting proline acted by a mechanism other than osmoprotection.

In *E. coli* and *S. enterica*, proline biosynthesis is initiated by γ -glutamyl kinase (ProB; EC 2.7.2.11), catalyzing the phosphorylation of glutamate to generate γ -glutamyl phosphate (Figure 3.1B). γ -glutamyl phosphate is labile and susceptible to nucleophilic attack, including spontaneous cyclization in solution (38). ProB is thought to form an enzyme aggregate with the second enzyme in the proline biosynthetic pathway, glutamate 5-semialdehyde dehydrogenase (ProA; EC 1.2.1.41), to avoid exposure of the labile intermediate to the cellular milieu (38). A previous report described variants of ProB or ProA in *E. coli* that exacerbated γ -glutamyl phosphate accumulation, leading to selective reactivity with thiol containing amino acids *in vivo* and *in vitro* (39). It was plausible that the primary amine attached to the β -carbon of Dap reacted with γ -glutamyl phosphate, or the subsequent proline intermediate, glutamate 5-semialdehyde. This scenario was supported by literature describing reactivity between Dap and electrophilic carbonyl groups (11). The *E. coli* ProA and ProB enzymes were purified from strains harboring the appropriate ASKA (A Complete Set of *E. coli* K-12 ORF Archive) library constructs described by Kitagawa *et al.* (32). The impact of Dap on ProAB activity was tested *in vitro* by monitoring the conversion of

glutamate (12 mM) to glutamate 5-semialdehyde based on the ProAB-dependent oxidation of NADPH ($\lambda_{\max} = 340$ nm). ProAB activity was not significantly different with (6.2 ± 0.2 nmol NADPH oxidized/ $\mu\text{M ProB min}^{-1}$) or without (5.6 ± 0.2 nmol NADPH oxidized/ $\mu\text{M ProB min}^{-1}$) Dap (10 mM) included in the assay, indicating that Dap did not inhibit γ -glutamyl kinase or glutamate 5-semialdehyde dehydrogenase activities directly. Similar assays consisting of ProAB and glutamate (with and without NADPH) were incubated overnight in the presence of Dap (10 mM) and analyzed by HPLC or submitted for LC-MS analysis to determine if a Dap-conjugated metabolite was formed with γ -glutamyl phosphate or glutamate 5-semialdehyde. Prior to HPLC analysis, reactions were derivatized with *o*-phthalaldehyde (OPA), and peaks corresponding to glutamate (Ex: 340 nm; Em: 455 nm) and Dap ($\lambda_{\max} = 420$ nm) were readily detected, while no additional peaks that would reflect a Dap-derivatized proline intermediate were detected (data not shown). Mass spectrometry similarly failed to identify a novel Dap derivative.

It was possible that Dap inhibited the final enzyme in the proline pathway, pyrroline 5-carboxylate reductase (ProC; EC 1.5.1.2). ProC catalyzes the NAD(P)H-dependent reduction of 1-pyrroline-5-carboxylate (P5C) to proline (Figure 3.1B). Previous reports demonstrated that strains lacking ProC activity excreted P5C, capable of cross-feeding a *proAB* null mutant strain (Berg and Rossi, 1974). Wild type strains of *E. coli* and *S. enterica* do not excrete P5C or proline due to tight regulation of flux through the proline pathway (40). A wild type *E. coli* strain carrying a feedback-resistant variant of ProB (ProB^{D107N}) did cross-feed a *proC* null mutant strain (31). Based on these phenotypic reports, experiments were designed to test whether Dap altered the cross-feeding by P5C or proline. A plasmid encoding *S. enterica* ProAB^{D107N} downstream of the arabinose-inducible promoter of pBAD24 was generated. The resulting construct (pDM1462) was

transformed into wild type and *proC* mutant strains, generating producer strains intended to excrete proline (DM15352) and P5C (DM15356), respectively.

A series of feeding experiments were performed and the data, some of it shown in Table 2, supported the hypothesis that Dap inhibits ProC *in vivo*. The wild type strain containing pDM1462 (DM15352) was able to cross-feed *proAB* (DM5846) and *proC* (TT9667) null mutants overlaid on glucose minimal medium (with or without DAP) containing arabinose. These data indicated that DM15352 excreted proline. The corresponding empty vector control (DM15353) failed to stimulate growth (data not shown). The *proC* mutant containing pDM1462 (DM15356) failed to cross-feed the *proC* null strain on either medium, consistent with the absence of a functional ProC (Table 3.2). Critically, when inoculated into a lawn of a *proAB* mutant on minimal medium, strain DM15356 both grew at the inoculation site and stimulated growth of the lawn. The growth of DM15356 indicated that a *proAB* mutant (DM5846) generated enough proline from the P5C provided (by DM15356) to feed the inoculating strain. In contrast, when Dap was added to the medium, DM15356 failed to grow at the site of inoculation or stimulate growth of the *proAB* reporter strain. The simplest explanation for these results in total is that Dap inhibited ProC in DM5846, and prevented it from a) growing, and b) producing proline to feed DM15356. The inhibition of ProC-dependent growth by Dap was always overcome by feeding proline directly. Because these observations were made *in vivo*, it is formally possible that the inhibition of ProC by Dap occurs indirectly following an interaction between Dap and another component of the cellular milieu.

Mutants lacking DpaL are sensitive to Dap due to altered pantothenate synthetase activity. The data above indicated that proline biosynthesis is the first critical target of Dap *in vivo*. If DpaL was removed from the metabolic network, additional Dap would accumulate and

potentially uncover distinct targets of Dap toxicity. Deleting the gene encoding DpaL prevented growth of *S. enterica* in the presence of 0.25 mM Dap and 1 mM proline (Figure 3.2). Nutrient requirements of the *dpaL* mutant strain (DM14881) were determined on solid minimal glucose medium containing 1mM Dap and 1 mM proline. Only the coenzyme A precursor, pantothenate, stimulated growth. Liquid analysis corroborated this phenotype and showed that pantothenate (100 μ M), in addition to proline, was required for growth of a *dpaL* mutant strain in the presence of Dap (Figure 3.2). These data were consistent with the absence of DpaL causing increased accumulation of Dap that led to the inhibition of pantothenate biosynthesis, in addition to proline biosynthesis.

In bacteria, pantothenate is generated by pantothenate synthetase (PanC; EC 6.3.2.1) through the ATP-dependent ligation of β -alanine and pantoate. PanC was considered a potential target of inhibition by Dap due to the similarity of β -alanine and Dap, which differ by a single amino group bound to the α -carbon of Dap. An untargeted screen of amino acid inhibitors of PanC from *E. coli* offered preliminary evidence that Dap could negatively affect pantothenate synthetase activity *in vitro* (41). Similarly, growth experiments with *Corynebacterium diphtheriae* demonstrated that Dap antagonized the growth stimulation afforded by β -alanine (42). *S. enterica* PanC activity was measured *in vitro* by a coupled assay monitoring the oxidation of NADH (A_{340nm}) in the presence of Dap. Control experiments showed Dap had no effect on the activity of the coupling enzymes. When Dap was added to PanC reactions lacking β -alanine, a background rate of PanC-dependent NADH oxidation was detected (Figure 3.3). PanC affinity for Dap ($K_m = 8.1$ mM) was approximately ten-fold less than for β -alanine ($K_m = 0.66$ mM; Bazurto and Downs, 2014). These data suggested Dap could interfere with pantothenate production *in vivo*, thereby eliciting a pantothenate requirement when Dap accumulation was provoked.

The cause of detectable PanC activity when Dap, but not β -alanine, was present in the reactions was investigated. It was formally possible that the stock of Dap had contaminating β -alanine or alternatively that Dap was serving as a substrate for PanC, leading to the formation of a pantothenate analog. PanC reactions were set up containing the canonical PanC substrates, or Dap in lieu of β -alanine, and the reaction products were analyzed in each case. The completed reactions, and the corresponding unreacted controls, were derivatized with OPA and separated by high performance liquid chromatography. Comparing HPLC traces between the Dap stock and a β -alanine standard ruled out β -alanine contamination in the Dap stock and indicated that a unique PanC product had been formed when Dap was present (data not shown). The identity of the Dap-dependent PanC product was identified by mass spectrometry. Aliquots from the PanC reactions described above were analyzed by electrospray ionization mass spectrometry in the positive mode after elution from a liquid chromatography column. The data showed that, as expected, pantothenate was formed in reactions containing β -alanine ($m/z = 220$; Figure 3.4A). In reactions containing Dap instead of β -alanine, no pantothenate was formed and a major chemical species with a mass-to-charge ratio ($m/z = 235$) that matched the predicted product formed through the condensation of pantoate and Dap was present (Figure 3.4B). Together these data established that Dap had the ability to inhibit pantothenate production in *S. enterica*, and suggested that *in vivo*, Dap would be converted to the pantothenate analog, 2-aminopantothenate, at some frequency. The observation that intact DpaL enzyme prevented Dap from causing a pantothenate limitation in *S. enterica* highlighted the role of DpaL in mitigating Dap stress.

RidA quenches 2AA produced by DpaL *in vitro*. The α,β -elimination reaction catalyzed by DpaL acting on Dap as a substrate was predicted to proceed through a 2AA intermediate, followed by spontaneous conversion to pyruvate (18). This suggested the DpaL enzyme could

belong to a growing class of PLP-dependent enzymes that contribute to 2AA stress in the absence of RidA. Addition of RidA to enzymatic reactions that released 2AA into solution led to detectable increases in the rate of 2AA hydrolysis to pyruvate *in vitro* (23, 36). Recombinant DpaL protein was purified and assayed in the presence and absence of RidA. In the absence of RidA, recombinant DpaL displayed specific activity (4.9 $\mu\text{mol}/\text{min}/\text{mg}$) consistent with previous reports (Figure 3.5) (15). Adding RidA to the reaction at a 3:1 active site ratio of RidA (trimer) to DpaL (dimer) resulted in a ~64 % increase in the rate of pyruvate formation at 6 mM Dap (10.8 nmol/min without RidA versus 17.3 nmol/min with RidA) (Figure 3.5). At high concentrations of Dap (≥ 48 mM), RidA had no effect on the rate of pyruvate formation (Figure 3.5). A possible interpretation of these data is that when Dap concentrations are elevated, RidA hydrolase activity becomes inhibited. A physiological significance of this finding is unlikely given the artificially high concentrations of Dap required to inhibit RidA *in vitro*. Nonetheless, this observation differs from the previously observed direct sequestration of 2AA by cysteine (23, 43), in that elevated concentrations of Dap only inhibited reactions containing RidA. The generation and release of 2AA by DpaL *in vitro* suggested that this enzyme contributed to 2AA stress *in vivo*.

DpaL influences the sensitivity of a *ridA* strain to Dap. The potential for DpaL to contribute to 2AA stress in *S. enterica* was tested by growing a *ridA* strain (DM14829) with 0.25 mM Dap. In the presence of Dap a *ridA* mutant had a growth defect that could not be rescued by proline and/or pantothenate (Figure 3.6). To clarify the cause of the growth defect, a *ridA dpaL* double mutant strain (DM14882) was constructed and tested under appropriate growth conditions. Disrupting *dpaL* in a *ridA* background eliminated Dap sensitivity of the *ridA* strain when proline and pantothenate were included in the growth medium (Figure 3.6). When compared to data presented in Figure 3.2, it was apparent that growth of the *ridA dpaL* mutant was not restored to

the same level as the *dpaL* single mutant despite proline and pantothenate supplementation, implicating additional nutrient limitation(s) caused by the *ridA* mutation. Isoleucine, added in combination with proline and pantothenate, restored full growth of the *ridA dpaL* strain (Figure 3.6). Importantly, growth of the *ridA* strain (DM14829) was not restored wherever Dap was added to the growth medium. These data were consistent with a model wherein DpaL degrades Dap and releases 2AA into the cellular milieu, leading to 2AA stress and growth inhibition in the absence of RidA. This scenario was supported by the finding that the addition of glycine partially alleviated the Dap sensitivity of a *ridA* strain (data not shown). Glycine relieves the growth inhibition caused by 2AA damage of serine hydroxymethyltransferase (GlyA; EC 2.1.2.1) in strains lacking RidA (22, 44).

Previous work showed isoleucine biosynthesis is negatively impacted by 2AA produced from endogenous serine in the absence of *ridA* (19, 20, 45). Endogenously generated 2AA inhibited the final step of the isoleucine pathway catalyzed by transaminase B (IlvE; EC 2.6.1.42), and reduced flux to isoleucine without causing an isoleucine-limited growth defect in minimal glucose medium (19, 20). It was possible that a combined effect of 2AA (from serine) and Dap on the isoleucine biosynthetic pathway explained the stimulatory effect of isoleucine on growth of the *ridA dpaL* (DM14882) strain in the presence of Dap. Biosynthetic threonine dehydratase (IlvA) catalyzes the first committed step in isoleucine biosynthesis and is susceptible to inhibition by amino acids structurally related to threonine, including serine (46, 47). When monitored *in vitro*, Dap displayed mixed inhibition of IlvA with respect to threonine ($K_i = 1.7$ mM) (Figure 3.7). The conversion of Dap to pyruvate by IlvA could not be detected under the conditions tested (data not shown). The mixed nature of inhibition is consistent with the ability of amino acids to bind to allosteric sites on the enzyme while simultaneously competing with threonine substrate for access

to the IlvA active site (47). *In vivo* data demonstrated a role for RidA in preventing metabolic stress caused by 2AA generated from the degradation of Dap mediated by DpaL. Abolishing DpaL in a *ridA* strain alleviated 2AA stress caused by Dap, but uncovered a minor isoleucine requirement likely stemming from the combined inhibition of IlvA by Dap and damage to the isoleucine pathway caused by Dap-independent 2AA production.

Conclusions. Results presented in this report shed light on the mechanisms of Dap toxicity in *S. enterica* and demonstrated the importance of DpaL and RidA in mitigating sensitivity to Dap (Figure 3.8). *In vivo*, Dap elicited a proline requirement in wild type *S. enterica* despite the presence of an intact DpaL enzyme. In the absence of DpaL, Dap accumulation led to the inhibition of pantothenate synthetase, causing a pantothenate limitation. Lastly, the inhibition of threonine dehydratase by Dap contributed to a detectable isoleucine deficiency in the absence of both DpaL and RidA.

These insights raise questions as to whether or not Dap inhibits similar metabolic processes in other organisms. Enteric bacteria including *E. coli* and *S. enterica* maintain low levels of intracellular proline and are unable to induce proline biosynthesis in response to osmotic stress, instead relying on uptake from the extracellular environment (37). Therefore, enteric bacteria may be particularly susceptible to disrupted proline biosynthesis caused by Dap in the absence of an abundant extracellular supply of proline. *Staphylococcus aureus* is known to produce Dap as a key intermediate in siderophore biosynthesis when grown in the presence of mammalian serum (12), yet displays a conditional proline auxotrophy when grown under these conditions despite the presence of all genes necessary for proline production in the genome (48). Perhaps our findings highlight the need to temporally coordinate Dap and proline production to prevent inhibitory cross-talk, thereby favoring iron acquisition (i.e. Dap production) over proline production in the context

of infection. The finding that Dap specifically inhibits pyrroline 5-carboxylate reductase (ProC) may in part explain the presence of alternative routes to proline in *S. aureus* speculated to be induced under low-iron conditions (48), where Dap production would likely be elevated.

The conserved function of pantothenate synthetase among bacteria, plants and fungi suggests that organisms that rely on *de novo* coenzyme A production may be sensitive to excessive Dap accumulation. *Mycobacterium tuberculosis* was attenuated when PanC activity was disrupted, confirming that *de novo* pantothenate biosynthesis is important for the pathogenic lifestyle of some organisms (49, 50). Furthermore, these findings may inform future drug discovery efforts, as the majority of pantothenate synthetase inhibitors described to date have been analogues of ATP or pantoate (35). Although Dap serves as a precursor to many secondary metabolites and antibiotics, data presented here and elsewhere (42, 51) show that Dap itself elicits antimicrobial effects and may influence microbial community dynamics in the environment. The potential toxicity of Dap suggests that organisms that produce Dap endogenously likely regulate Dap concentrations in the cell, or have developed alternative metabolic strategies to circumvent nutrient limitations caused by Dap.

Diaminopropionate ammonia-lyase represents an additional generator of endogenous 2AA in *Salmonella*. These results confirm a pattern of 2AA generation mediated by fold-type II PLP-dependent enzymes acting on amino acid substrates. Homologs of DpaL have not been observed in any eukaryotic organisms to date, suggesting the dedicated capacity to degrade Dap is likely unique to prokaryotes (13, 18). However, many fold-type II PLP enzymes are found throughout each domain of life, suggesting that several mechanisms of endogenous 2AA production likely exist. This report corroborates previous findings related to cysteine detoxification by CdsH, showing that RidA participates in amino acid detoxification by preventing concomitant 2AA

stress. These findings also raise broader questions regarding the significance of 2AA. *S. enterica* degrades toxic levels of serine by an Fe-S dependent mechanism catalyzed by serine dehydratase (SdaA; EC 4.3.1.17). Our unpublished work and a recent report confirmed that the SdaA enzyme does not release a 2AA substrate for RidA (52). In light of alternative options, why employ a mechanism that releases potentially damaging 2AA? Perhaps RidA hydrolase activity confers a selective advantage to PLP-dependent 2AA release mechanisms that are less susceptible to oxidative damage in comparison to Fe-S dependent mechanisms. Alternatively, free 2AA may interact with cellular components in order to serve as an important regulatory signal akin to hydrogen peroxide (53). Regardless, the frequent co-occurrence of PLP-dependent eliminases and RidA homologs among distantly related organisms supports the argument for an evolutionarily conserved role of RidA in preventing 2AA stress (54).

ACKNOWLEDGEMENTS

The authors would like to thank Jannell Bazarro for the purified PanC protein and Kelsey Hodge-Hanson for the purified IlvA protein that was used in this study. This work was supported by competitive grant GM095837 from the National Institutes of Health (DMD).

3.5 REFERENCES

1. Linster CL, Van Schaftingen E, Hanson AD. 2013. Metabolite damage and its repair or pre-emption. *Nat Chem Biol* 9:72–80.
2. de Lorenzo V, Sekowska A, Danchin A. 2015. Chemical reactivity drives spatiotemporal organisation of bacterial metabolism. *FEMS Microbiol Rev* 39:96–119.
3. Wellner D, Meister A. 1981. A survey of inborn errors of amino acid metabolism and transport in man. *Annu Rev Biochem* 50:911–968.

4. Zhang X, Newman E. 2008. Deficiency in L-serine deaminase results in abnormal growth and cell division of *Escherichia coli* K-12. *Mol Microbiol* 69:870–881.
5. Park S, Imlay JA. 2003. High levels of intracellular cysteine promote oxidative DNA damage by driving the Fenton reaction. *J Bacteriol* 185:1942–1950.
6. Oguri T, Schneider B, Reitzer L. 2012. Cysteine catabolism and cysteine desulfhydrase (CdsH/STM0458) in *Salmonella enterica* serovar Typhimurium. *J Bacteriol* 194:4366–4376.
7. Rao SL. 1978. Sensitive and specific colorimetric method for determination of alpha,beta-diaminopropionic acid and *Lathyrus sativus* neurotoxin. *Anal Biochem* 86:386–395.
8. Zhao C, Song C, Luo Y, Yu Z, Sun M. 2008. L-2,3-Diaminopropionate: one of the building blocks for the biosynthesis of Zwittermicin A in *Bacillus thuringiensis* subsp. kurstaki strain YBT-1520. *FEBS Lett* 582:3125–3131.
9. Beasley FC, Cheung J, Heinrichs DE. 2011. Mutation of L-2, 3-diaminopropionic acid synthase genes blocks staphyloferrin B synthesis in *Staphylococcus aureus*. *BMC Microbiol* 11:199.
10. Xu Z, Sun Z, Li S, Xu Z, Cao C, Xu Z, Feng X, Xu H. 2015. Systematic unravelling of the biosynthesis of poly (L-diaminopropionic acid) in *Streptomyces albulus* PD-1. *Sci Rep* 5:17400.
11. Audic N, Potier G, Sasaki NA. 2013. New 2,3-diaminopropionic acid inhibitors of AGE and ALE formation. *Org Biomol Chem* 11:773–780.
12. Kobylarz MJ, Grigg JC, Takayama SJ, Rai DK, Heinrichs DE, Murphy MEP. 2014. Synthesis of L-2,3-diaminopropionic acid, a siderophore and antibiotic precursor. *Chem Biol* 21:379–388.
13. Kalyani JN, Ramachandra N, Kachroo AH, Mahadevan S, Savithri HS. 2012. Functional analysis of the genes encoding diaminopropionate ammonia lyase in *Escherichia coli* and *Salmonella enterica* serovar Typhimurium. *J Bacteriol* 194:5604–5612.
14. Nagasawa T, Satoda T, Tanizawa K, Yamada H. 1987. Diaminopropionate ammonia-lyase Of *Salmonella typhimurium*, p. 229–232. In *Biochemistry of Vitamin B6*. Springer.
15. Khan F, Jala VR, Rao NA, Savithri H. 2003. Characterization of recombinant diaminopropionate ammonia-lyase from *Escherichia coli* and *Salmonella typhimurium*. *Biochem Biophys Res Commun* 306:1083–1088.

16. Kalyani JN, Bisht S, Lakshmikanth M, Murthy MRN, Savithri HS. 2013. Identification of key amino acid residues in the catalytic mechanism of diaminopropionate ammonialyase from *Salmonella typhimurium*. FEBS J 280:5039–5051.
17. Rajaram V, Rajaganapathi J, Khan F, Savithri HS, Murthy MRN. 2003. Crystallization and preliminary X-ray diffraction studies on recombinant diaminopropionate ammonia lyase from *Escherichia coli*. Acta Crystallogr D Biol Crystallogr D59:1668–1669.
18. Bisht S, Rajaram V, Bharath SR, Kalyani JN, Khan F, Rao AN, Savithri HS, Murthy MRN. 2012. Crystal structure of *Escherichia coli* diaminopropionate ammonia-lyase reveals mechanism of enzyme activation and catalysis. J Biol Chem 287:20369–20381.
19. Schmitz G, Downs DM. 2004. Reduced transaminase B (IlvE) activity caused by the lack of *yjgF* is dependent on the status of threonine deaminase (IlvA) in *Salmonella enterica* serovar Typhimurium. J Bacteriol 186:803–810.
20. Christopherson MR, Schmit GE, Downs DM. 2008. YjgF is required for isoleucine biosynthesis when *Salmonella enterica* is grown on pyruvate medium. J Bacteriol 190:3057–3062.
21. Flynn JM, Downs DM. 2013. In the absence of RidA, endogenous 2-aminoacrylate inactivates alanine racemases by modifying the pyridoxal 5'-phosphate cofactor. J Bacteriol 195:3603–3609.
22. Flynn JM, Christopherson MR, Downs DM. 2013. Decreased coenzyme A levels in *ridA* mutant strains of *Salmonella enterica* result from inactivated serine hydroxymethyltransferase: *ridA* mutants are deficient in one carbon metabolism. Mol Microbiol 89:751–759.
23. Ernst DC, Lambrecht JA, Schomer RA, Downs DM. 2014. Endogenous synthesis of 2-aminoacrylate contributes to cysteine sensitivity in *Salmonella enterica*. J Bacteriol 196:3335–3342.
24. Way JC, Davis MA, Morisato D, Roberts DE, Kleckner N. 1984. New Tn10 derivatives for transposon mutagenesis and for construction of *lacZ* operon fusions by transposition. Gene 32:369–379.
25. Castilho BA, Olfson P, Casadaban MJ. 1984. Plasmid insertion mutagenesis and *lac* gene fusion with mini-mu bacteriophage transposons. J Bacteriol 158:488–495.
26. Balch WE, Wolfe RS. 1976. New approach to the cultivation of methanogenic bacteria: 2-mercaptoethanesulfonic acid (HS-CoM)-dependent growth of *Methanobacterium ruminantium* in a pressurized atmosphere. Appl Environ Microbiol 32:781–791.

27. Schmieger H. 1972. Phage P22-mutants with increased or decreased transduction abilities. *Mol Gen Genet MGG* 119:75–88.
28. Chan RK, Botstein D, Watanabe T, Ogata Y. 1972. Specialized transduction of tetracycline resistance by phage P22 in *Salmonella typhimurium*. II. Properties of a high-frequency-transducing lysate. *Virology* 50:883–898.
29. Downs DM, Petersen L. 1994. *apbA*, a new genetic locus involved in thiamine biosynthesis in *Salmonella typhimurium*. *J Bacteriol* 176:4858–4864.
30. Datsenko KA, Wanner BL. 2000. One-step inactivation of chromosomal genes in *Escherichia coli* K-12 using PCR products. *Proc Natl Acad Sci* 97:6640–6645.
31. Dandekar AM, Uratsu SL. 1988. A single base pair change in proline biosynthesis genes causes osmotic stress tolerance. *J Bacteriol* 170:5943–5945.
32. Kitagawa M, Ara T, Arifuzzaman M, Ioka-Nakamichi T, Inamoto E, Toyonaga H, Mori H. 2006. Complete set of ORF clones of *Escherichia coli* ASKA library (A Complete Set of *E. coli* K-12 ORF Archive): Unique Resources for Biological Research. *DNA Res* 12:291–299.
33. Pérez-Arellano I, Gil-Ortiz F, Cervera J, Rubio V. 2004. Glutamate-5-kinase from *Escherichia coli*: gene cloning, overexpression, purification and crystallization of the recombinant enzyme and preliminary X-ray studies. *Acta Crystallogr D Biol Crystallogr* 60:2091–2094.
34. Bazurto JV, Downs DM. 2014. Amino-4-imidazolecarboxamide ribotide directly inhibits coenzyme A biosynthesis in *Salmonella enterica*. *J Bacteriol* 196:772–779.
35. Tuck KL, Saldanha SA, Birch LM, Smith AG, Abell C. 2006. The design and synthesis of inhibitors of pantothenate synthetase. *Org Biomol Chem* 4:3598.
36. Lambrecht JA, Flynn JM, Downs DM. 2012. Conserved YjgF protein family deaminates reactive enamine/imine intermediates of pyridoxal 5'-phosphate (PLP)-dependent enzyme reactions. *J Biol Chem* 287:3454–3461.
37. Csonka LN. 1989. Physiological and genetic responses of bacteria to osmotic stress. *Microbiol Rev* 53:121–147.
38. Gamper H, Moses V. 1974. Enzyme organization in the proline biosynthetic pathway of *Escherichia coli*. *Biochim Biophys Acta* 354:75–87.

39. Veeravalli K, Boyd D, Iverson BL, Beckwith J, Georgiou G. 2011. Laboratory evolution of glutathione biosynthesis reveals natural compensatory pathways. *Nat Chem Biol* 7:101–105.
40. Berg CM, Rossi JJ. 1974. Proline excretion and indirect suppression in *Escherichia coli* and *Salmonella typhimurium*. *J Bacteriol* 118:928–934.
41. Miyatake K, Nakano Y, Kitaoka S. 1978. Enzymological properties of pantothenate synthetase from *Escherichia coli* B. *J Nutr Sci Vitaminol (Tokyo)* 24:243–253.
42. Kjerulf-Jensen K, Schmidt V. 1945. The antigrowth effects of diaminopropionic acid on *Corynebacterium diphtheriae*. *Acta Pharmacol Toxicol (Copenh)* 1:346–350.
43. Kredich NM, Foote LJ, Keenan BS. 1973. The stoichiometry and kinetics of the inducible cysteine desulfhydrase from *Salmonella typhimurium*. *J Biol Chem* 248:6187–6196.
44. Ernst DC, Downs DM. 2016. 2-aminoacrylate stress induces a context-dependent glycine requirement in *ridA* strains of *Salmonella enterica*. *J Bacteriol* 198:536–543.
45. Lambrecht JA, Schmitz GE, Downs DM. 2013. RidA proteins prevent metabolic damage inflicted by PLP-dependent dehydratases in all domains of life. *MBio* 4:e00033-13.
46. Harris CL. 1981. Cysteine and growth inhibition of *Escherichia coli*: threonine deaminase as the target enzyme. *J Bacteriol* 145:1031–1035.
47. Burns RO, Hofler JG, Luginbuhl GH. 1979. Threonine deaminase from *Salmonella typhimurium*. Substrate-specific patterns of inhibition in an activator site-deficient form of the enzyme. *J Biol Chem* 254:1074–1079.
48. Li C, Sun F, Cho H, Yelavarthi V, Sohn C, He C, Schneewind O, Bae T. 2010. CcpA mediates proline auxotrophy and Is required for *Staphylococcus aureus* pathogenesis. *J Bacteriol* 192:3883–3892.
49. Kumar A, Casey A, Odingo J, Kesicki EA, Abrahams G, Vieth M, Masquelin T, Mizrahi V, Hipskind PA, Sherman DR, Parish T. 2013. A high-throughput screen against pantothenate synthetase (PanC) identifies 3-biphenyl-4-cyanopyrrole-2-carboxylic acids as a new class of inhibitor with activity against *Mycobacterium tuberculosis*. *Plos One* 8:e72786.
50. Devi PB, Samala G, Sridevi JP, Saxena S, Alvala M, Salina EG, Sriram D, Yogeewari P. 2014. Structure-guided design of thiazolidine derivatives as *Mycobacterium tuberculosis* pantothenate synthetase inhibitors. *ChemMedChem* 9:2538–2547.

51. Garcia-Hernandez M, Kun E. 1957. Inhibition of enzymic transamination of aspartic acid by hydroxyaspartate, 2,3-diaminosuccinate and 2,3-diaminopropionate. *Biochim Biophys Acta* 24:78–82.
52. Xu XL, Grant GA. 2016. Mutagenic and chemical analyses provide new insight into enzyme activation and mechanism of the type 2 iron-sulfur l-serine dehydratase from *Legionella pneumophila*. *Arch Biochem Biophys* 596:108–117.
53. Rhee SG. 2006. Cell signaling. H₂O₂, a necessary evil for cell signaling. *Science* 312:1882–1883.
54. Niehaus TD, Gerdes S, Hodge-Hanson K, Zhukov A, Cooper AJ, ElBadawi-Sidhu M, Fiehn O, Downs DM, Hanson AD. 2015. Genomic and experimental evidence for multiple metabolic functions in the RidA/YjgF/YER057c/UK114 (Rid) protein family. *BMC Genomics* 16:382.
55. Hughes KT, Roth JR. 1985. Directed formation of deletions and duplications using Mud (*Ap*, *lac*). *Genetics* 109:263–282.
56. Guzman LM, Belin D, Carson MJ, Beckwith J. 1995. Tight regulation, modulation, and high-level expression by vectors containing the arabinose pBAD promoter. *J Bacteriol* 177:4121–4130.

TABLE 3.1. Bacterial strains and plasmids

Strain or plasmid	Genotype or description	Source
Strains		
TT9667	<i>proC693::MudA</i>	Lab collection
DM5846	<i>proAB::Tn10d(Tc)</i>	Lab collection
DM14224	<i>E. coli</i> BL21-AI / pDM1451	This study
DM14828	Wild type LT2	This study
DM14829	<i>ridA1::Tn10d(Tc)</i>	This study
DM14881	<i>dpaL::Kn</i>	This study
DM14882	<i>ridA1::Tn10d(Tc) dpaL::Kn</i>	This study
DM15352	Wt / pDM1462	This study
DM15353	Wt / pBAD24	This study
DM15356	<i>proC693::MudA</i> / pDM1462	This study
DM15357	<i>proC693::MudA</i> / pBAD24	This study
Plasmids		
pDM1451	pET15b - DpaL ^{Wt}	This study
pDM1457	pBAD24 - ProAB ^{Wt}	This study
pDM1462	pBAD24 - ProAB ^{D107N}	This study

Tn10d(Tc) indicates a transposition-defective mini-Tn10 (24). MudA indicates a transposition defective Mu element (55). Plasmids constructed using pET15b (Novagen) and pBAD24 (56) are described in the *Materials and methods*.

TABLE 3.2. Dap inhibits ProC *in vivo*

Reporter strain ^a	Media ^b	Producer strain ^c	
		Wt/pDM1462 (DM15352)	<i>proC</i> /pDM1462 (DM15356)
<i>proAB</i> (DM5846)	- Dap	+ ^d	+
	+ Dap	+	-
<i>proC</i> (TT9667)	- Dap	+	-
	+ Dap	+	-

^aProline auxotrophs served as reporter strains for P5C or proline utilization. Strains were grown in rich medium then embedded in soft-agar overlaid on minimal growth medium lacking proline.

^bGrowth was assessed on minimal glucose medium containing arabinose (1.3 mM). Dap was added to the growth medium at a final concentration of 0.25 mM, where indicated.

^cProducer strains were grown on NB agar. Single colonies were stabbed into agar overlays of the reporter strain.

^dCross-feeding was designated as growth (+) or no growth (-) based on turbidity of the reporter strain after 48 hours at 37°C. Outgrowth of the producer strains (not shown) from the sites of inoculation is described in the text.

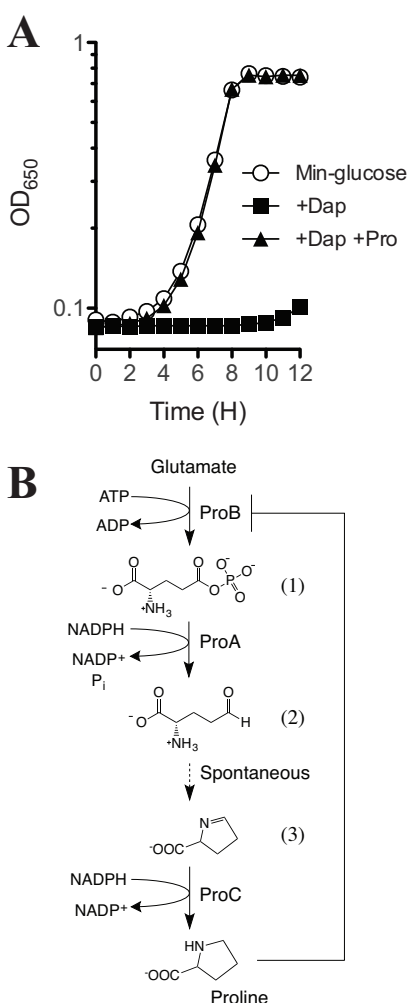


FIGURE 3.1. L-2,3-diaminopropionate elicits a proline requirement in *S. enterica*. A) Wild type *S. enterica* (DM14828) was grown at 37°C in glucose minimal medium containing no addition (open circle); 0.25 mM Dap (closed square); or 0.25 mM Dap and 1 mM proline (closed triangle). The data reflect experiments performed in triplicate. Error bars representing the standard deviation are not visible because the replicates deviated less than 5 % from the mean. B) Proline biosynthesis in *S. enterica* occurs in four steps, beginning with the ATP-dependent phosphorylation of glutamate, generating γ -glutamyl 5-phosphate (1). The conversion of glutamate 5-semialdehyde (2) to 1-pyrroline-5-carboxylate (3) occurs spontaneously (dashed line). Proline feedback-regulates the first enzyme (ProB) in the pathway.

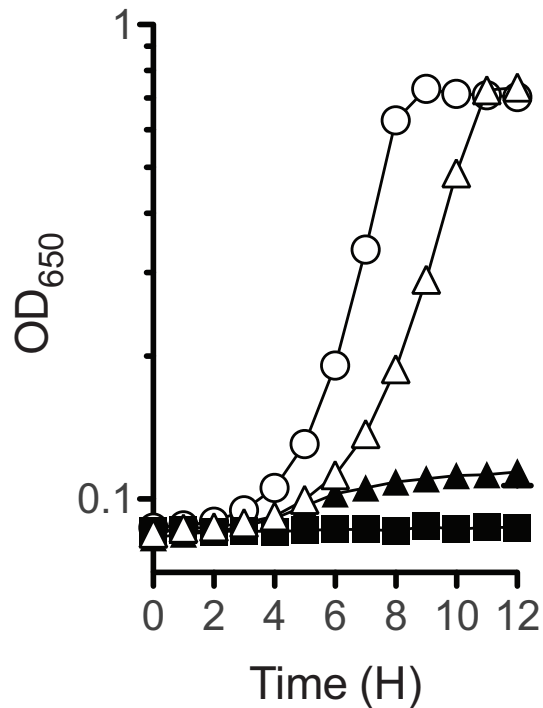


FIGURE 3.2. Pantothenate and proline are required for growth of a *dpaL* mutant in the presence of Dap. A *dpaL* mutant strain (DM14881) was grown at 37°C in glucose minimal medium containing no addition (open circle); 0.25 mM Dap (closed square); 0.25 mM Dap and 1 mM proline (closed triangle); or 0.25 mM Dap, 1 mM proline, and 0.1 mM pantothenate (open triangle). The data reflect experiments performed in triplicate. Error bars representing the standard deviation are not visible as the replicates deviated less than 5 % from the mean. Growth with Dap and pantothenate together was indistinguishable from Dap alone under the conditions tested (data not shown).

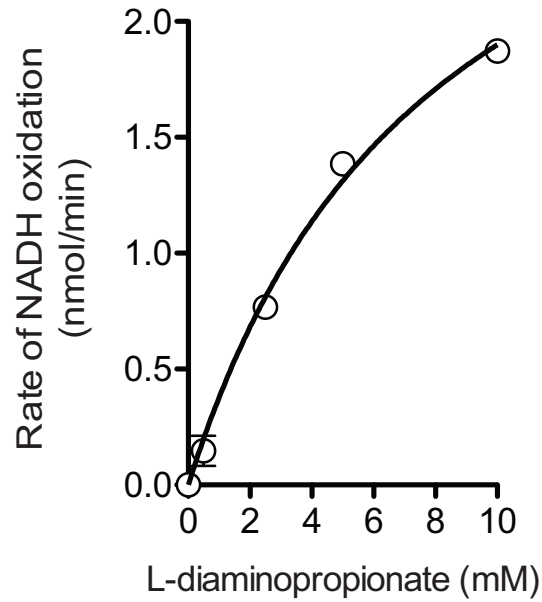


FIGURE 3.3. L-2,3-diaminopropionate serves as a substrate for pantothenate synthetase.

PanC activity was measured by a coupled assay, relying on the oxidation of NADH ($\Delta A_{340\text{nm}}$), in the presence of increasing concentrations of Dap. The initial rate of NADH oxidation in the presence of Dap was determined in the absence of β -alanine. Observed rates were completely dependent on the addition of enzymes and co-substrates as outlined in *Experimental procedures*. Data are plotted as the average and standard deviation of three independent experiments. The data were fit with a curve in GraphPad Prism 5.0f using the Michaelis-Menten equation.

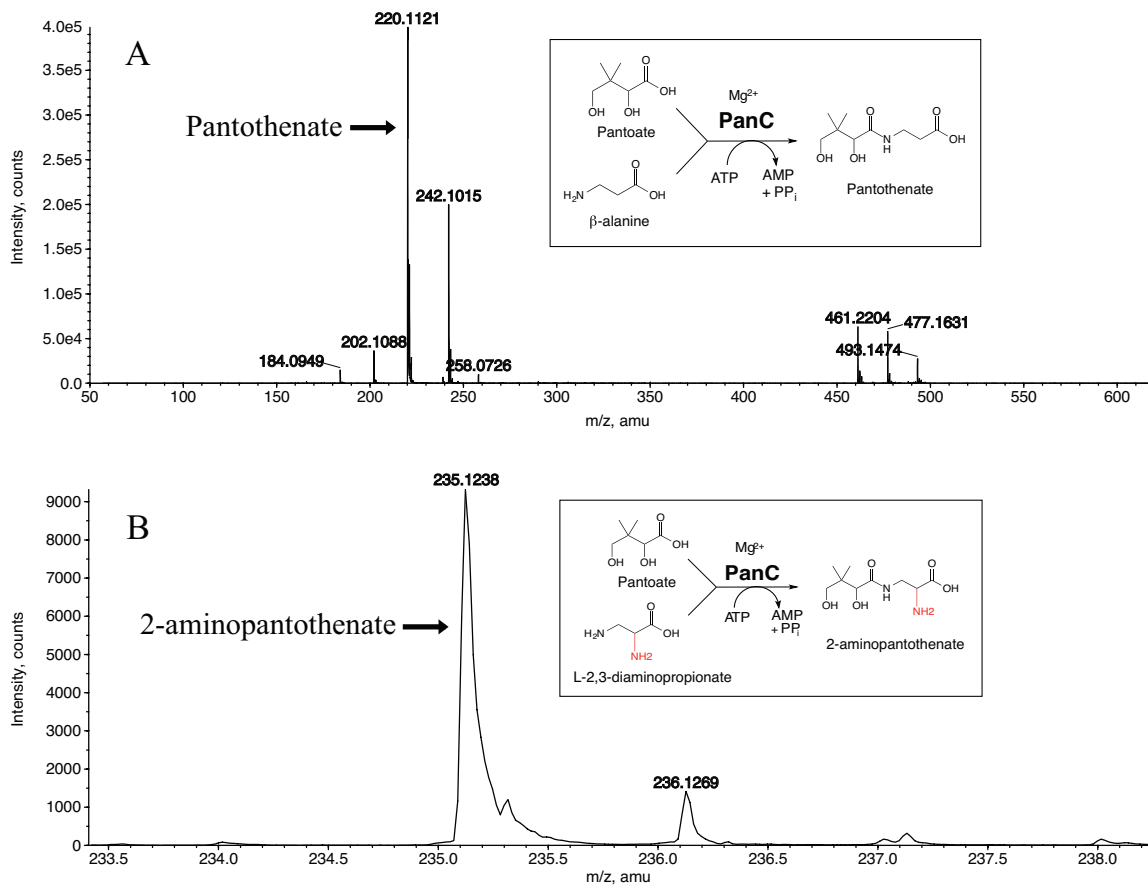


FIGURE 3.4. L-2,3-diaminopropionate reacts with pantoate in the presence of PanC to form a pantothenate analog. PanC assays containing pantoate, ATP and A) β -alanine or B) L-2,3-diaminopropionate as substrates were carried out for 16 hours. PanC was removed by size-exclusion filtration and samples were submitted for LC/MSD-TOF analysis in the positive mode. Insets show the reaction components and anticipated products, pantothenate (219 g/mol; $m/z = 220$) and 2-aminopantothenate (234 g/mol; $m/z = 235$), respectively.

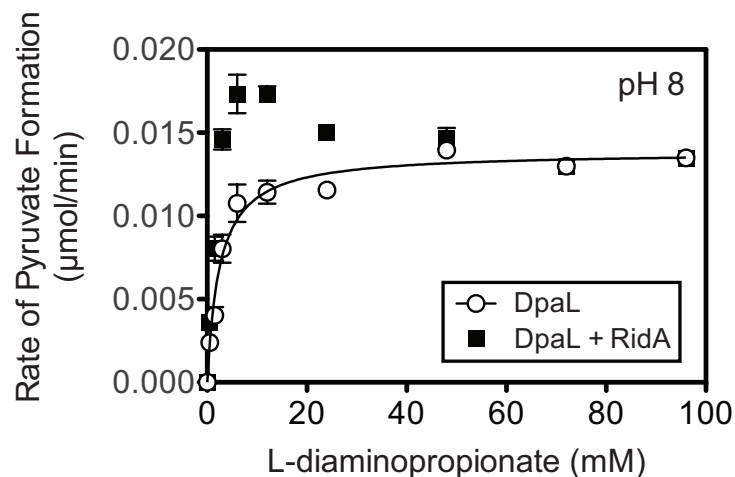


FIGURE 3.5. Diaminopropionate ammonia-lyase (DpaL) generates a 2AA substrate for RidA *in vitro*. Reactions consisted of DpaL (0.2 μ M) alone (open circle) or DpaL and RidA (0.9 μ M) (closed square). Assays were performed in triplicate and are plotted as the average and standard deviation. The data from DpaL-only assays were fit with a curve in GraphPad Prism 5.0f using the Michaelis-Menten equation.

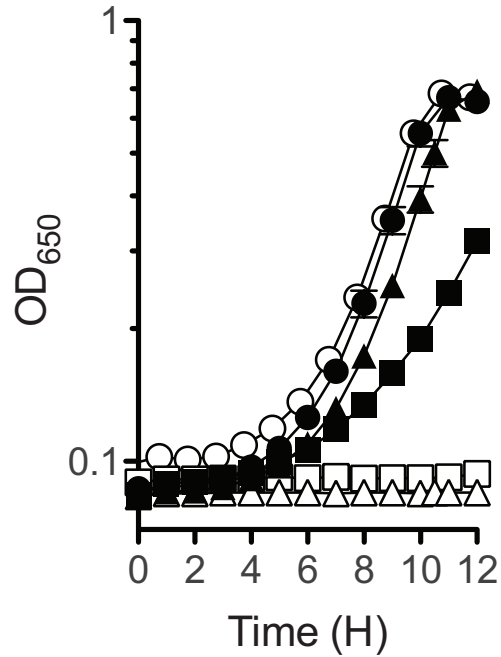


FIGURE 3.6. DpaL influences the sensitivity of a *ridA* strain to inhibition by Dap. A *ridA* strain (DM14829, open symbols) and a *ridA dpaL* strain (DM14882, closed symbols) were grown in glucose minimal medium containing no addition (circles); 0.25 mM Dap, 1 mM proline, and 0.1 mM pantothenate (squares); or 0.25 mM Dap, 1 mM proline, 0.1 mM pantothenate, and 1 mM L-isoleucine (triangles). Experiments were performed in triplicate and plotted as the average and standard deviation.

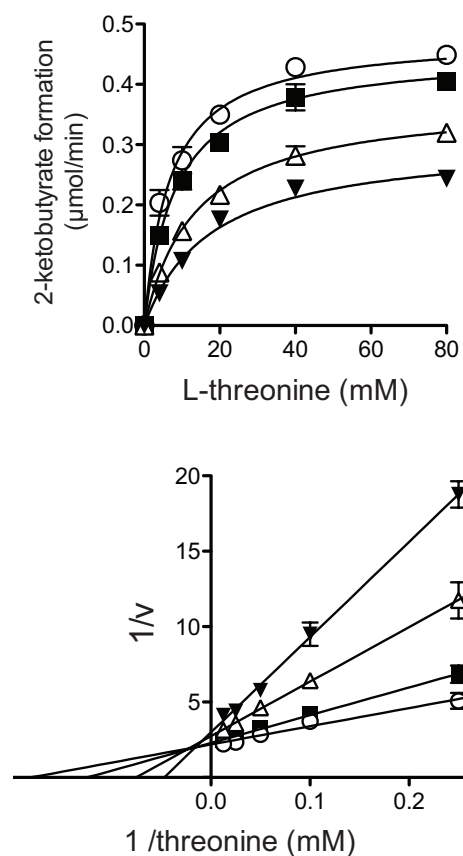


FIGURE 3.7. L-2,3-diaminopropionate inhibits IlvA. IlvA assays were performed in the presence of varying concentrations of Dap: 0 mM (open circle; $R^2 = 0.97$), 0.5 mM (closed square; $R^2 = 0.98$), 2.5 mM (open triangle; $R^2 = 0.97$), and 5 mM (closed inverted triangle; $R^2 = 0.98$). Data are plotted as the average and standard deviation of three independent experiments performed in parallel. (Top) The data were fit according to a mixed model of inhibition using GraphPad Prism 5.0f. (Bottom) Lineweaver-Burke analysis demonstrates mixed inhibition.

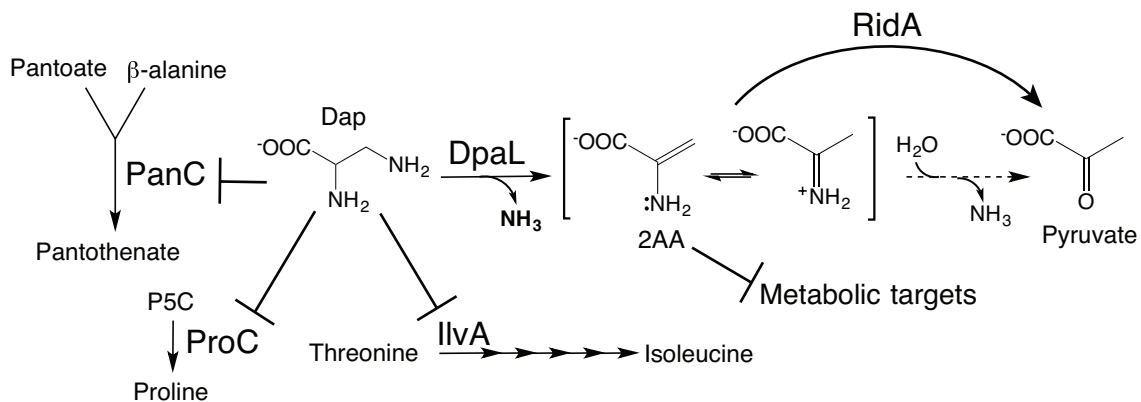


FIGURE 3.8. Proposed role of L-2,3-diaminopropionate (Dap) in the metabolic network. Dap negatively impacts metabolism in *S. enterica* by directly inhibiting proline, pantothenate and isoleucine biosynthesis. Dap also serves as a precursor to 2-aminoacrylate (2AA), leading to 2AA stress in the absence of RidA.

CHAPTER 4

2-AMINOACRYLATE STRESS INDUCES A CONTEXT-DEPENDENT GLYCINE REQUIREMENT IN *RIDA* STRAINS OF *SALMONELLA ENTERICA*¹

¹Ernst DC, Downs DM. 2016. *Journal of Bacteriology* 198:536–543.

Reprinted here with permission of the publisher.

4.1 ABSTRACT

The reactive enamine, 2-aminoacrylate (2AA), is a metabolic stressor capable of damaging cellular components. Members of the broadly conserved Rid (RidA/YER057c/UK114) protein family mitigate 2AA stress *in vivo* by facilitating enamine/imine hydrolysis. Previous work showed that 2AA accumulation in *ridA* strains of *Salmonella enterica* led to the inactivation of multiple target enzymes, including serine hydroxymethyltransferase (GlyA). However, the specific cause of a *ridA* strains inability to grow during periods of 2AA stress had yet to be determined. Work presented here shows that glycine supplementation suppressed all 2AA-dependent *ridA* strain growth defects described to date. Depending on the metabolic context, glycine appeared to suppress *ridA* strain growth defects by eliciting a GcvB small RNA-dependent regulatory response or by serving as a precursor to one-carbon units produced by the glycine cleavage complex (GCV). In either case, the data suggest that GlyA is the most physiologically sensitive target of 2AA inactivation in *S. enterica*. The universally conserved nature of GlyA among free-living organisms highlights the importance of RidA in mitigating 2AA stress.

Importance. The RidA stress response prevents 2-aminoacrylate (2AA) damage from occurring in prokaryotes and eukaryotes alike. 2AA inactivation of serine hydroxymethyltransferase (GlyA) from *Salmonella enterica* restricts glycine and one-carbon production, ultimately reducing fitness of the organism. The co-occurrence of genes encoding 2AA production enzymes and serine hydroxymethyltransferase (SHMT) in many genomes may in-part underlie the evolutionary selection for Rid proteins to maintain appropriate glycine and one-carbon metabolism throughout life.

4.2 BACKGROUND

Rid (RidA/YER057c/UK114) proteins are found throughout each kingdom of life, indicating these proteins serve fundamental roles in cellular processes. Bioinformatics analyses identified eight subgroups within the Rid protein family (1). The archetypal RidA subfamily is broadly distributed, and includes the best-studied RidA enzyme from *Salmonella enterica*, while the remaining seven Rid subgroups are primarily restricted to bacteria. In *S. enterica*, RidA is known to pre-empt metabolic damage caused by the unbound reactive enamine, 2-aminoacrylate (2AA) (2). In the absence of RidA, 2AA persisted in solution long enough to inactivate multiple target enzymes *in vivo* and *in vitro* (2–4). RidA proteins isolated from organisms spanning the tree of life displayed similar enamine/imine deaminase activity (5, 6), suggesting RidA enzymes serve a conserved role in preventing 2AA stress.

2AA stress arises as a consequence of some pyridoxal 5'-phosphate (PLP)-dependent enzyme activities. Previous analysis of *S. enterica* showed that PLP-dependent serine/threonine dehydratases (IlvA/TdcB; EC 4.3.1.19), cysteine desulfhydrase (CdsH; EC 4.4.1.1), and diaminopropionate ammonia-lyase (DpaL; EC 4.3.1.15) generated free 2AA from exogenous serine, cysteine and diaminopropionate, respectively, leading to complete growth inhibition in the absence of RidA (7, 8) (D. C. Ernst, M. E. Anderson and D. M. Downs, submitted for publication). In the absence of exogenous 2AA precursors, basal IlvA activity produced sufficient 2AA from endogenous serine to cause a minor growth defect in *ridA* strains grown in minimal glucose medium (9). The minor growth defect coincided with measureable 2AA inactivation of several PLP-dependent target enzymes, including serine hydroxymethyltransferase (SHMT) (GlyA, EC 2.1.2.1), alanine racemases (Alr/DadX, EC 5.1.1.1) and transaminase B (IlvE, EC 2.6.1.42) (2–4). Isoleucine prevented IlvA-dependent

2AA production from serine (endogenous or exogenous) and restored growth of *ridA* strains to wild type levels through feedback-inhibition of IlvA (9). Isoleucine failed to restore growth to a *ridA* strain grown in the presence of exogenous cysteine or diaminopropionate (8) (D. C. Ernst, M. E. Anderson and D. M. Downs, submitted for publication), or when containing a feedback-resistant variant of IlvA (IlvA^{L447F}) and grown in minimal glucose medium (10). Taken together, these data showed that isoleucine limitation alone could not explain the growth defects displayed by a *ridA* strain faced with 2AA stress.

Of the 2AA targets described to date, GlyA was inactivated to the greatest extent in *ridA* strains relative to wild type (20% of wild type activity in minimal glucose medium) (4). GlyA catalyzes the reversible transfer of a hydroxymethyl group from serine to tetrahydrofolate (THF), forming glycine and the one-carbon unit, 5,10-methylene-tetrahydrofolate (5,10-mTHF) (Figure 4.1). Glycine can be further catabolized by the glycine cleavage complex (GCV) to generate additional one-carbon units. Alternatively, glycine may serve as a proteinaceous amino acid, metabolic precursor, or regulatory signal (11). Work published by Flynn *et al.* demonstrated that *ridA* strains grown aerobically on glucose as the sole carbon source experienced a defect in one-carbon metabolism stemming from 2AA damage to GlyA (4). The one-carbon limitation diminished coenzyme A (CoA) biosynthesis, leading to pyruvate accumulation in the growth medium that correlated with a minor growth defect of the *ridA* strain. The CoA precursor pantothenate stimulated CoA production in a *ridA* strain but failed to restore wild type growth. In contrast, glycine restored both growth and CoA production to wild type levels in a *ridA* strain grown in minimal glucose medium (4). Building on this previous work, results presented herein demonstrate that glycine alleviates all *ridA*-dependent growth defects. However, the mechanism by which glycine suppresses these growth defects depends on the metabolic context. This work

underlines the crucial role played by RidA in protecting GlyA from 2AA damage to facilitate efficient glycine and one-carbon metabolism. The ubiquity of GlyA homologs among free-living organisms may in-part explain the broad conservation of RidA enzymes.

4.3 MATERIALS AND METHODS

Bacterial strains, media and chemicals. All strains used for this study are derivatives of *Salmonella enterica* serovar Typhimurium LT2 and are listed with their respective genotypes in Table 4.1. Tn10d(Tc) refers to the transposition-defective mini-Tn10 (Tn10 Δ 16 Δ 17) described by Way *et al.* (12). Each strain was constructed for this study.

Minimal growth medium consisted of no-carbon E medium (NCE) supplemented with 1 mM MgSO₄ (13) and trace elements (14). Glucose (11 mM) or pyruvate (50 mM) were provided as the sole carbon source where indicated. Difco nutrient broth (NB; 8 g/liter) with sodium chloride (5 g/liter) was used as rich medium. Difco BiTek agar (15 g/liter) was added for solid medium. When added, final amino acid and vitamin concentrations were as follows: L-serine, 5 mM; L-cysteine, 0.25 mM; L-2,3-diaminopropionate, 0.1 mM; L-isoleucine, 1 mM; glycine, 0.67 mM; methionine, 1 mM; pantothenate, 0.1 mM; thiamine, 0.1 μ M. Antibiotics were added at the following final concentrations when necessary for rich and minimal medium, respectively: 20 and 10 μ g/ml tetracycline; 20 and 5 μ g/ml chloramphenicol; 50 and 12.5 μ g/ml kanamycin. L-2,3-diaminopropionate was purchased from Chem-Impex International, Inc., Wood Dale, IL. All other chemicals were purchased from Sigma-Aldrich Chemical Company, St. Louis, MO.

Genetic techniques. Strains were constructed by transductional crosses using the high-frequency general transducing mutant of bacteriophage P22 (HT105/1, *int*-201) (15). Methods used to perform transductions, remove phage contamination from cells and identify phage-free

recombinants were described previously (16, 17). Gene replacements were made using the λ -red recombineering strategy described by Datsenko and Wanner (18). Primers *gcvB_Wanner_For* (5'-ACTTCCTGAGCCGGAACGAAAAGTTTTATCGGAATGCGTGGTGTAG GCTGGAGCTGCTTC-3') and *gcvB_Wanner_Rev* (5'-AGCACCGCAATATGG CCGTGCTACATTAATCACTATGGACCATATGAATATCCTCCTTAG-3') were used to insert a genetic marker at the *gcvB* locus, forming *gcvB32::Kn*. The *gcvP* locus was disrupted previously, forming *gcvP3I::Cm*. All gene replacements were reconstructed in the appropriate isogenic strain backgrounds for this study.

Growth phenotypes were assessed in solid medium using agar overlays or in liquid medium using growth curves as described previously (19). Growth curves were performed as follows: an overnight NB culture of the relevant strain was pelleted and resuspended in an equal volume of saline (85 mM), and 5 μ l was used to inoculate 195 μ l of growth medium contained within each well of a 96-well microtitre plate (Corning). Microtitre plates were incubated at 37°C while shaking and growth was monitored by the change in optical density (OD) at 650nm (OD₆₅₀) using a BioTek Elx808 plate reader. All growth experiments were performed in triplicate and the resulting data were plotted using GraphPad Prism 5.0f, generating curves in log₁₀-format that display the average and standard deviation of the replicates. Specific growth rates (μ) were calculated according to the following equation: $\ln(X/X_0)/T$, where X is OD₆₅₀, X₀ is the starting OD₆₅₀ of the exponential growth period monitored, and T is time in hours.

Transaminase B (IlvE) assays. IlvE activity was measured in crude lysates as previously described (8). Cultures were grown at 37°C with aeration to stationary phase in 2 ml of NB. Cells were pelleted and resuspended in an equal volume of saline (85 mM NaCl), and 100 μ l was used to inoculate 5 ml of minimal glucose medium. Where appropriate, isoleucine (1

mM) or glycine (0.67 mM) were included in the growth medium. Cultures were returned to 37°C and incubated ~6-8 hrs while shaking until an OD₆₅₀ of 1 was achieved. Cultures were chilled on ice, then pelleted (8,000 x g) at 4°C. Cell pellets were gently resuspended in NCE medium (1 ml), then harvested by centrifugation as above and frozen at -20°C until assayed. Upon thawing, cell pellets were resuspended in 250 µl of 50 mM potassium phosphate buffer (pH 8.0). An aliquot of the cell suspension (30 µl) was added to 150 µl of buffer containing 50 nM PLP, 10 nM 2-ketoglutarate and 10% PopCulture (Merck). Reactions were pre-equilibrated for 10 minutes at 37°C, then initiated by adding 20 µl of 0.2 mM isoleucine. After 20 minutes, the reactions were terminated by adding 2,4-dinitrophenylhydrazine (DNPH), and the amount of 2-ketomethylvalerate (2KMV) produced was quantified to assess IlvE activity. Following derivatization with DNPH, the relevant hydrazone was extracted with toluene, washed with hydrochloric acid (0.5 N) and treated with sodium hydroxide (1.5 N) to allow chromophore formation. The absorbance of the chromophore-containing aqueous layer was measured spectrophotometrically at 540nm using a Spectramax M2, and compared to a standard curve of 2KMV generated using the same extraction and chromophore development procedure. Cell-free extracts were generated and the amount of protein in each extract was quantified using the bicinchoninic acid (BCA) assay (Pierce). IlvE activity is reported as nmol 2KMV formed/mg of protein/min. The data are displayed as the average and standard deviation of three independent experiments. Statistical significance ($p < 0.01$) was determined by conducting one-way analysis of variance (ANOVA) and Tukey's post-test using GraphPad Prism 5.0f.

4.4 RESULTS AND DISCUSSION

Glycine alleviates growth arrest caused by 2AA. The effect exogenous glycine had on growth of a *ridA* strain in minimal glucose medium was reported previously (4). Glycine suppressed the minor growth defect of a *ridA* strain and prevented pyruvate accumulation, suggesting that glycine limitation may contribute to alternative *ridA* phenotypes. Consistent with previous reports, the addition of serine, cysteine or diaminopropionate to cultures of a *ridA* strain grown in minimal glucose medium completely prevented growth as a consequence of 2AA production (7, 8) (D. C. Ernst, M. E. Anderson and D. M. Downs, submitted for publication) (Table 4.2). Additionally, a *ridA* strain did not grow with pyruvate as the sole carbon source (10) (Table 4.2). The impact of exogenous glycine on these phenotypes was quantified in liquid cultures containing minimal glucose medium and the respective 2AA precursors, or in minimal medium containing pyruvate as the sole carbon source. The addition of glycine (0.67 mM) to cultures of a *ridA* strain (DM14829) containing 5 mM serine restored growth (Figure 4.2), resulting in a specific growth rate (μ) of 0.34 h^{-1} (Table 4.2). Although the same final cell density was achieved, the *ridA* strain grew slower than wild type (DM14828; $\mu = 0.60 \text{ h}^{-1}$) in the presence of serine and glycine, suggesting that additional metabolic deficiencies persisted in the *ridA* strain. Growth was similarly restored when glycine was added to *ridA* cultures containing 0.25 mM cysteine ($\mu = 0.30 \text{ h}^{-1}$) or 0.1 mM diaminopropionate ($\mu = 0.43 \text{ h}^{-1}$), or when pyruvate served as the carbon source ($\mu = 0.33 \text{ h}^{-1}$) (Table 4.2). In each case, the growth rate of *ridA* cultures supplemented with glycine remained less than the respective wild type cultures, but the final cell densities were equivalent (data not shown). Additional amino acids and vitamins were tested for their ability to suppress *ridA* strain growth defects caused by 2AA stress induced by serine or cysteine added to the growth medium. Previous reports described the stimulatory effect

threonine and isoleucine had on growth of *ridA* strains inhibited by exogenous serine (9, 20). None of the remaining common amino acids or coenzyme precursors, including pyridoxal, thiamine or pantothenate, significantly stimulated growth of the *ridA* strain in the presence of serine or cysteine (data not shown). These observations suggest that the perturbation of glycine metabolism was the most sensitive defect encountered by *ridA* strains challenged with 2AA stress, and showed that glycine significantly alleviated all *ridA* strain growth defects identified to date.

It was possible that glycine suppressed the growth defect of the *ridA* strain by preventing 2AA formation and/or accumulation. To test this possibility, the influence of glycine on transaminase B (IlvE) activity was assessed in a *ridA* background. Previous studies demonstrated the susceptibility of IlvE to free 2AA inactivation by covalent modification of the enzyme (2, 9), rendering IlvE a reliable proxy for endogenous 2AA levels. IlvE activity was measured in crude lysates of wild type and *ridA* strains grown to stationary phase ($OD_{650} \approx 1$) in minimal glucose medium containing the appropriate additions. IlvE activity was significantly reduced ($p < 0.01$) in a *ridA* background (234 nmol/min/mg) relative to the wild type control (370 nmol/min/mg) when grown in minimal glucose medium, while isoleucine (1 Mm) added to the growth medium preserved IlvE activity in the *ridA* strain (333 nmol/min/mg) as compared to wild type (334 nmol/min/mg) (Figure 4.3), consistent with previous reports (9). When glycine (0.67 Mm) was present in the growth medium, IlvE activity in a *ridA* strain (232 nmol/min/mg) remained significantly reduced ($p < 0.01$) relative to wild type (395 nmol/min/mg) (Figure 4.3). These data showed that exogenous glycine did not prevent 2AA formation/accumulation or concomitant damage caused to IlvE. Thus, a simple scenario suggested that glycine restored growth to a *ridA* strain under 2AA stress by bypassing a target of that stress (i.e. GlyA).

GcvB, but not GCV, is required to suppress *ridA* strain sensitivity to exogenous serine. Glycine serves as an amino acid building block in protein biosynthesis throughout life. Glycine can also function as a metabolic precursor, contributing to the production of one-carbon units and a variety of core metabolites (Figure 4.1). Additionally, glycine influences the regulation of metabolism, coordinating the production of metabolic enzymes with the nutrient state of the cell (21). A genetic approach was taken to tease apart the relative benefit of glycine to a *ridA* strain experiencing 2AA stress. A genetic marker inserted in *gcvP*, which encodes the P-protein of the glycine cleavage complex (GCV), prevented further catabolism of glycine to 5,10-Mthf, carbon dioxide and ammonia. If the benefit of glycine to a *ridA* strain was due to restored one-carbon units, the lesion in *gcvP* was predicted to abolish glycine rescue of a *ridA* strain grown in the presence of exogenous serine. Instead, the *ridA gcvP* double mutant strain (DM14839) grew biphasically in minimal glucose medium containing 5 Mm serine even in the absence of exogenous glycine (Figure 4.4). The biphasic growth consisted of a primary (~15 h) slow growth phase ($\mu = 0.06 \text{ h}^{-1}$), followed by a faster secondary growth phase ($\mu = 0.28 \text{ h}^{-1}$) (Table 4.2). Growth of the *gcvP* single mutant strain (DM14838) was similar to the wild type strain under the conditions tested (Table 4.2). These data indicated that glycine accumulation in the absence of GCV directly suppressed the *ridA* strain growth defect (Figure 4.4). The addition of glycine to *ridA gcvP* (DM14839) cultures containing serine circumvented the initial slow growth phase and enabled monophasic growth, achieving a growth rate ($\mu = 0.18 \text{ h}^{-1}$) intermediate to the biphasic growth rates observed in the absence of glycine (Table 4.2; Figure 4.5A). Together, these data demonstrated that GCV was not essential for glycine suppression of *ridA* strain sensitivity to exogenous serine.

A genetic marker inserted into the *gcvB* locus to prevent transcription of the GcvB sRNA was used to assess whether glycine was required for regulatory purposes. The GcvB sRNA was previously shown to negatively regulate translation of a number of amino acid uptake and biosynthesis enzymes in response to glycine accumulation in *S. enterica* (22). The regulatory cascade leading to GcvB production is initiated when glycine disrupts the protein complex formed between GcvA and GcvR, freeing GcvA to activate transcription of *gcvB* and other target genes (Figure 4.1). The *ridA gcvB* double mutant (DM14837) did not grow in minimal medium containing 5 mM serine, while growth of the *gcvB* single mutant (DM14836) was indistinguishable from wild type (DM14828) (Table 4.2). Including glycine in the growth medium did not stimulate growth of the *ridA gcvB* strain (DM14837) in minimal medium containing serine (Table 4.2; Figure 4.5A), demonstrating that the GcvB sRNA was essential for glycine suppression of serine sensitivity in a *ridA* strain. Genetic experiments found that deleting the major serine transporter regulated by GcvB, SstT, had no impact on serine sensitivity or glycine suppression phenotypes in a *ridA* background (data not shown).

GCV is necessary and sufficient for glycine effect in moderate 2AA stress scenario.

The impact of *gcvP* or *gcvB* on additional *ridA* phenotypes was tested to determine if the mechanism of glycine suppression was conserved. In contrast to the results seen with exogenous serine, the *ridA gcvP* strain (DM14389) was unable to grow when cysteine or diaminopropionate were included in the growth medium despite the addition of glycine (Table 4.2; Figure 4.5B). Similarly, glycine failed to stimulate growth of the *ridA gcvP* strain when pyruvate was provided as the sole carbon source (Table 4.2). Disruption of the GcvB sRNA had no impact on the growth response of a *ridA* strain to cysteine, diaminopropionate or pyruvate (Table 4.2). Growth of the *ridA gcvB* double mutant strain (DM13897) was restored to roughly the same rate as the

ridA single mutant strain when glycine was added to cultures containing cysteine ($\mu = 0.31 \text{ h}^{-1}$) (Figure 4.5B) or diaminopropionate ($\mu = 0.51 \text{ h}^{-1}$), or when pyruvate served as the sole carbon source ($\mu = 0.35 \text{ h}^{-1}$). These data demonstrated that glycine suppression of *ridA* strain sensitivity to cysteine, diaminopropionate or pyruvate relied on an intact GCV, but was unaffected by the GcvB sRNA. The conclusion drawn from these data is that the stimulation of one-carbon production by GCV-mediated catabolism of glycine was required to support growth of a *ridA* strain inhibited by 2AA produced from cysteine or diaminopropionate, or when pyruvate served as the carbon source.

A genetic strategy was devised to address the contradicting mechanisms of glycine suppression observed for a *ridA* strain inhibited by exogenous serine compared to the alternative sources of growth inhibition (i.e. cysteine, diaminopropionate and pyruvate). To bypass the variable of serine uptake, the *ilvA219* allele encoding an IlvA variant (IlvA^{L447F}) resistant to feedback inhibition by isoleucine (23) was introduced into the appropriate strain backgrounds to exacerbate 2AA production from endogenous serine, as previously described (9, 10). Consistent with previous reports, the uncontrolled activity of IlvA^{L447F} in an *ilvA219 ridA* background (DM14831) inhibited growth in minimal glucose medium (Figure 4.6A), achieving a final cell density (Final OD₆₅₀ = 0.22) more than 2-fold less than the *ilvA219* single mutant strain (DM14830) (Final OD₆₅₀ = 0.57) (Table 4.3). These data were consistent with a nutrient limitation caused by increased 2AA stress in the *ilvA219 ridA* strain. Adding glycine to the growth medium stimulated growth of the *ilvA219 ridA* strain, reaching the same final cell density as the *ilvA219* single mutant (Final OD₆₅₀ = 0.58). A lesion in *gcvP* prevented glycine from stimulating growth of the *ilvA219 ridA gcvP* mutant strain (DM14843), while the inactivation of *gcvB* in the *ilvA219 ridA gcvB* strain (DM14841) did not affect glycine stimulation (Figure

4.6B). The data showed that glycine suppressed the growth defect of a *ridA* strain caused by endogenous serine in a GCV-dependent manner, counter to the GcvB sRNA requirement for glycine suppression of the growth defect caused by exogenous serine described above. These data suggest that there is no inherent difference in the metabolic consequences encountered by a *ridA* strain experiencing 2AA stress, regardless of the source of 2AA. The different mechanistic determinants of glycine suppression observed between endogenous versus exogenous serine stress conditions likely reflects the disparate 2AA burdens caused by unequal levels of serine accumulation inside the cell.

GCV is dispensable for growth of an *ilvA219 ridA* strain when downstream products of one-carbon metabolism are provided directly. The necessity of GCV to allow glycine to stimulate growth of the *ilvA219 ridA* strain suggested that products of one-carbon metabolism were limiting. In *S. enterica*, one-carbon units are required for DNA methylation reactions and the biosynthesis of purines, thiamine, methionine, pantothenate and histidine (24). The impact of these metabolites on growth of the *ilvA219 ridA* strain in minimal glucose medium was compared to that of glycine (Table 4.3). Thiamine (0.1 μ M), pantothenate (0.1 mM) and methionine (1 mM) independently restored growth of the *ilvA219 ridA* strain to the same final cell density as the glycine supplemented cultures (Table 4.3). Furthermore, the disruption of *gcvP* in the *ilvA219 ridA gcvP* strain (DM14843) had little impact on the growth suppression afforded by these metabolites, suggesting that the need for an intact GCV was bypassed by directly feeding downstream products requiring one-carbon units instead of glycine. None of the products of one-carbon metabolism (i.e. thiamine, pantothenate, methionine) stimulated growth of a *ridA* (DM14828) strain inhibited by exogenous serine, cysteine or diaminopropionate (data not shown), perhaps reflecting altered growth requirements caused by different levels of 2AA damage inside the cell. Histidine had no

impact on growth of any of the strains grown under the conditions described for Table 4.3 (data not shown). The addition of adenine as a purine source further diminished the already low level of growth displayed by the *ilvA219 ridA* strain in minimal glucose medium (data not shown), possibly through feedback inhibition of the shared pathway for thiamine production. These data suggest that in an *ilvA219 ridA* background, 2AA damage to GlyA limits the production of one-carbon units required for the biosynthesis of thiamine, pantothenate or methionine. The ability of these metabolites to suppress the growth defect independently may reflect a one-carbon sparing phenomenon. Alternatively, because coenzyme A and methionine are known to stimulate production of thiamine in *S. enterica* (25), these data may indicate that a thiamine limitation is the key to the growth defect observed for the *ilvA219 ridA* strain.

Conclusions. The aim of this study was to determine why strains of *S. enterica* lacking RidA were unable to grow when challenged with 2AA. The data support a model in which the growth-limiting defect of *ridA* strains is 2AA inactivation of GlyA, which causes a disruption in glycine and one-carbon production. Exogenous glycine suppressed the growth defects of a *ridA* strain caused by cysteine, diaminopropionate or pyruvate only when *gcvP* was intact, suggesting glycine was used to generate additional one-carbon units via GCV. Similarly, when 2AA was produced from endogenous serine by an isoleucine-insensitive variant of IlvA, glycine suppression required a functional GCV.

Surprisingly, the ability of glycine to allow growth of a *ridA* strain in the presence of exogenous serine required the regulatory GcvB small RNA, but not a functional GCV. The concentration of exogenous serine (5 mM) supplied to cultures was 20-50 times greater than cysteine (0.25 mM) or diaminopropionate (0.1 mM), and approximately 70 times greater than levels endogenous serine (based on intracellular serine concentrations determined for *E. coli*)

(26). Therefore, it is reasonable to predict that exogenous serine resulted in a large pool of endogenous 2AA, leading to broad inactivation of target enzymes, including but not limited to GlyA. In this scenario, *gcvP*-dependent one-carbon production alone was insufficient to overcome the metabolic needs of the cell despite glycine supplementation. We propose that *ridA* strains grown in the presence of exogenous serine experience substantial damage to targets aside from GlyA, eliciting one or more nutritional requirements in addition to glycine. The addition of glycine serves to rewire the metabolic network by eliciting a GcvB-dependent regulatory response to overcome 2AA stress caused by exogenous serine. The GcvB regulon consists of over 50 targets in *S. enterica* (22) and it is likely that growth in the presence of high 2AA stress required the cumulative effect of genes in the regulon. Significantly, the lack of GcvB would result in derepression of the major serine transporter (SstT), and indirectly (via Lrp) reduce the expression of *sdaA* (27). SdaA (EC 4.3.1.17) is an Fe-S cluster serine dehydratase that degrades serine without releasing the reactive 2AA species (Chen and Downs, unpublished; G. Grant, personal communication). Thus, the lack of GcvB could contribute to enhanced serine uptake and similarly prevent efficient degradation of serine by a non-toxic route (i.e. SdaA), thereby exacerbating 2AA stress to the point where one-carbon production by GCV would be insufficient to restore growth to a *ridA* strain.

In the absence of exogenous serine, glycine was required to suppress alternative *ridA* growth defects by stimulating one-carbon production, catalyzed by GCV. The phenotypic data presented herein are consistent with biochemical data presented by Flynn *et al.* that showed GlyA activity was reduced (20% of wild type activity) in *ridA* strains grown in minimal glucose medium, leading to a downstream deficiency in one-carbon units (4). In the absence of an extreme 2AA burden (i.e. exogenous serine), the stimulation of one-carbon production by GCV

and glycine was sufficient to restore growth in the presence of exogenous cysteine, diaminopropionate or pyruvate, or when 2AA was produced from endogenous serine by the isoleucine-insensitive variant of IlvA, suggesting a one-carbon limitation is the primary defect encountered by *ridA* strains under the growth conditions tested. Because thiamine, methionine and pantothenate individually stimulated growth of an *ilvA219 ridA* strain, consistent with one-carbon units being spared, it remains to be seen if one of these metabolites alone is primarily limiting for growth.

Insights gained from our work in *S. enterica* inform our understanding of the RidA paradigm in other organisms. Serine hydroxymethyltransferase (SHMT, EC 2.1.2.1) is one of only two PLP-dependent enzymes encoded in genomes of all free-living organisms, the other being aspartate aminotransferase (EC 2.6.1.1) (28). Future work is needed to address whether or not SHMT inactivation by 2AA elicits similar glycine or one-carbon requirements in other organisms. It is feasible that alternative metabolic configurations may preclude SHMT inactivation from drastically impacting growth given that alternative strategies of glycine production from threonine have been described (29, 30). In such cases, different targets of 2AA inactivation (e.g. aspartate aminotransferase) may have a greater impact on organism fitness. Nonetheless, several organisms produce one or more isozymes of SHMT, and in some cases SHMT is predicted to co-localize with RidA homologs throughout the cell. For example, the RidA homolog (At3g20390) from *Arabidopsis thaliana* is targeted to the plastid (6), while SHMT (AtSHMT3) activity can also be detected there (31). In *Saccharomyces cerevisiae*, the SHM1 isozyme of SHMT and the yeast RidA homolog (Yil051cp) both localize to the mitochondria (32, 33). In some mammalian cell lines, RidA-like UK114 is produced in the cytoplasm (34), while SHMT isozymes are found in both the cytosol and mitochondria (35).

Developing a better understanding of the link between RidA homologs and SHMT may lead to better chemotherapeutics to combat diseases such as cancer, as tumor cells rely heavily on flux through SHMT to meet the rampant demand for glycine and one-carbon units necessary for rapid cell growth and division (36–38). Interestingly, UK114 serves as a cytotoxic tumor antigen in some forms of cancer (39), perhaps reflecting a reliance by cancer cells on UK114 to preserve efficient SHMT activity. Future investigation of connections between Rid enzymes and glycine and one-carbon metabolism are warranted given the importance of this node of metabolism throughout life.

4.5 REFERENCES

1. Niehaus TD, Gerdes S, Hodge-Hanson K, Zhukov A, Cooper AJ, ElBadawi-Sidhu M, Fiehn O, Downs DM, Hanson AD. 2015. Genomic and experimental evidence for multiple metabolic functions in the RidA/YjgF/YER057c/UK114 (Rid) protein family. *BMC Genomics* 16:382.
2. Lambrecht JA, Schmitz GE, Downs DM. 2013. RidA proteins prevent metabolic damage inflicted by PLP-dependent dehydratases in all domains of life. *mBio* 4:e00033-13-e00033-13.
3. Flynn JM, Downs DM. 2013. In the absence of RidA, endogenous 2-aminoacrylate inactivates alanine racemases by modifying the pyridoxal 5'-phosphate cofactor. *J Bacteriol* 195:3603–3609.
4. Flynn JM, Christopherson MR, Downs DM. 2013. Decreased coenzyme A levels in *ridA* mutant strains of *Salmonella enterica* result from inactivated serine hydroxymethyltransferase: *ridA* mutants are deficient in one carbon metabolism. *Mol Microbiol* 89:751–759.
5. Lambrecht JA, Flynn JM, Downs DM. 2012. Conserved YjgF protein family deaminates reactive enamine/imine intermediates of pyridoxal 5'-phosphate (PLP)-dependent enzyme reactions. *J Biol Chem* 287:3454–3461.
6. Niehaus TD, Nguyen TND, Gidda SK, ElBadawi-Sidhu M, Lambrecht JA, McCarty DR, Downs DM, Cooper AJL, Fiehn O, Mullen RT, Hanson AD. 2014. *Arabidopsis* and *Maize*

RidA proteins preempt reactive enamine/imine damage to branched-chain amino acid biosynthesis in plastids. *Plant Cell* 7:3010–3022.

7. Enos-Berlage JL, Langendorf MJ, Downs DM. 1998. Complex metabolic phenotypes caused by a mutation in *yjgF*, encoding a member of the highly conserved YER057c/YjgF family of proteins. *J Bacteriol* 180:6519–6528.
8. Ernst DC, Lambrecht JA, Schomer RA, Downs DM. 2014. Endogenous synthesis of 2-aminoacrylate contributes to cysteine sensitivity in *Salmonella enterica*. *J Bacteriol* 196:3335–3342.
9. Schmitz G, Downs DM. 2004. Reduced transaminase B (IlvE) activity caused by the lack of *yjgF* is dependent on the status of threonine deaminase (IlvA) in *Salmonella enterica* serovar Typhimurium. *J Bacteriol* 186:803–810.
10. Christopherson MR, Schmit GE, Downs DM. 2008. YjgF is required for isoleucine biosynthesis when *Salmonella enterica* is grown on pyruvate medium. *J Bacteriol* 190:3057–3062.
11. Stauffer G. 2004. Regulation of Serine, Glycine, and One-Carbon Biosynthesis. *EcoSal Plus*.
12. Way JC, Davis MA, Morisato D, Roberts DE, Kleckner N. 1984. New Tn10 derivatives for transposon mutagenesis and for construction of *lacZ* operon fusions by transposition. *Gene* 32:369–379.
13. Vogel HJ, Bonner DM. 1956. Acetylornithinase of *Escherichia coli*: partial purification and some properties. *J Biol Chem* 218:97–106.
14. Balch WE, Wolfe RS. 1976. New approach to the cultivation of methanogenic bacteria: 2-mercaptoethanesulfonic acid (HS-CoM)-dependent growth of *Methanobacterium ruminantium* in a pressurized atmosphere. *Appl Environ Microbiol* 32:781–791.
15. Schmieger H. 1972. Phage P22-mutants with increased or decreased transduction abilities. *Mol Gen Genet MGG* 119:75–88.
16. Chan RK, Botstein D, Watanabe T, Ogata Y. 1972. Specialized transduction of tetracycline resistance by phage P22 in *Salmonella typhimurium*. II. Properties of a high-frequency-transducing lysate. *Virology* 50:883–898.
17. Downs DM, Petersen L. 1994. *apbA*, a new genetic locus involved in thiamine biosynthesis in *Salmonella typhimurium*. *J Bacteriol* 176:4858–4864.

18. Datsenko KA, Wanner BL. 2000. One-step inactivation of chromosomal genes in *Escherichia coli* K-12 using PCR products. *Proc Natl Acad Sci* 97:6640–6645.
19. Petersen L, Enos-Berlage J, Downs DM. 1996. Genetic analysis of metabolic crosstalk and its impact on thiamine synthesis in *Salmonella typhimurium*. *Genetics* 143:37.
20. Christopherson MR, Lambrecht JA, Downs D, Downs DM. 2012. Suppressor analyses identify threonine as a modulator of *ridA* mutant phenotypes in *Salmonella enterica*. *PLOS ONE* 7:e43082.
21. Modi SR, Camacho DM, Kohanski MA, Walker GC, Collins JJ. 2011. Functional characterization of bacterial sRNAs using a network biology approach. *Proc Natl Acad Sci* 108:15522–15527.
22. Sharma CM, Papenfort K, Pernitzsch SR, Mollenkopf H-J, Hinton JCD, Vogel J. 2011. Pervasive post-transcriptional control of genes involved in amino acid metabolism by the Hfq-dependent GcvB small RNA: GcvB regulon. *Mol Microbiol* 81:1144–1165.
23. LaRossa RA, Van Dyk TK, Smulski DR. 1987. Toxic accumulation of alpha-ketobutyrate caused by inhibition of the branched-chain amino acid biosynthetic enzyme acetolactate synthase in *Salmonella typhimurium*. *J Bacteriol* 169:1372–1378.
24. Matthews RG. 1996. One-carbon metabolism. In *Escherichia coli* and *Salmonella typhimurium*. *Cell Mol Biol* 506–513.
25. Palmer LD, Dougherty MJ, Downs DM. 2012. Analysis of ThiC variants in the context of the metabolic network of *Salmonella enterica*. *J Bacteriol* 194:6088–6095.
26. Bennett BD, Kimball EH, Gao M, Osterhout R, Van Dien SJ, Rabinowitz JD. 2009. Absolute metabolite concentrations and implied enzyme active site occupancy in *Escherichia coli*. *Nat Chem Biol* 5:593–599.
27. Tani TH, Khodursky A, Blumenthal RM, Brown PO, Matthews RG. 2002. Adaptation to famine: a family of stationary-phase genes revealed by microarray analysis. *Proc Natl Acad Sci* 99:13471–13476.
28. Percudani R, Peracchi A. 2003. A genomic overview of pyridoxal-phosphate-dependent enzymes. *EMBO Rep* 4:850–854.
29. Newman EB, Kapoor V, Potter R. 1976. Role of L-threonine dehydrogenase in the catabolism of threonine and synthesis of glycine by *Escherichia coli*. *J Bacteriol* 126:1245–1249.

30. Ogawa H, Gomi T, Fujioka M. 2000. Serine hydroxymethyltransferase and threonine aldolase: are they identical? *Int J Biochem Cell Biol* 32:289–301.
31. Zhang Y, Sun K, Sandoval FJ, Santiago K, Roje S. 2010. One-carbon metabolism in plants: characterization of a plastid serine hydroxymethyltransferase. *Biochem J* 430:97–105.
32. Kastanos EK, Woldman YY, Appling DR. 1997. Role of mitochondrial and cytoplasmic serine hydroxymethyltransferase isozymes in *de novo* purine synthesis in *Saccharomyces cerevisiae*. *Biochemistry (Mosc)* 36:14956–14964.
33. Kim J-M, Yoshikawa H, Shirahige K. 2001. A member of the YER057c/yjgf/Uk114 family links isoleucine biosynthesis and intact mitochondria maintenance in *Saccharomyces cerevisiae*. *Genes Cells* 6:507–517.
34. Chong CL, Huang SF, Hu C p., Chen YL, Chou HY, Chau GY, Shew JY, Tsai YL, Chen CT, Chang C, Chen ML. 2008. Decreased expression of UK114 is related to the differentiation status of human hepatocellular carcinoma. *Cancer Epidemiol Biomarkers Prev* 17:535–542.
35. Tibbetts AS, Appling DR. 2010. Compartmentalization of mammalian folate-mediated one-carbon metabolism. *Annu Rev Nutr* 30:57–81.
36. Locasale JW. 2013. Serine, glycine and one-carbon units: cancer metabolism in full circle. *Nat Rev Cancer* 13:572–583.
37. Amelio I, Cutruzzolá F, Antonov A, Agostini M, Melino G. 2014. Serine and glycine metabolism in cancer. *Trends Biochem Sci* 39:191–198.
38. Labuschagne CF, van den Broek NJF, Mackay GM, Vousden KH, Maddocks ODK. 2014. Serine, but not glycine, supports one-carbon metabolism and proliferation of cancer cells. *Cell Rep* 7:1248–1258.
39. Bartorelli A, Bussolati B, Millesimo M, Gugiotta P, Bussolati G. 1996. Antibody-dependent cytotoxic activity of human cancer cells expressing UK114 membrane antigen. *Int J Oncol* 8:543–548.

TABLE 4.1 Bacterial strains

Bacterial strain	Genotype
DM14828	Wild type LT2
DM14829	<i>ridA1::Tn10d(Tc)</i> ^a
DM14830	<i>ilvA219</i>
DM14831	<i>ilvA219 ridA1::Tn10d(Tc)</i>
DM14836	<i>gcvB32::Kn</i>
DM14837	<i>ridA1::Tn10d(Tc) gcvB32::Kn</i>
DM14838	<i>gcvP31::Cm</i>
DM14839	<i>ridA1::Tn10d(Tc) gcvP31::Cm</i>
DM14840	<i>ilvA219 gcvB32::Kn</i>
DM14841	<i>ilvA219 ridA1::Tn10d(Tc) gcvB32::Kn</i>
DM14842	<i>ilvA219 gcvP31::Cm</i>
DM14843	<i>ilvA219 ridA1::Tn10d(Tc) gcvP31::Cm</i>

^a *Tn10d(Tc)* refers to the transposition-defective mini-*Tn10* (*Tn10Δ16Δ17*) (12)

TABLE 4.2 Glycine improves growth rates of *ridA* strains inhibited by 2AA

Growth medium ^b	Growth rate ^a (h ⁻¹)					
	DM14828 (Wt)	DM14829 (<i>ridA</i>)	DM14838 (<i>gcvP</i>)	DM14839 (<i>ridA gcvP</i>)	DM14836 (<i>gcvB</i>)	DM14837 (<i>ridA gcvB</i>)
Min-glucose	0.56	0.42	0.52	0.33	0.51	0.42
+Gly	0.52	0.52	0.38	0.23	0.59	0.51
+Ser	0.57	NG	0.59	0.28	0.59	NG
+Ser +Gly	0.60	0.34	0.58	0.18	0.59	NG
+Cys	0.50	NG	0.54	NG	0.57	NG
+Cys +Gly	0.57	0.30	0.52	NG	0.54	0.31
+Dap	0.58	NG	0.52	NG	0.56	NG
+Dap +Gly	0.57	0.43	0.45	NG	0.49	0.51
Min-pyruvate	0.41	NG	0.40	NG	0.44	NG
+Gly	0.42	0.33	0.35	NG	0.41	0.35

^a Specific growth rates (μ) were calculated as $\ln(X/X_0)/T$, where X represents OD₆₅₀, X₀ is the initial OD₆₅₀ of the exponential growth period monitored and T is time in hours. Gray bars represent the ratio of the observed growth rate to the maximal growth rate from the data set ($\mu = 0.6 \text{ h}^{-1}$). Data shown are the average of three independent cultures. The standard deviation was less than 0.05 in all cases. Growth was assessed within 20 hours following inoculation.

^b Glucose (11 mM) or pyruvate (50 mM) were provided as the carbon source as indicated. Amino acid supplements were added at the following final concentrations: 0.67 mM glycine (Gly); 5 mM serine (Ser); 0.25 mM cysteine (Cys); 0.1 mM diaminopropionate (Dap).

^c Average growth rates less than 0.05 h^{-1} were designated as no-growth (NG).

^d The displayed growth rate reflects the secondary growth phase of a biphasic growth pattern; the primary growth rate was 0.06 h^{-1} .

TABLE 4.3 Metabolites that require one-carbon units for their production bypass the need to restore one-carbon production via GCV in *ilvA219 ridA* strains grown in minimal medium

Strain	Genotype	Final cell density ^a (OD ₆₅₀)						
		Min-glu ^b	+Gly	+Thi	+Pan	+Met	+Ade	+Ade +Thi
DM14830	<i>ilvA219</i>	0.70	0.70	0.73	0.76	0.74	0.69	0.72
DM14831	<i>ilvA219 ridA</i>	0.20	0.67	0.58	0.71	0.62	0.11	0.49
DM14842	<i>ilvA219 gcvP</i>	0.66	0.68	0.70	0.75	0.76	0.70	0.70
DM14843	<i>ilvA219 ridA gcvP</i>	0.17	0.17	0.48	0.68	0.64	0.11	0.49
DM14840	<i>ilvA219 gcvB</i>	0.67	0.69	0.72	0.75	0.75	0.69	0.69
DM14841	<i>ilvA219 ridA gcvB</i>	0.15	0.68	0.57	0.70	0.62	0.15	0.48

^a The displayed data represent the average cell densities of cultures grown in triplicate based on OD₆₅₀ readings taken after 15 hours of growth. Standard deviations were less than 0.03 in all cases. Gray bars reflect the ratio of the observed final OD₆₅₀ to the maximal OD₆₅₀ from the data set (OD₆₅₀ = 0.76)

^b Growth was assessed in minimal glucose medium containing the following concentrations of the indicated supplements: 0.67 mM glycine, 0.1 μM thiamine, 0.1 mM pantothenate, or 1 mM methionine.

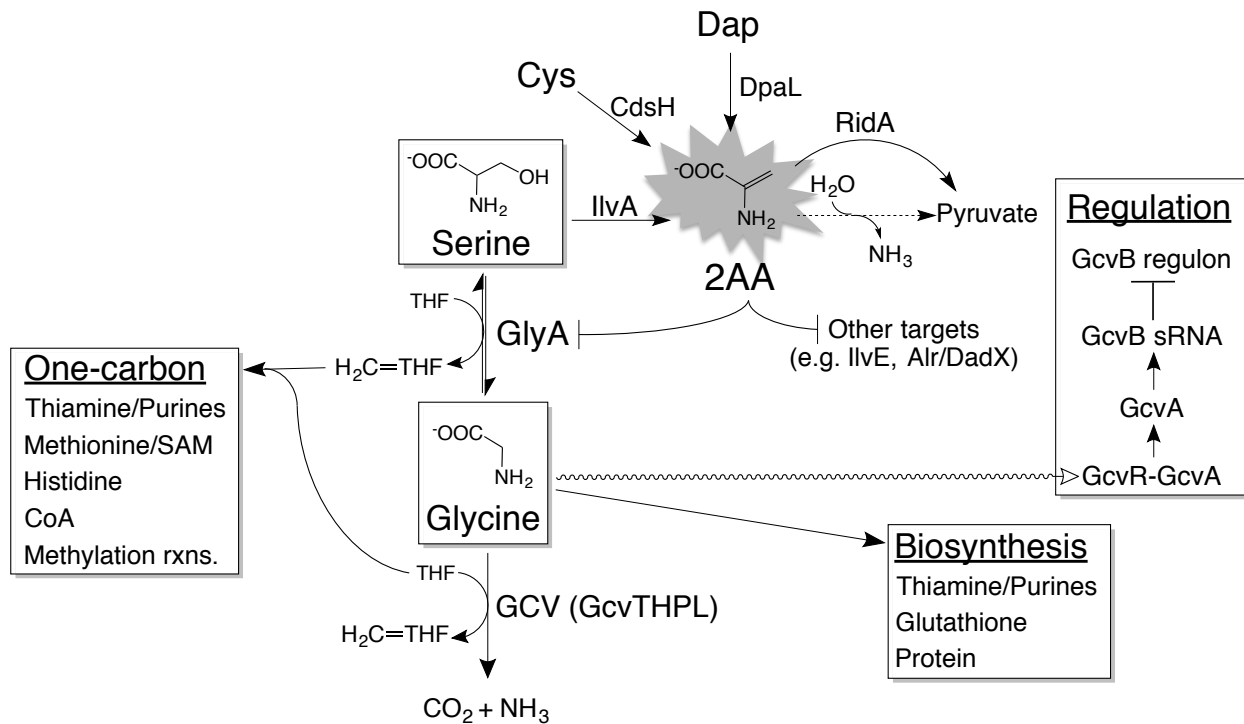


FIGURE 4.1. Connections between 2-aminoacrylate (2AA) and the glycine metabolic node.

2AA is produced from serine, cysteine and diaminopropionate by IlvA, CdsH and DpaL, respectively. In the absence of RidA, 2AA persists in solution long enough to inactivate target enzymes, including GlyA. Damage to GlyA restricts flux to glycine, simultaneously reducing the amount of tetrahydrofolate (THF) converted to one-carbon units ($\text{H}_2\text{C=THF}$). Excess glycine can be converted to additional one-carbon units by the glycine cleavage complex (GCV) or can be incorporated into protein production or other biosynthetic pathways. Alternatively, glycine may serve as a regulatory molecule (undulating line), disrupting the complex formed between GcvR-GcvA, freeing GcvA to activate transcription of the GcvB sRNA, leading to post-transcriptional regulation of the GcvB regulon. The spontaneous conversion from 2AA to pyruvate (dashed line) is slow enough to allow 2AA accumulation and damage to occur.

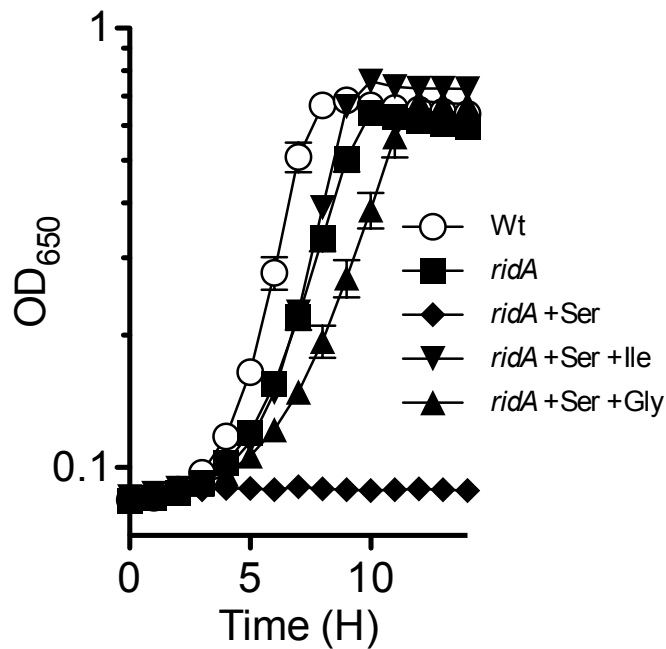


FIGURE 4.2. Glycine restores growth to *ridA* strains inhibited by 2AA produced from serine. Growth of the wild type strain (DM14828; open circles) in minimal glucose medium is compared to growth of the *ridA* strain (DM14829; closed symbols) in minimal glucose medium containing: no addition (squares), 5 mM serine (diamonds), 5 mM serine and 1 mM isoleucine (inverted triangles) or 5 mM serine and 0.67 mM glycine (triangles). The displayed data represent the average and standard deviation of three independent cultures. Growth of the wild type strain was not significantly improved by exogenous glycine or serine.

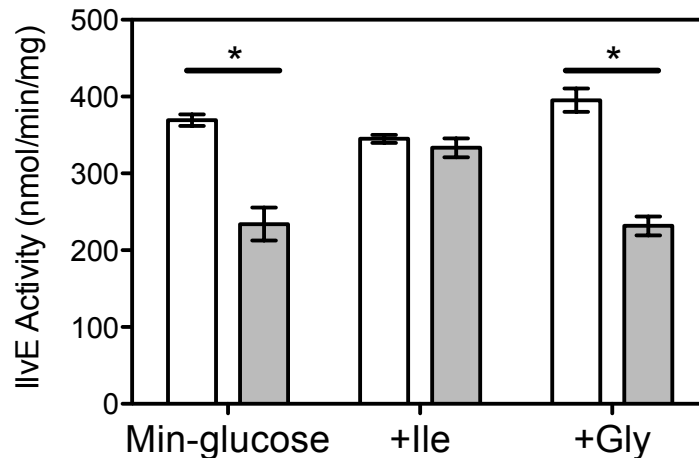


FIGURE 4.3. Glycine does not directly prevent IlvA-dependent 2AA production from endogenous serine *in vivo*. IlvE activity was measured as a proxy for 2AA accumulation in wild type (DM14828; white bars) and *ridA* (DM14829; gray bars) strains grown in minimal glucose medium alone (Min-glucose), with 1mM isoleucine added (+Ile), or with 0.67 mM glycine added (+Gly). The data are reported as nmol of 2-ketomethylvalerate produced per minute per mg of crude lysate. Experiments were performed in triplicate and are reported as the average and standard deviation about the mean. The data were analyzed by one-way ANOVA and Tukey's test using GraphPad Prism 5.0f to identify significantly reduced activities ($p < 0.01$) for a given growth condition, indicated by the asterisks.

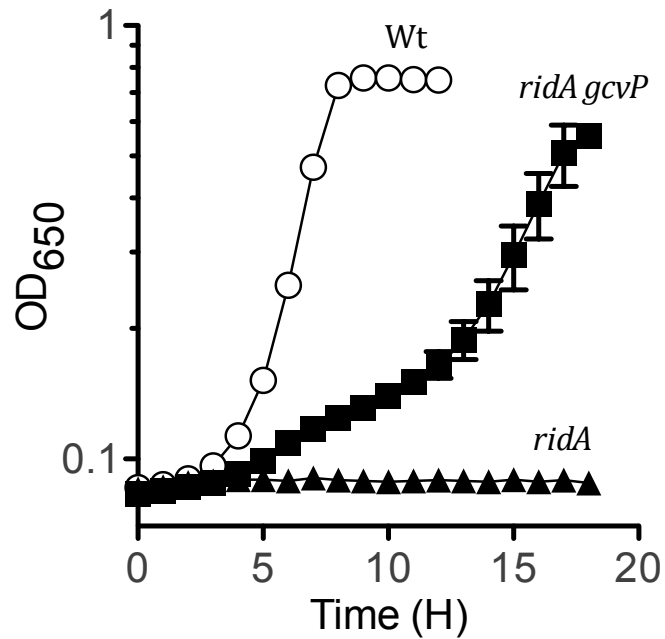


FIGURE 4.4. The disruption of *gcvP*, encoding a component of GCV, stimulates growth of a *ridA* strain inhibited by exogenous serine. Growth curves were performed in minimal glucose medium containing 5 mM serine. The data show the average and standard deviation of three independent cultures. The relevant genotypes are indicated as Wt (DM14828; open circles), *ridA* (DM14829; closed triangles) and *ridA gcvP* (DM14839; closed squares). Growth of the *gcvP* single mutant strain (DM14838; not shown) was indistinguishable from wild type.

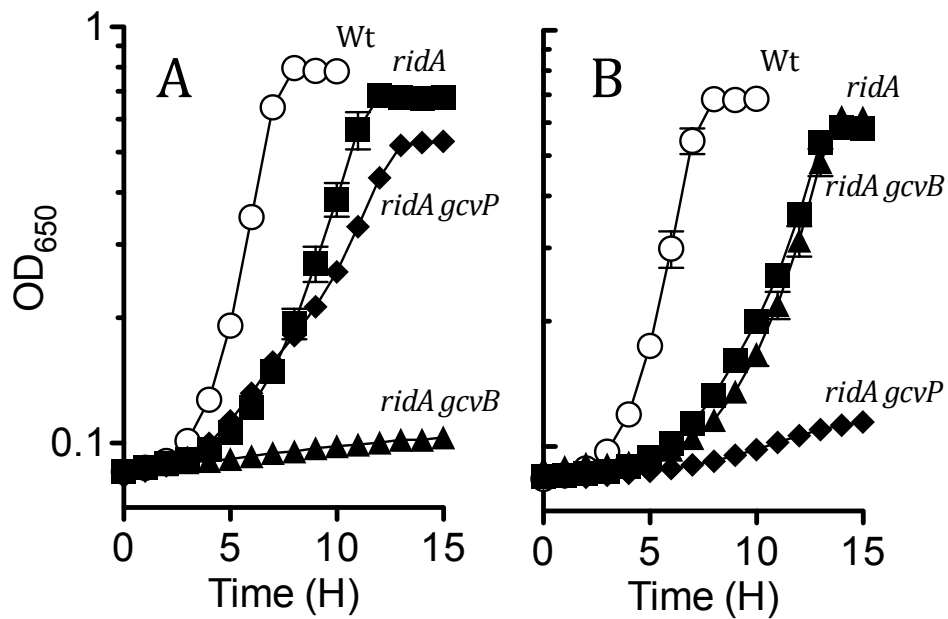


FIGURE 4.5. The metabolic components required for glycine to suppress the growth defect of a *ridA* strain are based on the source of metabolic stress. Growth of the indicated strains was assessed in minimal glucose glycine (0.67 mM) media containing 5 mM serine (A) or 0.25 mM cysteine (B). The average and standard deviation of three independent cultures is plotted for Wt (DM14828; open circles), *ridA* (DM14829; squares), *ridA gcvB* (DM14837; triangles) and *ridA gcvP* (DM14839; diamonds). Growth of the *gcvB* (DM14836) or *gcvP* (DM14838) single mutant strains was identical to wild type (data not shown).

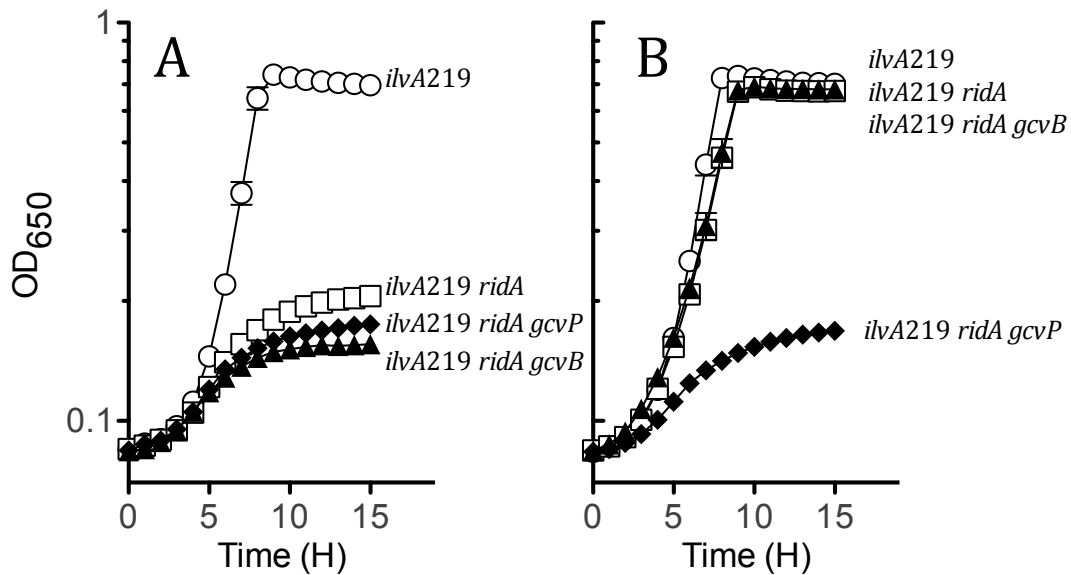


FIGURE 4.6. GCV is necessary for glycine to stimulate growth of a *ridA* strain inhibited 2AA produced from endogenous serine. Strains were grown in minimal glucose medium lacking additions (A) or supplemented with 0.67 mM glycine (B). The strains displayed include *ilvA219* (DM14830; open circles), *ilvA219 ridA* (DM14831; open squares), *ilvA219 ridA gcvB* (DM14841; closed triangles) and *ilvA219 ridA gcvP* (DM14843; closed diamonds). The data shown reflect the average and standard deviation of three independent cultures.

CHAPTER 5

MMF1P COUPLES AMINO ACID METABOLISM TO MITOCHONDRIAL DNA MAINTENANCE IN *SACCHAROMYCES CEREVISIAE*¹

¹Ernst DC, Downs DM. To be submitted to *mBio*.

5.1 ABSTRACT

A variety of metabolic deficiencies and human diseases arise from the disruption of mitochondrial enzymes and/or loss of mitochondrial DNA. Mounting evidence shows eukaryotes have conserved enzymes that prevent accumulation of reactive metabolites that cause stress in the mitochondrion. 2-aminoacrylate is a reactive enamine that is an obligatory intermediate in the breakdown of serine. In prokaryotes, members of the broadly conserved RidA family (PF14588) prevent metabolic stress by deaminating 2-aminoacrylate to pyruvate. Here, we demonstrate that unmanaged 2-aminoacrylate accumulation in *Saccharomyces cerevisiae* mitochondria causes transient metabolic stress and the irreversible loss of mitochondrial DNA. The RidA family protein Mmf1p deaminates 2-aminoacrylate and preempts metabolite mediated damage, which preserves normal metabolic function in mitochondria and prevents loss of the mitochondrial genome.

Significance. Deleterious reactive metabolites are produced as a consequence of many intracellular biochemical transformations. Importantly, reactive metabolites that appear short-lived *in vitro* have the unappreciated potential to persist within crowded intracellular environments, leading to pervasive cell damage and diminished fitness. To overcome metabolite damage, organisms utilize enzymatic reactive-metabolite defense systems to rid the cell of deleterious metabolites. In this report, we describe the importance of the RidA/YER057c/UK114 enamine/imine deaminase family in preventing 2-aminoacrylate stress in eukaryotes. *Saccharomyces cerevisiae* lacking the enamine/imine deaminase Mmf1p are shown to experience pleiotropic growth defects and fail to maintain their mitochondrial genome. Our results provide the first line of evidence that uncontrolled 2-aminoacrylate stress derived from mitochondrial serine metabolism negatively impacts mitochondrial DNA maintenance in eukaryotes.

5.2 BACKGROUND

RidA/YER057c/UK114 family proteins ([PF14588](#)) are ubiquitous; phylogenetic analysis identified the archetypal RidA throughout all three domains of life, with additional subgroups (Rid1-7) present in prokaryotes (1, 2). Biochemical genetic studies in the bacterium *Salmonella enterica* determined that RidA proteins are deaminases that hydrolyze the reactive enamine 2-aminoacrylate (2AA), and other substrates, to ketoacids (3–8). In cellular metabolism, 2AA is generated by pyridoxal 5'-phosphate (PLP)-dependent α,β -eliminase enzymes as an intermediate in the conversion of amino acids to pyruvate (3, 4, 7). Following release from the enzyme, 2AA can be spontaneously converted to pyruvate by solvent water (7). Although 2AA can covalently modify enzymes *in vitro* (9–15), the potential for intracellular enamine damage was initially dismissed because of the short (~ 1.5 s) half-life of 2AA in water (16). However, biochemical and genetic data demonstrate that in the absence of RidA, unbound 2AA persists *in vivo* and inactivates PLP-dependent enzymes (1, 17, 18). These data indicate that the cellular milieu lacks sufficient free water needed to rapidly hydrolyze 2AA, and provides the framework for phenotypes displayed by *ridA* mutants (6, 17–20).

Little is known about eukaryotic Rid proteins, although early reports suggested involvement in a variety of cellular processes mediated by undefined mechanisms (21–30). Interestingly, the mitochondrial RidA protein Mmf1p influences mitochondrial DNA (mtDNA) stability in *Saccharomyces cerevisiae* (29, 30). Characterization of enamine deaminase activity *in vitro* and genetic complementation analyses *in vivo* suggest that RidA proteins from the three domains of life share a conserved cellular function (7, 28). Here, we identify 2AA generation as the cause of irreversible mtDNA loss in *S. cerevisiae* lacking Mmf1p. Furthermore, 2AA stress elicits a growth defect that is distinct from the respiratory deficiency caused by mtDNA loss. This study establishes

the role of Mmflp in preventing 2AA stress in a eukaryote, and highlights damage that results from reactive metabolite imbalance in mitochondria.

5.3 MATERIALS AND METHODS

Strains, media and chemicals. *Saccharomyces cerevisiae* strain YJF153 (*MATa* HO::*dsdAMX4*) was derived from an oak tree isolate (YPS163) and provided by Justin Fay (Washington University) (31). Rich medium (YP) consisted of 20 g/L peptone (Fisher Scientific) and 10 g/L yeast extract (Becton Dickinson). Minimal medium (S medium) contained 1.7 g/L yeast nitrogen base without amino acids or nitrogen (Sunrise Science; #1500-100) and 5 g/L ammonium sulfate. Either dextrose (D; 20 g/L) or glycerol (G; 30 g/L) were provided as the sole carbon source. Solid medium was made by adding 20 g/L Difco agar (Becton Dickinson). Antibiotics used for deletion-marker selection were added to the following final concentrations: 400 µg/ml geneticin (G418; Gold Biotechnology), 200 µg/ml hygromycin B (Gold Biotechnology) and 100 µg/ml nourseothricin sulfate (cloNAT; Gold Biotechnology). A lower concentration of geneticin (200 µg/ml) was used for maintenance of strains with confirmed G418 resistance. Isoleucine or threonine were added to minimal growth medium at a final concentration of 1 mM.

Escherichia coli strain BL21-AI was used for recombinant protein overproduction. Standard *E. coli* growth medium (LB broth) consisted of 10 g/L tryptone, 5 g/L yeast extract and 10 g/L NaCl. Superbroth containing tryptone (32 g/L), yeast extract (20 g/L), sodium chloride (5 g/L) and sodium hydroxide (0.2 g/L) was used when high cell densities were required for protein overproduction. Ampicillin (150 µg/ml) was added to the growth medium as needed. Reagents and chemicals were purchased from Sigma Aldrich unless otherwise specified.

Genetic techniques and growth methods. Gene disruptions in *S. cerevisiae* were made following the standard gene replacement method described by Hegemann and Heick (32), resulting in the strains listed in table 5.1. Disruption cassettes were amplified using the appropriate primers and plasmid templates listed in table 5.2. Purified DNA (1 μ g) was transformed into *S. cerevisiae* by incubating cells suspended in 33 % PEG-3350, 100 mM lithium acetate and 0.28 mg/ml salmon sperm DNA at 30°C for 30 minutes followed by a 30-minute heat-shock at 42°C. The transformed cells were recovered in rich medium containing dextrose (YPD) for one hour at 30°C, and subsequently plated on solid YPD containing the relevant selection agent. Colonies that arose after 2-3 days of incubation were transferred to selective medium and individual colonies were screened via PCR for the appropriate genetic recombinants.

For growth analyses, yeast strains were revived from -80°C freezer stocks and streaked for isolation on YPD. Single colonies were inoculated into 2 ml YPD cultures and incubated at 30°C while shaking (200 rpm) overnight. Turbid cultures were i) 10-fold serial diluted with NaCl for spot plating (10 μ l) on solid medium or ii) inoculated (1%) into 5 ml of SD medium to monitor growth over time based on the change in OD₆₀₀. Growth curves were plotted as the average and standard deviation of three independent cultures using GraphPad Prism 7.0. Specific growth rates (μ) were calculated based on the equation $\ln(X/X_0)/T$, where X represents OD₆₀₀, X_0 is the initial OD₆₀₀ of the linear growth period monitored and T is time in hours.

Molecular techniques. Plasmids were constructed using standard molecular techniques. DNA was amplified using Q5 DNA polymerase (New England BioLabs) with primers purchased from Eton Bioscience Inc. (Research Triangle Park, NC). Plasmids were isolated using the Wizard Plus SV miniprep kit (Promega), and PCR products were purified using the E.Z.N.A DNA isolation kit (Omega Biotek). Restriction endonucleases used for molecular cloning were

purchased from New England BioLabs. T4 ligase (Thermo Scientific) was used to ligate inserts to vectors. The plasmids and primers are listed in table 5.2. Plasmids pUG6, pUG74 and pUG75 were used as templates for drug cassette amplification (EUROSCARF). Plasmid pFA6a-*kanMX* was provided by David Garfinkel (University of Georgia). The pSF episomal shuttle vector (Sigma Aldrich; Prod. # OGS542) containing a *TEF1* promoter, *TPII* terminator and geneticin (yeast)/ampicillin (bacteria) resistance markers was used to express *MMF1* in *S. cerevisiae* (pDM1481); full-length *MMF1* was PCR amplified for cloning using mmf1_pSF_NcoI_F and mmf1_pSF_XbaI_R. Constructs for protein overproduction were made using pET20b (Novagen) as the vector backbone. Primers were designed to amplify *MMF1* (mmf1_NdeI_F_truncated_pET20, mmf1_XhoI_R) or *ILV1* (ilv1_NdeI_F_truncated_pET20, ilv1_Not1_R_pET20) lacking the N-terminal mitochondrial targeting sequences and ligated into pET20b following restriction enzyme digestion of the insert and vector, forming pDM1463 and pDM1467, respectively. The full-length allele of *ILV1* was cloned into pET20b to make pDM1469. All constructs were transformed into DH5 α following ligation and selected on LB medium containing the appropriate drug. Plasmid inserts were confirmed by sequence analysis performed at Eton Bioscience Inc. Constructs pDM1467 and pDM1469 were used as templates for site directed mutagenesis to generate pDM1536 and pDM1540, respectively. Site directed mutants of *ILV1* were made by amplifying pDM1467 and pDM1469 with Q5 polymerase and primer ilv1_R416F, changing the codon for arginine-416 (AGA) to phenylalanine-416 (TTC), generating allele *ILV1-1*. Following transformation into DH5 α , site directed mutants were confirmed by Sanger sequencing (Eton Bioscience). Plasmid pDM1540 served as a template to amplify the *ILV1-1* allele for integration into the chromosome at the *ilv1::natMX* locus of DMy18. Replacement of the *natMX* drug cassette in DMy18 with the feedback-resistant *ILV1-1* allele

restored isoleucine prototrophy to DM_y43 and abolished nourseothricin sulfate resistance. Integration of the appropriate allele in DM_y43 was confirmed by sequence analysis (Eton Bioscience Inc.).

Purification of Mmflp₍₂₁₋₁₄₇₎. Mmflp₂₁₋₁₄₇, lacking the N-terminal amino acids required for mitochondrial localization, was purified from an *E. coli* BL21-AI strain containing pDM1463. An overnight culture of DM15531 grown in 10 ml of superbrotth containing ampicillin was inoculated into 2 liters of superbrotth with ampicillin. Cultures were grown for 3 h at 37°C with aeration (200 rpm) until an OD₆₅₀ of 0.5 was reached. Fresh arabinose was added to a final concentration of 0.02%, and cultures were shifted to 30°C and incubated for an additional 16 h while shaking. Cells were harvested by centrifugation and resuspended in binding buffer consisting of 50 mM Tris-HCl (pH 8), 200 mM sodium chloride, 10 mM imidazole, 1 mM TCEP and 10% glycerol. Lysozyme (1 mg/ml), phenylmethylsulfonyl fluoride (100 g/ml), and DNase (25 g/ml) were added to the cell suspension and incubated on ice for 1 h. Cells were lysed using the Constant Systems Limited One Shot (United Kingdom) system by passing cells through the disruptor one time with the pressure set to 21,000 psi. Following lysis, the extract was clarified, filtered, and injected onto a HisTrap HP Ni-sepharose column (5 ml). The column was washed with five column volumes of binding buffer with 40 mM imidazole added. Mmflp was eluted by increasing the concentration of imidazole from 40-300 mM over 10 column volumes, and 3 ml fractions were collected and analyzed by SDS-PAGE to determine protein purity. Fractions containing pure protein (> 99%) were pooled and concentrated by centrifugation with a 4,000-molecular-weight-cutoff filter unit (Millipore). The concentrated protein sample was transferred to storage buffer containing 10 mM HEPES and 10% glycerol using a PD-10 desalting column (GE Healthcare). Protein yield as determined using the BCA assay (Pierce) was approximately 14 mg/ml. Protein

aliquots were frozen in liquid nitrogen and stored at -80°C.

Purification of Ilv1p₍₄₆₋₅₇₆₎ and Ilv1p₍₄₆₋₅₇₆₎R416F. Plasmids encoding Ilv1p₄₆₋₅₇₆ (pDM1467) and Ilv1p₍₄₆₋₅₇₆₎R416F (pDM1536) were transformed into *E. coli* BL21-AI for protein purification. The resulting strains were inoculated into 10 ml of superbroth containing ampicillin and grown overnight at 37°C. Overnight cultures were subcultured into 2 liters of superbroth containing ampicillin and grown at 37°C until OD₆₅₀ of 0.7 was reached. Arabinose (0.02%) was added to induce expression, and cultures were shifted to 30°C for 16 h. Cells were harvested at 4°C by centrifugation (15 min at 8,000 g) and resuspended in binding buffer containing 50 mM potassium phosphate (pH 8), 500 mM sodium chloride, 10 mM imidazole, 1 mM TCEP, 10 µM PLP, and 10% glycerol. Lysozyme (1 mg/ml), phenylmethylsulfonyl fluoride (100 g/ml), and DNase (25 g/ml) were added to each cell suspension, which then sat on ice for 1 h. Cells were mechanically lysed using a French pressure cell (5 passes at 10,342 kPa). Each resulting lysate was clarified by centrifugation (45 min at 48,000 g) and filtered through a membrane with 0.45 µm pores. Filtered lysates were loaded onto HisTrap HP Ni-sepharose columns (5 ml), and the columns were washed with five column volumes of binding buffer containing 40 mM imidazole. Protein was eluted by increasing the concentration of imidazole in the elution buffer from 40-300 mM over 10 column volumes. Purified protein was concentrated by centrifugation with a 10,000-molecular-weight-cutoff filter unit (Millipore), and the buffer was replaced with 50 mM Tris-HCl (pH 7.5) containing 10 µM PLP and 10% glycerol using a PD-10 desalting column (GE Healthcare). Protein recovery as determined by the BCA assay (Pierce) was approximately 10.8 mg/ml for Ilv1p₄₆₋₅₇₆ and 13 mg/ml for Ilv1p₍₄₆₋₅₇₆₎R416F. Protein aliquots were frozen in liquid nitrogen and stored at -80°C.

Ilv1p generation of pyruvate assays. Ilv1p₍₄₆₋₅₇₆₎ serine dehydratase activity was assayed in the presence or absence of Mmf1p or RidA from *S. enterica* as previously described (7). The activity of purified RidA was previously confirmed (3). Reactions (300 μ l) consisted of 50 mM CHES pH 9.5, 0.6 μ M Ilv1p₍₄₆₋₅₇₆₎ and Mmf1p₍₂₁₋₁₄₇₎ (1.3 μ M) or RidA (1.3 μ M). Experiments were performed in triplicate and measured in a 96-well quartz plate using a SpectraMax M2 (Molecular Devices) microplate reader. Reactions were initiated by adding L-serine and monitored continuously at 230 nm for 120 s. Initial rates were determined based on the increase in A230 corresponding to pyruvate production. A standard curve of pyruvate concentrations relative to A230 was generated and used to calculate reaction rates, reported as μ mol of pyruvate produced per minute. The data, reported as the average and standard deviation of three independent experiments, were fit with curves based on the Michaelis-Menten equation using GraphPad Prism 7.0. The above procedure was used to compare Ilv1p₍₄₆₋₅₇₆₎ and Ilv1p₍₄₆₋₅₇₆₎R416F catalytic efficiency, with the sole change being 50 mM potassium phosphate pH 8 was used instead of 50 mM CHES pH 9.5.

Inhibition of Ilv1p variants by isoleucine assays. The sensitivity of Ilv1p₍₄₆₋₅₇₆₎ and Ilv1p₍₄₆₋₅₇₆₎R416F to allosteric regulation by isoleucine was determined *in vitro*. Reactions (300 μ l) consisted of 50 mM potassium phosphate pH 8 and 0.6 μ M Ilv1p₍₄₆₋₅₇₆₎ or 0.6 μ M Ilv1p₍₄₆₋₅₇₆₎R416F. Isoleucine was added to assays at a final concentration of 3.3 mM. Experiments were performed in triplicate and measured in a 96-well quartz plate using a SpectraMax M2 (Molecular Devices) microplate reader. Reactions were initiated by adding 120 mM L-serine and monitored continuously at 230 nm for 120 s. Initial rates were determined based on the increase in A230 corresponding to pyruvate formation. A standard curve of pyruvate concentrations relative to A230 was generated and used to calculate reaction rates, reported as μ mol of pyruvate produced per

minute. The reaction rates for a single concentration of serine added are reported as the average and standard deviation of three independent experiments.

Microscopy. Strains were grown in YPD to full-density overnight, then diluted to $OD_{600} = 0.1$ in complete synthetic dextrose medium (Sunrise Science; # 1001-010) the following morning. Cultures were then grown at 30°C and 200 rpm for 4 hours. Cells were harvested by centrifugation (2 minutes at 2,000 x g) and resuspended in mounting medium consisting of 10 mM HEPES pH 7.4 and 5 % dextrose. Cells were again pelleted and washed in an equal volume of mounting medium. The mitochondrial matrix was stained with 1 μ M Rhodamine B (Molecular Probes) for 20 minutes, followed by 3 minutes of staining with 10 μ M SYTO 18 (Molecular Probes) to detect mitochondrial DNA. Cells were pelleted and resuspended in fresh mounting medium, to which 2 μ l of ProLong Live Antifade reagent (Thermo Fisher) was added. Tubes containing cells and antifade reagent were transferred to a sealed box at 4°C overnight. The next morning, 20 μ ls of cell suspension were mounted on a glass slide and imaged using the DeltaVision microscope system (GE Life Sciences) equipped with an Olympus IX-71 inverted microscope and a xenon arc lamp as the illumination source for exciting fluorophores. Rhodamine B was visualized with excitation at 555 nm and emission at 627 nm and SYTO 18 was visualized with excitation at 490 nm and emission at 507 nm. Figures were generated by merging Z stacks of Rhodamine B and SYTO 18 images and the resulting merged images were deconvoluted using a conservative ratio and fifteen processing cycles using the automated softWoRx 6.5.2 (GE) image acquisition software. A quick projection was generated and the resulting images were exported to Adobe Illustrator 21.0.2. Images were cropped and resized without adjusting features related to contrast or brightness. Cell borders were generated in Adobe Illustrator by outlining each cell boundary as determined from a white light snapshot.

Effect of serine on respiratory capacity. A 50 μ l aliquot of strain DMy20 (ρ^+ *cha1* Δ *mmf1* Δ) grown ~12 hours in YPD medium at 30°C was used to inoculate 5 ml cultures containing SD medium with or without 5 mM serine added. Cultures were incubated at 30°C with shaking (200 rpm) for up to 72 hours and aliquots were taken at the indicated time-points following inoculation, serially diluted to 10^5 - 10^1 in NaCl and plated (10 μ l) on YPD and YPG plates. Images were acquired after ~48 hours of growth at 30°C and are representative of two independent experiments.

Rifampicin resistance frequency of *S. enterica* lacking *ridA*. The *in vivo* mutagenicity of 2-aminoacrylate was tested in a *ridA* strain of *S. enterica* known to accumulate 2AA when grown on minimal glucose medium (17). Cultures containing minimal glucose medium (5 ml) were inoculated with a single colony of wild type *S. enterica* LT2 (DM9404) or the isogenic *ridA3::MudJ* mutant strain (DM3480). Cultures were incubated at 37°C for 48 hours, pelleted and resuspended in NaCl solution at one-tenth the original volume and 100 μ l aliquots ($\sim 10^9$ CFU) were plated on solid rich medium containing 8 g/L nutrient broth, 5 g/L sodium chloride, 15 g/L agar and 60 μ g/ml rifampicin. Spontaneous rifampicin-resistant mutants were counted following 48 hours of incubation at 37°C and the average and standard deviation from three independent experiments are reported.

4.4 RESULTS AND DISCUSSION

Disruption of *MMF1* leads to a growth defect and loss of mtDNA. The *MMF1* locus of *S. cerevisiae* strain YJF153 (31) was replaced with a drug cassette by targeted gene disruption and the drug marker was resolved to generate mutant strain DMy22 (*mmf1* Δ 0). A plasmid expressing *MMF1*, or an empty vector (pSF-TEF1-G418; Sigma) was introduced into DMy22, the wild type

parent (ρ^+), and a chemically-induced cytoplasmic petite (ρ^-) derived from the wild type strain. The resulting strains were assessed for growth on minimal medium containing a fermentable (dextrose) and non-fermentable (glycerol) carbon substrate (Figure 5.1A). The *mmf1* Δ mutant had two significant growth phenotypes: i) an inability to grow on glycerol and ii) a reduced ability to grow on dextrose. Plasmid-borne *MMF1* failed to restore growth on glycerol, consistent with the irreversible loss or mutation of mtDNA observed in ρ^0 or ρ^- cytoplasmic petites (33) (Figure 5.1A). Results of deconvolution microscopy confirmed that the *mmf1* Δ mutant lacked detectable mtDNA, and therefore, was likely a ρ^0 -cytoplasmic petite (see below). In contrast, growth of the *mmf1* Δ mutant on dextrose was restored to the same level as the ρ^- control by providing plasmid-borne *MMF1*. This indicated that transient metabolic deficiencies distinguishable from the respiratory defect were encountered by strains lacking Mmf1p. The addition of isoleucine, and to a lesser extent threonine (an isoleucine precursor), restored growth of the ρ^0 *mmf1* Δ mutant on dextrose (Figure 5.1B), but not glycerol. Together these data distinguished the reversible and irreversible consequences of the *mmf1* Δ mutation, and each was considered in turn.

Ilv1p-generated 2-aminoacrylate causes a growth defect in the absence of Mmf1p. The data above supports a model where both the growth defect and mtDNA loss are a consequence of the toxic accumulation of 2AA in mitochondria lacking Mmf1p. The growth defect of a ρ^0 *mmf1* Δ mutant on dextrose is reminiscent of a *ridA* mutant phenotype in *S. enterica* (19). In this case, 2AA generated by serine/threonine dehydratase (IlvA; EC 4.3.1.19) accumulates and compromises growth. Isoleucine allosterically inhibits IlvA, prevents 2AA generation and restores growth. Two nuclear encoded serine/threonine dehydratases (EC 4.3.1.19) are active in the *S. cerevisiae* mitochondrion. Ilv1p is the biosynthetic serine/threonine dehydratase required for isoleucine biosynthesis (34), and Cha1p is a catabolic dehydratase induced by serine or threonine (35). Much

like the bacterial enzyme IlvA, Ilv1p catalyzes the first committed step in isoleucine biosynthesis, is subject to feedback inhibition by isoleucine, and uses serine as an alternative substrate to threonine (36) (Figure 5.2A). *In vitro*, Ilv1p dehydrated serine and released 2AA, which Mmf1p used as a substrate leading to an increased rate of pyruvate formation (Figure 5.2B). On a per mole basis, the 2AA-hydrolyzing activity of Mmf1p was indistinguishable from the well-characterized RidA enzyme from *S. enterica* (Figure 5.2B). These data support the hypothesis that the absence of Mmf1p leads to accumulation of 2AA following serine dehydration.

Taken together, the data favored a scenario depicted in Figure 5.2A and suggested the growth-stimulating role of isoleucine was exerted via the allosteric inhibition of Ilv1p. If true, preventing allosteric inhibition of Ilv1p would abolish the benefit of isoleucine in cells lacking Mmf1p. To test this hypothesis, an allosterically resistant variant of Ilv1p (Ilv1p^{R416F}) was analyzed. *In vitro*, recombinant Ilv1p₍₄₆₋₅₇₆₎^{R416F} was insensitive to isoleucine concentrations that completely inhibited the wild-type enzyme (Figure 5.2C). Importantly, the catalytic efficiency of serine dehydration by the variant enzyme was not significantly different than the wild-type enzyme (Figure 5.2D). Wild type *ILV1* was replaced with the full-length allele (*ILV1-1*) encoding Ilv1p^{R416F} to generate a strain where 2AA production by Ilv1p could not be inhibited. Isoleucine failed to completely reverse the growth defect of the *mmf1Δ* mutant strain expressing Ilv1p^{R416F} in minimal synthetic dextrose (SD) medium (Figure 5.2E). Therefore, isoleucine improves growth of the *mmf1Δ* mutant strain in part through allosteric inhibition of Ilv1p, and not by satisfying an isoleucine limitation. Taken together, these data show that Ilv1p generates 2AA from endogenous serine, and growth is limited unless Mmf1p or isoleucine quenches 2AA or inhibits Ilv1p activity, respectively.

Cha1p increases 2-aminoacrylate stress when exogenous serine is present. The ρ^0 *mmf1Δ* mutant characterized above was constructed on rich medium (YPD) containing isoleucine,

so feedback inhibition prevented Ilv1p from generating significant 2AA. Therefore, if 2AA stress contributes to mtDNA loss, an additional enzyme would be required to generate 2AA in the presence of isoleucine. The catabolic Ser/Thr dehydratase Cha1p is a logical source of 2AA since *CHAI* expression is induced by serine, which is present in YPD, and the enzyme is insensitive to regulation by isoleucine (35). Growth analysis in SD medium plus isoleucine, with or without serine, confirmed that Cha1p contributed to 2AA stress in the absence of Mmf1p (Figure 5.3A). Both the ρ^0 *mmf1* Δ and ρ^0 *mmf1* Δ *cha1* Δ mutants grew in medium with isoleucine, but the addition of serine only compromised growth of the ρ^0 *mmf1* Δ mutant, indicating *CHAI* is required for sensitivity to exogenous serine. These data indicate 2AA is produced following induction of Cha1p by exogenous serine, and Ilv1p is feedback-inhibited by isoleucine. The increased level of 2AA compromises growth in the absence of *MMFI*. Unlike a *ridA* mutant in *S. enterica* (37), the growth defect of the ρ^0 *mmf1* Δ mutant was not reversed by the addition of common nutritional supplements (i.e., amino acids or vitamins). This result suggests the cellular deficiencies underpinning the 2AA-dependent growth defect of *mmf1* Δ mutant strains in minimal medium are more complex than those caused by a single compromised enzyme.

Disruption of serine dehydratase-dependent 2-aminoacrylate production preserves mtDNA in the absence of *MMFI*. Despite the connection between Mmf1p and 2AA, it remained possible that the irreversible loss of mtDNA in an *mmf1* Δ mutant strain was unrelated to 2AA accumulation. However, data from order-dependent genetic manipulations and growth analyses demonstrate that 2AA stress specifically causes mtDNA loss (Figure 5.3B). First, *CHAI* was disrupted in a ρ^+ *MMFI* background. Second, *MMFI* was disrupted in the *cha1* Δ strain while Ilv1p was inhibited by isoleucine in the YPD-based selection medium. This resulted in a ρ^+ *cha1* Δ *mmf1* Δ double mutant with unique properties. Significantly, introducing the genetic lesions in this

order preempts the production of 2AA, and results in a strain that respire glycerol (Figure 5.3B) and maintains its mtDNA (Figure 5.4A). Therefore, preventing both Ilv1p and Cha1p serine dehydratase activity renders Mmf1p non-essential for mtDNA maintenance. The inversely constructed *mmf1Δ CHA1* strain lost the ability to respire glycerol, and subsequent disruption of *CHA1* in the absence of *MMF1* did not restore growth on glycerol (Figure 5.3B). These results demonstrate that disruption of *MMF1* prior to *CHA1* leads to permanent loss of mtDNA, as supported by mitochondrial staining of the ρ^0 *mmf1Δ cha1Δ* strain (Figure 5.4A). Thus, identical genotypes constructed in opposing series result in dramatically different outcomes with regard to mtDNA stability. These data support the conclusion that the preemptive disruption of *CHA1*, coupled with isoleucine-mediated inhibition of Ilv1p, blocks 2AA production in the mitochondrial matrix and bypasses the need for Mmf1p to maintain the mitochondrial genome.

The ρ^+ *cha1Δ mmf1Δ* mutant maintains wild-type growth indefinitely when propagated on medium containing isoleucine. However, when the inhibition of Ilv1p was lifted by removing isoleucine, a growth defect of the ρ^+ *cha1Δ mmf1Δ* mutant strain ($\mu = 0.16$) relative to the ρ^+ wild-type control ($\mu = 0.45$) was detected (Figure 5.4B). Isoleucine supplementation restored the growth rate of ρ^+ *cha1Δ mmf1Δ* strain ($\mu = 0.44$) to the same level as the ρ^+ wild-type control ($\mu = 0.48$). A parallel result was observed with the respiration-deficient ρ^0 *mmf1Δ cha1Δ* mutant strain where the addition of isoleucine increased the growth rate to the level of the ρ^- wild-type control ($\mu = 0.26$) (Figure 5.4B). These data show that the ρ^+ *cha1Δ mmf1Δ* mutant is susceptible to 2AA stress and experiences diminished growth when cultured on minimal medium. However, the respiratory capacity of the ρ^+ *cha1Δ mmf1Δ* mutant was maintained indefinitely during growth on minimal medium (Figure 5.5). This result suggests that mtDNA is stable in spite of the growth defect given the moderate level of 2AA stress generated by Ilv1p on minimal medium. Enhancing flux through

Ilv1p to increase 2AA stress severely diminished the ability of the ρ^+ *cha1* Δ *mmf1* Δ mutant to respire glycerol after growth on minimal medium supplemented with 5 mM serine (Figure 5.5). Taken together, these data indicate that in the absence of Mmf1p, Ilv1p acts on endogenous serine to generate moderate 2AA stress that elicits a minor and reversible growth defect akin to the bacterial paradigm (5). However, exogenous serine stimulates production (via Ilv1p and/or Cha1p) of sufficient 2AA to cause irreversible loss of the mitochondrial genome.

Conclusions. Our work shows that accumulation of 2AA causes metabolic stress and loss of mtDNA in *S. cerevisiae*. Furthermore, Mmf1p prevents 2AA accumulation in the *S. cerevisiae* mitochondrion. Two consequences of 2AA accumulation in the mitochondrion were identified: the irreversible loss of mtDNA giving rise to respiration-deficient ρ^0 cytoplasmic petites and a transient growth defect on fermentable carbon substrates. The latter phenotype is reminiscent of the growth defects caused by 2AA stress in *S. enterica* (6, 19) and other organisms (8, 28). PLP-dependent enzymes are the only targets of 2AA damage characterized to date (38), suggesting the *mmf1* Δ strain growth defect is due to inhibition of one or more (of 10 possible) target PLP enzymes in the mitochondrion (39) (Figure 5.6). 2AA is not mutagenic *in vivo* when queried with a bacterial system (Table 5.3), making it unlikely that direct DNA damage by 2AA causes the loss of mtDNA. We suggest loss of mtDNA is caused by the stress 2AA exerts on the mitochondrial metabolic network. Specifically, we favor a model in which 2AA damages multiple mitochondrial PLP-dependent enzymes, ultimately leading to destabilization and loss of the mitochondrial genome (Figure 5.6). The independent disruption of mitochondrial PLP-dependent enzymes involved in heme biosynthesis (Hem1p; EC 2.3.1.37), iron-sulfur cluster biogenesis (Nfs1p; EC 2.8.1.7), one-carbon metabolism (Shm1p; EC 2.1.2.1), and aspartate metabolism (Aat1p; EC 2.6.1.1) have been reported to influence mtDNA stability to varying degrees (40–43). Given the variety of PLP-

dependent enzymes that individually impact mtDNA stability, it is reasonable that a combination of partially defective enzymes could result in mtDNA loss. Consistently, preliminary work shows that Hem1p is targeted by 2AA in an *mmf1Δ* strain (data not shown). Further understanding of how 2AA leads to loss of mtDNA may uncover a novel stress response pathway in mitochondria.

Our work identified a lethal consequence of uncontrolled reactive metabolite accumulation in the mitochondrion. Synthesis of 2AA is unavoidable in PLP-dependent serine dehydration, resulting in the need for RidA proteins (e.g., Mmf1p) to prevent accumulation of this reactive metabolite. Strikingly, when *S. cerevisiae* is exposed to serine, *CHA1* and *MMF1* are the two most highly expressed genes (44), suggesting these enzymes act in concert to safely reduce serine levels in the mitochondrion. Interestingly, Cha1p is reported to be a component of the mitochondrial nucleoid in *S. cerevisiae* (45), perhaps reflecting an added benefit of Cha1p-dependent physical stabilization of the nucleoid during periods of elevated serine catabolism and 2AA production. The Mmf1p homolog in humans, UK114 ([PF01042](#)), is variably described as a tumor antigen, calpain activator or translation inhibitor in diverse animal cell types (21, 26, 46–48). Importantly, UK114 can substitute for Mmf1p to maintain the mitochondrial genome in *S. cerevisiae* (29), which argues in favor of an evolutionarily conserved biological function. PLP-dependent serine dehydratases are broadly distributed among eukaryotes, which emphasizes the breadth of 2AA stress (49–51). Furthermore, many cell types, including cancer cells and neurons, require high serine levels to promote growth and proliferation (52–54), predisposing certain cell types to high concentrations of a known 2AA precursor. Our work provides a framework for understanding the physiological role of Mmf1p and other eukaryotic RidA proteins, in addition to dissecting the mechanism by which 2AA stress causes loss of mtDNA.

ACKNOWLEDGEMENTS

The authors would like to thank David Garfinkel for technical guidance and David Garfinkel, Zachary Lewis and Jorge Escalante for critical reading of this manuscript. We thank Justin Fay (Washington University) for generously providing strain YJF153. Muthugapatti Kandasamy (University of Georgia) assisted with microscopy. This work was supported by funding from the NIH (GM095837) to D.M.D.

4.5 REFERENCES

1. Lambrecht JA, Schmitz GE, Downs DM. 2013. RidA proteins prevent metabolic damage inflicted by PLP-dependent dehydratases in all domains of life. *MBio* 4:e00033-13.
2. Niehaus TD, Gerdes S, Hodge-Hanson K, Zhukov A, Cooper AJ, ElBadawi-Sidhu M, Fiehn O, Downs DM, Hanson AD. 2015. Genomic and experimental evidence for multiple metabolic functions in the RidA/YjgF/YER057c/UK114 (Rid) protein family. *BMC Genomics* 16:382.
3. Ernst DC, Lambrecht JA, Schomer RA, Downs DM. 2014. Endogenous synthesis of 2-aminoacrylate contributes to cysteine sensitivity in *Salmonella enterica*. *J Bacteriol* 196:3335–3342.
4. Ernst DC, Anderson ME, Downs DM. 2016. L-2,3-diaminopropionate generates diverse metabolic stresses in *Salmonella enterica*. *Mol Microbiol* 101:210–223.
5. Enos-Berlage JL, Langendorf MJ, Downs DM. 1998. Complex metabolic phenotypes caused by a mutation in *yjgF*, encoding a member of the highly conserved YER057c/YjgF family of proteins. *J Bacteriol* 180:6519–6528.
6. Christopherson MR, Schmit GE, Downs DM. 2008. YjgF is required for isoleucine biosynthesis when *Salmonella enterica* is grown on pyruvate medium. *J Bacteriol* 190:3057–3062.
7. Lambrecht JA, Flynn JM, Downs DM. 2012. Conserved YjgF protein family deaminates reactive enamine/imine intermediates of pyridoxal 5'-phosphate (PLP)-dependent enzyme reactions. *J Biol Chem* 287:3454–3461.

8. Borchert AJ, Downs DM. 2017. The response to 2-aminoacrylate differs in *Escherichia coli* and *Salmonella enterica*, despite shared metabolic components. *J Bacteriol* 199:e00140-17.
9. Walsh C. 1982. Suicide substrates: mechanism-based enzyme inactivators. *Tetrahedron* 38:871–909.
10. Rando RR. 1974. Irreversible inhibition of aspartate aminotransferase by 2-amino-3-butenic acid. *Biochemistry (Mosc)* 13:3859–3863.
11. Relyea NM, Tate SS, Meister A. 1974. Affinity labeling of the active center of l-aspartate- β -decarboxylase with β -chloro-l-alanine. *J Biol Chem* 249:1519–1524.
12. Wang EA, Kallen R, Walsh C. 1981. Mechanism-based inactivation of serine transhydroxymethylases by D-fluoroalanine and related amino acids. *J Biol Chem* 256:6917–6926.
13. Ueno H, Likos JJ, Metzler DE. 1982. Chemistry of the inactivation of cytosolic aspartate aminotransferase by serine O-sulfate. *Biochemistry (Mosc)* 21:4387–4393.
14. Likos JJ, Ueno H, Feldhaus RW, Metzler DE. 1982. A novel reaction of the coenzyme of glutamate decarboxylase with L-serine O-sulfate. *Biochemistry (Mosc)* 21:4377–4386.
15. Kishore GM. 1984. Mechanism-based inactivation of bacterial kynureninase by beta-substituted amino acids. *J Biol Chem* 259:10669–10674.
16. Hillebrand GG, Dye JL, Suelter CH. 1979. Formation of an intermediate and its rate of conversion to pyruvate during the tryptophanase-catalyzed degradation of S-o-nitrophenyl-L-cysteine. *Biochemistry (Mosc)* 18:1751–1755.
17. Flynn JM, Christopherson MR, Downs DM. 2013. Decreased coenzyme A levels in *ridA* mutant strains of *Salmonella enterica* result from inactivated serine hydroxymethyltransferase: *ridA* mutants are deficient in one carbon metabolism. *Mol Microbiol* 89:751–759.
18. Flynn JM, Downs DM. 2013. In the absence of RidA, endogenous 2-aminoacrylate inactivates alanine racemases by modifying the pyridoxal 5'-phosphate cofactor. *J Bacteriol* 195:3603–3609.
19. Schmitz G, Downs DM. 2004. Reduced transaminase B (IlvE) activity caused by the lack of *yjgF* is dependent on the status of threonine deaminase (IlvA) in *Salmonella enterica* serovar Typhimurium. *J Bacteriol* 186:803–810.

20. Christopherson MR, Lambrecht JA, Downs D, Downs DM. 2012. Suppressor analyses identify threonine as a modulator of *ridA* mutant phenotypes in *Salmonella enterica*. PLOS ONE 7:e43082.
21. Farkas A, Nardai G, Csermely P, Tompa P, Friedrich P. 2004. DUK114, the *Drosophila* orthologue of bovine brain calpain activator protein, is a molecular chaperone. Biochem J 383:165–170.
22. Oka T, Tsuji H, Noda C, Sakai K, Hong Y, Suzuki I, Muñoz S, Natori Y. 1995. Isolation and characterization of a novel perchloric acid-soluble protein inhibiting cell-free protein synthesis. J Biol Chem 270:30060–30067.
23. Deaconescu AM, Roll-Mecak A, Bonanno JB, Gerchman SE, Kycia H, Studier FW, Burley SK. 2002. X-ray structure of *Saccharomyces cerevisiae* homologous mitochondrial matrix factor 1 (Hmf1). Proteins Struct Funct Genet 48:431–436.
24. Deriu D. 2003. Structure and oligomeric state of the mammalian tumour-associated antigen UK114. Acta Crystallogr D Biol Crystallogr D59:1676–1678.
25. Manjasetty BA, Delbrück H, Pham D-T, Mueller U, Fieber-Erdmann M, Scheich C, Sievert V, Büsow K, Neisen FH, Weihofen W. 2004. Crystal structure of *Homo sapiens* protein hp14. 5. PROTEINS Struct Funct Bioinforma 54:797–800.
26. Michetti M, Viotti PL, Melloni E, Pontremoli S. 1991. Mechanism of action of the calpain activator protein in rat skeletal muscle. Eur J Biochem 202:1177–1180.
27. Antonenkov VD, Ohlmeier S, Sormunen RT, Hiltunen JK. 2007. UK114, a YjgF/Yer057p/UK114 family protein highly conserved from bacteria to mammals, is localized in rat liver peroxisomes. Biochem Biophys Res Commun 357:252–257.
28. Niehaus TD, Nguyen TND, Gidda SK, ElBadawi-Sidhu M, Lambrecht JA, McCarty DR, Downs DM, Cooper AJL, Fiehn O, Mullen RT, Hanson AD. 2014. *Arabidopsis* and *Maize* RidA proteins preempt reactive enamine/imine damage to branched-chain amino acid biosynthesis in plastids. Plant Cell 7:3010–3022.
29. Oxelmark E, Marchini A, Malanchi I, Magherini F, Jaquet L, Hajibagheri MAN, Blight KJ, Jauniaux J-C, Tommasino M. 2000. Mmf1p, a novel yeast mitochondrial protein conserved throughout evolution and involved in maintenance of the mitochondrial genome. Mol Cell Biol 20:7784–7797.
30. Kim J-M, Yoshikawa H, Shirahige K. 2001. A member of the YER057c/yjgf/Uk114 family links isoleucine biosynthesis and intact mitochondria maintenance in *Saccharomyces cerevisiae*. Genes Cells 6:507–517.

31. Li XC, Fay JC. 2017. Cis-regulatory divergence in gene expression between two thermally divergent yeast species. *Genome Biol Evol* 9:1120–1129.
32. Hegemann JH, Heick SB. 2011. Delete and repeat: a comprehensive toolkit for sequential gene knockout in the budding yeast *Saccharomyces cerevisiae*. *Methods Mol Biol* 765:189–206.
33. Day M. 2013. Yeast petites and small colony variants: for everything there is a season, p. 1–41. *In* Sariaslani, S, Gadd, GM (eds.), *Advances in Applied Microbiology*.
34. Ryan ED, Kohlhaw GB. 1974. Subcellular localization of isoleucine-valine biosynthetic enzymes in yeast. *J Bacteriol* 120:631–637.
35. Bornaes C, Ignjatovic MW, Schjerling P, Kielland-Brandt MC, Holmberg S. 1993. A regulatory element in the *CHAI* promoter which confers inducibility by serine and threonine on *Saccharomyces cerevisiae* genes. *Mol Cell Biol* 13:7604–7611.
36. Ahmed SI, Bollon AP, Rogers SJ, Magee PT. 1976. Purification and properties of threonine deaminase from *Saccharomyces cerevisiae*. *Biochimie* 58:225–232.
37. Ernst DC, Downs DM. 2016. 2-aminoacrylate stress induces a context-dependent glycine requirement in *ridA* strains of *Salmonella enterica*. *J Bacteriol* 198:536–543.
38. Downs DM, Ernst DC. 2015. From microbiology to cancer biology: the Rid protein family prevents cellular damage caused by endogenously generated reactive nitrogen species. *Mol Microbiol* 96:211–219.
39. Whittaker JW. 2016. Intracellular trafficking of the pyridoxal cofactor. Implications for health and metabolic disease. *Arch Biochem Biophys* 592:20–26.
40. Whittaker MM, Penmatsa A, Whittaker JW. 2015. The Mtm1p carrier and pyridoxal 5'-phosphate cofactor trafficking in yeast mitochondria. *Arch Biochem Biophys* 568:64–70.
41. Sliwa D, Dairou J, Camadro J-M, Santos R. 2012. Inactivation of mitochondrial aspartate aminotransferase contributes to the respiratory deficit of yeast frataxin-deficient cells. *Biochem J* 441:945–953.
42. Luzzati M. 1975. Isolation and properties of a thymidylate-less mutant in *Saccharomyces cerevisiae*. *Eur J Biochem* 56:533–538.
43. Li J, Kogan M, Knight SA, Pain D, Dancis A. 1999. Yeast mitochondrial protein, Nfs1p, coordinately regulates iron-sulfur cluster proteins, cellular iron uptake, and iron distribution. *J Biol Chem* 274:33025–33034.

44. Godard P, Urrestarazu A, Vissers S, Kontos K, Bontempi G, van Helden J, Andre B. 2007. Effect of 21 different nitrogen sources on global gene expression in the yeast *Saccharomyces cerevisiae*. *Mol Cell Biol* 27:3065–3086.
45. Chen XJ, Wang X, Kaufman BA, Butow RA. 2005. Aconitase couples metabolic regulation to mitochondrial DNA maintenance. *Science* 307:714–717.
46. Bussolati G, Geuna M, Bussolati B, Millesimo M, Botta M, Bartorelli A. 1997. Cytolytic and tumor inhibitory antibodies against UK114 protein in the sera of cancer patients. *Int J Oncol* 10:779–785.
47. Funaro A, Horenstein AL, Ghisolfi G, Bussolati B, Bartorelli A, Bussolati G. 1999. Identification of a 220-kDa membrane tumor-associated antigen by human anti-UK114 monoclonal antibodies selected from the immunoglobulin repertoire of a cancer patient. *Exp Cell Res* 247:441–450.
48. Rorbach J, Minczuk M. 2012. The post-transcriptional life of mammalian mitochondrial RNA. *Biochem J* 444:357–373.
49. Snell K. 1984. Enzymes of serine metabolism in normal, developing and neoplastic rat tissues. *Adv Enzyme Regul* 22:325–400.
50. Sun L, Bartlam M, Liu Y, Pang H, Rao Z. 2005. Crystal structure of the pyridoxal-5'-phosphate-dependent serine dehydratase from human liver. *Protein Sci* 14:791–798.
51. Yamada T, Komoto J, Kasuya T, Takata Y, Ogawa H, Mori H, Takusagawa F. 2008. A catalytic mechanism that explains a low catalytic activity of serine dehydratase like-1 from human cancer cells: crystal structure and site-directed mutagenesis studies. *Biochim Biophys Acta BBA - Gen Subj* 1780:809–818.
52. Labuschagne CF, van den Broek NJF, Mackay GM, Vousden KH, Maddocks ODK. 2014. Serine, but not glycine, supports one-carbon metabolism and proliferation of cancer cells. *Cell Rep* 7:1248–1258.
53. Amelio I, Cutruzzolá F, Antonov A, Agostini M, Melino G. 2014. Serine and glycine metabolism in cancer. *Trends Biochem Sci* 39:191–198.
54. de Koning TJ, Snell K, Duran M, Berger R, SURTEES R, others. 2003. L-serine in disease and development. *Biochem J* 371:653–661.

TABLE 5.1. Strain list

Strain	Relevant Genotype
YJF153*	MATa HO:: <i>dsdAMX4</i>
DMy13	<i>mmf1::kanMX</i> (ρ^0)
DMy16	<i>cha1::hphMX</i>
DMy17	<i>mmf1::kanMX cha1::hphMX</i> (ρ^0)
DMy18	<i>ilv1::natMX</i>
DMy20	<i>cha1::hphMX mmf1::kanMX</i>
DMy23	YJF153 (ρ^-)
DMy21	<i>mmf1::hphMX-loxP</i> (ρ^0)
DMy22	<i>mmf1Δ0</i> (ρ^0)
DMy31	YJF153 / pDM1481
DMy32	YJF153 / pSF-empty
DMy33	<i>mmf1Δ0</i> (ρ^0) / pDM1481
DMy34	<i>mmf1Δ0</i> (ρ^0) / pSF-empty
DMy35	YJF153 (ρ^-) / pDM1481
DMy36	YJF153 (ρ^-) / pSF-empty
DMy43	<i>ilv1Δ0::ILV1-1**</i>
DMy46	<i>ilv1Δ0::ILV1-1 mmf1::kanMX</i>
DM15531	<i>E. coli</i> BL21-AI / pDM1463
DM15533	<i>E. coli</i> BL21-AI / pDM1467
DM15910	<i>E. coli</i> BL21-AI / pDM1536

*All yeast strains were constructed in a YJF153 strain background. **Allele *ILV1-1* encodes Ilv1p^{R416F} feedback-resistant variant.

TABLE 5.2. Plasmids and primers used in this study.

Plasmids	Description	Source
pDM1463	pET20- <i>mmf1</i> ₍₂₁₋₁₄₇₎	This study.
pDM1467	pET20- <i>ilv1</i> ₍₄₆₋₅₇₆₎	This study.
pDM1481	pSF- <i>mmf1</i>	This study.
pDM1536	pET20- <i>ilv1</i> ₍₄₆₋₅₇₆₎ R416F	This study.
pDM1540	pET20- <i>ilv1</i> -R416F	This study.
pSF	pSF-TEF1-TPI1-G418	Sigma Aldrich
pFA6a-KanMX	TEF1-kanMX-tAgTEF1	D. Garfinkel
pUG6	loxP-pAgTEF1-kanMX-tAgTEF1-loxP	EUROSCARF
pUG74	loxP-pAgTEF1-natMX-tAgTEF1-loxP	EUROSCARF
pUG75	loxP-pAgTEF1-hphMX-tAgTEF1-loxP	EUROSCARF

Primers	Sequence
insMX_BM	GGATGTATGGGCTAAATG
insMX_CM	CCTCGACATCATCTGCC
mmf1_insMX_F	GTA AAAAGGACAACACATACACACAAATATATTACCAATACAGCTGAAGCTTCGTACGC
mmf1_insMX_R	ATCGCAAGTGGAAAAAGGCAGTAAAGAAGTTTCAATCCTGCATAGGCCACTAGTGGATCTG
mmf1_A	GGCGGTGATCTTAGAAGACC
mmf1_B	AGATAGAACCTTGAACAGGC
mmf1_C	GGTTCTATCTCTGAGAAGGC
mmf1_D	CACCCAAACAACACACGG
ilv1_insMX_F	CAAGCCACATTTAAACTAAGTCAATTACACAAAAGTTAGTGCAGCTGAAGCTTCGTACGC
ilv1_insMX_R	AACAAGTTGTTGCGTAAATTTATAAAGTAAATTGTCGGTTGCATAGGCCACTAGTGGATC
ilv1_A	CGCAGCGGGTAGCAAATT
ilv1_B	GAGTAACATACACGCGCTG
ilv1_C	TTCCCTGAAAGACCAGGTG
ilv1_D	AGACGGGAAGACAAACCTAC
cha1_insMX_F	AGTGCTGGATAGACAAGAGACAGGAAAATTAACCAGCGAGCAGCTGAAGCTTCGTACGC
cha1_insMX_R	AAGGGCAAATTTGATGCTTCAACGAAAAAGTTATTGGATTTCATAGGCCACTAGTGGATC
cha1_A	AAGGGACAATATGAGGAGGA
cha1_B	GCATTACCGCCAGA ACTAG
cha1_C	ATTAGCTGCGGATGACATTG
cha1_D	GGATATGTTGATGCTTACTTCC
T7_promoter_F	TAATACGACTCACTATAGGG
T7_promoter_R	TATGCTAGTTATTGCTCAGCG
mmf1_NdeI_F_truncated_pET20	GGCATATGATAACAACATTGACCCCGGTC
mmf1_XhoI_R	GGCTCGAGATTCTTTTCAACAGCGATAAC
ilv1_NdeI_F_truncated_pET20	GAGACATATGCACTCTGAATTGAAATTGGATG
ilv1_NotI_R_pET20	GAGAGCGGCCGCATATTTCAAGAATTTTGATAAAC
mmf1_pSF_NcoI_F	GAGACCATGGCCTTTTAAAGAAATTCGGTTTGGAG
mmf1_pSF_XbaI_R	GAGATCTAGATCAATTCTTTTCAACAGCGATAAC
ilv1_R416F	ATGCAAAAAGATCATCCACCCATTCTCTGTTACTGAATTCTCTTACC
ilv1_QC_replacement_F	CAAGCCACATTTAAACTAAGTCAATTACACAAAAGTTAGTGCAGCTACTCTACTAAA
ilv1_QC_replacement_R	GTTGCGTAAATTTATAAAGTAAATTGTCGGTTTAAATTTCAAGAATTTTGATAAAC

TABLE 5.3. Frequency of rifampicin resistant colonies in wild-type and *ridA* strains of *S. enterica*

Strain	Genotype	CFU/10 ⁹ cells
DM9404	Wild type	43 ± 3
DM3480	<i>ridA3::MudJ</i>	42 ± 1

The values reported indicate the average and standard deviation of three independent experiments. CFU; colony forming unit.

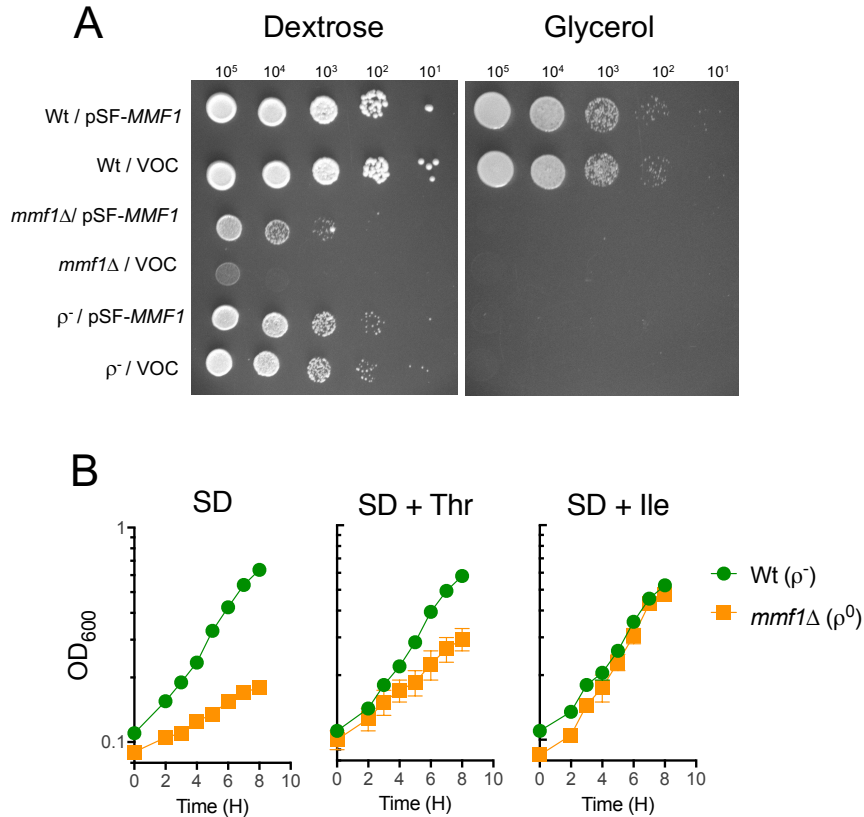


FIGURE 5.1. Yeast lacking *Mmf1p* cannot respire glycerol and have a growth defect on glucose. (A) Growth of wild-type (ρ^+), petite wild-type (ρ^-) and *mmf1*Δ mutant strains on synthetic dextrose (SD) and synthetic glycerol (SG) solid media. An *MMF1* expression plasmid (pSF-*MMF1*) or the empty vector (pSF) were transformed into each strain prior to growth analyses. (B) Growth of a ρ^0 *mmf1*Δ mutant and petite wild-type (ρ^-) in liquid SD medium supplemented with isoleucine or threonine as indicated. Data indicate the average and standard deviation of three independent cultures.

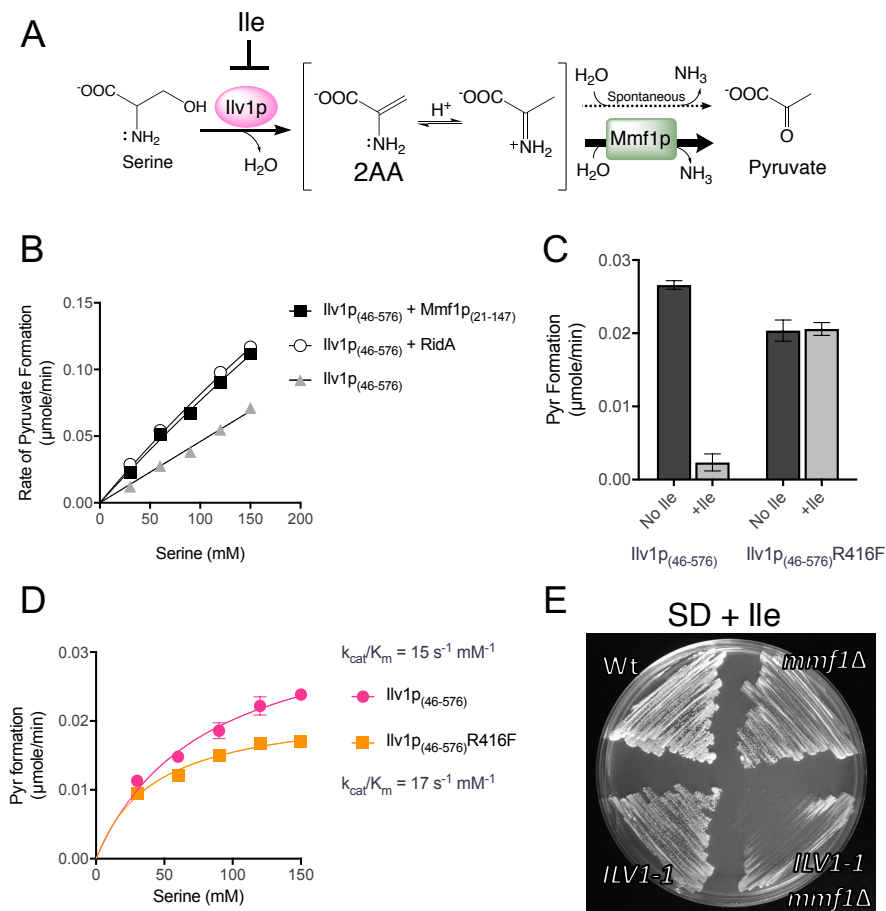


FIGURE 5.2. Ilv1p generates 2AA stress in yeast lacking Mmf1p. (A) The scheme of Ilv1p-mediated pyruvate formation, showing 2AA as an unbound intermediate that can be hydrolyzed to pyruvate by solvent water or Mmf1p. Isoleucine allosterically inhibits Ilv1p activity and prevents 2AA formation. (B) The rate of serine to pyruvate conversion by Ilv1p₍₄₆₋₅₇₆₎ is enhanced similarly by adding Mmf1p₍₂₁₋₁₄₇₎ (*S. cerevisiae*) or RidA (*S. enterica*). Data represent the average and standard deviation of three independent experiments, with error bars not exceeding the symbol boundaries. (C) The serine dehydratase activity of the purified Ilv1p₍₄₆₋₅₇₆₎-R416F variant is insensitive to a concentration of isoleucine (3.3 mM) that completely inhibited the wild-type enzyme. Data represent the average and standard deviation of three independent experiments. (D) Ilv1p₍₄₆₋₅₇₆₎-R416F has similar catalytic efficiency for serine dehydration relative to the wild-type enzyme. Data indicate the average and standard deviation of three independent experiments. (E) Inserting the *ILV1-1* allele encoding Ilv1p^{R416F} into a ρ^0 *mmf1* Δ strain prevented isoleucine from restoring full-growth to the double mutant when compared to the ρ^0 *mmf1* Δ single mutant following 48 hours of incubation on solid SD + Ile (1 mM) medium at 30°C.

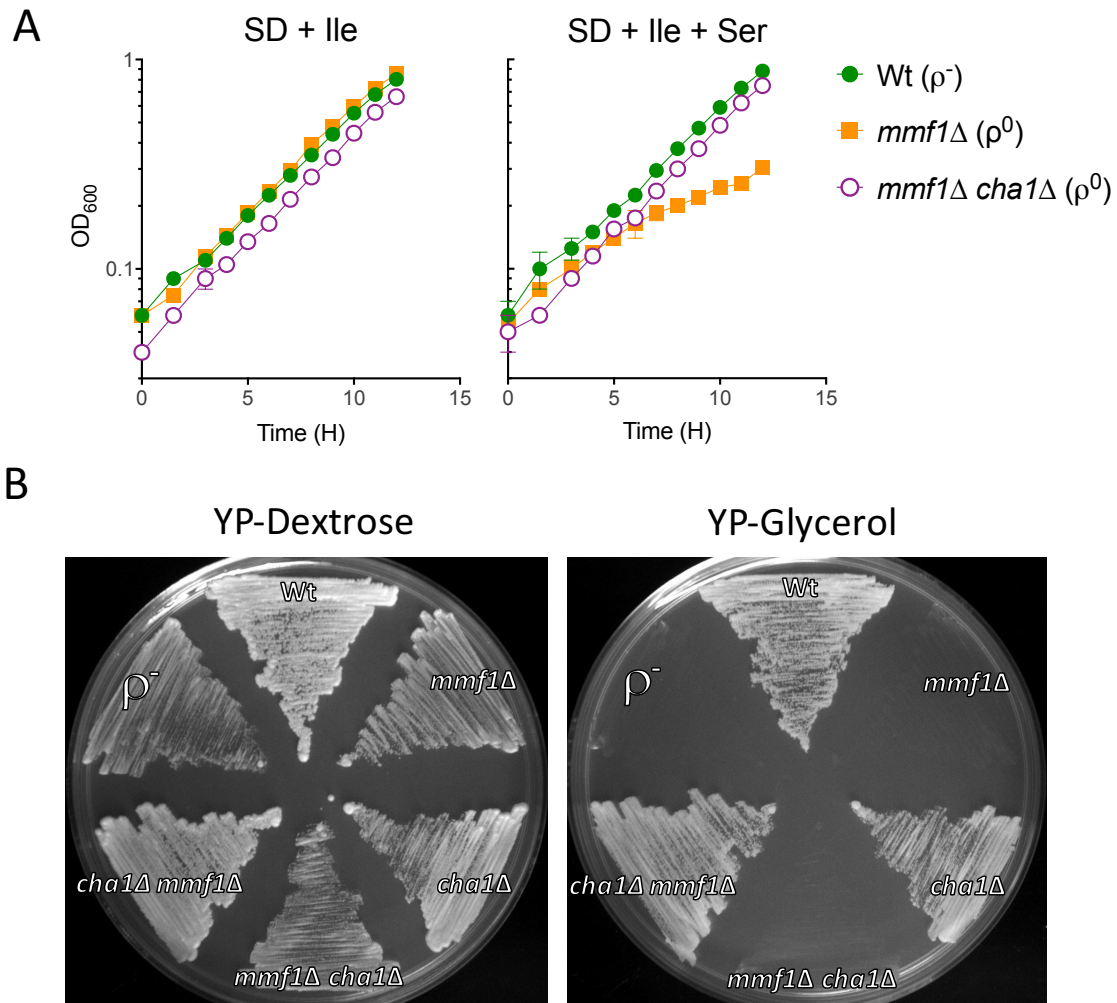


FIGURE 5.3. Cha1p contributes to 2AA generation when serine is provided exogenously. (A) Disruption of *CHAI* prevents conversion of exogenous serine to 2AA, thereby alleviating exogenous serine sensitivity in a $\rho^0 mmf1\Delta cha1\Delta$ background. Data are displayed as the average and standard deviation of three independent experiments. **(B)** Preventing 2AA production by simultaneously inhibiting the activity of Ilv1p (with isoleucine) and deleting *CHAI* renders Mmf1p non-essential for mtDNA maintenance despite the presence of serine in the growth medium. All mutants were constructed in the order indicated by the genotype and selected on YPD medium prior to streaking on the displayed YPD or YPG plates. Growth was recorded after 48 hours at 30°C.

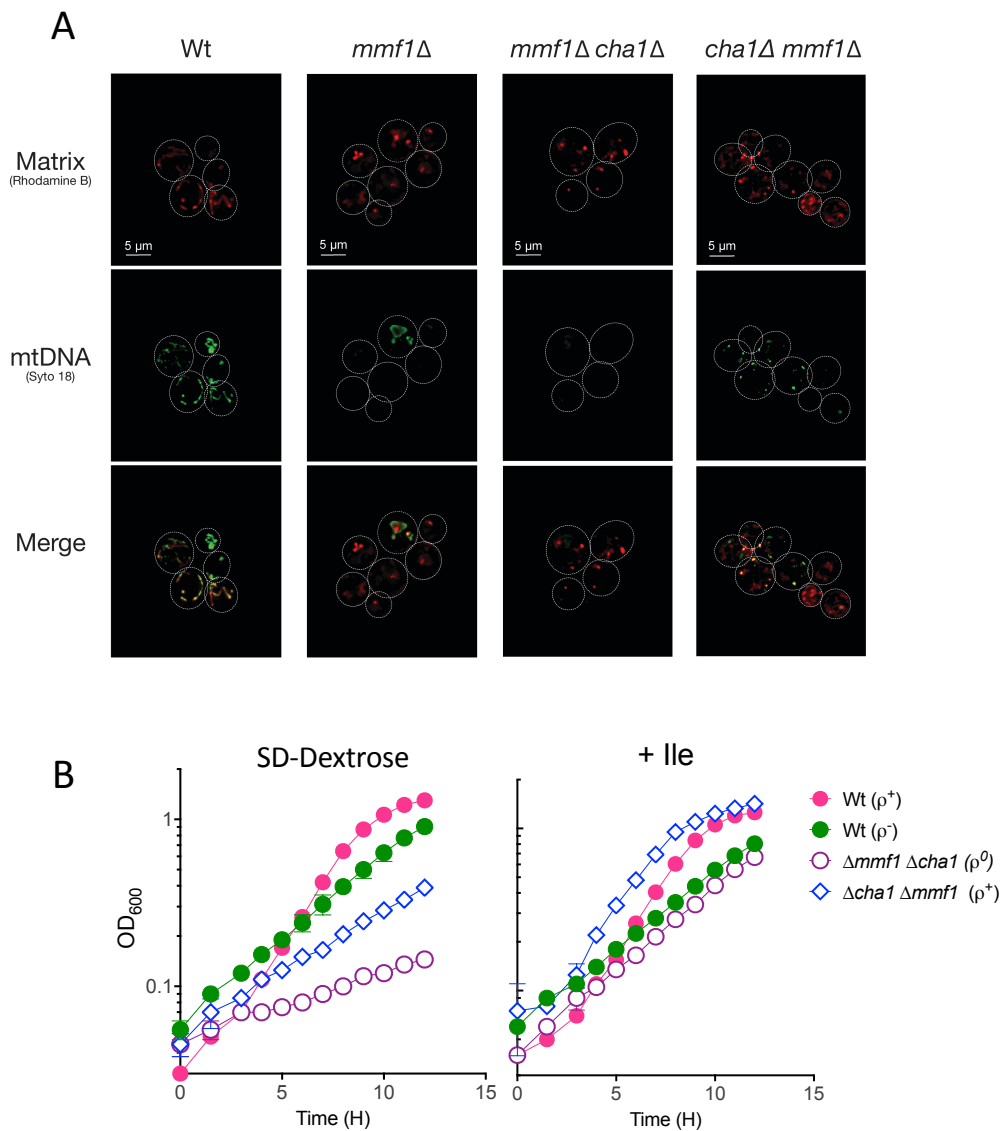


FIGURE 5.4. Mmf1p is dispensable for mtDNA maintenance in the absence of 2AA generators. (A) Microscopy (100x magnification) confirms the disruption of *MMF1* prior to *CHA1* leads to loss of mtDNA following selection on YPD. Conversely, disruption of *CHA1* coupled with feedback inhibition of Ilv1p during propagation on YPD preserves mtDNA following subsequent disruption of *MMF1*. (B) Although the ρ^+ *cha1* Δ *mmf1* Δ mutant maintains respiratory capacity, it remains sensitive to moderate 2AA stress when Ilv1p activity is restored by removing isoleucine from the growth medium. Data displayed are the average and standard deviation of three independent cultures.

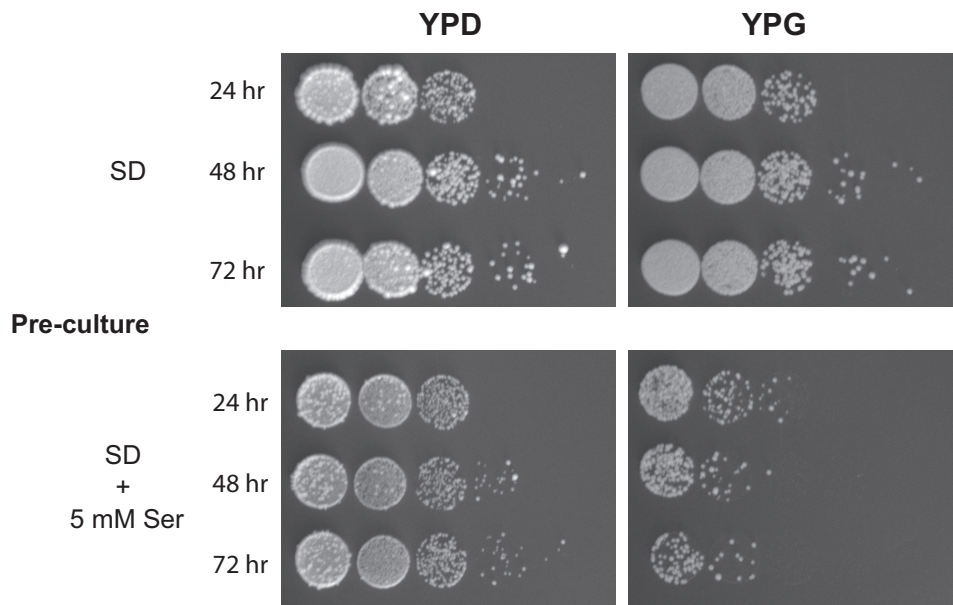


FIGURE 5.5. Serine diminishes the respiratory capacity of a ρ^+ *cha1* Δ *mmf1* Δ strain grown in minimal medium. Dilution plating (10^5 - 10^1) of DMy20 (ρ^+ *cha1* Δ *mmf1* Δ) pre-cultured up to 72 hours in minimal SD medium with 5 mM serine reveals a diminished capacity to respire glycerol relative to the minimal SD medium control.

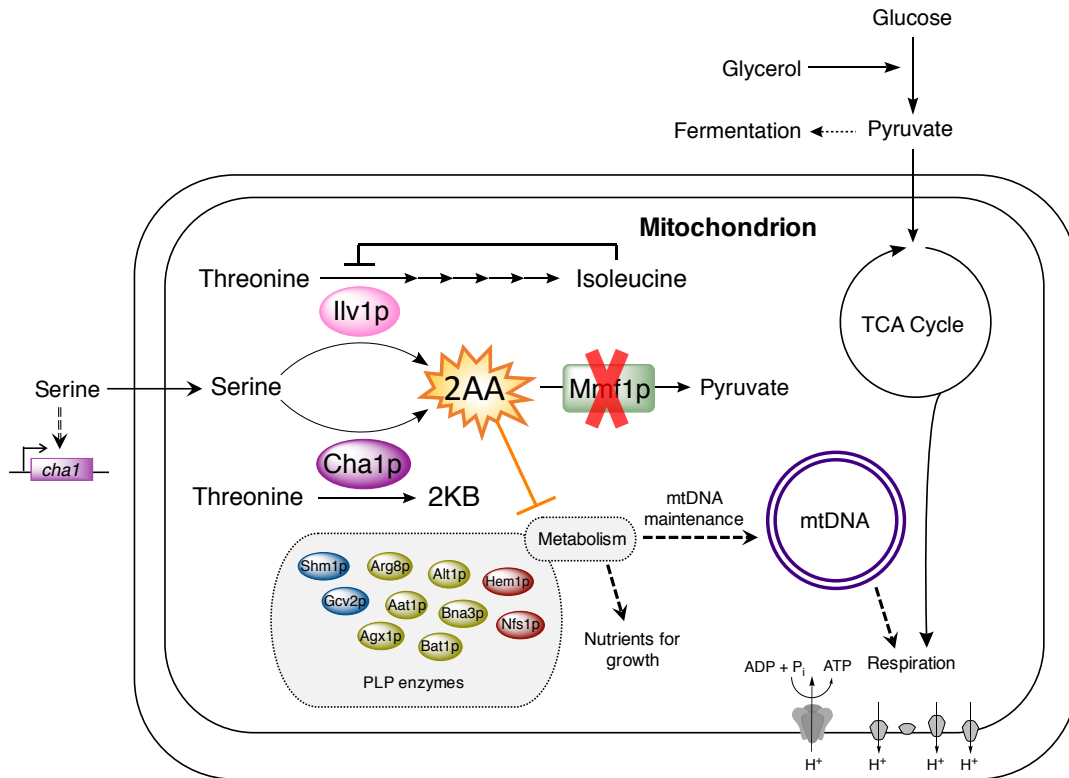


FIGURE 5.6. Model of 2AA stress in the yeast mitochondrion. PLP-dependent serine dehydratases active in the yeast mitochondrion (Ilv1p and Cha1p) generate 2AA through the dehydration of serine. Unless Mmf1p is present to prevent 2AA accumulation, metabolic stress arises, ultimately causing loss of the mitochondrial genome. The precedence for 2AA damaging PLP-dependent enzymes suggests the negative influence of 2AA on mtDNA maintenance is indirect and likely due to damage of one or more target PLP-dependent enzymes. 2KB=2-ketobutyrate, 2AA=2-aminoacrylate, CHA1 and ILV1 encode serine/threonine dehydratases (EC 4.3.1.19).

CHAPTER 6

ENHANCED CYSTATHIONINE β -LYASE PRODUCTION SUPPRESSES 2-
AMINOACRYLATE STRESS IN *SALMONELLA ENTERICA*¹

¹Ernst DC, Christopherson MR, Downs DM. To be submitted to *Journal of Bacteriology*.

6.1 ABSTRACT

Reactive enamine stress caused by intracellular 2-aminoacrylate accumulation leads to pleiotropic growth defects in a variety of organisms. Members of the well-conserved RidA/YER057c/UK114 protein family prevent enamine stress by enhancing the breakdown of 2-aminoacrylate to pyruvate. In *Salmonella enterica*, the disruption of RidA allows unbound 2-aminoacrylate to accumulate and inactivate a variety of pyridoxal 5'-phosphate-dependent enzymes. This study was carried out to identify robustness in the *S. enterica* metabolic network required to overcome 2-aminoacrylate stress in the absence of RidA. Multicopy suppressor analysis revealed that overproduction of the methionine biosynthetic enzyme cystathionine β -lyase (MetC; EC 4.4.1.8) alleviated the pleiotropic consequences of 2-aminoacrylate stress in a *ridA* mutant strain. The cystathionase activity of MetC was not required for suppression of *ridA* phenotypes. Although MetC overproduction reduced 2-aminoacrylate levels *in vivo*, MetC failed to use 2-aminoacrylate as a substrate *in vitro*. The data support a model where MetC acts on a non-cystathionine substrate to generate a metabolite that reduces 2-aminoacrylate levels, representing a potential non-enzymatic mechanism of 2-aminoacrylate depletion.

6.2 BACKGROUND

Metabolism is guided by the chemical reactivity of molecules in the cell. Inherent to this reactivity is the potential for deleterious reactions to take place between molecules in a heterogeneous and crowded intracellular milieu (1). Examples abound of reactive metabolites spontaneously damaging macromolecules (i.e. DNA, protein) in the cell, with well-characterized damage repair systems in place to counteract such damage (2, 3). Increasingly, examples of metabolite damage caused by promiscuous enzyme activities or spontaneous reactions between

unstable molecules have been described (4). In many cases, dedicated metabolite damage repair systems are necessary to prevent deleterious metabolites from reaching toxic levels in the cell.

The reactive enamine stressor 2-aminoacrylate (2AA) is produced by pyridoxal 5'-phosphate (PLP)-dependent enzymes associated with amino acid metabolism (5). Due to the short half-life of unbound 2AA *in vitro* (5), a role for this reactive metabolite *in vivo* was previously overlooked. However, detailed biochemical and genetic studies demonstrated that 2AA could persist intracellularly and inactivate a variety of target PLP-dependent enzymes, leading to numerous metabolic deficiencies (6–8). Pioneering studies in *Salmonella enterica* defined the role of RidA/YER057c/UK114 family proteins in preserving metabolic network integrity by hydrolyzing 2AA and preventing its accumulation inside the cell (9) (Figure 6.1A). Comparing *S. enterica* to the closely related gram-negative bacterium *Escherichia coli* revealed that these organisms differed in their susceptibility to enamine accumulation and 2AA stress despite their shared metabolic components (10, 11). Strains of *S. enterica* lacking RidA were unable to grow on minimal glucose medium containing serine or on minimal pyruvate medium due to 2AA stress generated by the biosynthetic serine/threonine dehydratase (IlvA; EC 4.3.1.19) (12). In contrast, *E. coli* lacking RidA only experienced a growth defect on the aforementioned media when IlvA activity was artificially increased (11). These studies showed that the mere presence of IlvA or RidA served as a poor predictor of enamine stress susceptibility, and suggested that the organization of the metabolic network influenced 2AA homeostasis.

The present study was carried out to identify robustness in the metabolic network of *S. enterica* required to prevent 2AA stress in the absence of RidA. Multicopy suppressor analysis showed that overexpression of *metC* in strains lacking RidA preserved wild-type growth under 2AA stress conditions. MetC is a PLP-dependent cystathionine β -lyase enzyme that catalyzes the

penultimate step in methionine biosynthesis (Figure 6.1B). The cystathionase activity of MetC was not required for suppression of *ridA* mutant phenotypes, nor did the MetC protein directly interact with 2AA to limit accumulation. The data support a model whereby MetC acts on alternative substrate(s) to generate a metabolite prone to react with 2AA.

6.3 MATERIALS AND METHODS

Bacterial strains, media and chemicals. Strains used in this study were derived from *Salmonella enterica* serovar Typhimurium LT2 and are listed along with their genotype in Table 6.1. Tn10d(Tc) is the transposition-defective mini-Tn10 (Tn10 Δ 16 Δ 17) described by Way et al. (13). MudJ refers to the transposition defective Mu element Mud1734 described previously (14).

Rich growth medium consisted of Difco nutrient broth (NB; 8 g/liter) and sodium chloride (5 g/liter). Minimal medium was composed of no-carbon E salts (NCE) with 1 mM magnesium sulfate (15), trace elements (16) and either glucose (11 mM) or pyruvate (50 mM) as the sole carbon source. Difco BiTek agar (15 g/liter) was added to make solid growth medium. When necessary, amino acids were added to minimal medium as follows: 5 mM serine, 0.3 mM methionine, 0.25 mM homocysteine, 1 mM isoleucine and 0.67 mM glycine. Antibiotics were added at the following final concentrations to rich and minimal medium, respectively: 20 and 5 g/ml of chloramphenicol, and 50 and 12.5 g/ml of kanamycin, 20 and 10 g/ml of tetracycline. Amino acids, including L-cystine dihydrochloride, and antibiotics were purchased from Sigma Aldrich (St. Louis, MO).

Genetic techniques and growth analyses. Strains were constructed by transductional crosses using the high-frequency general transducing mutant of bacteriophage P22 (HT105/1, *int*-201) (17). Techniques used to perform transductions, eliminate phage contamination from

cells, and identify phage-free recombinants were described previously (18). Strains were freshly streaked to solid NB medium prior to growth curves. Individual colonies were inoculated into 2 ml of NB broth and grown overnight at 37°C and 200 rpm. Cell growth was measured in liquid as described previously (19), where 5 µl of NB overnight was used to inoculate 195 µl of growth medium contained within each well of a 96-well microtiter plate (Corning). Microtiter plates were incubated at 37°C with shaking, and growth was monitored by the change in optical density at 650 nm (OD₆₅₀) using a BioTek Elx808 plate reader. All growth experiments were performed in triplicate, and the resulting data were plotted using GraphPad Prism 7.0, generating curves in log₁₀-format that display the averages and standard deviations of the replicates. When final ODs are reported, growth analyses were performed by inoculating 100 µl of NB overnight into 5 ml cultures contained within 30 ml cultures tubes and incubated at 37°C and 200 rpm.

Molecular methods and library construction. Library construction was described previously (see Downs lab). Two sequential stop codons were engineered by site-directed mutagenesis into the beginning of the *metC* sequence using primers MetC-SDMfor and MetC-SMDrev. The DNA changes A10T and C13A, corresponding to amino acids K4 (ochre) and Q5 (amber), respectively, were introduced into the pSR43 multicopy suppressor plasmid using a standard Quickchange protocol (Stratagene) to generate the plasmid pMC10. The addition of pSR43 to a *metC* mutant (DM9386) complemented growth in minimal glucose medium lacking methionine, while pMC10 failed to restore growth to a *metC* mutant (DM9387). Plasmid pSW-*metC* was constructed previously by blunt-end cloning the *metC* ORF into pSU19. Plasmid pDM1480 was generated by cloning the *metC* into pBAD24. The *metC* ORF was amplified using primers MetC_For_KpnI and MetC_Rev_HindIII, digested with KpnI and HindIII and ligated into pBAD24 digested with the same restriction enzymes.

Crude cystathionase assays. MetC activity was assessed as the cystathionine-dependent formation of free thiols in cell-free extracts according to published protocol. Briefly, 25 ml cultures were grown to full density in Nutrient Broth with 20 $\mu\text{g/ml}$ chloramphenicol at 37 °C with shaking. Cells were pelleted by centrifugation and resuspended in 1 mL 0.85% NaCl. Cells were lysed by sonication at 4 °C and cell debris removed by 10 min centrifugation at 4 °C. Cell-free extract was moved to a new tube, brought to a volume of 2.5 ml with 0.85% NaCl, and loaded onto a Sephadex G-25M PD-10 desalting column (Pharmacia). Proteins were eluted with 3.5 mL 0.85% saline and protein concentration was determined by Bradford assay (20). Approximately 30 μl of extract (corresponding to ~ 13 μg protein) was assayed at 30 °C in 200 μl total reaction volume containing 130 mM Tris pH 7.5, 0.02 mM PLP, and 1 mM 5,5'-dithiobis-(2-nitrobenzoic acid) (Sigma). A volume of 8 μl 50 mM cystathionine was added to a final concentration of 2 mM to start the reaction and absorbance at 412 nm was monitored over time. Experiments were performed in triplicate and reported as the average and standard deviation.

Transaminase B (IlvE) assays. IlvE activity was measured in permeabilized cell extracts as previously described (21). Strains were grown to late-log phase in 5 ml minimal glucose medium, pelleted, washed with 50 mM KPO_4 pH 8 and frozen overnight at -20°C. Frozen cell pellets were thawed on ice, resuspended in 50 mM KPO_4 pH 8 and lysed using PopCulture (Novagen). Aliquots of PLP (50 μM) and 2-ketoglutarate (10 mM) were mixed with ~ 30 μl of the permeabilized cell suspension, and isoleucine was added (20 mM) to initiate reactions. Reactions were incubated for 20 min at 37°C, and IlvE activity was determined based on the amount of 2-keto-3-methylvalerate (2KMV) formed. 2KMV was derivatized with 2,4-dinitrophenylhydrazine (DNPH) prior to hydrazone formation, followed by organic extraction. The organic layer was treated with 0.5 N HCl, then removed and mixed with 1.5 N NaOH to

allow chromophore formation. Absorbance of the resulting aqueous layer (containing the chromophore) was measured at 540 nm using a Spectramax M2. The protein concentration of each lysate was determined using the bicinchoninic acid (BCA) assay (Pierce). Activity is reported as nmol 2KMV/min/mg protein per cell lysate. The resulting data was analyzed by one-way analysis of variance (ANOVA), using GraphPad Prism 7.0 and Tukey's test was used to assess significant changes in IlvE activity ($P = 0.01$).

MetC purification. MetC was amplified from *S. enterica* LT2 using primers MetC_For_NdeI containing an engineered 5' NdeI restriction site and MetC_Rev_XhoI containing an engineered XhoI site in place of the stop codon. Amplification was performed by PCR using cloned Pfu DNA polymerase. PCR conditions were as follows: denaturation at 95 °C for 1 min, annealing at 52 °C for 1 min, and extension at 72 °C for 1 min. The resulting 1.2 kB fragment was digested with NdeI and XhoI and ligated into the pET20b vector (Novagen) digested with NdeI and XhoI. The plasmid (pMC12) complemented *metC* mutant TT14 (data not shown). MetC was overexpressed from pMC12 in *E. coli* BL21(AI) according to the manufacturer's protocol (Novagen). Cells from the resulting cultures were broken at 15,000 psi in a French Pressure cell at 4 °C. Cell debris was removed by centrifugation (42,000 x g) for 30 min at 4 °C. Proteins were purified using a column containing Superflow Ni²⁺ resin (Qiagen) according to standard protocol (Novagen). Fractions containing MetC were concentrated at 30 psi under Argon gas using a 10,000 MWCO membrane (Amicon YM10). The protein was dialyzed in Binding Buffer and stored at –80 °C.

Serine dehydratase (IlvA) assays. IlvA was provided by K. Hodge-Hanson and was purified as previously described (5). RidA was the same as used in previously described assays (22). Reactions (300 µl) consisted of 50 mM Tris-HCl pH 9 and 0.6 µM IlvA. Reactions were

initiated by adding L-serine (60 mM) and monitored continuously at 230 nm for 120 seconds in a 96-well quartz plate using a SpectraMax M2 (Molecular Devices) microplate reader. Initial rates were determined based on the increase in A_{230} corresponding to pyruvate formation. The impact of RidA (0.3 μ M) or MetC (0.45 μ M) on the rate of pyruvate formation was assessed by adding the proteins to IlvA reactions at the indicated concentrations and monitoring changes in ΔA_{230} .

6.4 RESULTS AND DISCUSSION

***metC* is a multicopy suppressor of *ridA* mutant strain growth defects.** A plasmid library containing *Salmonella enterica* LT2 genomic DNA in pBR328 was transduced into a *ridA* strain (DM3480) and plated on rich medium containing chloramphenicol (20 μ g/ml). Transductants were screened for restored growth on minimal glucose medium containing serine (5 mM). Plasmids expressing putative multicopy suppressors were transduced to a naïve parental strain to confirm suppression and a representative plasmid, pSR43, was chosen for further characterization. The presence of pSR43 reversed the growth defect of a *ridA* mutant strain in minimal glucose medium containing serine (Figure 6.2A). Sequence analysis showed pSR43 contained a fragment of chromosomal DNA consisting of seven open reading frames, including four genes of unknown function, two genes encoding components of a TonB-dependent transport system and the *metC* gene encoding a PLP-dependent cystathionine β -lyase required for methionine biosynthesis (Figure 6.2B). The association of *ridA* mutant phenotypes with PLP-enzymes suggested *metC* could be involved in the suppression of serine sensitivity. Plasmid pSR43 was engineered to contain two sequential stop codons in *metC*, generating plasmid pMC10. A *ridA* mutant strain containing pMC10 (DM9407) failed to grow in the presence of serine (Figure 6.2A), allowing the conclusion that MetC was required for the multicopy suppression of pSR43.

The *metC* ORF was cloned into a pSU19 vector, forming pSW-*metC*, and a pBAD vector generating pDM1480. Unexpectedly, neither of the *metC* containing constructs restored growth to a *ridA* mutant on medium with serine. Both plasmids (and pSR43) restored full growth to a *metC* mutant on minimal medium, confirming that functional MetC was being produced. In addition to serine sensitivity, *ridA* mutants display an inability to grow on pyruvate as the sole carbon source (23). Expression of *metC* from pSW-*metC* failed to restore growth to a *ridA* mutant on pyruvate medium (Table 6.2). These data indicated that the presence of pSW-*metC* or pDM1480 could satisfy the methionine requirement of a *metC* mutant, but could not suppress the 2AA-dependent growth defect of *ridA* strains grown in the presence of serine or on pyruvate as a sole carbon source.

A simple interpretation of these results was that other genes on the pSR43 construct were required for suppression of *ridA* phenotypes. ExbB and ExbD form a complex with TonB to transduce energy to the outer membrane for use by TonB-dependent transporters (24). Therefore, the possibility that TonB was required for pSR43 suppression of *ridA* phenotypes was examined. After 24 hours, DM13226 (*ridA tonB* / pSR43) grew in the presence of 5 mM serine ($OD_{650} = 1.12 \pm 0.035$) while DM13225 (*ridA tonB* / pSU19) did not ($OD_{650} = 0.064 \pm 0.063$), indicating ExbB and ExbD were dispensable for suppression. The remaining genes of unknown function flanking *metC* (*yghA*, *yhjG*, *yghB* and *yqhC*) were independently determined to be non-essential for pSR43-mediated suppression of *ridA* phenotypes (data not shown).

In the absence of evidence for a role of additional proteins in the suppression by pSR43, strains were assayed for cystathionase activity. The data showed that strains carrying the pSR43 construct had approximately 40-fold higher cystathionase activity than strains carrying the *metC*-null pMC10 construct, and 10 to 50-fold higher cystathionase activity than strains with constructs

containing the *metC* ORF alone (Table 6.3). Thus, cystathionase activity positively correlated with suppression of *ridA* strain growth defects. However, the mere presence/organization of the DNA flanking *metC* in pSR43 led to greater MetC activity than could be achieved by expressing *metC* alone from pSW-*metC* or pDM1480. The significantly higher level of MetC activity in strains with pSR43 suggested a strong genomic context-dependent effect on *metC* expression. The mechanism of how the added genomic content of pSR43 influenced MetC activity was not pursued.

Cystathionine α,β -elimination is not required for MetC to suppress the growth defects of a *ridA* strain. The positive correlation between cystathionase activity and the suppression of *ridA* strain phenotypes indicated MetC was required, but did not prove that cystathionase activity was necessary *per se*. Methionine limits flux through the methionine biosynthetic pathway by feedback inhibition of MetA (25), thus diminishing the production of cystathionine. Adding methionine to cultures of a *ridA* strain containing pSR43 grown on minimal pyruvate medium or minimal glucose plus serine medium did not affect MetC suppression of *ridA* strain growth defects (data not shown). Furthermore, the disruption of *metB*, encoding cystathionine synthase, did not prevent pSR43 from suppressing the growth defect of a *metB ridA* (DM9567) strain grown in minimal glucose medium containing serine and methionine (data not shown). Thus, cystathionine was not required for MetC-dependent suppression of *ridA* strain phenotypes. In fact, one of the products of MetC-catalyzed cystathionine α,β -elimination, homocysteine, was toxic to a *ridA* strain when supplied exogenously in minimal glucose medium (Figure 6.3). Homocysteine accumulation is known to increase IlvA activity in *E. coli* (26), predictably leading to greater 2AA production. Isoleucine or glycine reversed the homocysteine sensitivity of a *ridA* strain, consistent with homocysteine exacerbating 2AA production via IlvA in *S. enterica* (18). The above data indicated that MetC, but not cystathionine, was required for the suppression of *ridA* strain growth

defects. It remained unclear if MetC overproduction reduced 2AA levels inside the cell or compensated for a damaged 2AA target in order to restore growth to a *ridA* strain.

MetC overproduction reduces 2AA accumulation by a mechanism that does not require allosteric inhibition of IlvA. A well-established indirect approach was used to monitor the impact of MetC overproduction on 2AA levels *in vivo*. Transaminase B (IlvE; EC 2.6.1.42) is a PLP-dependent enzyme that is inactivated by free 2AA; measuring IlvE activity in a *ridA* strain reflects the level of 2AA accumulation (21). IlvE activity was significantly reduced (55 nmol 2-KMV/min/mg) in a *ridA* strain carrying pMC10 relative to the wild-type control (120 nmol 2-KMV/min/mg) (Figure 6.4). In contrast, the IlvE activity of a *ridA* strain carrying pSR43 (90 nmol 2-KMV/min/mg) was not significantly different than the wild type control (122 nmol 2-KMV/min/mg) (Figure 6.4). The data indicated that MetC reduced 2AA levels in a *ridA* strain.

The serine sensitivity of a *ridA* mutant is suppressed by isoleucine (12) through a mechanism that requires allosteric inhibition of IlvA (23). It was possible that MetC overproduction ultimately diminished 2AA levels through the allosteric inhibition of IlvA. An IlvA variant (encoded by *ilvA219*) insensitive to allosteric regulation (21) was introduced to a *ridA* strain carrying pSR43. The presence of pSR43 maintained growth of the *ridA* mutant in the presence of serine (or on pyruvate) despite the inability to regulate IlvA activity (Table 6.4). Taken together, these data confirmed that MetC reduced 2AA accumulation *in vivo* without affecting the production of 2AA by IlvA. Therefore, MetC acted downstream of IlvA to sequester/degrade 2AA prior to target enzyme inactivation.

MetC does not sequester 2-aminoacrylate directly. MetC overproduction clearly reduced 2AA accumulation *in vivo*, but it was unclear if MetC directly interacted with 2AA or generated a product capable of sequestering 2AA. Pure MetC protein or RidA were added to

spectrophotometric assays containing IlvA and serine, and the rate of pyruvate formation was monitored. The addition of RidA to the reactions sped up the rate of pyruvate formation (data not shown) as described previously (5). In contrast, adding MetC to the reaction had no effect on the rate of pyruvate formation (data not shown), indicating MetC did not hydrolyze 2AA, nor did MetC bind and sequester 2AA. It was hypothesized that MetC could generate a reactive metabolite capable of reacting with 2AA. MetC is reported to have a broad substrate range (27) and is capable of generating reactive persulfide species (28). Therefore, we proposed a simple scenario where MetC provided with a cysteine persulfide precursor, such as cystine, could diminish IlvA-dependent pyruvate formation through persulfide-mediated 2AA sequestration (Figure 6.5). Verification of the model was hampered by our inability to provide the relevant intermediates directly *in vitro*. Attempts to enzymatically generate 2AA and cysteine persulfide in the same reaction via IlvA and MetC, respectively, failed to definitively show that 2AA and cysteine persulfide reacted to form a unique product (data not shown). Similarly, attempts to non-enzymatically generate cysteine persulfide from cystine using sodium sulfide inhibited IlvA activity, limiting the usefulness of this approach.

Conclusions. The results presented here indicate that MetC overproduction suppresses multiple growth defects displayed by a *ridA* mutant. The data indicate that suppression by MetC does not depend on cystathionase activity or the regulation of IlvA, nor does MetC directly bind 2AA. Cystathionine β -lyase enzymes are able to decompose a variety of sulfur containing amino acids of potential biological significance, including cystine, djenkolic acid, lanthionine and several other substrates (27). The broad substrate range used by MetC, coupled with the difficulty of replicating intracellular conditions, impeded efforts to identify a reactive metabolite generated by MetC that could sequester 2AA *in vitro*.

Our model predicts that a reactive persulfide generated by MetC is capable of sequestering 2AA to prevent stress in the absence of RidA. Precedence exists for cysteine being able to react with 2AA generated by cysteine desulfhydrase (CdsH; EC 4.4.1.1) in semi-pure enzyme assays, leading to the accumulation of a cyclized end-product (29). These data confirmed that despite the abundance of free water in the assays, the nucleophilic cysteine thiol could attack 2AA before spontaneous tautomerization and hydrolysis could take place. Cysteine persulfide (thiocysteine) is predicted to act either as a strong nucleophile capable of attacking 2AA, or an electrophile susceptible to attack by 2AA, depending on the sulfur atom considered (Figure 6.5). Thiocysteine is produced by a variety of promiscuous cystine lyases, including cystathionine lyases, and impacts the cellular thiol landscape in many organisms (30). Our inability to rigorously test the interaction between 2AA and thiocysteine *in vitro* warrants future work to explore the formation of a 2AA-persulfide conjugate *in vivo*. A variety of persulfide species beyond thiocysteine, derived from precursors other than cystine, play important roles in sulfur trafficking, protein persulfidation and other cellular processes (31). The benefit of an unbiased *in vivo* approach is that we will not be limited to exploring the impact of a single MetC substrate (e.g. cystine) on 2AA levels, since a variety of MetC substrates are present in *S. enterica*. Furthermore, conditions of the intracellular space, including molecular crowding and a lack of abundant free water, may be required for the proposed interaction between 2AA and a MetC metabolite to take place.

RidA represents the only mechanism of 2AA control that has been described to date (9). However, some organisms that seem capable of generating 2AA based on possessing type II PLP-enzymes lack a canonical RidA homolog, opening the possibility that non-RidA mechanisms of 2AA control exist in nature (32). Parallel studies seeking to identify 2AA control enzymes from RidA-deficient *Methanococcus maripaludis* identified an aspartate/glutamate racemase

(MMP0739; EC 5.1.1.13) capable of suppressing *S. enterica ridA* phenotypes, similar to MetC (Hodge-Hanson and Downs, unpublished data). These findings suggest that metabolic enzymes, when produced in the appropriate context, are capable of altering metabolic flux to diminish the accumulation of 2AA in the absence of RidA. Work comparing *Escherichia coli* and *S. enterica* showed that organisms with nearly identical metabolic components, including IlvA and RidA, differed in their susceptibility to 2-aminoacrylate stress (11). Insights from the present study may inform our understanding of how seemingly unrelated components of a given metabolic network buffer against 2AA accumulation, in addition to or in lieu of RidA activity. Continued investigation of cross-talk between 2AA and the metabolic network are warranted to better understand the subtle perturbations caused by 2AA. Although enzyme bound pyridoxal 5'-phosphate is the only metabolite we have identified as damaged by 2AA *in vivo*, it is likely that other metabolites in the crowded intracellular space are prone to react with 2AA. Our ability to detect such deleterious interactions may be limited in wild-type *S. enterica*, but through genetic intervention, we may be able to amplify the impact of 2AA-conjugated metabolite production to a phenotypically detectable level. Findings from this approach may not be relevant to the 2AA stress paradigm active in *S. enterica*, but may reflect relevant consequences of 2AA stress in other organisms.

6.5 REFERENCES

1. de Lorenzo V, Sekowska A, Danchin A. 2015. Chemical reactivity drives spatiotemporal organisation of bacterial metabolism. *FEMS Microbiol Rev* 39:96–119.
2. Cooke MS. 2003. Oxidative DNA damage: mechanisms, mutation, and disease. *FASEB J* 17:1195–1214.
3. Chondrogianni N, Petropoulos I, Grimm S, Georgila K, Catalgol B, Friguet B, Grune T, Gonos ES. 2014. Protein damage, repair and proteolysis. *Mol Aspects Med* 35:1–71.

4. Linster CL, Van Schaftingen E, Hanson AD. 2013. Metabolite damage and its repair or pre-emption. *Nat Chem Biol* 9:72–80.
5. Lambrecht JA, Flynn JM, Downs DM. 2012. Conserved YjgF protein family deaminates reactive enamine/imine intermediates of pyridoxal 5'-phosphate (PLP)-dependent enzyme reactions. *J Biol Chem* 287:3454–3461.
6. Flynn JM, Downs DM. 2013. In the absence of RidA, endogenous 2-aminoacrylate inactivates alanine racemases by modifying the pyridoxal 5'-phosphate cofactor. *J Bacteriol* 195:3603–3609.
7. Flynn JM, Christopherson MR, Downs DM. 2013. Decreased coenzyme A levels in *ridA* mutant strains of *Salmonella enterica* result from inactivated serine hydroxymethyltransferase: *ridA* mutants are deficient in one carbon metabolism. *Mol Microbiol* 89:751–759.
8. Lambrecht JA, Schmitz GE, Downs DM. 2013. RidA proteins prevent metabolic damage inflicted by PLP-dependent dehydratases in all domains of life. *mBio* 4:e00033-13-e00033-13.
9. Downs DM, Ernst DC. 2015. From microbiology to cancer biology: the Rid protein family prevents cellular damage caused by endogenously generated reactive nitrogen species. *Mol Microbiol* 96:211–219.
10. Bazurto JV, Farley KR, Downs DM. 2016. An unexpected route to an essential cofactor: *Escherichia coli* relies on threonine for thiamine biosynthesis. *mBio* 7:e01840–15.
11. Borchert AJ, Downs DM. 2017. The response to 2-aminoacrylate differs in *Escherichia coli* and *Salmonella enterica*, despite shared metabolic components. *J Bacteriol* 199:e00140-17.
12. Enos-Berlage JL, Langendorf MJ, Downs DM. 1998. Complex metabolic phenotypes caused by a mutation in *yjgF*, encoding a member of the highly conserved YER057c/YjgF family of proteins. *J Bacteriol* 180:6519–6528.
13. Way JC, Davis MA, Morisato D, Roberts DE, Kleckner N. 1984. New *Tn10* derivatives for transposon mutagenesis and for construction of *lacZ* operon fusions by transposition. *Gene* 32:369–379.
14. Castilho BA, Olfson P, Casadaban MJ. 1984. Plasmid insertion mutagenesis and *lac* gene fusion with mini-mu bacteriophage transposons. *J Bacteriol* 158:488–495.
15. Vogel HJ, Bonner DM. 1956. Acetylornithinase of *Escherichia coli*: partial purification and some properties. *J Biol Chem* 218:97–106.

16. Balch WE, Wolfe RS. 1976. New approach to the cultivation of methanogenic bacteria: 2-mercaptoethanesulfonic acid (HS-CoM)-dependent growth of *Methanobacterium ruminantium* in a pressurized atmosphere. *Appl Environ Microbiol* 32:781–791.
17. Schmieger H. 1972. Phage P22-mutants with increased or decreased transduction abilities. *Mol Gen Genet MGG* 119:75–88.
18. Ernst DC, Downs DM. 2016. 2-aminoacrylate stress induces a context-dependent glycine requirement in *ridA* strains of *Salmonella enterica*. *J Bacteriol* 198:536–543.
19. Petersen L, Enos-Berlage J, Downs DM. 1996. Genetic analysis of metabolic crosstalk and its impact on thiamine synthesis in *Salmonella typhimurium*. *Genetics* 143:37.
20. Bradford MM. 1976. A rapid and sensitive method for the quantitation of microgram quantities of protein utilizing the principle of protein-dye binding. *Anal Biochem* 72:248–254.
21. Schmitz G, Downs DM. 2004. Reduced transaminase B (IlvE) activity caused by the lack of *yjgF* is dependent on the status of threonine deaminase (IlvA) in *Salmonella enterica* serovar Typhimurium. *J Bacteriol* 186:803–810.
22. Ernst DC, Lambrecht JA, Schomer RA, Downs DM. 2014. Endogenous synthesis of 2-aminoacrylate contributes to cysteine sensitivity in *Salmonella enterica*. *J Bacteriol* 196:3335–3342.
23. Christopherson MR, Schmit GE, Downs DM. 2008. YjgF is required for isoleucine biosynthesis when *Salmonella enterica* is grown on pyruvate medium. *J Bacteriol* 190:3057–3062.
24. Noinaj N, Guillier M, Barnard TJ, Buchanan SK. 2010. TonB-dependent transporters: regulation, structure, and function. *Annu Rev Microbiol* 64:43–60.
25. Smith DA. 1961. Some aspects of the genetics of methionineless mutants of *Salmonella typhimurium*. *Microbiology* 24:335–353.
26. Roe AJ, O’Byrne C, McLaggan D, Booth IR. 2002. Inhibition of *Escherichia coli* growth by acetic acid: a problem with methionine biosynthesis and homocysteine toxicity. *Microbiology* 148:2215–2222.
27. Matsuo Y, Greenberg DM. 1959. A crystalline enzyme that cleaves homoserine and cystathionine. IV. Mechanism of action, reversibility, and substrate specificity. *J Biol Chem* 234:516–519.

28. Ida T, Sawa T, Ihara H, Tsuchiya Y, Watanabe Y, Kumagai Y, Suematsu M, Motohashi H, Fujii S, Matsunaga T, Yamamoto M, Ono K, Devarie-Baez NO, Xian M, Fukuto JM, Akaike T. 2014. Reactive cysteine persulfides and S-polythiolation regulate oxidative stress and redox signaling. *Proc Natl Acad Sci* 111:7606–7611.
29. Kredich NM, Foote LJ, Keenan BS. 1973. The stoichiometry and kinetics of the inducible cysteine desulfhydrase from *Salmonella typhimurium*. *J Biol Chem* 248:6187–6196.
30. Reitzer L. 2015. Death by cystine: an adverse emergent property from a beneficial series of reactions. *J Bacteriol* 197:3626–3628.
31. Mishanina TV, Libiad M, Banerjee R. 2015. Biogenesis of reactive sulfur species for signaling by hydrogen sulfide oxidation pathways. *Nat Chem Biol* 11:457–464.
32. Niehaus TD, Gerdes S, Hodge-Hanson K, Zhukov A, Cooper AJ, ElBadawi-Sidhu M, Fiehn O, Downs DM, Hanson AD. 2015. Genomic and experimental evidence for multiple metabolic functions in the RidA/YjgF/YER057c/UK114 (Rid) protein family. *BMC Genomics* 16:382.
33. Soberon X, Covarrubias L, Bolivar F. 1980. Construction and characterization of new cloning vehicles. IV. Deletion derivatives of pBR322 and pBR325. *Gene* 9:287–305.
34. Guzman LM, Belin D, Carson MJ, Beckwith J. 1995. Tight regulation, modulation, and high-level expression by vectors containing the arabinose pBAD promoter. *J Bacteriol* 177:4121–4130.
35. Bartolome B, Jubete Y, Martinez E, Cruz F de la. 1991. Construction and properties of a family of pACYC184-derived cloning vectors compatible with pBR322 and its derivatives. *Gene* 102:75–78.

TABLE 6.1. Strains, plasmids and primers used in this study.

Strain, plasmid or primer	Genotype, description or sequence
Strains	
DM3480	<i>ridA3</i> ::MudJ
DM5970	<i>ilvA219 ridA3</i> ::MudJ
DM7575	<i>ridA3</i> ::MudJ / pSR43
DM7576	<i>ridA3</i> ::MudJ / pSW
DM9384	<i>ilvA219 ridA3</i> ::MudJ / pSR43
DM9385	<i>ilvA219 ridA3</i> ::MudJ / pMC10
DM9386	<i>metC</i> ::Tn10d(Tc) / pSR43
DM9387	<i>metC</i> ::Tn10d(Tc) / pMC10
DM9404	Wild-type (isogenic to DM3480)
DM9405	Wild-type / pSR43
DM9407	<i>ridA3</i> ::MudJ / pMC10
DM9567	<i>ridA3</i> ::MudJ <i>metB</i> ::Tn10d(Tc)
DM13225	<i>ridA3</i> ::MudJ <i>tonB256</i> ::Tn10(d)Tc / pSU19
DM13226	<i>ridA3</i> ::MudJ <i>tonB256</i> ::Tn10(d)Tc / pSR43
DM14277	<i>ridA3</i> ::MudJ / pBAD24
DM14370	Wild-type / pBAD24
DM15535	Wild-type / pSU19
DM15536	Wild-type / pDM1480
DM15538	<i>ridA3</i> ::MudJ / pSU19
DM15539	<i>ridA3</i> ::MudJ / pDM1480
DM16218	Wild-type / pBR328
DM16219	<i>ridA3</i> ::MudJ / pBR328
Plasmids	
pBR328	Reference (33)
pBAD24	Reference (34)
pSU19	Reference (35)
pSW	<i>metC</i> cloned into the pSU19 multiple cloning site
pSR43	<i>metC</i> and flanking gDNA cloned into the pSU19 multiple cloning site
pMC10	pSR43 with two stop codons inserted in the <i>metC</i> ORF
pDM1480	<i>metC</i> cloned into the pBAD24 multiple cloning site
Primers	
MetC-SDMfor	CAGGAAACGCAACATGACGGATTAATAGTTGGATACCAAACCTGG
MetC-SMDrev	GCGTTTACCAGTTTGGTATCCAACCTATTAATCCGTCTATGTTGCG
MetC_For_NdeI	CATATGACGGATAAACAGTTGGATACCAAACCTGGTAAACGC
MetC_Rev_XhoI	CCCCGGCACTCGAGCACAATTC
MetC_For_KpnI	GAGAGGTACCAACGGATAAACAGTTGGATAC
MetC_Rev_HindIII	GAGATCTAGATTACACAATTCTGGCGAAGC

TABLE 6.2. Construct-dependent overexpression of *metC* alleviates *ridA* strain growth defects

Strain	Genotype	Growth (OD ₆₅₀) after 24 hours ^a		
		Glc	Glc + Ser	Pyr
DM7576	<i>ridA</i> / pSW	1.14	0.07	0.56
DM7575	<i>ridA</i> / pSR43	1.15	1.29	1.07
DM9407	<i>ridA</i> / pMC10	1.07	0.14	0.37
DM15539	<i>ridA</i> / pDM1480 ^b	1.37	0.11	N/A ^c

^a Average from three independent cultures. Error less than 0.2 absorbance units. Growth media: 11 mM Glucose (Glc), 5 mM serine (Ser), 50 mM pyruvate (Pyr). ^b Arabinose (0.1 %) was added to all growth medium for this strain. ^c The vector-only control (DM14277) grew in pyruvate medium containing arabinose. Otherwise, the vector-only control behaved like a *ridA* mutant strain.

TABLE 6.3. MetC activity correlates with phenotypic suppression of *ridA*

Strain	Genotype	MetC Activity
DM7576	<i>ridA</i> / pSW	0.2 ± 0.3
DM7575	<i>ridA</i> / pSR43	11.6 ± 1.9
DM9407	<i>ridA</i> / pMC10	0.3 ± 0.05
DM15539*	<i>ridA</i> / pDM1480	1.3 ± 0.8

MetC activity is reported as: $\Delta A_{412\text{nm}}/\text{mg}/\text{min}$. The data are reported as the average and standard deviation of three independent experiments. * Arabinose (0.1%) was added to cultures containing DM15539.

TABLE 6.4. MetC suppression does not require allosteric inhibition of IlvA

Strain	Genotype	Growth (OD ₆₅₀) after 12 hours [†]		
		Glc	Glc + Ser	Pyr
DM3480	<i>ridA</i>	1.26	0.16	0.32
DM5970	<i>ridA ilvA219</i>	0.51	0.1	0.13
DM9384	<i>ridA ilvA219</i> / pSR43	1.29	1.16	1.24
DM9385	<i>ridA ilvA219</i> / pMC10	0.36	0.07	0.12

[†] Average from three independent cultures. Error less than 0.2 absorbance units. Growth media:

11 mM Glucose (Glc), 5 mM serine (Ser), 50 mM pyruvate (Pyr).

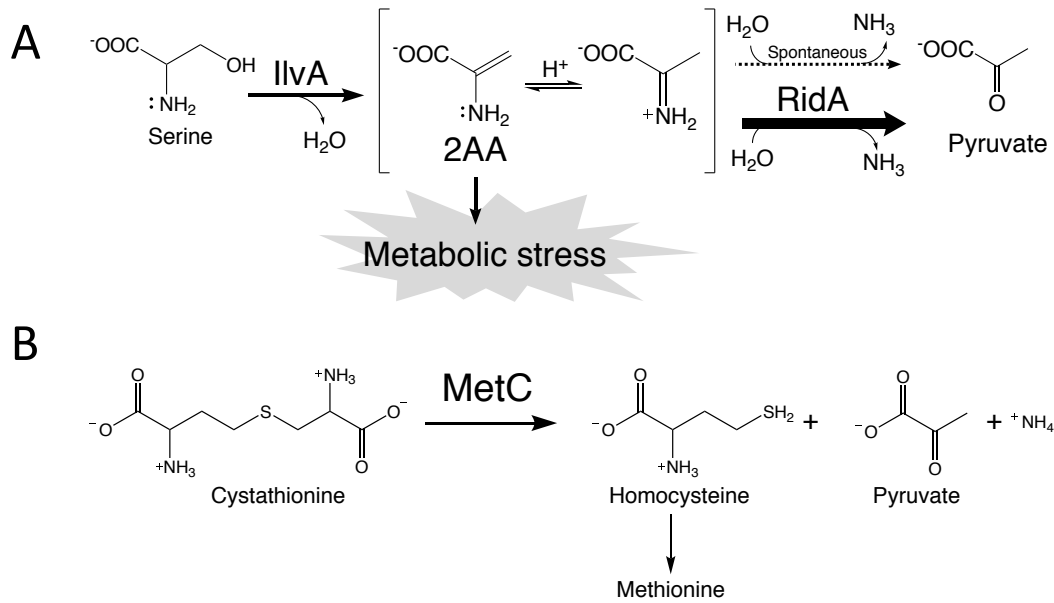


FIGURE 6.1. A) 2-aminoacrylate is produced in *Salmonella enterica* by the pyridoxal 5'-phosphate-dependent serine/threonine dehydratase IlvA. Following release from IlvA, 2AA can undergo spontaneous conversion to pyruvate, but some 2AA persists long enough to damage target enzymes and cause metabolic stress. However, RidA enhances 2AA hydrolysis and prevents endogenous metabolic stress. B) Cystathionine β -lyase encoded by *metC* is a pyridoxal 5'-phosphate-dependent enzyme that converts cystathionine to homocysteine, pyruvate and ammonia in the penultimate step of methionine biosynthesis.

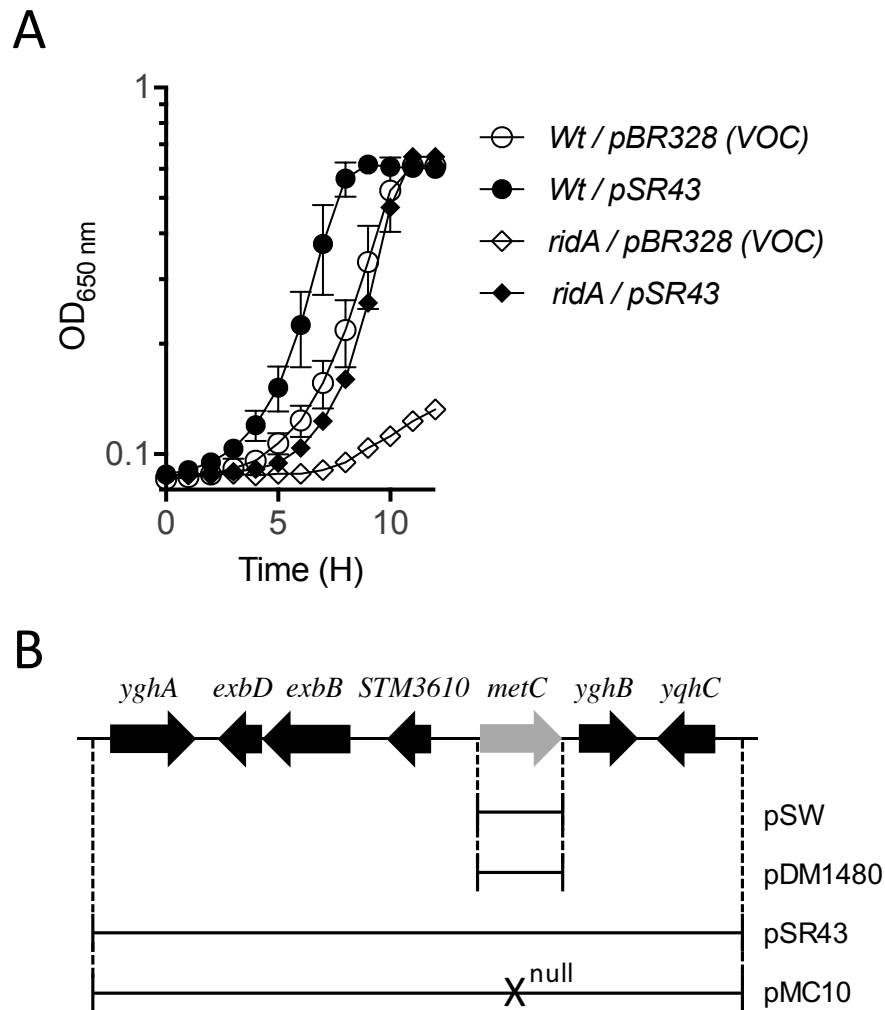


FIGURE 6.2. A) Growth of wild-type (circles) and *ridA* (diamonds) strains containing the empty pBR328 vector (open symbols) or pSR43 (closed symbols) in minimal glucose plus serine (5 mM) medium. Data reflect the average and standard deviation of experiments performed in triplicate in a 96-well plate format. B) The *metC* open reading frame was cloned into the multiple cloning site of pSU19 or pBAD24 to generate pSW and pDM1480, respectively. Alternatively, *metC* flanked by several upstream and downstream genes was cloned into pBR328 to generate pSR43. Site directed mutagenesis using pSR43 as a template was performed to generate a *metC*-null version of pSR43, pMC10.

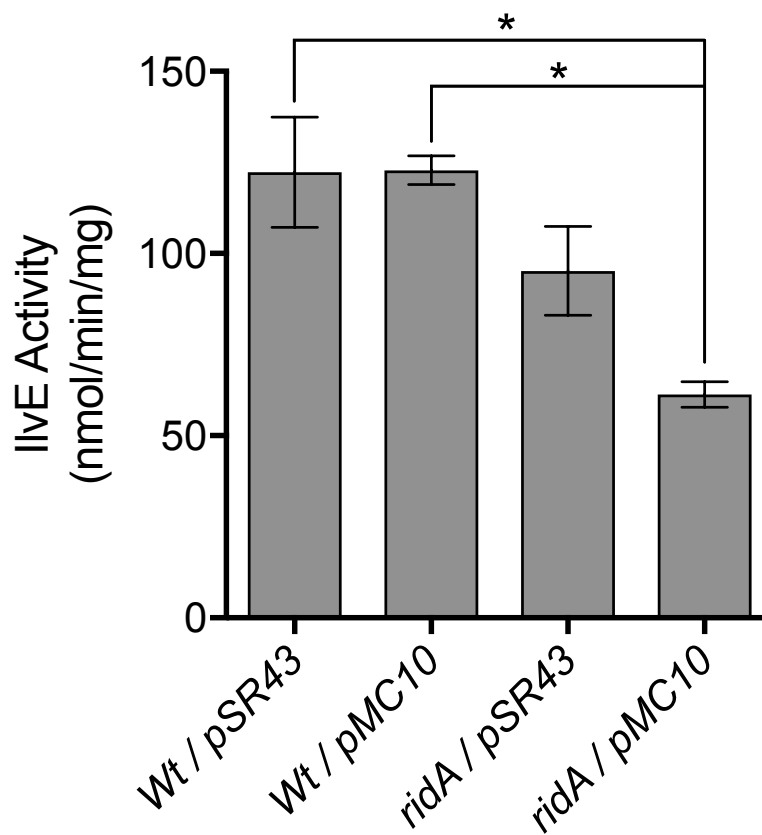


FIGURE 6.3. Transaminase B (IlvE) activity. IlvE activity was measured in crude extracts of wild-type or *ridA* strains containing pSR43 or pMC10 grown to late-log phase in minimal glucose medium. IlvE activity was normalized to crude protein concentration. Data display the average and standard deviation of three biological replicates.

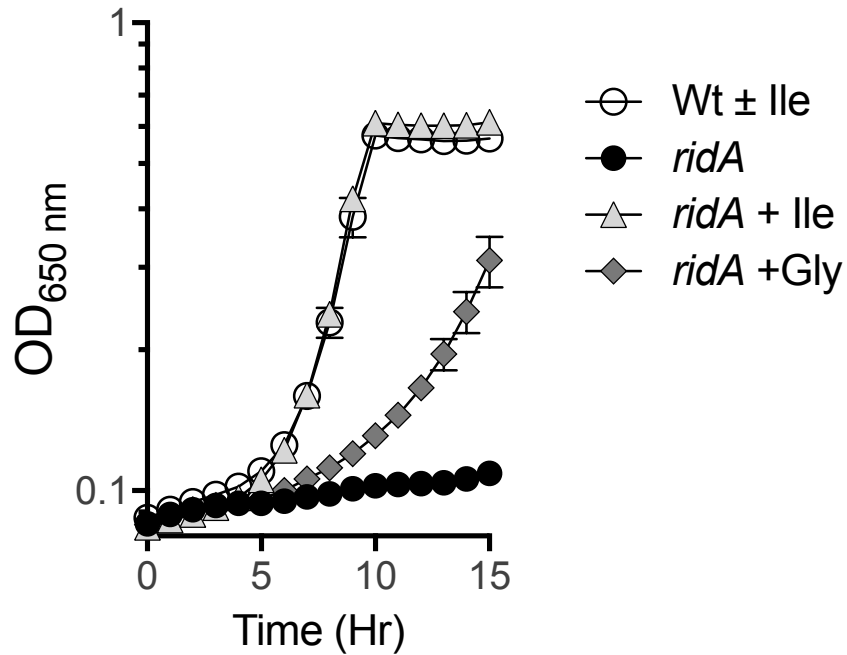


FIGURE 6.4. Homocysteine is the product of cystathionine β -elimination and is toxic to *ridA* strains grown in minimal glucose medium. Wild-type (open symbols) and *ridA* (closed symbols) strains were grown in minimal glucose medium containing 0.25 mM homocysteine. No supplements (circles), isoleucine (1 mM; triangles) or glycine (0.67 mM; diamonds) were added to cultures containing homocysteine. The data represent the average and standard deviation of three independent cultures.

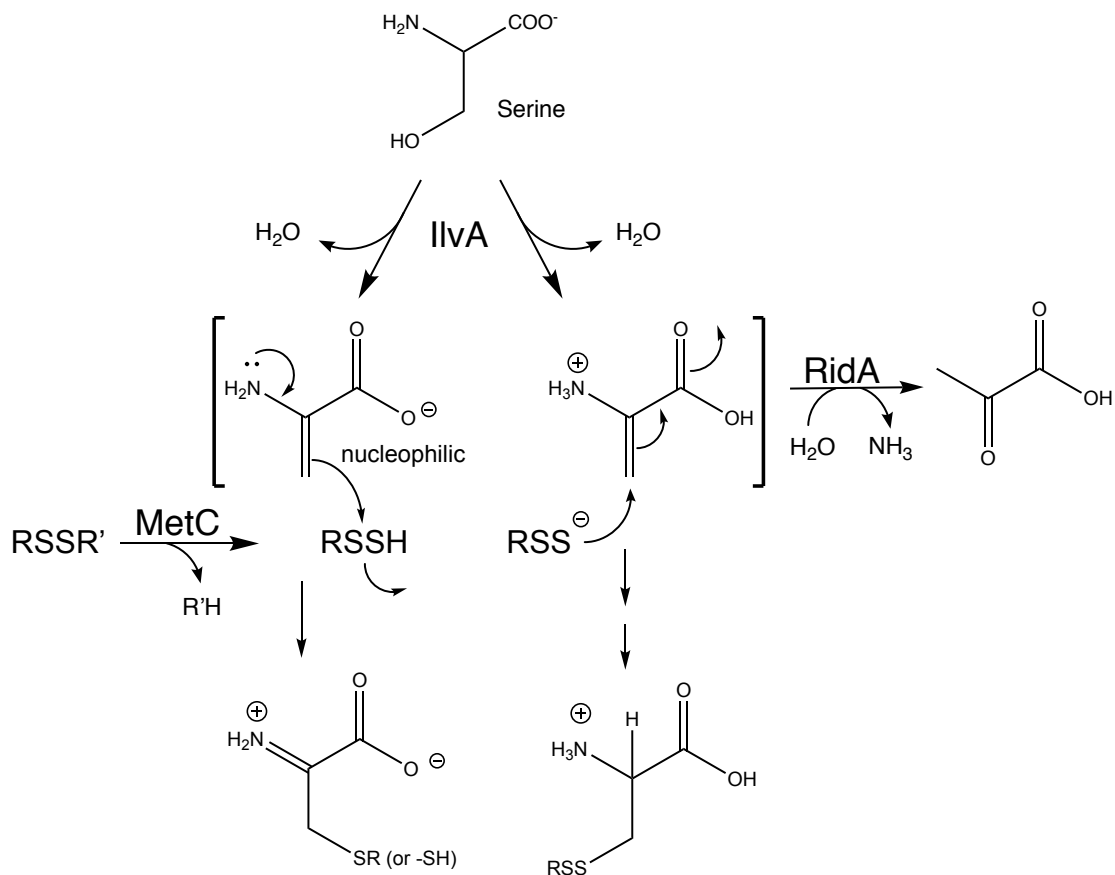


FIGURE 6.5. Proposed model of 2-aminoacrylate sequestration by MetC-generated persulfides. MetC can catalyze a variety of elimination reactions using sulfur-containing amino acid substrates. The elimination of pyruvate from cystine yields cysteine persulfide (thiocysteine) that can react with and sequester 2AA, thus alleviating 2AA stress in the absence of RidA.

CHAPTER 7

CONCLUSIONS

7.1 Multiple mechanisms of 2-aminoacrylate production are relevant *in vivo*.

Work presented in chapters 2 and 3 demonstrated that multiple routes to 2AA exist in *S. enterica*. When grown on minimal glucose medium, expression of the *ilv* operon is necessary to facilitate isoleucine, leucine and valine biosynthesis (1). As a consequence, IlvA is produced during growth on minimal glucose medium. Although IlvA serves a primary role in initiating isoleucine biosynthesis through the dehydration of threonine, it also has side-activity with serine (2). In this way, IlvA-generated 2AA can be viewed as a metabolic accident; the degradation of serine by IlvA does not appear to serve a specific purpose in the cell. Nonetheless, RidA housekeeping function is necessary to prevent minor 2AA accumulation during growth on minimal glucose medium, and becomes essential in order to maintain growth when serine is abundant.

In contrast to the scenario with IlvA, cysteine desulfhydrase (CdsH) and diaminopropionate ammonia lyase (DpaL) activity are virtually undetectable unless cysteine or diaminopropionate are provided to *S. enterica* (3, 4). Expression of *cdsH* is tightly controlled by a cysteine-responsive transcription factor, CutR (4). Once produced, CdsH shows strong cooperative kinetics, with a sharp increase in CdsH activity as the concentration of cysteine approaches 200 μM , approximately the level at which cysteine begins to exert a toxic effect in *E. coli* and *S. enterica* (4–6). The cooperative activity of CdsH reflects the need to rapidly degrade excessive intracellular cysteine to avoid cysteine toxicity, but once cysteine levels drop below $\sim 100\text{-}200 \mu\text{M}$,

cysteine degradation is halted to prevent CdsH from burning through the entire cysteine pool. Given our description of CdsH-mediated 2AA stress, the only way this strategy makes sense from an evolutionary perspective is when one considers RidA. The detoxification of cysteine via CdsH is futile in the absence of RidA, as it exacerbates 2AA stress despite getting rid of cysteine, essentially trading out one form of stress for another. Thus, RidA not only detoxifies the cell of 2AA, but it also acts as an essential component of upstream amino acid detoxification pathways. The general outlook is similar for the relationship between DpaL and RidA. Interestingly, CdsH and DpaL homologs appear restricted to prokaryotes, and are far less pervasive than PLP-dependent serine/threonine dehydratases, perhaps reflecting disparate requirements for amino acid detoxification that depend on the growth environment.

It is interesting to note that *S. enterica* encodes three Fe-S-dependent serine/threonine dehydratases involved in serine detoxification (7, 8). These enzymes do not release a 2AA substrate for RidA *in vitro* (9), nor do they contribute to 2AA stress *in vivo*. It has been proposed that Fe-S serine dehydratases offer i) a greater level of substrate discrimination and ii) an Fe-S cofactor for activation of the serine hydroxyl to promote efficient elimination (10). Regardless, the selective pressure to maintain Fe-S-dehydratases, instead of PLP-dependent dehydratases, may be interesting from an evolutionary perspective.

7.2 Damage to GlyA severely impacts growth of *S. enterica* exposed to 2AA stress.

The results from chapter 4 clarified the underlying cause of 2AA-mediated growth inhibition in *ridA* mutant strains. High levels of 2AA, regardless of the source of 2AA (i.e. serine, cysteine, diamino propionate), inhibit GlyA to such a degree that the cell is starved for glycine and/or one-carbon units. Of the four known enzymes damaged by endogenous 2AA,

GlyA is inhibited to the greatest extent in *ridA* strains relative to wild type (~80 % inactivation) (11). In most cases, 2AA stress elicits a requirement for one-carbon units that can be derived from glycine via the glycine cleavage complex (GCV). However, when *ridA* mutant strains are faced with a substantial exogenous serine burden (~ 5 mM), glycine restores growth in a GCV-independent manner. Our work showed that under high-serine stress, a *ridA* mutant strain requires glycine to activate the GcvB small RNA. The relevant target of GcvB was not identified, but in general, glycine activation of GcvB serves to limit translation of amino acid importers (12), perhaps limiting serine uptake and concomitant 2AA stress.

Somewhat surprisingly, recent work suggests GlyA is not the primary growth-limiting target of 2AA damage in *E. coli* (13). Instead, aspartate stimulates growth of *E. coli ridA* mutants undergoing 2AA stress. Comparative studies demonstrated that swapping 2AA-targeted enzymes from *S. enterica* with their *E. coli* counterparts, generating a hybrid *S. enterica ridA* strain with putative *E. coli* 2AA-target enzymes, failed to recapitulate the *E. coli* phenotypes in *S. enterica*. That is, a *ridA* mutant of *S. enterica* containing *E. coli* GlyA was still sensitive to serine, and sensitivity was overcome through glycine supplementation. These data suggest that the primary divergence between *E. coli* and *S. enterica* with regard to the RidA paradigm is not the level of PLP-enzyme sensitivity to 2AA inactivation, but rather, the organization of the metabolic network. In fact, the accumulation of 2AC in wild-type *E. coli* offers a clear example of how different network structures impact the serine/threonine metabolic node, leading to different reactive enamine accumulation outcomes (14).

7.3 RidA control of 2-aminoacrylate stress is conserved in eukaryotes.

Our foray into yeast metabolism confirmed that RidA 2AA deaminase activity is conserved in *S. cerevisiae*. Furthermore, the loss of 2AA deaminase activity provoked the loss of mtDNA in yeast lacking Mmf1p. In contrast to *S. enterica*, there appears to be a level of coordination between the catabolic PLP-dependent serine/threonine dehydratase (Cha1p) and Mmf1p; upon exposure to serine or threonine, expression of *cha1* and *mmf1* increase more than any other genes (15). The simultaneous upregulation of these genes may indicate Cha1p and Mmf1p act as components of a dedicated serine/threonine detoxification pathway, akin to CdsH or DpaL.

7.4 Future directions.

Exploration of the RidA paradigm in *S. enterica* has been extremely fruitful. However, a number of interesting questions still remain. For one, there is the question of what else might be inhibited by 2AA (in a *ridA* strain) that is beneath our current level of detection? Continuing to build-out the archetypal model of 2AA stress in *S. enterica*, especially through genetic perturbations, will uncover a wider range of possibilities that may be incredibly relevant in other systems. It is likely that numerous other PLP-dependent enzymes are susceptible to endogenous 2AA damage, but we will need to fine-tune the growth conditions and/or strain backgrounds to observe relevant phenotypes. Furthermore, the MetC suppression study presented in chapter 6 raises the interesting possibility that 2AA undergoes spontaneous reactions with other reactive metabolites *in vivo*. If so, to what extent are these spontaneous reactions contributing to 2AA quenching? As appreciation for the impact reactive enamines have on metabolism continues to

grow, there is a need to continue adding to the *S. enterica* RidA paradigm to push the boundaries of expectation in other organisms.

As it relates to yeast, preliminary work summarized in appendix A suggests yeast lacking Mmf1p are sensitive to ferrous iron. This likely indicates that the consequences of 2AA stress in yeast are different than those observed in *S. enterica* and *E. coli*. Continued investigation of Mmf1p function in yeast, and the consequences of 2AA stress in mitochondria, may be informative when investigating mammalian systems. Several reports indicate UK114 is localized to mitochondria in rats and humans (16). Beyond yeast, there is a strong argument to continue exploring fundamental aspects of the RidA paradigm in other model organisms; if we have only looked at three systems (e.g. *S. enterica*, *E. coli* and *S. cerevisiae*), and each system displays different consequences of 2AA accumulation, how many more possible outcomes are there in nature?

7.5 References

1. Berg CM, Shaw KJ. 1981. Organization and regulation of the *ilvGEDA* operon in *Salmonella typhimurium* LT2. *J Bacteriol* 145:984–989.
2. Burns RO, Hofler JG, Luginbuhl GH. 1979. Threonine deaminase from *Salmonella typhimurium*. Substrate-specific patterns of inhibition in an activator site-deficient form of the enzyme. *J Biol Chem* 254:1074–1079.
3. Kalyani JN, Ramachandra N, Kachroo AH, Mahadevan S, Savithri HS. 2012. Functional analysis of the genes encoding diaminopropionate ammonia lyase in *Escherichia coli* and *Salmonella enterica* serovar Typhimurium. *J Bacteriol* 194:5604–5612.
4. Oguri T, Schneider B, Reitzer L. 2012. Cysteine catabolism and cysteine desulfhydrase (CdsH/STM0458) in *Salmonella enterica* serovar Typhimurium. *J Bacteriol* 194:4366–4376.
5. Kredich NM, Foote LJ, Keenan BS. 1973. The stoichiometry and kinetics of the inducible cysteine desulfhydrase from *Salmonella typhimurium*. *J Biol Chem* 248:6187–6196.

6. Park S, Imlay JA. 2003. High levels of intracellular cysteine promote oxidative DNA damage by driving the Fenton reaction. *J Bacteriol* 185:1942–1950.
7. Zhang X, Newman E. 2008. Deficiency in L-serine deaminase results in abnormal growth and cell division of *Escherichia coli* K-12. *Mol Microbiol* 69:870–881.
8. Zhang X, El-Hajj ZW, Newman E. 2010. Deficiency in L-serine deaminase interferes with one-carbon metabolism and cell wall synthesis in *Escherichia coli* K-12. *J Bacteriol* 192:5515–5525.
9. Xu XL, Grant GA. 2016. Mutagenic and chemical analyses provide new insight into enzyme activation and mechanism of the type 2 iron-sulfur l-serine dehydratase from *Legionella pneumophila*. *Arch Biochem Biophys* 596:108–117.
10. Grabowski R, Hofmeister AE, Buckel W. 1993. Bacterial L-serine dehydratases: a new family of enzymes containing iron-sulfur clusters. *Trends Biochem Sci* 18:297–300.
11. Flynn JM, Christopherson MR, Downs DM. 2013. Decreased coenzyme A levels in *ridA* mutant strains of *Salmonella enterica* result from inactivated serine hydroxymethyltransferase: *ridA* mutants are deficient in one carbon metabolism. *Mol Microbiol* 89:751–759.
12. Sharma CM, Papenfort K, Pernitzsch SR, Mollenkopf H-J, Hinton JCD, Vogel J. 2011. Pervasive post-transcriptional control of genes involved in amino acid metabolism by the Hfq-dependent GcvB small RNA: GcvB regulon. *Mol Microbiol* 81:1144–1165.
13. Borchert AJ, Downs DM. 2017. The response to 2-Aminoacrylate differs in *Escherichia coli* and *Salmonella enterica*, despite shared metabolic components. *J Bacteriol* 199:e00140-17.
14. Bazurto JV, Farley KR, Downs DM. 2016. An unexpected route to an essential cofactor: *Escherichia coli* relies on threonine for thiamine biosynthesis. *mBio* 7:e01840–15.
15. Godard P, Urrestarazu A, Vissers S, Kontos K, Bontempi G, van Helden J, Andre B. 2007. Effect of 21 different nitrogen sources on global gene expression in the yeast *Saccharomyces cerevisiae*. *Mol Cell Biol* 27:3065–3086.
16. Mootha VK, Bunkenborg J, Olsen JV, Hjerrild M, Wisniewski JR, Stahl E, Bolouri MS, Ray HN, Sihag S, Kamal M, others. 2003. Integrated analysis of protein composition, tissue diversity, and gene regulation in mouse mitochondria. *Cell* 115:629–640.

APPENDIX A

SACCHAROMYCES CEREVISIAE LACKING MMF1P HAVE LOW HEME LEVELS AND ARE SENSITIVE TO IRON

A.1 Premise

As described in chapter 5, the loss of Mmf1p in *Saccharomyces cerevisiae* leads to loss of mitochondrial DNA. The loss of mitochondrial DNA occurs in a 2-aminoacrylate (2AA)-dependent manner; preemptively disrupting Ilv1p- and Cha1p-mediated 2AA production preserves mtDNA in an *mmf1*Δ mutant strain indefinitely. However, the link between 2AA production and loss of mtDNA remains unclear. Work in *Salmonella enterica* has identified a number of pyridoxal 5'-phosphate (PLP)-dependent enzymes that are inhibited by 2AA (1–3). Work presented in chapter 4 highlighted the significance of serine hydroxymethyltransferase (SHMT; GlyA) in being the primary growth-limiting target of 2AA damage in *S. enterica* (4). In *S. cerevisiae*, at least 12 PLP-dependent enzymes are localized to the mitochondrion (Table A.1) (5). Several of the mitochondrial PLP-dependent enzymes are redundant with cytosolic isozymes. For example, mitochondrial SHMT (Shm1p) is responsible for 5 % of the total serine hydroxymethyltransferase activity in *S. cerevisiae*, with the remaining 95 % contributed by the cytosolic isozyme (Shm2p) (6). Furthermore, yeast lacking both SHMT isozymes remain glycine prototrophs due to an alternative mechanism of glycine synthesis catalyzed by threonine aldolase (Gly1p).

The growth defect of a $\rho^0 \Delta mmf1$ mutant in minimal glucose medium was not improved through glycine supplementation (data not shown), counter to the observations made in *S. enterica*. This observation, coupled with redundancy in the *S. cerevisiae* SHMT/glycine enzymes, suggests other PLP-dependent enzymes may be damaged by 2AA and underlie the growth defects and/or loss of mtDNA experienced by *mmf1* Δ mutants. The preliminary data that follow reveal growth defects related to purines, heme and iron homeostasis in *mmf1* Δ mutant strains.

A.2 Construction and phenotypic characterization of a ρ^+ *mmf1* Δ mutant strain.

Given that glycine supplementation failed to improve growth of the ρ^0 *mmf1* Δ mutant on minimal glucose, a panel of diverse nutritional supplements was assessed (Table A.2). First, a ρ^+ *mmf1* Δ mutant strain (DMy41) was generated by inserting a drug marker (KanMx6) into the *mmf1* ORF and selecting for G418 resistance on solid YP-glycerol (YPG) medium containing 400 μ g/ml geneticin. As described previously, selection and propagation of *mmf1* Δ mutants on YPG does not result in loss of the mitochondrial genome (7, 8). When transferred to minimal glucose medium, the ρ^+ *mmf1* Δ mutant strain showed a growth defect relative to the ρ^+ wild type strain (YJF153), but maintained respiratory capacity (data not shown). The benefit of using a ρ^+ *mmf1* Δ mutant strain for supplementation analysis is that it provides robust growth relative to the severely inhibited ρ^0 *mmf1* Δ mutant on minimal glucose medium (data not shown), increasing the odds of detecting supplements that improve growth in strains experiencing 2AA stress.

The ρ^+ *mmf1* Δ mutant strain was grown overnight in YPG (5 ml) at 30 °C and 200 rpm. The following day, turbid cultures served as inoculum for generating soft-agar overlays on

synthetic dextrose (SD) medium. An aliquot (100 μ l) of the turbid culture was mixed with melted soft agar (3 ml) and poured over solid SD medium. Upon solidifying, supplements were spotted (5 μ l) on the agar surface and plates were incubated \sim 48 hours at 30 $^{\circ}$ C. Growth was qualitatively assessed based on the turbidity of the agar overlay; background growth in the absence of supplementation was undetectable (data not shown). Isoleucine was spotted on the agar overlays as an indicator of fully restored growth; the allosteric regulation of IlvA by isoleucine prevents 2AA stress in the ρ^{+} *mmf1* Δ mutant strain grown on minimal glucose medium. A number of purine-related supplements displayed mild growth-stimulating effects (Table A.2). A variety of metabolic precursors are required for *de novo* purine synthesis, including glycine and one-carbon units (6). Yeast lacking the mitochondrial SHMT (Shm1p) are typically proficient in purine synthesis (9), arguing against damage to mitochondrial Shm1p being relevant to the observed purine effect. However, one report described an obscure allele of *Shm1* (*tmp3*) with \sim 40 % of wild type SHMT activity that induced a requirement for methionine (also stimulatory; Table A.2), thymidine, adenine and histidine (10). Surprisingly, this report also showed that the *tmp3* allele resulted in the formation of ρ^{-} cytoplasmic petites. The influence of strain background and growth conditions on the activity of both yeast SHMT isozymes may indicate that Shm1p is required for purine synthesis and maintenance of mtDNA under specific conditions.

A.3 Strains lacking Mmf1p display a heme defect.

Additional supplements that improved growth of the ρ^{+} *mmf1* Δ mutant strain share a connection to iron metabolism. Aminolevulinic acid (ALA) promoted growth to a level intermediate between adenine and isoleucine (Table A.2), judged based on the density of the

growth halo (data not shown). ALA is the first dedicated intermediate in heme biosynthesis. The synthesis of ALA is catalyzed by Hem1p, a fold type II PLP-dependent ALA synthase (ALAS) that requires glycine and succinyl-CoA as substrates (11). Hem1p-like ALAS is found in all non-plant eukaryotes and α -proteobacteria, and performs an unusual dual-cleavage reaction that cleaves both amino acid substrate α -carbon bonds (12). Hem1p in yeast performs chemistry unrelated to the PLP-dependent ALAS in most bacteria, including *S. enterica*, that requires glutamate-1-semialdehyde as a substrate (13). Disruption of Hem1p results in loss of heme and auxotrophy for unsaturated fatty acids, ergosterol and methionine, and in some cases results in permanent damage to mtDNA (ρ^-) (14, 15).

To determine if a heme limitation exists in *mmf1* Δ mutant strains, total intracellular heme levels were quantified following the methods of Sassa (16). Cultures (20 ml) of ρ^+ wild type, ρ^- wild type and ρ^0 *mmf1* Δ strains were grown in YPD to a final OD₆₀₀ of 0.4. Cells were pelleted (5 min at 4 °C and 3,000 x g), resuspended in 1 ml ice-cold water, transferred to an amber microcentrifuge tube and repelleted for 5 min at 8,000 x g. Supernatant was discarded and the cell pellet was resuspended in 500 μ l of 20 mM oxalic acid, then transferred to a light-safe box at 4 °C overnight. The next day, 500 μ l of 2 M oxalic acid was added to each tube, mixed by pipetting and separated (500 μ l each) into two amber microcentrifuge tubes. One tube was heated at 98 °C for 30 min, while the other was stored in the dark at room temperature as the control. After 30 minutes, all tubes were centrifuged for 2 min at 16,000 x g. Aliquots (200 μ l) of each heated and unheated sample were transferred to a black 96-well plate and fluorescence was measured (Ex: 400 nm; Em: 620 nm) using a Gemini EM microplate reader (Molecular Devices). A standard curve was generated as above using hemin diluted in water. For each boiled sample, fluorescence of the corresponding non-heated sample was subtracted to correct for

background fluorescence. Fluorescence was normalized to dry cell weight, measured after evaporating aliquots (200 μ l) of the initial culture in an Eppendorf Vacufuge. The resulting data show that ρ^0 *mmf1* Δ mutants have severely diminished heme levels (\sim 9.5 nmol/g DCW) relative to the ρ^- (\sim 87 nmol/g DCW) or ρ^+ (\sim 116 nmol/g DCW) wild type controls (Figure A.1). These data are consistent with, but do not prove, Hem1p may be damaged in strains lacking Mmf1p. Future work is needed to confirm if the heme defect in strains lacking Mmf1p is caused by 2AA damage to Hem1p specifically. To assess the potential for Hem1p to be damaged by 2AA *in vivo*, recombinant Hem1p will be purified from a *S. enterica ridA* mutant strain engineered for robust 2AA production. Furthermore, Hem1 in yeast will be deleted to see how the resulting phenotype matches to *mmf1* Δ mutants; mtDNA maintenance in *hem1* Δ mutants can be influenced by the stain background. Finally, to confirm if Hem1p is specifically damaged by 2AA, ALAS assays will be performed in wild type and *mmf1* Δ strain backgrounds.

A.4 Iron chelation prevents 2AA-dependent loss of mtDNA.

In addition to ALA, the iron chelator bathophenanthrolinedisulfonic acid (BPS), and to a lesser extent ethylenediaminetetraacetic acid (EDTA), improved growth of the ρ^+ *mmf1* Δ mutant on SD medium. A representative plate displays the halo of turbidity (i.e. growth) generated by BPS spotted on top of the ρ^+ *mmf1* Δ strain embedded in agar on solid SD medium (Figure A.2). BPS is a potent ferrous iron (Fe^{2+}) chelator; spotting it on the agar surface presumably sequesters iron present in the growth medium. These data indicate that *mmf1* Δ mutants are sensitive to iron. A key fate of iron in yeast, aside from heme, is incorporation into iron-sulfur clusters. Mutants with defective iron-sulfur cluster biogenesis are known to experience iron sensitivity due to hyperaccumulation of iron in the mitochondrion (17). The hyperaccumulation of iron can drive

Fenton chemistry, leading to damage of mtDNA (18). The sole PLP-dependent enzyme directly involved in iron-sulfur cluster biogenesis is cysteine desulfurase (Nfs1p). This enzyme generates a persulfide required for cluster biogenesis, and *nfs1Δ* mutants are inviable (19). Although not tested here, it is formally possible that 2AA damages Nfs1p, contributing to iron sensitivity in an *mmf1Δ* mutant strain.

Based on the preceding data, we developed a model that predicts damage to heme biosynthesis and/or iron-sulfur biogenesis leads to iron accumulation in the mitochondrion, that in turn drives Fenton chemistry, leading to damage and eventual loss of mtDNA (Figure A.3). Following this logic, the loss of mtDNA could be prevented in an *mmf1Δ* mutant strain propagated on YPD as long as iron levels are kept sufficiently low. To test this hypothesis, the ρ^+ *mmf1Δ* mutant strain (DMy41) isolated and maintained on glycerol was streaked on YPD, YPD + 10 μ M BPS or YPG, then incubated for 48 hours at 30 °C. After two passages on the aforementioned media, two colonies from each condition were picked and streaked out on quadrants of the same YPG plate. Colonies passaged on YPG maintained their ability to respire glycerol (data not shown). Colonies passaged on YPD lost their ability to respire glycerol (data not shown). Lastly, one of the two colonies passaged on YPD + 10 μ M BPS maintained the ability to respire glycerol when transferred to YPG, indicating that the mitochondrial genome remained intact despite the loss of Mmf1p (data not shown). These data are preliminary, but they offer support for our model and warrant follow-up investigation to explore possible connections between iron homeostasis, 2-aminoacrylate toxicity and mtDNA maintenance. Experiments will be repeated with greater statistical power (i.e. hundreds of colonies) to assess the impact of iron chelation of mtDNA maintenance in the ρ^+ *mmf1Δ* strain.

A.4 Conclusions.

The connection between 2AA stress in the mitochondrion and loss of mtDNA remains unsettled. The data presented here offer clues for further investigation. To date, the only detectable consequence of intracellular 2AA accumulation has been damage to PLP-dependent enzymes. Evidence from *S. enterica* suggests 2AA is not mutagenic under standard growth conditions. Taken together, our model predicts that 2AA negatively influences mtDNA stability indirectly, by damaging one or more mitochondrial PLP-dependent enzymes. Many studies that connect mitochondrial PLP-dependent enzymes to mtDNA maintenance lack sufficient detail to discern the strain background or specific growth conditions necessary to elicit the described phenotypes. However, reports describe the role of disrupted iron homeostasis, stemming from damage to heme and/or Fe-S biogenesis, in prompting damage or loss of mtDNA (14, 19). One of the best known examples is frataxin (Yfh1p); the function of this enzyme is still somewhat obscure, but ultimately, frataxin facilitates loading of iron into Fe-S cluster biogenesis machinery (20). Mutations in the gene encoding frataxin elicit hyperaccumulation of iron in the mitochondrion that induces loss of mtDNA (21); this defect is countered by BPS-mediated iron chelation (22). Continued study of the metabolic consequences of 2AA accumulation in the yeast mitochondrion may inform future studies regarding 2AA stress in humans, especially given the well-conserved enzymes and pathways for heme and iron-sulfur cluster synthesis in yeast and humans. Following examples from the frataxin model, we can continue to investigate iron toxicity as it relates to 2AA stress in yeast mitochondria.

A.5 References

1. Flynn JM, Downs DM. 2013. In the absence of RidA, endogenous 2-aminoacrylate inactivates alanine racemases by modifying the pyridoxal 5'-phosphate cofactor. *J Bacteriol* 195:3603–3609.
2. Flynn JM, Christopherson MR, Downs DM. 2013. Decreased coenzyme A levels in *ridA* mutant strains of *Salmonella enterica* result from inactivated serine hydroxymethyltransferase: *ridA* mutants are deficient in one carbon metabolism. *Mol Microbiol* 89:751–759.
3. Lambrecht JA, Schmitz GE, Downs DM. 2013. RidA proteins prevent metabolic damage inflicted by PLP-dependent dehydratases in all domains of life. *MBio* 4:e00033-13.
4. Ernst DC, Downs DM. 2016. 2-aminoacrylate stress induces a context-dependent glycine requirement in *ridA* strains of *Salmonella enterica*. *J Bacteriol* 198:536–543.
5. Whittaker JW. 2016. Intracellular trafficking of the pyridoxal cofactor. Implications for health and metabolic disease. *Arch Biochem Biophys* 592:20–26.
6. Kastanos EK, Woldman YY, Appling DR. 1997. Role of mitochondrial and cytoplasmic serine hydroxymethyltransferase isozymes in *de novo* purine synthesis in *Saccharomyces cerevisiae*. *Biochemistry (Mosc)* 36:14956–14964.
7. Kim J-M, Yoshikawa H, Shirahige K. 2001. A member of the YER057c/yjgf/Uk114 family links isoleucine biosynthesis and intact mitochondria maintenance in *Saccharomyces cerevisiae*. *Genes Cells* 6:507–517.
8. Oxelmark E, Marchini A, Malanchi I, Magherini F, Jaquet L, Hajibagheri MAN, Blight KJ, Jauniaux J-C, Tommasino M. 2000. Mmflp, a novel yeast mitochondrial protein conserved throughout evolution and involved in maintenance of the mitochondrial genome. *Mol Cell Biol* 20:7784–7797.
9. Christensen KE, MacKenzie RE. 2006. Mitochondrial one-carbon metabolism is adapted to the specific needs of yeast, plants and mammals. *BioEssays* 28:595–605.
10. Luzzati M. 1975. Isolation and properties of a thymidylate-less mutant in *Saccharomyces cerevisiae*. *Eur J Biochem* 56:533–538.
11. Schulze JO, Schubert W-D, Moser J, Jahn D, Heinz DW. 2006. Evolutionary relationship between initial enzymes of tetrapyrrole biosynthesis. *J Mol Biol* 358:1212–1220.
12. Hunter GA, Ferreira GC. 2011. Molecular enzymology of 5-Aminolevulinic synthase, the gatekeeper of heme biosynthesis. *Biochim Biophys Acta BBA - Proteins Proteomics* 1814:1467–1473.

13. Pugh CE, Harwood JL, John RA. 1992. Mechanism of glutamate semialdehyde aminotransferase. Roles of diamino- and dioxo-intermediates in the synthesis of aminolevulinate. *J Biol Chem* 267:1584–1588.
14. Whittaker MM, Penmatsa A, Whittaker JW. 2015. The Mtm1p carrier and pyridoxal 5'-phosphate cofactor trafficking in yeast mitochondria. *Arch Biochem Biophys* 568:64–70.
15. Gollub EG, Liu KP, Dayan J, Adlersberg M, Sprinson DB. 1977. Yeast mutants deficient in heme biosynthesis and a heme mutant additionally blocked in cyclization of 2, 3-oxidosqualene. *J Biol Chem* 252:2846–2854.
16. Sassa S. 1976. Sequential induction of heme pathway enzymes during erythroid differentiation of mouse Friend leukemia virus-infected cells. *J Exp Med* 143:305–315.
17. Pelzer W, Mühlenhoff U, Diekert K, Siegmund K, Kispal G, Lill R. 2000. Mitochondrial Isa2p plays a crucial role in the maturation of cellular iron–sulfur proteins. *FEBS Lett* 476:134–139.
18. Gomez M, Pérez-Gallardo RV, Sánchez LA, Díaz-Pérez AL, Cortés-Rojo C, Meza Carmen V, Saavedra-Molina A, Lara-Romero J, Jiménez-Sandoval S, Rodríguez F, Rodríguez-Zavala JS, Campos-García J. 2014. Malfunctioning of the iron–sulfur cluster assembly machinery in *Saccharomyces cerevisiae* produces oxidative stress via an iron-dependent mechanism, causing dysfunction in respiratory complexes. *PLoS ONE* 9:e111585.
19. Li J, Kogan M, Knight SA, Pain D, Dancis A. 1999. Yeast mitochondrial protein, Nfs1p, coordinately regulates iron-sulfur cluster proteins, cellular iron uptake, and iron distribution. *J Biol Chem* 274:33025–33034.
20. Braymer JJ, Lill R. 2017. Iron–sulfur cluster biogenesis and trafficking in mitochondria. *J Biol Chem* 292:12754–12763.
21. Gakh O. 2005. Mitochondrial iron detoxification is a primary function of frataxin that limits oxidative damage and preserves cell longevity. *Hum Mol Genet* 15:467–479.
22. Foury F. 1999. Low iron concentration and aconitase deficiency in a yeast frataxin homologue deficient strain. *FEBS Lett* 456:281–284.

TABLE A.1. List of *S. cerevisiae* mitochondrial pyridoxal 5'-phosphate-dependent enzymes.

Mitochondrial PLP enzymes	Proteins	
	<i>S. cerevisiae</i>	<i>S. enterica</i>
α,β-eliminases		
Threonine dehydratase (anabolic)	Ilv1p*	IlvA*
L-serine/threonine dehydratase (catabolic)	Cha1p*	TdcB*
Transaminases		
Acetylmethionine aminotransferase	Arg8p	ArgD
Alanine:glyoxylate aminotransferase	Aat1p	-
Alanine transaminase	Alt1p	YfbQ
Aspartate aminotransferase	Aat1p	AspC
Branched-chain amino acid aminotransferase	Bat1p	IlvE [#]
Kynurenine aminotransferase	Bna3p	-
Other		
5-Aminolevulinate synthase	Hem1p	-
Cysteine desulfurase	Nfs1p	NifS
Glycine decarboxylase complex	Gcv2p	GcvP
Serine hydroxymethyltransferase	Shm1p	GlyA [#]

* Confirmed endogenous 2AA-stress generator.

Confirmed endogenous 2AA-stress target of inactivation.

TABLE A.2. Supplements that improve growth of a ρ^+ $\Delta mmf1$ mutant on minimal glucose medium.

Nutrient	Stock (mM)	Growth	Nutrient	Stock (mM)	Growth
Adenine	80	+	Isoleucine	60	+++
Adenosine	25		α -Ketobutyrate	60	
Alanine	94		α -Ketoglutarate	60	
Aminolevulinic acid	1	++	Ketoisovalerate	60	
Arginine	120		Leucine	60	
Asparagine	64		Lysine	75	
Aspartate	58		Methionine	60	+
Biotin	1		Nicotinic acid	20	
BPS	1	++	Oxaloacetate	20	+
Citrate	20		Ornithine	15	
Cysteine	42		Pantothenate	20	
Cytosine	25		Phenylalanine	60	
Diaminopimelic acid	20		Proline	400	
EDTA	10	+	Pyridoxal	20	
Glutamine	20		Serine	476	
Glycine	27		Succinate	20	
Glutamate	20	++	Thiamine	10	
Glutathione	10		Threonine	60	
Guanine	49	+	Tryptophan	20	
Guanosine	60	+	Tyrosine	16	
Histidinol	200		Thymine	32	
Histidine	15		Uracil	20	
Homoserine	60		Uridine	20	
Hypoxanthine	25	+	Valine	60	
Inosine	25	+			

Five microliter aliquots of the indicated stock solutions were spotted on agar overlays of DMy41 (ρ^+ $\Delta mmf1$). Growth was assessed after 48 hours; blank = no growth, + = minor growth, ++ = growth, +++ = growth comparable to ρ^+ Wt strain (YJF153). BPS, bathophenanthrolinedisulfonic acid.

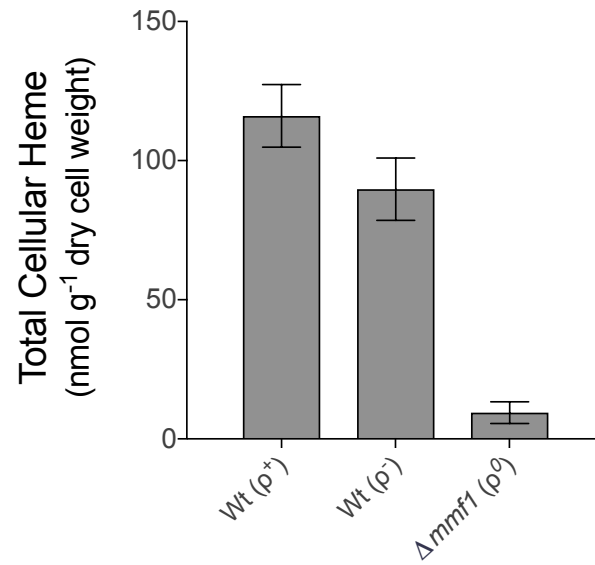


FIGURE A.1. Quantification of total cellular heme levels. The indicated strains were grown in YPD, washed and assayed for heme content. Data were corrected for background and normalized to dry cell weight (g⁻¹ DCW). Each bar represents the average and standard deviation of three independent cultures. Data were plotted using GraphPad Prism 7.

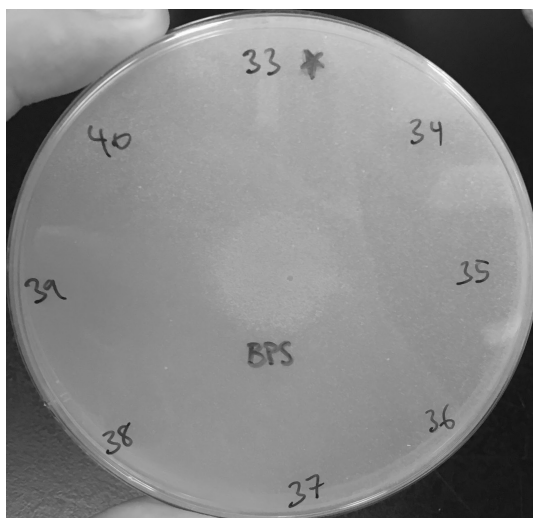


FIGURE A.2. Growth assay shows iron chelator stimulates growth of a ρ^+ $\Delta mmf1$ mutant on minimal glucose medium. An overnight culture of DMy41 was embedded in agar and overlaid on solid SD medium. Supplements were spotted around the periphery, or in the center of the plate. BPS (1 mM) was spotted in the middle of the plate. Image was acquired after ~ 48 hours at 30 °C and shows turbid growth where BPS was added to the plate.

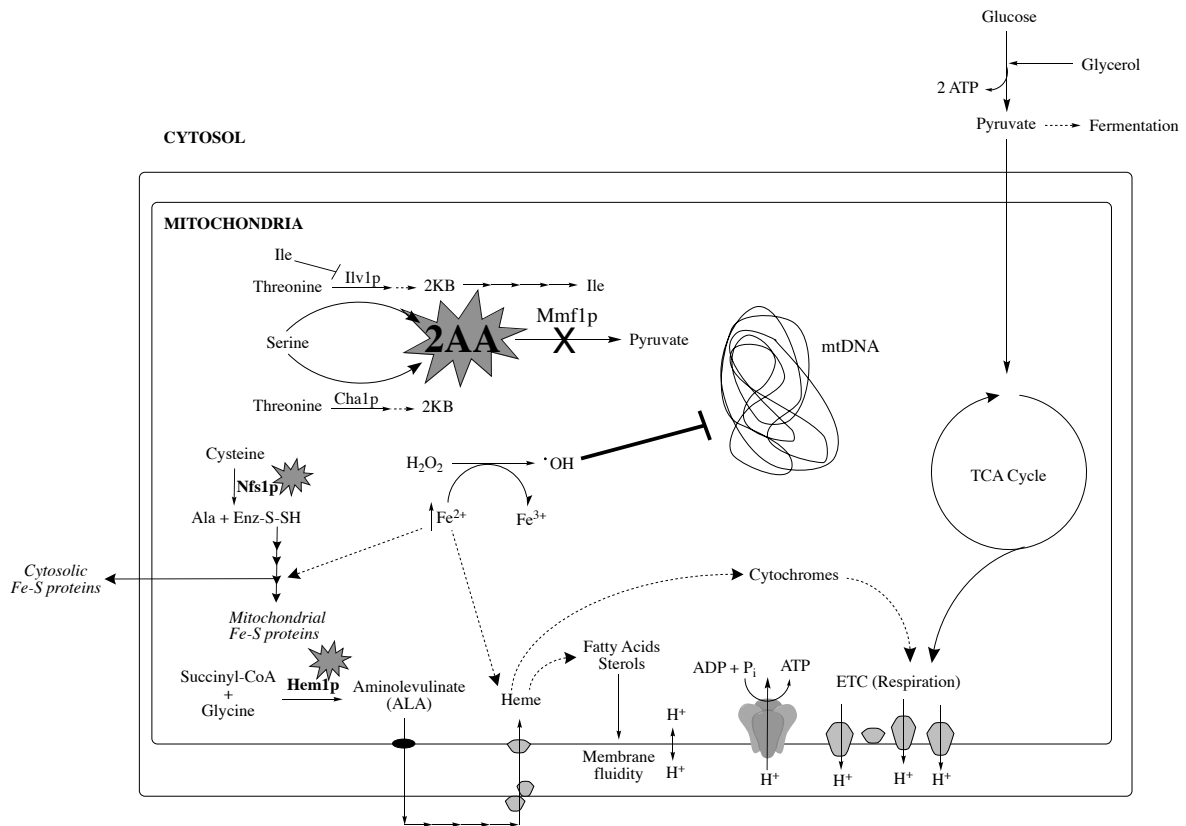


FIGURE A.3. Model of 2-aminoacrylate-disrupted iron homeostasis leading to mitochondrial DNA damage. Growth phenotypes indicate $\Delta mmf1$ mutant strains have reduced heme content and are sensitive to iron. Restricted synthesis of heme and/or iron-sulfur clusters prompts accumulation of ferrous (Fe^{2+}) iron in the mitochondrion. Ferrous iron can reduce hydrogen peroxide to the hydroxyl radical, leading to damage and potential loss of the mitochondrial genome.

APPENDIX B

THE *STM4195* GENE PRODUCT (PANS) TRANSPORTS COENZYME A PRECURSORS
IN *SALMONELLA ENTERICA*¹

¹Ernst DC, Downs DM. 2015. *Journal of Bacteriology* 197:1368–1377.
Reprinted here with permission of the publisher.

B.1 ABSTRACT

Coenzyme A (CoA) is a ubiquitous coenzyme involved in fundamental metabolic processes. CoA is synthesized from pantothenic acid by a pathway that is largely conserved among bacteria and eukaryotes, and consists of five enzymatic steps. While higher organisms, including humans, must scavenge pantothenate from the environment, most bacteria and plants are capable of *de novo* pantothenate biosynthesis. In *Salmonella enterica*, precursors to pantothenate can be salvaged, but subsequent intermediates are not transported due to their phosphorylated state and thus the pathway from pantothenate to CoA is considered essential. Genetic analyses identified the *stm4195* gene product of *Salmonella enterica* serovar Typhimurium as a transporter of pantothenate precursors, ketopantoate and pantoate, and to a lesser extent, pantothenate. Further results indicated that Stm4195 transports a product of CoA degradation that serves as a precursor to CoA and enters the biosynthetic pathway between PanC and CoaBC (*dfp*). The relevant CoA derivative is distinguishable from pantothenate, pantetheine and pantethine and has spectral properties indicating the adenine moiety of CoA is intact. Taken together, results herein provide evidence of a transport mechanism for the uptake of ketopantoate, pantoate and pantothenate, and demonstrate a role for Stm4195 in the salvage of a CoA derivative of unknown structure. The *stm4195* gene is renamed *panS* to reflect participation in pantothenate salvage that was uncovered herein.

B.2 BACKGROUND

Coenzyme A (CoA) is essential for reactions of central metabolism, where it facilitates the activation of carbonyl groups and acts in the biosynthesis and degradation of fatty acids, polyketides and nonribosomal peptides (1). Nine percent of known enzymatic activities are dependent on CoA or a thioester derivative (2). In eukaryotes and bacteria, CoA biosynthesis stems

from the vitamin, pantothenic acid (B₅), and many higher organisms rely on dietary pantothenate to satisfy their CoA requirement (1). In contrast, many plants, fungi and microorganisms such as *Escherichia coli* and *Salmonella enterica* possess the enzymes necessary for *de novo* biosynthesis of pantothenate from β -alanine and α -ketoisovalerate (Figure B.1) (1, 3). Briefly, aspartate α -decarboxylase (PanD; EC 4.1.1.11) catalyzes the production of β -alanine from L-aspartate. The activity of ketopantoate hydroxymethyltransferase (PanB; EC 2.1.2.11) converts the branch-point metabolite α -ketoisovalerate to ketopantoate, which is subsequently reduced to pantoate by ketopantoate reductase (PanE; EC 1.1.1.169). Acetohydroxyacid isomoreductase (IlvC; EC 1.1.1.86) catalyzes the same reduction of ketopantoate to pantoate, although much less efficiently than PanE, making the activities of PanE and IlvC partially redundant in the cell (4). Finally, pantothenate is produced by the ATP-dependent ligation of pantoate and β -alanine, catalyzed by pantothenate synthase (PanC; EC 6.3.2.1).

Many organisms actively transport pantothenate into the cell (1). *E. coli* and *S. enterica* have a sodium-dependent pantothenate permease (PanF) with high affinity for the substrate pantothenate ($K_t = 0.4 \mu\text{M}$ in *E. coli*) (5). Exogenous ketopantoate, pantoate and β -alanine stimulated pantothenate production in *E. coli* under various growth conditions, which suggested these intermediates were also salvaged by the cell (6). However, of these three, only the transport of β -alanine by CycA has been characterized (7).

In most bacteria, plants and mammals the formation of CoA from pantothenate requires five enzymatic steps (Figure B.1). The first committed step in CoA biosynthesis is the ATP-dependent phosphorylation of pantothenate to form 4'-phosphopantothenate catalyzed by pantothenate kinase (CoaA; EC 2.7.1.33) (6). Most organisms cannot salvage exogenous CoA or its phosphorylated intermediates, making the pathway beyond pantothenate essential for viability (2). An exception

is pantetheine, which is transported by an unknown mechanism, and phosphorylated by pantothenate kinase (CoaA) to generate 4'-phosphopantetheine, the substrate for phosphopantetheine adenylyltransferase (CoaD; EC 2.7.7.3) (2). Thus, exogenous pantetheine can bypass the need for the steps catalyzed by CoaBC (EC 4.1.1.36, 6.3.2.5), but requires CoaA (Figure B.1). The mechanism of pantetheine uptake in *E. coli* and *S. enterica* is PanF-independent, but otherwise uncharacterized (8). Following adenylation, dephospho-CoA is phosphorylated by dephospho-CoA kinase (CoaE; 2.7.1.24). CoA and its thioester derivatives allosterically inhibit pantothenate kinase, thus coordinating CoA biosynthesis with the metabolic state of the cell (9). As a result of this allosteric regulation, *E. coli* is capable of accumulating a 15-fold excess of pantothenate relative to CoA (6), a strategy that ensures rapid generation of CoA when a need arises.

Essential metabolic pathways can be used to gain insights about metabolic robustness and probe how the cell responds to perturbations in the metabolic network (10). If the primary ketopantoate reductase in *S. enterica*, PanE, is disrupted, the cellular CoA levels are decreased about ten-fold (11). However, in this strain the redundant ketopantoate reductase activity of IlvC produced sufficient CoA to support prototrophic growth (4). The low level of CoA present in a *panE* mutant caused multiple phenotypes that were used to detect metabolic integration of biochemical pathways (11). In the current study, a *panE ilvC* mutant strain that lacked all ketopantoate reductase activity was used to isolate suppressors in an effort to uncover alternative routes of CoA biosynthesis supported by robustness in the metabolic network. These studies uncovered a role for the previously uncharacterized open-reading frame, *panS* (previously *stm4195*), in CoA salvage and detected a novel CoA derivative that could be incorporated into the biosynthetic pathway.

B.3 MATERIALS AND METHODS

Bacterial strains, media and chemicals. All strains used in this study are derivatives of *Salmonella enterica* serovar Typhimurium LT2 and are listed with their genotype in Table B.1. *Tn10d*(Tc) refers to the transposition defective mini-*Tn10* (*Tn10*Δ16 Δ17) described by Way *et al.* (12), while *Tn10* refers to the full-length transposable element (13). MudJ refers to the Mud1734 transposon described previously (14) and *Tn10d*-Cam refers to the transposition defective *Tn10* specifying chloramphenicol resistance (15).

No-carbon E medium (NCE) supplemented with 1 mM MgSO₄ (16), trace minerals (17) and glucose (11 mM) as the sole carbon source was used as minimal medium. Difco nutrient broth (NB) (8 g/liter) with NaCl (5 g/liter) and Luria-Bertani broth were used as rich media. Difco BiTek agar (15 g/L) was added for solid medium. When necessary the branched-chain amino acids (BCAA) leucine, isoleucine and valine (plus ketoisovalerate) were added at a final concentration of 0.3 mM. Antibiotics were added as needed to reach the following concentrations in rich and minimal medium, respectively: tetracycline 20 and 10 μg/ml; ampicillin 30 and 15 μg/ml; and chloramphenicol 20 and 5 μg/ml. Coenzyme A sodium salt hydrate, D-pantothenic acid and D-pantethine were purchased from Sigma-Aldrich. Pantetheine was made by adding dithiothreitol (20 mM final) to a stock of 20 mM pantethine and incubating at room temperature overnight. Ketopantoate and pantoate were synthesized from their respective lactonized forms using the method of Primerano and Burns (4).

Genetic methods. All transductional crosses were performed using the high-frequency general transducing mutant of bacteriophage P22 (HT105/1, *int*-201) (18). Methods for performing transductional crosses, purification of transductants from phage and the identification of phage-free recombinants have been described previously (19, 20). All mutant strains were constructed

using standard genetic techniques. The *panE* and *ilvC* loci were replaced with chloramphenicol and kanamycin drug resistance cassettes, respectively, using the λ -Red recombinase system described by Datsenko and Wanner (21). Insertions in *stm4195*, *panF* and *dfp* were generated using similar methods. When necessary, drug cassettes were resolved using the Flp-*FRT* recombination method previously described (21). Nomenclature used herein associated with *stm4195* follows classical genetic format; the gene locus is denoted *stm4195*, the gene product is referred to as Stm4195 and genetic lesions affecting expression isolated here are referred to by allele names *stm4195p1-11* to reflect their impact on the promoter.

Mutant isolation. Eleven cultures of DM6486 (*panE675::MudJ ilvC2104::Tn10*) were grown overnight in LB medium. Cells were pelleted and resuspended in an equal volume of saline solution (85 mM). Approximately 10^8 cells from each cell suspension were spread onto solid glucose medium containing 1% Difco vitamin-assay casamino acids (CAAs). Plated cultures were incubated at 37 °C for a period of 24-48 h. The resulting mutant colonies were streaked out on non-selective medium. Phenotypes were confirmed by patching mutant isolates to non-selective rich medium, which were then replica-printed to selective plates after a period of 6-12 hr at 37 °C. A representative mutant strain displaying CAA-dependent growth, DM13708 (*panE675::MudJ ilvC2104::Tn10 stm4195p1*), was used to generate a pool of ~60,000 cells with random Tn10d-Cam insertions throughout the chromosome. A P22 lysate grown on this pool and standard genetic approaches identified Tn10d-Cam insertions linked to the causative suppressor mutation. The site of insertion was determined by sequence analyses using degenerate primers and those specific to the Tn10d-Cam (22). DNA sequence was obtained at the University of Wisconsin Biotechnology Center.

Phenotypic analysis. Nutritional requirements were determined on solid media and in liquid growth media as described below.

(i) *Liquid growth.* Strains to be analyzed were grown in LB broth overnight. Cultures were pelleted and resuspended in an equal volume of glucose minimal medium supplemented with BCAA. Cultures were then returned to 37 °C for a period of 2-3 hours in order to deplete metabolite pools until growth of the appropriate strains abated. Following metabolite depletion, 2 µl of the cell suspension was added to 198 µl of the desired medium contained in each well of a 96-well microtitre plate. Cultures were grown at 37 °C while shaking using the Biotek EL808 ultra microplate reader. Cell density was measured as the absorbance at 650 nm. The specific growth rate was determined as $[\mu = \ln(X/X_0)/T]$, in which X is the optical density during the linear growth phase and T is time.

(ii) *Solid media.* Nutritional requirements were determined using soft agar overlays containing cells of the relevant strain. Compounds were spotted on the overlay and growth was scored after 24-48 h at 37 °C.

Quantification of Coenzyme A pool size. Overnight cultures of the strains to be analyzed were grown in LB broth. Cultures were pelleted and resuspended in saline solution. Culture flasks containing 200 ml of glucose minimal medium supplemented with 0.2 % CAA were inoculated to a starting OD₆₅₀ of 0.02. Growth was carried out at 37 °C while shaking until a final OD₆₅₀ of 0.6 was achieved. Cells were pelleted and stored at -80 °C until ready for analysis. CoA levels were determined by the method of Allred and Guy (23).

Molecular methods. The *stm4195* gene was amplified by PCR with Herculase II Fusion DNA polymerase (Agilent) using primers *stm4195_NcoI_F* (5'-GAGACCATGGCCATGCTCGCCGTCATTACC-3') and *stm4195_XbaI_R* (5'-GAGATCTAGATTAATTTACCTTTGCCGTTT-

3'). The resulting PCR product was gel purified, digested with *NcoI* (Promega) and *XbaI* (Promega) and ligated into *NcoI/XbaI*-cut pBAD24 (24). Constructs were transformed into *Escherichia coli* strain DH5 α and screened for vectors containing inserts. Plasmid inserts were confirmed by sequencing. Plasmids containing the appropriate insert (designated pDM1397) were purified and transformed into the relevant strains.

Bioinformatic analysis. The *S. enterica* LT2 genome sequence (25) was used to analyze the chromosomal region immediately 5' of the *stm4195* translation start site. Promoter predictions were made using BPROM (Soft Berry). Protein sequence alignments were performed using Clustal Omega (EBI) and formatted using BoxShade (SIB). Chromosomal gene cluster analysis was performed using the SEED subsystem based approach as previously described (26).

Formation and characterization of a transported, biologically active CoA derivative. Coenzyme A (Sigma) was dissolved in water to a final concentration of 100 mM. Aliquots were heated at 98 °C for 0-5 h using an Eppendorf Mastercycler nexus. Individual samples from each time-point were pooled and filtered using a 0.22 μ m centrifuge tube filter (Costar) prior to testing for biological activity as described in the text. Dephospo CoA was formed by incubating a 100 mM stock of CoA (100 μ l) with 2 Units of rAPid alkaline phosphatase (Roche) at 37 °C for 2 hours. The resulting sample was resolved by HPLC.

Biologically active samples were analyzed via HPLC using an anion exchange column (250 x 4.6 mm) packed with Partisil-10 SAX resin (Phenomenex). The column was equipped with a NH₂ SecurityGuard cartridge (Phenomenex). The analysis method was adapted from Jackowski and Rock (27). A linear gradient of monobasic potassium phosphate running from 0.05 M to 0.9 M was introduced to the column over the course of 60 minutes at a flow rate of 1 ml/min. β -mercaptoethanol was included in the mobile phase at a final concentration of 1 mM. Mobile-phase

delivery was carried out using the Shimadzu Prominence LC-20AT pump system and peak absorbance from 200-400 nm was followed by a Shimadzu SPD-M20A diode array detector. Elution fractions were collected using the FRC-10A fraction collector (Shimadzu). When necessary, fractions were concentrated by evaporation using the Eppendorf Vacufuge. Concentrated samples with biological activity were further resolved and salts were removed by injection onto a Gemini C18 reverse-phase column (Phenomenex). Hexafluoro-2-propanol (HFIP; Sigma), used as an ion pairing reagent, was dissolved in water to a final concentration of 800 mM and adjusted to a final pH of 7 with triethylamine. The HFIP solution was divided and mixed 1:1 with either water or 100 % methanol, forming mobile phase A and B, respectively. The flow rate was adjusted to 0.5 ml/minute and samples were eluted during a 10 minute isocratic step of 95 % mobile phase A and 5 % mobile phase B, followed by a 20 minute gradient to 100 % mobile phase B. Isolated fractions were again concentrated and tested for biological activity. Samples with biological activity had maximal absorbance at 259 nm. Biologically active fractions were then dried, resuspended in 50 % methanol/water and submitted for mass-spectrometry analysis at the University of Georgia Proteomic and Mass Spectrometry core facility.

B. 4 RESULTS AND DISCUSSION

A *panE ilvC* strain requires branched-chain amino acids (BCAA) and pantothenate for growth on glucose minimal medium (Figure B.2). Mutations that allowed strain DM6486 (*panE ilvC*) to grow in the absence of exogenous pantothenate, potentially by altering metabolic flux, were sought on minimal medium supplemented with BCAA. The desired mutants were not found, despite looking for both spontaneous and diethyl sulfate induced mutations. It was considered formally possible that mutations that restored pantoate synthesis could be deleterious to the

function of another pathway and thus generate a new growth requirement. To account for this possibility, the growth medium was supplemented with vitamin-free casamino acids (CAA). The parental strain showed the expected requirement for pantothenate or pantoate on this medium, which confirmed that pantothenate was not present in the CAA solution to levels sufficient to allow growth.

Eleven independent, spontaneously arising, derivatives of DM6486 (*panE ilvC*) were isolated on glucose minimal medium supplemented with 1 % CAA. Growth of the eleven isolates was quantified in liquid medium and each grew when pantothenate or CAA was added to the medium. The data in Figure B.2 show the growth of a representative revertant strain, DM13708. Growth of each of the revertant strains was less than wild-type, both in rate and final density, and proportional to the concentration of CAA added (data not shown). Growth of these strains was not supported by the simultaneous addition all 20 common amino acids, suggesting a minor component of the CAA was responsible for growth of the revertant strains. While the revertant strains had detectable total CoA levels, concentrations were less than 50 % of the amount found in a *panE* strain, indicating that CoA synthesis was only partially restored (Table B.2).

Transposition events lead to pantothenate-independent growth of the *panE ilvC* strain. Standard genetic techniques identified a modified transposon (*zxx10185::Tn10d-Cam*) that was linked by transduction to the causative lesion in all eleven strains. Sequence analysis identified the causative lesions in each revertant strain in a region on the chromosome depicted in Figure B.3A. Ten of the eleven strains contained an insertion of IS10-right (IS10-R), the active element in transposon *Tn10*, 28 base pairs upstream of the predicted translation start site of *stm4195* (*stm4195pl*; Figure B.3B). The reading frame of the transposase gene encoded by IS10-R was oriented in the opposite direction relative to *stm4195* and shared 100 % identity with the *E. coli*

IS10-R, encoding a functional transposase flanked by inverted repeats (28, 29). The IS10-R is presumed to have originated from the non-defective Tn10 insertion present in *ilvC* of the parent strain (DM6486). The frequency with which this class of suppressor mutations was isolated suggested that the sequence upstream of *stm4195* contained a hot-spot for DNA insertion (30). Sequence analysis of the chromosome-IS10-R junction sites revealed a 9-bp duplication of chromosomal DNA flanking the IS10-R element (Figure B.3B). The 9-bp sequence showed symmetry similar to previously characterized insertion hot-spots (31, 32). Previous studies have demonstrated that the presence of a functional transposase in the genome can increase the activation of “silent” genes 5-25-fold (33). IS10-R possesses a strong promoter that reads out of the transposase coding region (pOUT) and potentiates the activation of adjacent genes (Figure B.3B) (34).

The remaining mutation was a single C-to-T transition 76 base pairs upstream of the *stm4195* translation start site (*stm4195p3*; Figure B.3B). The promoter prediction tool BPROM (SoftBerry) indicated the base substitution was in the -10 region of the promoter of *stm4195*. The substitution resulted in a sigma 70 recognition site closer to the -10 consensus sequence (35). Based on the sequence data, the saturation of the mutant hunt and the precedent in the literature (33, 36), we hypothesized that increased expression of *stm4195* was the mechanism of suppression.

Increased expression of *stm4195* allows growth of pantothenate auxotrophs with casamino acids. A construct encoding *stm4195* transcribed by the arabinose-inducible pBAD promoter (pDM1397) was introduced into strain DM6486 (*panE ilvC*). Growth of the resulting strain (DM13947) in the absence of pantothenate, but presence of CAA (0.2 %), was restored only when *stm4195* expression was induced (Figure B.4). These data confirmed that increased expression of *stm4195* mimicked the effect of the mutations described above. Further, expression

of *stm4195* from pDM1397 restored growth to a *panC* strain (DM13950) in the presence of CAA (Figure B.4). These data allowed the conclusion that expression of *stm4195* in the presence of CAA overcame the need for pantothenate synthesis.

Stm4195 is annotated as a Na⁺-dependent transporter (25). Protein domain analysis of Stm4195 identified a single conserved domain (COG0385) belonging to the sodium bile acid symporter superfamily (SBF; cl19217), which includes transmembrane proteins involved in bile acid transport and resistance to arsenic compounds (37). The Stm4195 homolog from *Neisseria meningitidis* (ASBT_{NM}), which is 41 % identical and 59 % similar to the protein in *S. enterica*, has been characterized biochemically as a sodium-dependent bile acid symporter (38). Protein alignments showed that several residues essential for interacting with Na⁺ ions and a bile acid substrate in ASBT_{NM} were conserved in Stm4195 (Figure B.5) (38). The transmembrane prediction tool, TMHMM (Center for Biological Sequence Analysis), predicted Stm4195 consists of 9 transmembrane helices. Taken together, the data were consistent with an impurity in the CAA being transported by Stm4195 to restore growth to a pantothenate auxotroph.

Commercially available intermediates of the CoA biosynthetic pathway were used to explore the substrate specificity of the predicted transporter. Pantoate and ketopantoate were provided in a range of concentrations to *panE ilvC* and *panB* strains, respectively, that carried an inducible *stm4195* construct (pDM1397) or the vector only control (pEmpty). The chromosomal *stm4195* gene was inactivated (*stm4195::Kn*) to clarify interpretation of the results. Relevant data are presented in Figure B.6. A *panE ilvC stm4195* strain grew on glucose minimal medium in the presence of 0.1-100 μM pantoate only when *stm4195* was expressed *in trans* (Figure B.6A). The *panE ilvC stm4195* strains containing either pDM1397 or pEmpty had the same growth characteristics in the presence of pantothenate (100 μM). Concentrations of pantoate equal to or

exceeding 1 mM resulted in growth of a *panE ilvC stm4195* strain containing the empty vector control, while concentrations of pantoate below 0.1 μ M did not allow growth of a *panE ilvC stm4195* strain despite *stm4195* expression *in trans* (data not shown). Ketopantoate (1-100 μ M) provided to a *panB stm4195* strain rescued growth only when *stm4195* was expressed *in trans* (Figure B.6B). Exogenous ketopantoate greater than or equal to 1 mM rescued growth independent of *stm4195* expression (data not shown). The minimal concentration of pantothenate required for growth of a pantothenate auxotroph (DM14206) was not altered by *stm4195* expression. Disruption of the *panF* gene in a *panE ilvC stm4195* background (DM14575) prevented growth in the presence of exogenous pantothenate (100 μ M; data not shown). However, the introduction of pDM1397 (DM14577) completely restored growth in the presence of 100 μ M pantothenate, and allowed limited growth with 10 μ M pantothenate. In contrast, the strain carrying the empty vector control (DM14576) failed to grow in either case (data not shown). Together these data indicated that Stm4195 functioned in the transport of pantoate, ketopantoate and pantothenate. Notably, 10 μ M pantothenate failed to support growth in DM14577 to the level allowed by 10 μ M pantoate or ketopantoate in DM14206 or DM14273, respectively. These results indicated that Stm4195 had a higher affinity for pantoate and ketopantoate than pantothenate. The ability of high concentrations (\geq 1 mM) of pantoate or ketopantoate to suppress the need for Stm4195 production in a *panE ilvC stm4195* or *panB stm4195* background, respectively, indicated that at least one alternative, less-sensitive mechanism of pantoate and ketopantoate uptake exists in *S. enterica*. Exogenous pantotheine (reduced) or pantethine (oxidized) rescued growth of a *panE ilvC* strain completely lacking *stm4195*, indicating Stm4195 was not required for the transport of these metabolites (data not shown).

The experiments with known intermediates of pantothenate biosynthesis above failed to recapitulate the phenotype seen with CAA as the source of CoA. Specifically, the relevant metabolite in CAA supported growth of a *panC* strain only when *stm4195* was expressed *in trans* despite the status of *panF*. Since Stm4195 had protein features in common with bile acid symporters, the impact of bile salts on *stm4195*-dependent growth of a pantothenate auxotroph was tested. The addition of bile salts (0-0.5 % w/v) to the growth medium failed to rescue growth of a *panE ilvC stm4195* mutant expressing *stm4195 in trans*, indicating that a component of bile salts was not used in CoA biosynthesis (data not shown). The presence of bile salts in the growth medium (0-0.5 % w/v) did not significantly alter growth of DM14206 when supplied CAA (data not shown), suggesting Stm4195 had a higher affinity for the relevant metabolite in CAA than bile salts.

A derivative of CoA is transported by Stm4195. Though considered unlikely, it was formally possible that Stm4195 was facilitating the transport of CoA itself. When crystals of pure CoA were spotted on a soft agar overlay containing DM13708 (*panE ilvC stm4195p1*), a small but noticeable zone of growth was visible after 18 h incubation at 37 °C. The concentration of CoA required to see a growth response was inconsistent with the technical analysis of the vitamin-assay grade CAA composition and suggested the growth was due to a breakdown product or contaminating precursor of CoA. A 100 mM solution of CoA was heated at 98 °C and aliquots were taken over time and spotted on arabinose-containing soft agar overlays of DM14206 (*panE ilvC stm4195 pDM1397*) and DM14207 (*panE ilvC stm4195 pEmpty*). The data in Figure B.7 showed that the factor promoting *stm4195*-dependent growth of DM14206 increased over time, and had little to no effect on growth of the empty vector control. Similar results were obtained with *panC* strains with and without expression of *stm4195*. These data supported the hypothesis

that heating CoA accelerated its breakdown or transformation, thus enriching for a substrate of Stm4195 that feeds into the CoA biosynthetic pathway downstream of pantothenate. Incubation of CoA with acid, base, alkaline phosphatase or dithiothreitol failed to generate a factor active in growth assays. HPLC analysis of alkaline phosphatase-treated CoA revealed chromatogram peaks not observed in the untreated CoA sample that were consistent with the formation of dephospho-CoA, suggesting dephospho-CoA was not a substrate for Stm4195. Interestingly, heating acetyl-CoA (100 mM) failed to generate a biologically active compound that stimulated growth of DM14206 (data not shown). These data suggested either the acetyl moiety of acetyl-CoA prevented the requisite breakdown/transformation or the acetyl group altered the structure of the resulting compound such that it was not recognized for transport by Stm4195.

The biologically active compound derived from heating CoA was enriched by HPLC passage over an anion exchange column. During HPLC fractionation, absorbance was monitored from 200-400 nm and fractions were collected over a 30 min mobile phase gradient. Representative chromatographs of untreated CoA and heat-treated CoA displaying the absorbance at 259 nm are shown in Figure B.8A and B.8B, respectively. Eluted fractions were assessed for biological activity by spotting 5 μ l of filtered aliquots on agar overlays of DM14206 in the presence of arabinose. Only the fractions collected between 5-7 minutes displayed biological activity. The sample collected from 5-7 minutes was further subjected to reverse-phase HPLC and revealed three peaks with maximal absorbance at 259 nm (Figure B.8C). Of these peaks, the fraction with a retention time of 10.5 minutes had biological activity. MS/MS analyses both in the positive and negative ion mode failed to definitively identify the active compound and a genetic approach was taken to pursue the physiological role of the relevant compound.

S. enterica strains lacking *dfp* (*coaBC*) are viable if provided with exogenous pantetheine. Once inside the cell, pantetheine can be phosphorylated to enter the CoA biosynthetic pathway (Figure B.1). Growth data in Figure B.9 showed that the *stm4195*-dependent growth allowed by heated CoA required *dfp*. The expression of *stm4195* supported growth of a *panC* strain supplied with heated CoA (1 mM; Figure B.9A), whereas *stm4195* expression failed to support growth of the *dfp* strain grown under the same conditions (Figure B.9B). These results supported the conclusion that a biologically active compound was transported by Stm4195 and entered the CoA pathway between PanC and CoaBC. Pantothenate kinase (encoded by *coaA*) is an essential enzyme and represents the only enzymatic step between PanC and CoaBC. The temperature sensitive allele, *coaA1*(Ts) (11), was used to probe the role of this enzyme in salvaging the CoA breakdown compound. Strains carrying the *coaA1* allele grow at 30 °C, but not at 42 °C (11). Heat-treated CoA (~1.5 mM) failed to support growth of DM14525 (*coaA1 stm4195* pDM1397) at 42 °C (data not shown). However, as an essential gene, there is no positive control for growth at 42 °C, which prevented solid conclusions from these data (Figure B.1). In total, the data herein supported the conclusion that Stm4195 catalyzed the transport of a CoA-derived product that enters the CoA biosynthetic pathway after PanC, but upstream of CoaBC.

Conclusions. The Stm4195 protein from *Salmonella enterica* is annotated as a Na⁺-dependent transporter with a single conserved domain (COG0385) that places it in the sodium bile acid symporter superfamily (SBF). Physiological work described here showed that Stm4195 is unlikely to transport bile salts, and rather transports precursors to CoA. Genetic analyses showed that Stm4195 transports pantoate, ketopantoate with high affinity, pantothenate with low affinity and a CoA-derived product of unknown structure. Figure B.10 summarizes what is known about the CoA derivative and the Stm4195 protein from this study. The demonstration that a CoA

derivative can be salvaged to satisfy the cellular requirement for this coenzyme suggests this compound (or related compounds) may exist in the environment and Stm4195 is present to scavenge it. Further study is required to determine if CoA salvage is the primary function of Stm4195 or rather a consequence of enzymatic promiscuity. Nonetheless, it seems appropriate to rename Stm4195 as PanS (pantothenate salvage) given the demonstrated impact of this protein on pantothenate and CoA metabolism in *Salmonella*.

Sodium bile acid superfamily (SBF) proteins are found across domains of life and the work here augments our understanding of this family and provides an activity that is likely to be important in organisms besides *S. enterica*. Additional members of the SBF superfamily include the solute carrier family 10 (SLC10) transporters found in eukaryotes. Approximately 320 distinct human transporters belong to one of 43 SLC families (39). SLC10 comprises the sodium bile acid cotransporter family, however not all members of the SLC10 family are involved in bile acid transport (39). Stm4195 is >20 % identical to SLC10A1 and SLC10A2 from *Homo sapiens*. Until now, the study of SBF family proteins, including SLC10 family members, has focused largely on the contribution these transporters make to the metabolism of bile acids and structurally related steroidal compounds, including cholesterol. Several SBF family proteins have been viewed as promising drug targets for cholesterol-lowering treatment (40). Our work highlights the need to consider alternative solutes that may serve as substrates for these transporters in various contexts.

The *stm4195* mRNA transcript has been described as a direct target of negative regulation by the Hfq-dependent small RNA, GcvB (41). The GcvB regulon consists largely of amino acid transporters, and to our knowledge, Stm4195 represents the first vitamin-salvaging transporter to be identified in this regulon. As part of the GcvB regulon, Stm4195 production is coordinated with the nutrient state of the cell, ensuring Stm4195 production is greatest when nutrients are scarce.

Further study to address the *in situ* relevance of Stm4195, and homologs found in other potentially pathogenic bacteria, is warranted based on interest in developing antimicrobial drugs that specifically target CoA biosynthesis in these organisms (2). If organisms possess a salvage mechanism which bypasses several steps of the *de novo* CoA pathway, accounting for the bypassed steps may pinpoint enzyme targets that are optimal for drug development. In contrast to the artificial production of CoA-derived products described here, it is possible that organisms growing in complex microbial communities are exposed to related CoA-degradation products as a result of bacterial cell lysis, host environment, and/or the activity of extracellular phosphatases/hydrolases acting on CoA directly to yield substrates for Stm4195 and related transporters. The complete range of substrates recognized by Stm4195 remains to be determined. Studies such as the one herein provide evidence that addressing metabolic robustness with *in vivo* tools can lead to new knowledge of mechanisms used in metabolic integration. This work provides fertile ground for continued efforts to understand mechanisms of metabolic integration that could influence drug targeting, synthetic biology, antibiotic development and more.

ACKNOWLEDGEMENTS

This work was supported by USPHS grant R01 GM047296 from the N.I.H. to D.M.D. Mass spectrometry was done by the University of Georgia Proteomic and Mass Spectrometry core facility.

B.5 REFERENCES

1. Leonardi R, Zhang YM, Rock CO, Jackowski S. 2005. Coenzyme A: back in action. *Prog Lipid Res* 44:125–153.
2. Spry C, Kirk K, Saliba KJ. 2008. Coenzyme A biosynthesis: an antimicrobial drug target. *FEMS Microbiol Rev* 32:56–106.
3. Webb ME, Smith AG, Abell C. 2004. Biosynthesis of pantothenate. *Nat Prod Rep* 21:695–721.
4. Primerano DA, Burns RO. 1983. Role of acetohydroxy acid isomeroreductase in biosynthesis of pantothenic acid in *Salmonella typhimurium*. *J Bacteriol* 153:259–269.
5. Vallari DS, Rock CO. 1985. Isolation and characterization of *Escherichia coli* pantothenate permease (panF) mutants. *J Bacteriol* 164:136–142.
6. Jackowski S, Rock C. 1981. Regulation of coenzyme A biosynthesis. *J Bacteriol* 148:926–932.
7. Schneider F, Kramer R, Burkovski A. 2004. Identification and characterization of the main B-alanine uptake system in *Escherichia coli*. *Appl Microbiol Biotechnol* 65:576–582.
8. Balibar CJ, Hollis-Symynkywicz MF, Tao J. 2011. Pantethine rescues phosphopantothenoylcysteine synthetase and phosphopantothenoylcysteine decarboxylase deficiency in *Escherichia coli* but not in *Pseudomonas aeruginosa*. *J Bacteriol* 193:3304–3312.
9. Vallari D, Jackowski S, Rock C. 1987. Regulation of pantothenate kinase by coenzyme A and its thioesters. *J Biol Chem* 262:2468–2471.
10. Koenigsknecht MJ, Downs DM. 2010. Thiamine biosynthesis can be used to dissect metabolic integration. *Trends Microbiol* 18:240–247.
11. Frodyma M, Rubio A, Downs D. 2000. Reduced flux through the purine biosynthetic pathway results in an increased requirement for coenzyme A in thiamine synthesis in *Salmonella enterica* serovar Typhimurium. *J Bacteriol* 182:236–240.
12. Way JC, Davis MA, Morisato D, Roberts DE, Kleckner N. 1984. New Tn10 derivatives for transposon mutagenesis and for construction of *lacZ* operon fusions by transposition. *Gene* 32:369–379.

13. Kleckner N, Chan RK, Tye B-K, Botstein D. 1975. Mutagenesis by insertion of a drug-resistance element carrying an inverted repetition. *J Mol Biol* 97:561–575.
14. Castilho BA, Olfson P, Casadaban MJ. 1984. Plasmid insertion mutagenesis and *lac* gene fusion with mini-mu bacteriophage transposons. *J Bacteriol* 158:488–495.
15. Elliot T, Roth JR. 1988. Characterization of Tn10d-Cam: A transposition-defective Tn10 specifying chloramphenicol resistance. *Mol Gen Genet MGG* 213:332–338.
16. Vogel HJ, Bonner DM. 1956. Acetylornithinase of *Escherichia coli*: partial purification and some properties. *J Biol Chem* 218:97–106.
17. Balch WE, Wolfe RS. 1976. New approach to the cultivation of methanogenic bacteria: 2-mercaptoethanesulfonic acid (HS-CoM)-dependent growth of *Methanobacterium ruminantium* in a pressurized atmosphere. *Appl Environ Microbiol* 32:781–791.
18. Schmieger H. 1972. Phage P22-mutants with increased or decreased transduction abilities. *Mol Gen Genet MGG* 119:75–88.
19. Chan RK, Botstein D, Watanabe T, Ogata Y. 1972. Specialized transduction of tetracycline resistance by phage P22 in *Salmonella typhimurium*. II. Properties of a high-frequency-transducing lysate. *Virology* 50:883–898.
20. Downs DM, Petersen L. 1994. *apbA*, a new genetic locus involved in thiamine biosynthesis in *Salmonella typhimurium*. *J Bacteriol* 176:4858–4864.
21. Datsenko KA, Wanner BL. 2000. One-step inactivation of chromosomal genes in *Escherichia coli* K-12 using PCR products. *Proc Natl Acad Sci* 97:6640–6645.
22. Sun S, Berg OG, Roth JR, Andersson DI. 2009. Contribution of gene amplification to evolution of increased antibiotic resistance in *Salmonella typhimurium*. *Genetics* 182:1183–1195.
23. Allred JB, Guy DG. 1969. Determination of coenzyme A and acetyl CoA in tissue extract. *Anal Biochem* 29:293–299.
24. Guzman LM, Belin D, Carson MJ, Beckwith J. 1995. Tight regulation, modulation, and high-level expression by vectors containing the arabinose pBAD promoter. *J Bacteriol* 177:4121–4130.
25. McClelland M, Sanderson KE, Spieth J, Clifton SW, Latreille P, Courtney L, Porwollik S, Ali J, Dante M, Du F, Hou S, Layman D, Leonard S, Nguyen C, Scott K, Holmes A, Grewal N, Mulvaney E, Ryan E, Sun H, Florea L, Miller W, Stoneking T, Nhan M,

- Waterston R, Wilson RK. 2001. Complete genome sequence of *Salmonella enterica* serovar Typhimurium LT2. *Nature* 413:852–856.
26. Overbeek R, Begley T, Butler RM, Choudhuri JV, Chuang H-Y, Cohoon M, Crecy-Lagard V de, Diaz N, Disz T, Edwards R, Fonstein M, Frank ED, Gerdes S, Glass EM, Goesmann A, Hanson A, Iwata-Reuyl D, Jensen R, Jamshidi N, Krause L, Kubal M, Larsen N, Linke B, McHardy AC, Meyer F, Neuweger H, Olsen G, Olson R, Osterman A, Portnoy V, Pusch GD, Rodionov DA, Ruckert C, Steiner J, Stevens R, Thiele I, Vassieva O, Ye Y, Zagnitko O, Vonstein V. 2005. The subsystems approach to genome annotation and its use in the project to annotate 1000 genomes. *Nucleic Acids Res* 33:5691–5702.
 27. Jackowski S, Rock CO. 1984. Metabolism of 4'-phosphopantetheine in *Escherichia coli*. *J Bacteriol* 158:115–120.
 28. Foster TJ, Davis MA, Roberts DE, Takeshita K, Kleckner N. 1981. Genetic organization of transposon Tn10. *Cell* 23:201–213.
 29. Halling SM, Simons RW, Way JC, Walsh RB, Kleckner N. 1982. DNA sequence organization of IS10-right of Tn10 and comparison with IS10-left. *Proc Natl Acad Sci* 79:2608–2612.
 30. Ross DG, Swan J, Kleckner N. 1979. Nearly precise excision: a new type of DNA alteration associated with the translocatable element Tn10. *Cell* 16:733–738.
 31. Halling SM, Kleckner N. 1982. A symmetrical six-base-pair target site sequence determines Tn10 insertion specificity. *Cell* 28:155–163.
 32. Lee SY, Butler D, Kleckner N. 1987. Efficient Tn10 transposition into a DNA insertion hot spot in vivo requires the 5-methyl groups of symmetrically disposed thymines within the hot-spot consensus sequence. *Proc Natl Acad Sci* 84:7876–7880.
 33. Wang A, Roth JR. 1988. Activation of silent genes by transposons Tn5 and Tn10. *Genetics* 120:875–885.
 34. Simons RW, Hoopes BC, McClure WR, Kleckner N. 1983. Three promoters near the termini of IS10: pIN, pOUT, and pIII. *Cell* 34:673–682.
 35. Hook-Barnard I, Johnson XB, Hinton DM. 2006. *Escherichia coli* RNA polymerase recognition of a 70-dependent promoter requiring a -35 DNA element and an extended -10 TGn motif. *J Bacteriol* 188:8352–8359.
 36. Graña D, Youderian P, Susskind MM. 1985. Mutations that improve the ant promoter of *Salmonella* phage P22. *Genetics* 110:1–16.

37. Marchler-Bauer A, Zheng C, Chitsaz F, Derbyshire MK, Geer LY, Geer RC, Gonzales NR, Gwadz M, Hurwitz DI, Lanczycki CJ, Lu F, Lu S, Marchler GH, Song JS, Thanki N, Yamashita RA, Zhang D, Bryant SH. 2013. CDD: conserved domains and protein three-dimensional structure. *Nucleic Acids Res* 41:D348–D352.
38. Hu N-J, Iwata S, Cameron AD, Drew D. 2011. Crystal structure of a bacterial homologue of the bile acid sodium symporter ASBT. *Nature* 478:408–411.
39. Geyer J, Wilke T, Petzinger E. 2006. The solute carrier family SLC10: more than a family of bile acid transporters regarding function and phylogenetic relationships. *Naunyn Schmiedebergs Arch Pharmacol* 372:413–431.
40. Geyer J, Doring B, Meerkamp K, Ugele B, Bakhiya N, Fernandes CF, Godoy JR, Glatt H, Petzinger E. 2007. Cloning and functional characterization of human sodium-dependent organic anion transporter (SLC10A6). *J Biol Chem* 282:19728–19741.
41. Sharma CM, Papenfort K, Pernitzsch SR, Mollenkopf H-J, Hinton JCD, Vogel J. 2011. Pervasive post-transcriptional control of genes involved in amino acid metabolism by the Hfq-dependent GcvB small RNA: GcvB regulon. *Mol Microbiol* 81:1144–1165.

TABLE B.1. Bacterial strains

Strain ^a	Genotype ^b
LT2	Wild type
DM3547	<i>panC617::Tn10d(Tc)</i>
DM6486	<i>panE675::MudJ ilvC2104::Tn10</i>
DM13708	<i>panE675::MudJ ilvC2104::Tn10 stm4195p1</i>
DM13710	<i>panE675::MudJ ilvC2104::Tn10 stm4195p3</i>
DM13950	<i>panC617::Tn10d(Tc) / pDM1397</i>
DM13951	<i>panC617::Tn10d(Tc) / pEmpty</i>
DM13947	<i>panE675::MudJ ilvC2104::Tn10 / pDM1397</i>
DM13948	<i>panE675::MudJ ilvC2104::Tn10 / pEmpty</i>
DM14101	<i>panE675::MudJ ilvC2104::Tn10 zxx10185::Tn10d-Cam stm4195p1</i>
DM14206	Δ <i>panE802</i> Δ <i>ilvC3218</i> <i>stm4195-2::Kn / pDM1397</i>
DM14207	Δ <i>panE802</i> Δ <i>ilvC3218</i> <i>stm4195-2::Kn / pEmpty</i>
DM14273	<i>panB611::Tn10d(Tc) stm4195-2::Kn / pDM1397</i>
DM14274	<i>panB611::Tn10d(Tc) stm4195-2::Kn / pEmpty</i>
DM14459	<i>dfp2::Kn / pDM1397</i>
DM14460	<i>dfp2::Kn / pEmpty</i>
DM14525	<i>zxx8038::Tn10d(Tc) coaA1 stm4195-2::Kn / pDM1397</i>
DM14526	<i>zxx8038::Tn10d(Tc) coaA1 stm4195-2::Kn / pEmpty</i>
DM14575	Δ <i>panE802</i> Δ <i>ilvC3218</i> <i>stm4195-2::Kn panF803::Cam</i>
DM14576	Δ <i>panE802</i> Δ <i>ilvC3218</i> <i>stm4195-2::Kn panF803::Cam / pEmpty</i>
DM14577	Δ <i>panE802</i> Δ <i>ilvC3218</i> <i>stm4195-2::Kn panF803::Cam / pDM1397</i>

^aAll strains are derivatives of *Salmonella enterica* subsp. *enterica* serovar Typhimurium LT2.

^b*Tn10* denotes a full-length *Tn10* with a functional transposase (13). *Tn10d(Tc)* indicates a transposition-defective mini-*Tn10* (12). *MudJ* refers to the *MudJ1734* mobile genetic element (14).

TABLE B.2. The *stm4195p1* allele allows a low level of CoA synthesis

Strain	Relevant genotype	CoA level ^a (nmol/mg, dry weight)	Ratio of CoA levels (wt/mutant)	Growth rate ^b (h ⁻¹)
LT2	Wild type	0.464 ± 0.051		0.508 ± 0.005
DM6486	<i>panE ilvC</i>	NG ^c		NG ^c
DM12653	<i>panE</i>	0.034 ± 0.005	13.5	0.498 ± 0.004
DM13708	<i>panE ilvC stm4195p1</i>	0.013 ± 0.006	35.4	0.255 ± 0.002

^aCoA levels (nanomoles per milligram of dry cell weight) were determined from cultures grown at 37 °C in culture flasks containing minimal medium with glucose (11 mM) as the sole carbon source and supplemented with vitamin-free casamino acids (0.2 % w/v). The data are displayed as the average and standard deviation of three independent cultures.

^bGrowth curves were performed in a 96-well plate. Minimal growth medium contained glucose (11 mM) supplemented with casamino acids (0.2 % w/v). The specific growth rate was determined as $\mu = \ln(X/X_0)/T$. The data are displayed as the average and standard deviation of three independent cultures.

^cStrain was unable to grow under the conditions tested.

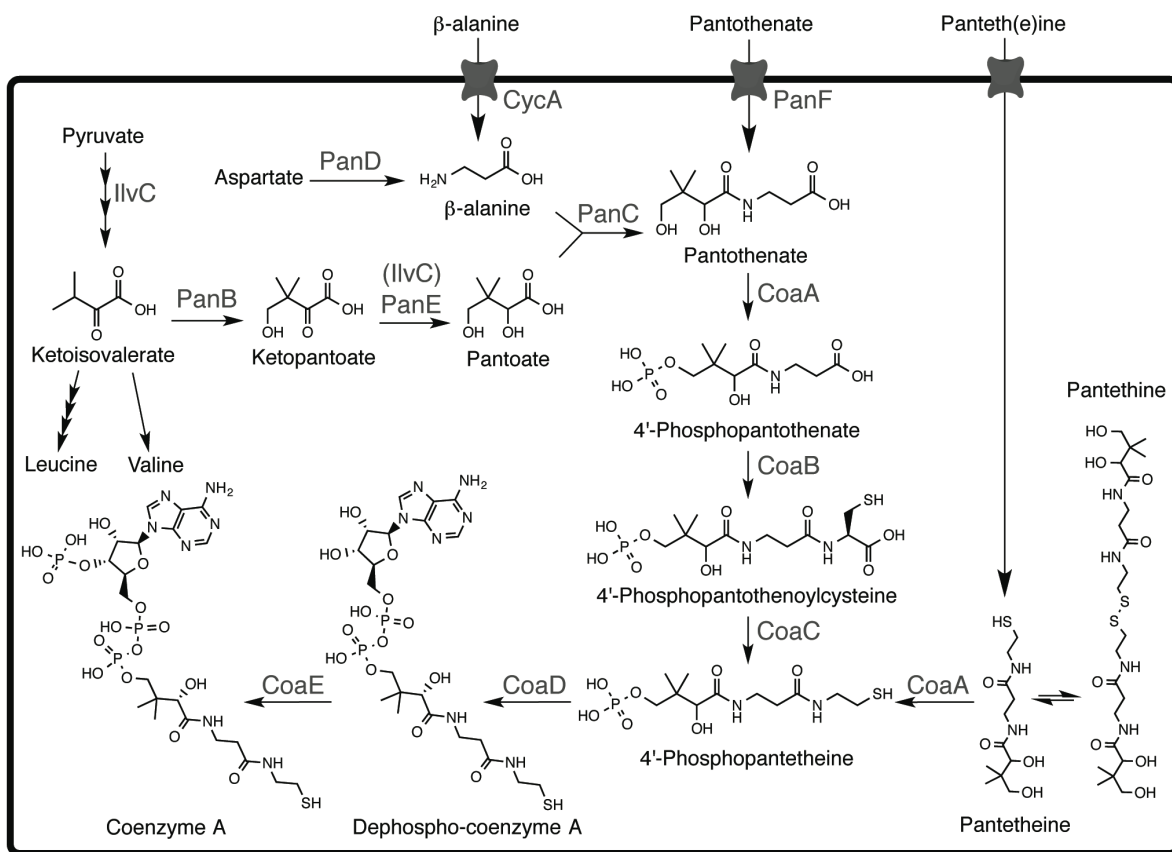


FIGURE B.1. Pantothenate and Coenzyme A biosynthesis in *Salmonella enterica*. Known biosynthetic enzymes, salvage enzymes and metabolic intermediates involved in CoA biosynthesis and salvage are depicted.

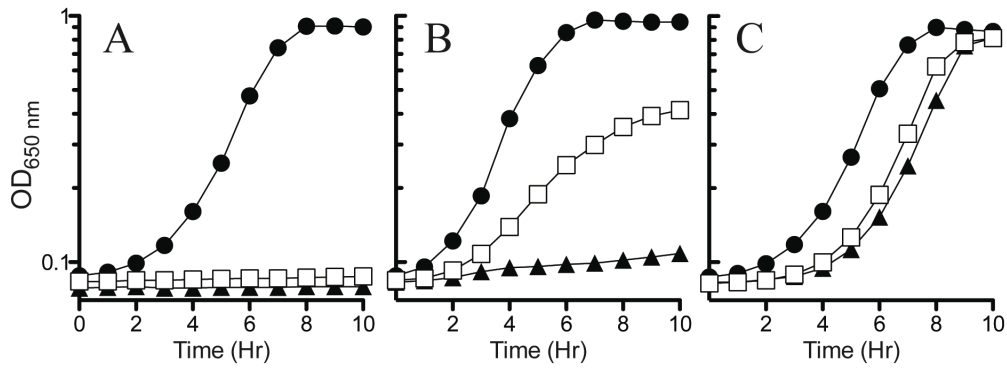


FIGURE B.2. The *stm4195p1* allele restores growth to a *panE ilvC* strain. Cultures were grown in glucose minimal medium containing BCAA with: (A) no additional supplements; (B) vitamin-free casamino acids (0.2 %); or (C) pantothenate (100 μ M). Strains shown in each panel are wild type LT2 (circles), *panE ilvC* (DM6486; triangles), and *panE ilvC stm4195p1* (DM13708; open squares). The data displayed are representative of three independent cultures.

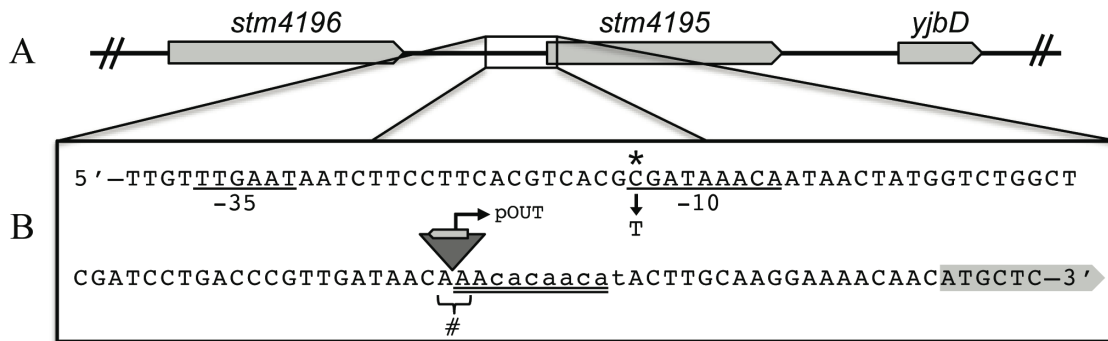


FIGURE B.3. Mutations in the chromosome upstream of *stm4195* restored growth to a *panE ilvC* strain when grown in the presence of CAA. A) The open reading frame organization in the relevant genomic region is depicted. B) The sequence upstream of the *Stm4195* coding region has been expanded. The predicted -10/-35 promoter regions are underlined. Lowercase letters depict the regulatory binding site for the small RNA repressor, GcvB (41). Allele *stm4195p1* contains an IS10-R insertion, indicated by the inverted triangle, inserted 24 bps upstream of the *stm4195* start codon (hash symbol (#)). The coding sequence of the transposase gene encoded by IS10-R is indicated, as is the promoter reading out of the IS10-R coding region (pOUT). The double-underlined region indicates the 9 bp insertion-site recognition sequence that is found duplicated at both ends of the IS10-R insertion (31). The position of allele *stm4195p3* (C to T) is denoted with an asterisk (*) and is in the predicted -10 region, 76 bp upstream of the *stm4195* start codon.

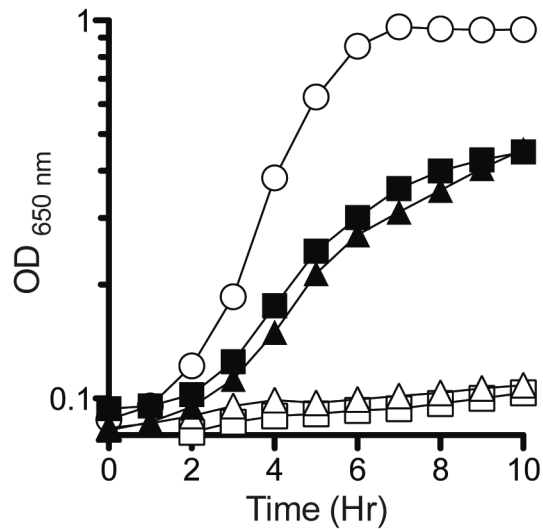


FIGURE B.4. Expression of *stm4195 in trans* suppresses growth defect in the presence of casamino acids. *panE ilvC* (squares) strains containing pDM1397 (DM13947; filled) or the vector only control (DM13948; empty) and *panC* (triangles) strains containing pDM1397 (DM13950; filled) or vector only control (DM13951; empty) were grown in minimal medium containing casamino acids (0.2 % w/v) and arabinose (1 %). Growth was compared relative to wild type (circles). The data displayed are representative of three independent cultures.

```

ASBT_NM      1  MNILSKISSF I G K T F S L W A A L F A A A F F A P D T F K W A G P Y I P W L L G I I M F G
STM4195     1  M-----LAV I T R L F P L W A L L L S L T A Y Y T P S T F T P V G P W V A T L L M I M F G

ASBT_NM     51  M G L T L K P S D F D I L F K H P K V V I I G V I A Q F A I M P A T A W L L S K L L N L P A E I A V
STM4195     45  M G V H L N V D D E K R V L S R P A P V A A G I F L H Y L V M P L A A W L L A L L F K M P P D L S A

ASBT_NM     101  G V I L V G C C P G G T A S N V M T Y L A R G N V A L S V A V T S V S T L I S P L L T P A I F L M L
STM4195     95  G M V L V G S V A S G T A S N V M I Y L A K G D V A L S V T I S S V S T L V G V A T P L L T R L Y

ASBT_NM     151  A G E M L E I Q A A G M L M S I V K M V L L P I V L G L I V H K V L G S K T E K L T D A L P L V S V
STM4195     145  V D A H I Q V D V M G M L L S I L Q I V V I P I T L G L V I H H L F P R V V K V V K P Y L P A F S M

ASBT_NM     201  A A I V L I I G A V V G A S K G K I M E S G L L I F A V V V L H N G I G Y L L G F F A A K W T G L P
STM4195     195  V C I L A I I S A V V A G S A S H I A S V G F M V I I A V I L H N T L G L L G G Y W G G R L F G F D

ASBT_NM     251  Y D A Q K T L T I E V G M Q N S G L A A A L A A A H F A A A P V V A V P G A L F S V W H N I S G S L
STM4195     245  E S T C R T L A I E V G M Q N S G L A A A L G K I Y F -- G P L A A L P G A L F S V W H N I S G S L

ASBT_NM     301  L A T Y W A A K A G K H K K P G S E N L Y F Q
STM4195     293  L A G Y W S G K P I V E K S G E T A K V -- N

```

FIGURE B.5. Alignment of Stm4195 from *Salmonella enterica* and a homolog from *Neisseria meningitidis* (ASBT_{NM}; NMB0705). Asterisks (*) indicate residues from ASBT_{NM} that coordinate sodium with their side chains (38). Hash symbols (#) indicate residues from ASBT_{NM} important for binding taurocholate (38). Identical residues and similar residues are highlighted black and gray, respectively.

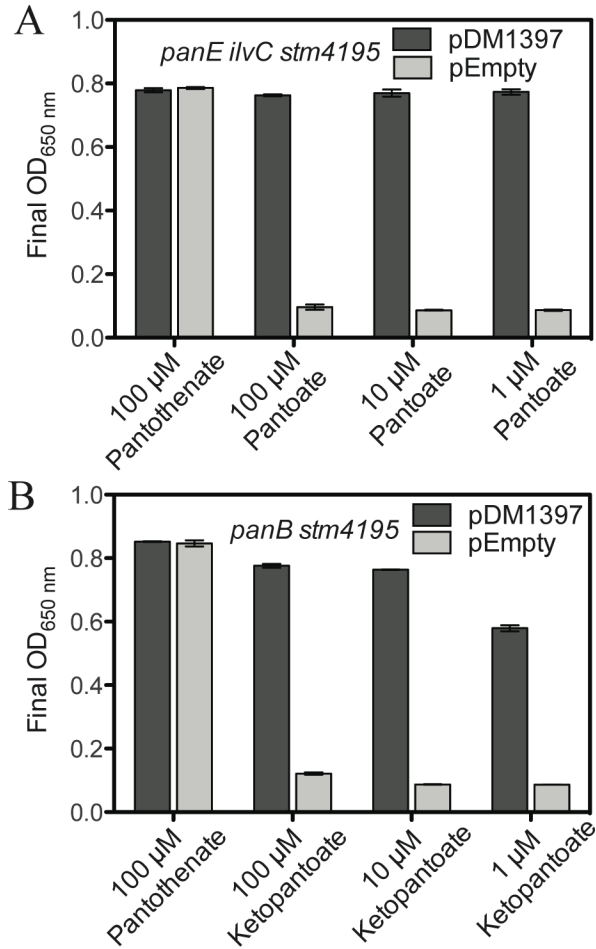


FIGURE B.6. Expression of *stm4195* facilitates ketopantoate and pantoate uptake. A) Supplements were added at the indicated concentrations to *panE ilvC stm4195* strains containing pDM1397 (DM14206) or the empty vector control (DM14207) grown in glucose minimal medium containing BCAA and 1 % arabinose. B) *panB stm4195* strains carrying pDM1397 (DM14273) or the empty vector control (DM14274) were examined as described for A. The data from three independent cultures are represented as the average and standard deviation of the OD_{650 nm} at 12 hours (all cultures reached stationary phase at ~12 hours).

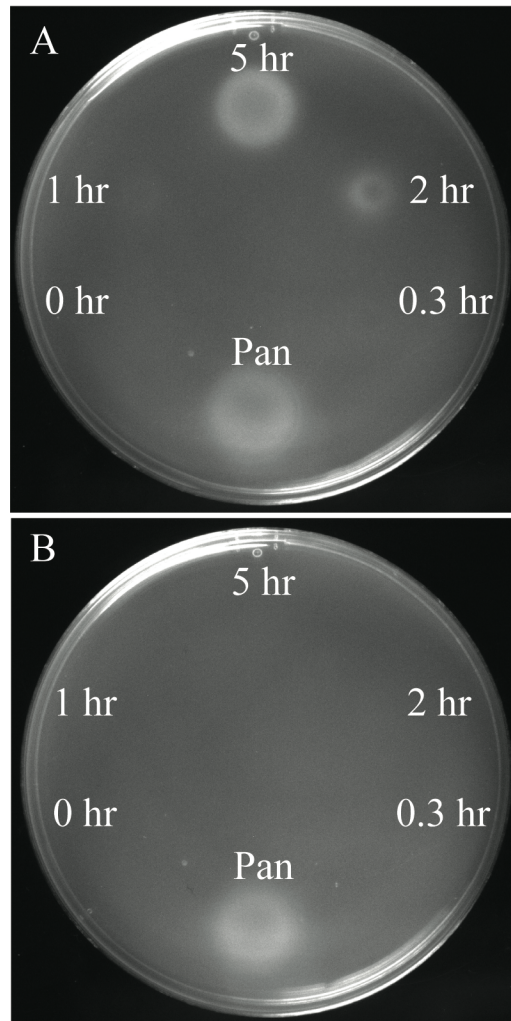


FIGURE B.7. Heated CoA produces substrates of *Stm4195*. A 100mM solution of CoA dissolved in water was heated at 98 °C and 5 μ l aliquots were taken at the indicated time points and spotted on soft-agar overlays of **A)** *panE ilvC stm4195* pDM1397 (DM14206) and **B)** *panE ilvC stm4195* pEmpty (DM14207) strains grown on glucose minimal medium containing BCAA and 1 % arabinose. Five microliters of pantothenate (Pan; 100 μ M) was added as a positive control. Pictures were taken after 48 hours of growth at 37 °C.

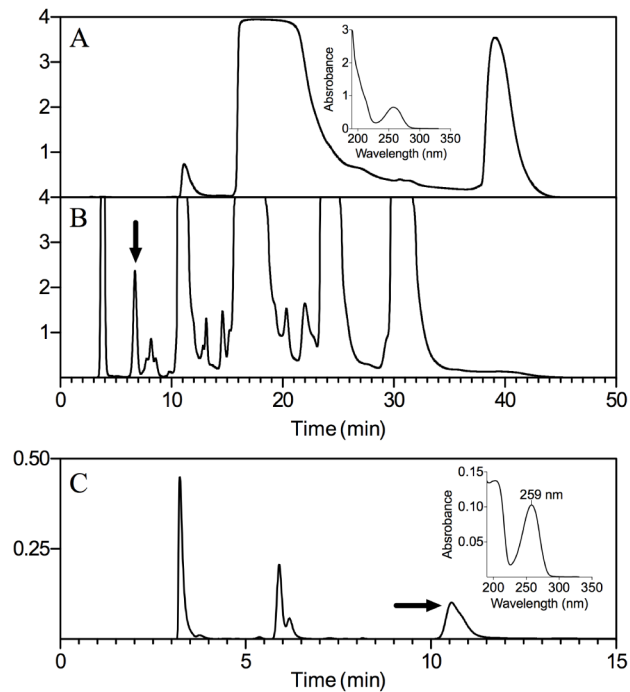


FIGURE B.8. HPLC separation of CoA breakdown products. A) 100 μ l of 100 mM untreated CoA was separated using an anion-exchange column while monitoring absorbance at 259 nm. The inset displays the absorption spectrum of pure coenzyme A (eluted at ~15 minutes). B) 100 μ l of 100 mM heat-treated CoA (98 $^{\circ}$ C for 5 hours) was separated using an anion-exchange column while monitoring absorbance at 259 nm. Peak-fractions were collected and tested for biological activity. The arrow indicates the only peak that displayed biological activity in *stm4195*-dependent growth assays. C) The biologically-active fraction collected in B was further resolved by reverse-phase chromatography while monitoring absorbance at 259 nm. The arrow indicates the peak that displayed *stm4195*-dependent biological activity. The inset displays the absorption spectrum of the relevant peak from C, with maximal absorbance at 259 nm.

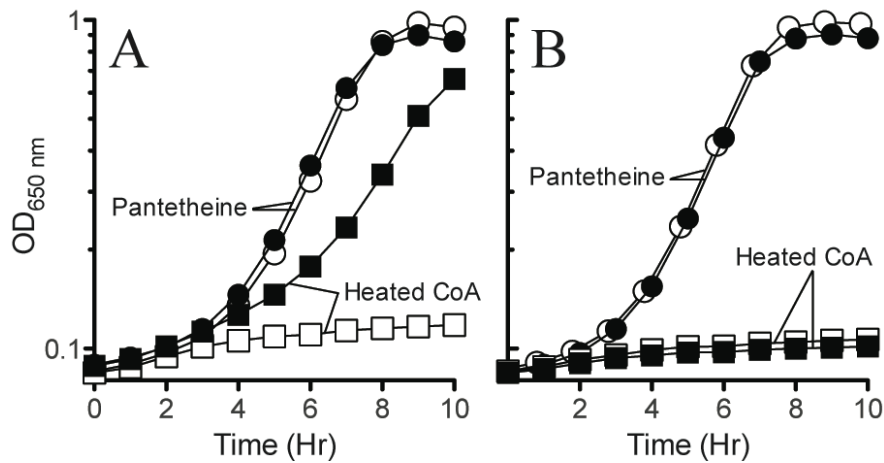


FIGURE B.9. *stm4195*-dependent growth requires CoaBC (*dfp*). *stm4195*-dependent growth of *panC* and *dfp* strains was tested on glucose minimal medium containing BCAA, 1 % arabinose and 1.25 mM boiled CoA (squares) or 100 μ M pantetheine (circles). A) Growth of *panC* strains carrying pDM1397 (DM13950; filled symbols) or pEmpty (DM13951; open symbols). B) Growth of *dfp* strains carrying pDM1397 (DM14459; filled symbols) or pEmpty (DM14460; open symbols). The growth data are representative of three independent cultures.

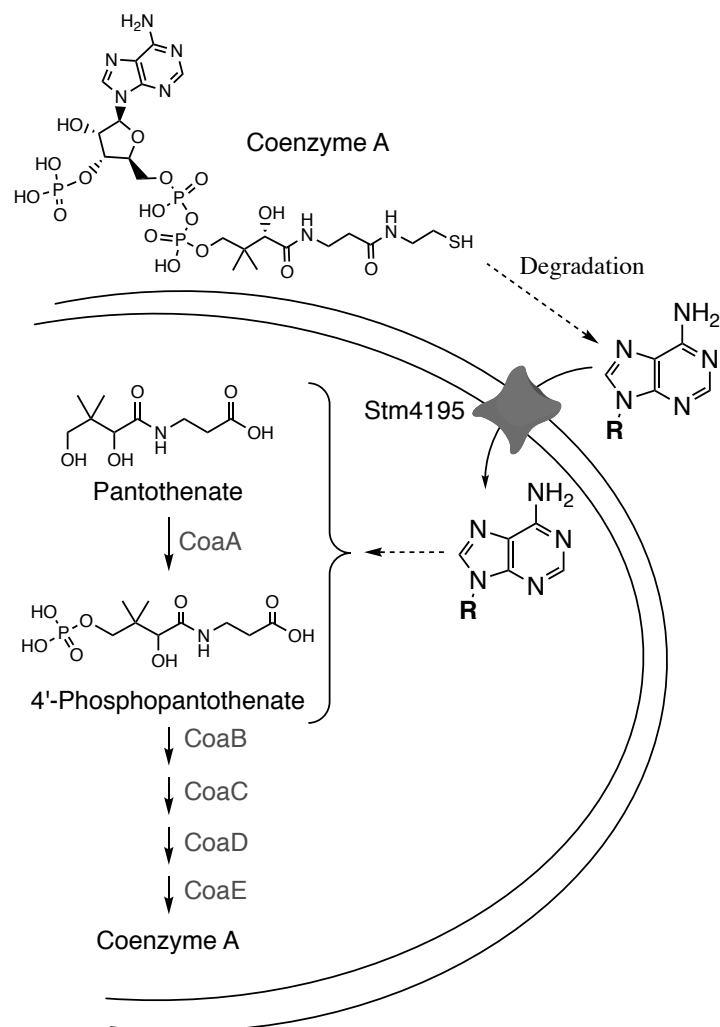


FIGURE B.10. Model of Stm4195-mediated salvage of CoA derived product(s). Stm4195 facilitates the uptake of a substrate derived from CoA that has spectral properties indicative of an intact adenine moiety. Spontaneous or enzymatic cleavage is required to release a compound that feeds into the pathway upstream of CoaBC.

APPENDIX C

PERTURBATION OF THE METABOLIC NETWORK IN *SALMONELLA ENTERICA* REVEALS CROSS-TALK BETWEEN COENZYME A AND THIAMINE PATHWAYS

C.1 BACKGROUND

There is a growing appreciation for the impact perturbations in a given pathway can have on seemingly unrelated metabolic pathways in the cell (1, 2). Subtle connections between seemingly unrelated pathways can be enhanced through mutant analysis in order to better understand the underlying metabolic cross-talk. For example, constraining any essential metabolic pathway requires that a cell overcome the disruption or risk cell death. The mechanisms used by a cell to overcome perturbations in the metabolic network reveals inherent robustness in the system and often uncovers connections between biochemical processes and pathways previously considered distinct. The analyses of cellular responses to perturbations in the metabolic network was successful in uncovering emergent mechanisms of thiamine biosynthesis in *Salmonella enterica* (3). Thiamine biosynthesis is similar to coenzyme A (CoA) biosynthesis in that both result in the production of an essential nutrient, and the flux of carbon and energy required for both products is low when compared to other essential molecules (3). It has been previously shown that disrupting the primary ketopantoate reductase found in *Salmonella enterica*, PanE, results in an approximately ten-fold reduction in total CoA levels (4). Importantly, the redundant ketopantoate reductase activity of the branched-chain amino acid biosynthetic enzyme, acetohydroxyacid

isomoreductase (IlvC), produces sufficient pantoate to support CoA biosynthesis (5). Thus, a *panE* mutant maintains ~ 10 % of wild type CoA levels due to IlvC ketopantoate reductase activity.

Previous work identified a link between intracellular CoA levels and thiamine biosynthesis (Figure C.1). Thiamine pyrophosphate is an essential cofactor, and is made of two independently synthesized moieties, 4-methyl-5-(2-hydroxyethyl)-thiazole phosphate (THZ-P) and 4-amino-5-(hydroxymethyl)-2-methylpyrimidine phosphate (HMP-P). Mutations in *panE* reduce CoA levels in the cell and cause a conditional HMP-P auxotrophy in *S. enterica* (6, 7). Disruption of *panE* only results in an HMP-P auxotrophy when flux through the shared purine/HMP-P biosynthetic pathway is compromised by eliminating or inhibiting the first shared pathway enzyme, PurF (4, 6, 7). Purines repress expression of *purF* and allosterically inhibit the PurF enzyme (8–10). The effect of CoA levels on thiamine production was narrowed down to the conversion of AIR to HMP-P *in vivo* (11), which is catalyzed by the HMP-P synthase ThiC (12, 13). ThiC is a member of the radical *S*-adenosylmethionine (SAM) superfamily of enzymes that use a [4Fe-4S] cluster to initiate radical catalysis (12, 13). CoA and acetyl-CoA do not exhibit any demonstrable effect on ThiC activity *in vitro* (14). Thus, an unknown connection exists between CoA and ThiC *in vivo*. To better understand this link, a genetic approach was taken to observe mutations that could restore growth to a purine-sensitive *panE* strain. To exacerbate the growth defect, wild-type *thiC* was replaced with previously described alleles (*thiC**) encoding variants with altered ThiC activity (15). In this compromised background, suppressors were isolated that restored growth to the *thiC* panE* mutant on minimal glucose medium. Perhaps unsurprisingly, suppressors were isolated that contained mutations in the *ilvC* transcriptional regulator, *ilvY*. The mutations isolated in *ilvY* are expected to increase *ilvC* transcription, leading

to greater ketopantoate reductase activity, increased CoA levels and improved thiamine production.

C.2 MATERIALS AND METHODS

Bacterial strains, media and chemicals. All strains used in this study are derivatives of *Salmonella enterica* serovar Typhimurim LT2 and are listed with their genotype in Table C.1. *Tn10d*(Tc) refers to the transposition defective mini-*Tn10* (*Tn10*Δ16 Δ17) described by Way et al. (16). *MudJ* refers to the *Mud1734* transposon described previously (17). *Tn10d*-Cm refers to the transposition defective *Tn10* specifying chloramphenicol resistance (18).

No-carbon E medium (NCE) supplemented with 1mM MgSO₄ (19), trace minerals (20) and glucose (11mM) as the sole carbon source was used as minimal medium. Difco nutrient broth (NB) (8g/liter) with NaCl (5g/liter) and Luria-Bertani broth (LB) were used as rich media. Difco BiTek agar (15g/L) was added for solid medium. When necessary the branched-chain amino acids leucine, isoleucine and valine (plus ketoisovalerate) were added at a final concentration of 0.3 mM. Antibiotics were added as needed to reach the following concentrations in rich and minimal medium, respectively: tetracycline 20 and 10 ug/ml; ampicillin 30 and 15 ug/ml; and chloramphenicol 20 and 5 ug/ml. Arabinose (0.1 %) was added to cultures when necessary for induction of the *araBAD* promoter.

Genetic methods. All transductional crosses were performed using the high-frequency general transducing mutant of bacteriophage P22 (HT105/1, *int*-201) (21). Methods for performing transductional crosses, purification of transductants from phage and the identification of phage-free recombinants have been described previously (6, 22). All mutant strains were constructed

using standard genetic techniques. Gene replacements were made using the λ -Red recombinase system described by Datsenko and Wanner (23).

Mutant isolation. Five cultures each of DM13651 (*zxx-8029::Tn10d(Tc) thiC1128 panE::Cm*) and DM13652 (*zxx-8029::Tn10d(Tc) thiC1129 panE::Cm*) were grown overnight in NB medium. Cells were pelleted and resuspended in an equal volume of saline solution (85mM). Approximately 10^8 cells from each cell suspension were spread onto solid minimal glucose medium. DES (5 μ l) was spotted in the middle of plates containing DM13652. Plated cultures were incubated at 37° C for a period of ~72 hours. The resulting mutant colonies were streaked out on non-selective medium. Phenotypes were confirmed by patching mutant isolates to non-selective rich medium, which were then replica-printed to selective plates after a period of 6-12 h at 37 °C. A representative mutant strain displaying robust growth on minimal glucose medium, DM13897 (*zxx-8029::Tn10d(Tc) thiC1129 panE::Cm ilvY3213*), was selected for mapping. First, the chloramphenicol marker was resolved FRT-site recombination by transforming the strain with pCP20 (23). The plasmid was cured and the phenotype was reconfirmed. The chloramphenicol-sensitive strain (DM13963) used to generate a pool of ~60,000 cells with random *Tn10d*-Cam insertions throughout the chromosome. A P22 lysate grown on this pool and standard genetic approaches identified *Tn10d*-Cam insertions linked to the causative suppressor mutation. The site of insertion was determined by sequence analyses using degenerate primers and those specific to the *Tn10d*-Cam (24). DNA sequence was obtained at the University of Wisconsin Biotechnology Center. Transductional crosses confirmed that the *Tn10d*-Cam linked to the originally mapped suppressor was linked to the other suppressors described here.

Phenotypic analysis. Nutritional requirements were determined in liquid growth. Strains to be analyzed were grown in NB broth overnight. Cultures were pelleted and resuspended in an

equal volume of saline. Aliquots (5 μ l) of the cell suspension were used to inoculate 200 μ l of the desired medium contained in each well of a 96-well microtitre plate. Cultures were grown at 37 °C while shaking at 250 rpm using the Biotek EL808 ultra microplate reader. Cell density was measured as the absorbance at 650 nm. The specific growth rate was determined as $[\mu = \ln(X/X_0)/T]$, in which X_0 is the initial optical density during the linear, X is the final optical density during the linear growth phase and T is time.

Molecular methods. The *ilvY* gene was amplified by PCR with Herculase II Fusion DNA polymerase (Agilent) using primers STM4195_NcoI_F (5'-GAGACCATGGCCATGCTCGCCGTCATTACC-3') and STM4195_XbaI_R (5'-GAGATCTAGATTAATTTACC TTTGCCGTTT-3'). The resulting PCR product was gel purified, digested with *NcoI* (Promega) and *XbaI* (Promega) and ligated into *NcoI/XbaI*-cut pBAD24 (25). Constructs were transformed into *Escherichia coli* strain DH5 α and screened for vectors containing inserts. Plasmid inserts were confirmed by sequencing. Plasmids containing the appropriate insert were purified and transformed into the relevant strains.

C.3 RESULTS AND DISCUSSION

ThiC variants cause a pantothenate or thiamine auxotrophy in a Δ *panE* background.

A previous report described “adenine sensitive” ThiC variants (ThiC^{E281K} and ThiC^{V267M}) based on their inability to support thiamine-independent growth when adenine was added to the growth medium (15). Preliminary work described growth properties of these strains (26); the ThiC variant strains were assessed for their ability to support thiamine-independent growth. In strains containing ThiC variants and a lesion in *panE*, either pantothenate or thiamine were required to support growth (Table C.2). This finding is consistent with previous findings demonstrating subtle effects

of CoA on ThiC activity; ThiC must be compromised in other ways (i.e. less-active ThiC variants) to exacerbate the CoA-dependent thiamine phenotype. Taken together, the combination of ThiC^{E218K} or ThiC^{V267M} with a lesion in *panE* generated strains unable to grow on minimal glucose medium. These strains were used to isolate suppressors to explore unforeseen connections between CoA levels and flux through ThiC.

Suppressors of *panE* ThiC-variant strains have mutations in *ilvY*. Multiple suppressors were isolated and triaged according to redundant growth phenotypes. Growth of a representative suppressor (DM13897) was compared to the respective thiamine-deficient parent strain (DM13652) in minimal glucose medium (Figure C.2). The parent strain was unable to grow without thiamine or pantothenate, while the suppressor grew on minimal glucose medium alone. Thus, the suppressor restored thiamine biosynthesis either directly or indirectly. The suppressor mutation from DM13897 was mapped and identified as a point mutation in *ilvY*, changing basepair 703 from a C-to-A, corresponding to amino acid change L235M (Figure C.3). Suppressors linked to the same region of the chromosome in other isolates also contained mutations in *ilvY*. DM13892 had a G-to-T mutation at basepair 272, corresponding to amino acid change G92V and DM13896 a G-to-A transition at basepair 710, corresponding to amino acid change C237V. IlvY is a positive regulator of *ilvC*; *ilvY* is expressed divergently from *ilvC* and the *ilvYC* locus represents a prototypic LysR-type regulated system (27). IlvY binds to the *ilvC* operator but requires the binding of IlvC substrates (either α -acetolactate or α -acetohydroxybutyrate), acting as coinducers, to activate transcription of *ilvC* (28). The residue changes in the observed IlvY variants either fall within or just upstream of the predicted effector binding domain. In *E. coli*, amino acid substitutions in the effector binding domain led to constitutive expression of *ilvC* (29). Therefore, the IlvY variants described here are predicted to activate constitutive *ilvC* expression.

Overexpression of *ilvC* or an *ilvY* suppressor allele, but not wild-type *ilvY*, restores growth to the *panE* ThiC-variant strain. A representative *ilvY* allele (*ilvY3213*) was cloned into pBAD24 to test if the mutation in *ilvY* correlated with overexpression of *ilvC*. The expression of *ilvC* from a pBAD plasmid restored growth to a thiamine-limited *panE thiC1129* strain (DM13994) on minimal glucose medium (Figure C.4). Similarly, expression of plasmid borne *ilvY3213* restored growth to strain DM13996 on minimal glucose medium (Figure C.4). Importantly, plasmid borne expression of wild-type *ilvY* failed to restore growth. Taken together, these data indicate that *ilvY3213* is dominant, as expression of *ilvY3213* in an *ilvY*⁺ background restored growth to the thiamine-deficient parent strain. Furthermore, the similar phenotype achieved by expressing *ilvC* or *ilvY3213* *in trans* is consistent with *ilvY3213* serving to constitutively activate *ilvC* expression. Moving forward, reporter assay experiments will be performed by fusing the *ilvC* promoter to *lacZ* and assessing the impact on the described IlvY variants on *ilvC* promoter output. Finally, total intracellular CoA levels will be assessed in each of the parent strain and suppressor strain backgrounds to determine if the reported *ilvY* alleles restore thiamine biosynthesis by increasing CoA levels. Given current data, we propose the model depicted in figure C.5, where mutations in the *ilvY* effector binding domain produce constitutively-active variants capable of inducing expression of *ilvC*, even in the absence of coinducer molecules. The constitutive expression of *ilvC* is expected to increase IlvC-dependent ketopantoate reductase activity, leading to improved CoA biosynthesis in the *panE* strain background.

C.4 ACKNOWLEDGMENTS

Lauren Palmer isolated and characterized ThiC variants and performed growth analyses reported in Table C.2. All subsequent work was performed by Dustin Ernst.

C.4 REFERENCES

1. Downs DM. 2006. Understanding microbial metabolism. *Annu Rev Microbiol* 60:533–559.
2. Kim J, Copley SD. 2012. Inhibitory cross-talk upon introduction of a new metabolic pathway into an existing metabolic network. *Proc Natl Acad Sci* 109:E2856–E2864.
3. Koenigsnecht MJ, Downs DM. 2010. Thiamine biosynthesis can be used to dissect metabolic integration. *Trends Microbiol* 18:240–247.
4. Frodyma M, Rubio A, Downs D. 2000. Reduced flux through the purine biosynthetic pathway results in an increased requirement for coenzyme A in thiamine synthesis in *Salmonella enterica* serovar Typhimurium. *J Bacteriol* 182:236–240.
5. Primerano DA, Burns RO. 1983. Role of acetohydroxy acid isomeroreductase in biosynthesis of pantothenic acid in *Salmonella typhimurium*. *J Bacteriol* 153:259–269.
6. Downs DM, Petersen L. 1994. *apbA*, a new genetic locus involved in thiamine biosynthesis in *Salmonella typhimurium*. *J Bacteriol* 176:4858–4864.
7. Frodyma ME, Downs D. 1998. The *panE* gene, encoding ketopantoate reductase, maps at 10 minutes and is allelic to *apbA* in *Salmonella typhimurium*. *J Bacteriol* 180:4757–4759.
8. Rolfes RJ, Zalkin H. 1988. Regulation of *Escherichia coli purF*. Mutations that define the promoter, operator, and purine repressor gene. *J Biol Chem* 263:19649–19652.
9. Rolfes RJ, Zalkin H. 1988. *Escherichia coli* gene *purR* encoding a repressor protein for purine nucleotide synthesis. Cloning, nucleotide sequence, and interaction with the *purF* operator. *J Biol Chem* 263:19653–19661.
10. Zhou G, Smith JL, Zalkin H. 1994. Binding of purine nucleotides to two regulatory sites results in synergistic feedback inhibition of glutamine 5-phosphoribosylpyrophosphate amidotransferase. *J Biol Chem* 269:6784–6789.

11. Allen S, Zilles JL, Downs DM. 2002. Metabolic flux in both the purine mononucleotide and histidine biosynthetic pathways can influence synthesis of the hydroxymethyl pyrimidine moiety of thiamine in *Salmonella enterica*. *J Bacteriol* 184:6130–6137.
12. Martinez-Gomez NC, Downs DM. 2008. ThiC is an [Fe-S] cluster protein that requires AdoMet to generate the 4-amino-5-hydroxymethyl-2-methylpyrimidine moiety in thiamin synthesis. *Biochemistry (Mosc)* 47:9054–9056.
13. Chatterjee A, Li Y, Zhang Y, Grove TL, Lee M, Krebs C, Booker SJ, Begley TP, Ealick SE. 2008. Reconstitution of ThiC in thiamine pyrimidine biosynthesis expands the radical SAM superfamily. *Nat Chem Biol* 4:758–765.
14. Palmer LD, Downs DM. 2013. The thiamine biosynthetic enzyme ThiC catalyzes multiple turnovers and is inhibited by S-adenosylmethionine (AdoMet) metabolites. *J Biol Chem* 288:30693–30699.
15. Palmer LD, Dougherty MJ, Downs DM. 2012. Analysis of ThiC variants in the context of the metabolic network of *Salmonella enterica*. *J Bacteriol* 194:6088–6095.
16. Way JC, Davis MA, Morisato D, Roberts DE, Kleckner N. 1984. New Tn10 derivatives for transposon mutagenesis and for construction of *lacZ* operon fusions by transposition. *Gene* 32:369–379.
17. Castilho BA, Olfson P, Casadaban MJ. 1984. Plasmid insertion mutagenesis and *lac* gene fusion with mini-mu bacteriophage transposons. *J Bacteriol* 158:488–495.
18. Elliot T, Roth JR. 1988. Characterization of Tn10d-Cam: A transposition-defective Tn10 specifying chloramphenicol resistance. *Mol Gen Genet MGG* 213:332–338.
19. Vogel HJ, Bonner DM. 1956. Acetylornithinase of *Escherichia coli*: partial purification and some properties. *J Biol Chem* 218:97–106.
20. Balch WE, Wolfe RS. 1976. New approach to the cultivation of methanogenic bacteria: 2-mercaptoethanesulfonic acid (HS-CoM)-dependent growth of *Methanobacterium ruminantium* in a pressurized atmosphere. *Appl Environ Microbiol* 32:781–791.
21. Schmieger H. 1972. Phage P22-mutants with increased or decreased transduction abilities. *Mol Gen Genet MGG* 119:75–88.
22. Chan RK, Botstein D, Watanabe T, Ogata Y. 1972. Specialized transduction of tetracycline resistance by phage P22 in *Salmonella typhimurium*. II. Properties of a high-frequency-transducing lysate. *Virology* 50:883–898.

23. Datsenko KA, Wanner BL. 2000. One-step inactivation of chromosomal genes in *Escherichia coli* K-12 using PCR products. *Proc Natl Acad Sci* 97:6640–6645.
24. Sun S, Berg OG, Roth JR, Andersson DI. 2009. Contribution of gene amplification to evolution of increased antibiotic resistance in *Salmonella typhimurium*. *Genetics* 182:1183–1195.
25. Guzman LM, Belin D, Carson MJ, Beckwith J. 1995. Tight regulation, modulation, and high-level expression by vectors containing the arabinose pBAD promoter. *J Bacteriol* 177:4121–4130.
26. Palmer LD. 2014. Characterization of thiamine biosynthetic enzymes and their integration in the metabolic network of *Salmonella enterica*. Ph.D., University of Georgia.
27. Rhee KY, Opel M, Ito E, Hung S, Arfin SM, Hatfield GW. 1999. Transcriptional coupling between the divergent promoters of a prototypic LysR-type regulatory system, the *ilvYC* operon of *Escherichia coli*. *Proc Natl Acad Sci* 96:14294–14299.
28. Wek RC, Hatfield G. 1988. Transcriptional activation at adjacent operators in the divergent-overlapping *ilvY* and *ilvC* promoters of *Escherichia coli*. *J Mol Biol* 203:643–663.
29. Biel AJ, Umbarger HE. 1981. Mutations in the *ilvY* gene of *Escherichia coli* K-12 that cause constitutive expression of *ilvC*. *J Bacteriol* 146:718–724.

TABLE C.1. Bacterial strains

Strain	Genotype
LT2	Wild type
DM13650	<i>zxx-8029::Tn10d(Tc) panE::Cm</i>
DM13651	<i>zxx-8029::Tn10d(Tc) thiC1128 panE::Cm</i>
DM13652	<i>zxx-8029::Tn10d(Tc) thiC1129 panE::Cm</i>
DM13892	<i>zxx-8029::Tn10d(Tc) thiC1128 panE::Cm ilvY3215</i>
DM13896	<i>zxx-8029::Tn10d(Tc) thiC1129 panE::Cm ilvY3214</i>
DM13897	<i>zxx-8029::Tn10d(Tc) thiC1129 panE::Cm ilvY3213</i>
DM13931	<i>zxx-8029::Tn10d(Tc) thiC1129 ΔpanE</i>
DM13956	<i>zxx-8029::Tn10d(Tc) thiC1129 ΔpanE zxx-3911::Tn10(Cm)</i>
DM13957	<i>zxx-8029::Tn10d(Tc) thiC1129 ΔpanE zxx-3911::Tn10(Cm) ilvY3213</i>
DM13963	<i>zxx-8029::Tn10d(Tc) thiC1129 ΔpanE ilvY3213</i>
DM13993	<i>zxx-8029::Tn10d(Tc) thiC1129 ΔpanE / pBAD24</i>
DM13994	<i>zxx-8029::Tn10d(Tc) thiC1129 ΔpanE / pBAD24-ilvC</i>
DM13995	<i>zxx-8029::Tn10d(Tc) thiC1129 ΔpanE / pBAD24-ilvY</i>
DM13996	<i>zxx-8029::Tn10d(Tc) thiC1129 ΔpanE / pBAD24-ilvY3213</i>

TABLE C.2. Growth of *panE* strains containing “adenine-sensitive” ThiC variants.^a

Strain	ThiC variant	Specific Growth Rate			Final Cell Yield		
		Min	+ Pant	+ Thi	Min	+ Pant	+ Thi
DM13650	ThiC ^{WT}	0.41	0.67	0.50	0.75	0.84	0.71
DM13651	ThiC ^{E281K}	0.03	0.67	0.50	0.15	0.89	0.75
DM13652	ThiC ^{V267M}	0.01	0.70	0.54	0.14	0.88	0.77

^a Strains were grown in NCE medium supplemented with glucose (11 mM) and the indicated additions. Min, minimal medium; Pant, pantothenate; Thi, thiamine. Growth rate is reported as $\mu = \ln(X/X_0)/T$, and the final cell yield is A_{650} after 12 h of growth. Data shown are the average of three independent cultures. All standard deviations were less than 0.03.

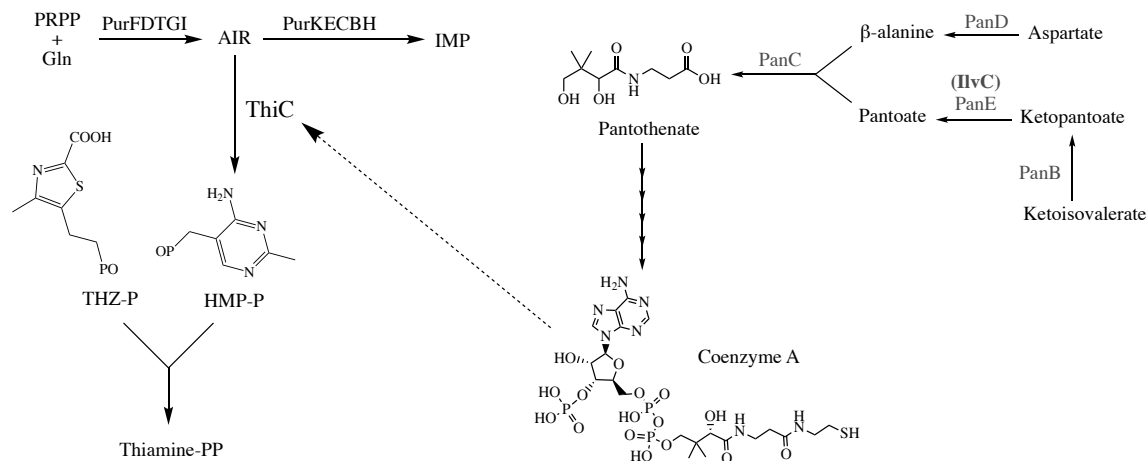


FIGURE C.1. Connection between ThiC-dependent thiamine production and coenzyme A.

(Left) The thiamine pathway branches off of the purine biosynthetic pathway at the branch-point metabolite aminoimidazole ribotide (AIR). ThiC catalyzes synthesis of HMP-P from AIR, which is subsequently condensed with THZ-P to form thiamine-pyrophosphate. (Right) Coenzyme A is synthesized from pantothenate in five steps. The production of the pantoate is predominantly catalyzed by PanE. The branched-chain amino acid biosynthetic enzyme acetohydroxyacid isomoreductase (IlvC) has ketopantoate reductase activity as well.

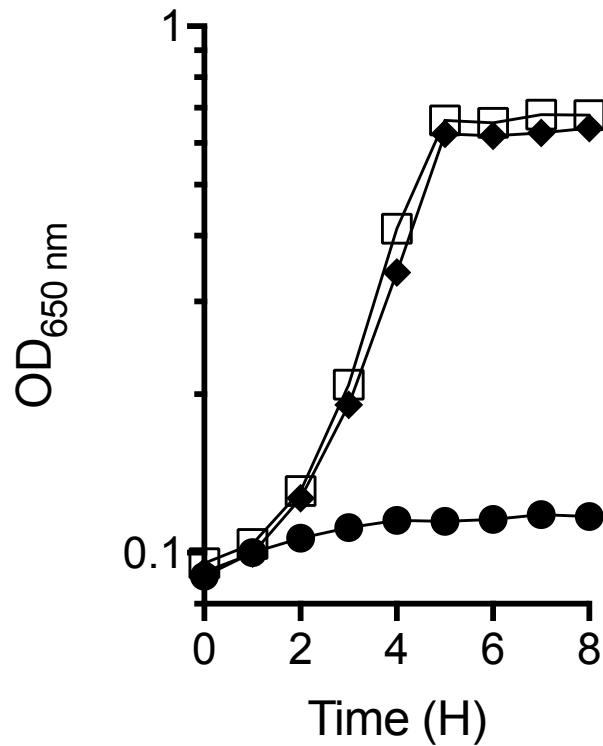


FIGURE C.2. Suppressor mutations restore growth to a *thiC1129 panE::Cm* (DM13652) strain on minimal glucose medium. The parent strain (circles) is unable to grow on minimal glucose medium, but a representative suppressor (DM13897) restores growth on minimal glucose medium (diamonds). The strains grow equally well when thiamine (100 nm) or pantothenate (100 μ M) are added to growth medium (squares). Each growth curve displays representative data from three independent cultures.

```

VDLRDLKTFLLHLAESRHFGRSARAMHVSPSTLSRQIQRLEEDLGQPLFVRDNRTVTLTEA 60
GEELRVFAQOTLLQYQQLRHTLDQQGPSLSGVG92VELHIFCSVTAAYSHLPPILDRFRAEHPSV 120
EIKLTTGDAADAMEKVVVTGEADLAIAGKPETLPGAVAFSMLLENLAVVLIAPALPCPVRNQ 180
VSVDKPDWSTVPPFIMADQGPVRRRIELWFRRHKISNPQIYATVGGHEAMVSMVALGCGVA 240
LLPEVVLENSPEPVRNRVMILERSDEKTPFELGVCAQKKRLHEPLIDAFWKILPN 295

```

FIGURE C.3. Protein alignment of wild-type IlvY with IlvY variants from suppressor mutants. The solid underlined section indicates the N-terminal helix-turn-helix and the dashed underline section identifies the C-terminal substrate binding domain. Variant residues in IlvY^{G92V} (*ilvY3215*), IlvY^{L235M} (*ilvY3213*), and IlvY^{C237Y} (*ilvY3214*) are indicated above their position in the IlvY primary sequence.

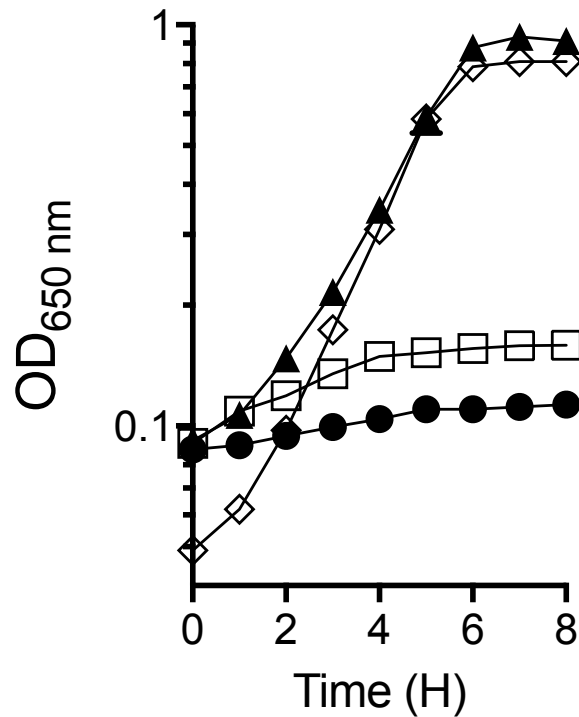


FIGURE C.4. Expression of *ilvY3213* or *ilvC*, but not wild-type *ilvY*, restores growth to a *thiC1129 ΔpanE* strain grown on minimal medium. All strains were grown in glucose minimal medium containing 0.1 % arabinose. Growth of a *thiC1129 ΔpanE* strain containing empty pBAD24 (DM13993; open squares), pBAD24-*ilvC* (DM13994; triangles), pBAD24-*ilvY* (DM13995; circles) and pBAD24-*ilvY3213* (DM13996; open diamonds) are plotted as a function of time. Data are representative of three independent cultures.

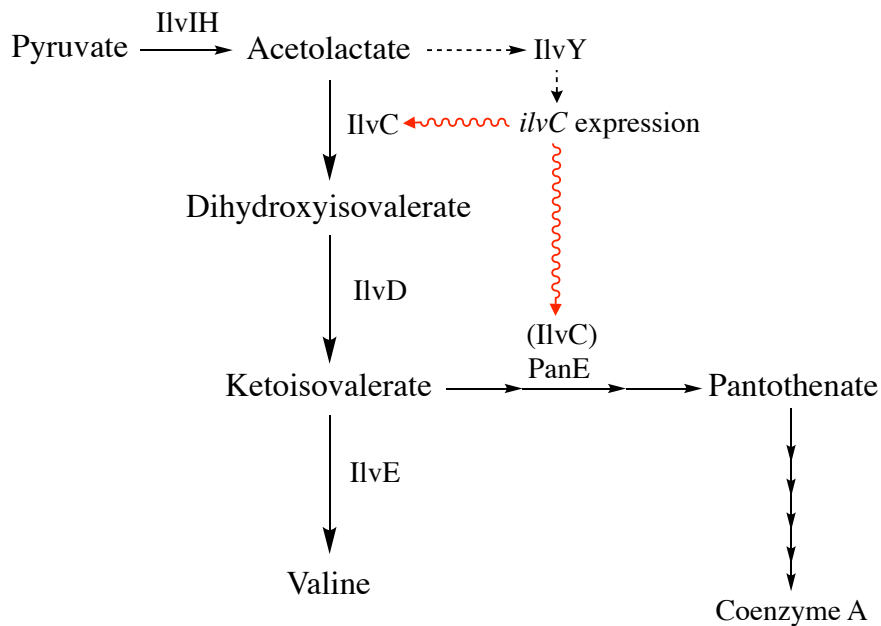


FIGURE C.5. Model of constitutive IlvY activation of IlvC production. In an “adenine-sensitive” ThiC-variant strain, disruption of *panE* reduces coenzyme A levels, limiting flux through ThiC and starving the cell for thiamine. The IlvY variants described here are predicted to constitutively activate expression of *ilvC*, enhancing ketopantoate reductase activity in the cell, leading to increased CoA levels that improve ThiC-variant activity to restore thiamine production.